A HYBRID APPROACH FOR QUANTITATIVE EVALUATION OF RESIDUAL TORQUE OF LOOSE BOLTS IN BOLTED JOINTS USING PASSIVE AND ACTIVE ACOUSTO-ULTRASONICS:

THEORY, SIMULATION AND EXPERIMENTAL VALIDATION

ZHEN ZHANG

Ph.D

The Hong Kong Polytechnic University

This programme is jointly offered by

The Hong Kong Polytechnic University and

Tongji University

2018

The Hong Kong Polytechnic University

Department of Mechanical Engineering

Tongji University

School of Aerospace Engineering and Applied Mechanics

A Hybrid Approach for Quantitative Evaluation of Residual Torque of Loose Bolts in Bolted Joints Using Passive and Active Acousto-ultrasonics: *Theory, Simulation and Experimental Validation*

Zhen ZHANG

A Thesis Submitted in Partial Fulfillment of the Requirements

for the Degree of Doctor of Philosophy

June 2017

CERTIFICATE OF ORIGINALITY

I hereby declare that this thesis is my own work and that, to the best of my knowledge and belief, it reproduces no material previously published or written, nor material that has been accepted for the award of any other degree or diploma, except where due acknowledgment has been made in the text.

_____________________________ (Signature)

ZHANG Zhen (Name of student)

ABSTRACT

Bolted joints are one of the most common elements to assemble structural components for engineering assets. To sustain structural integrity, cut down maintenance cost, and extend service lives of bolted structures, it is highly desirable to characterize bolt loosening in engineering structures as accurately as possible when the bolt loosening is still at its embryo stage. To serve the task of detection of bolt loosening, a diversity of nondestructive evaluation (*NDE*) and structural health monitoring (*SHM*) approaches have been well developed, based on the use of linear and nonlinear features of acousto-ultrasonics.

In this *Ph.D.* study, theoretical analyses are firstly conducted to correlate the linear/nonlinear features of acoustic waves to the residual torque of a loose joint, which facilitates understanding of the detection philosophy of bolt loosening. Subsequently, bolt loosening-related linear/nonlinear indices are established using the linear and nonlinear features of acousto-ultrasonics. Specifically, for the linear passive acoustic method using acoustic emission (*AE*), microcontact theory is used to derive a qualitative relationship between extracted *AE* parameters and contact conditions at the interface of a joint. In the active linear acoustic method using vibration modal parameters (*VMP*), resonant frequency and damping ratio are theoretically linked to the tightening status of a joint. In the active acoustic method using wave energy dissipation (*WED*) of *GUWs*, a linear index is defined based on *WED* to identify the tightening condition of multi-type (e.g., single-lap, cross-lap and hybrid lap) bolted joints. Given the necessity of identifying early bolt loosening in the multi-type joints, three nonlinear indices are constructed theoretically using the magnitudes of *SOH*, *TOH* and modulated sidebands.

To validate the theoretical development, the proposed indices using linear and nonlinear acoustic features, are comparatively adopted to detect bolt loosening in both aluminum-aluminum (*Al-Al*) and composite-composite (*C-C*) bolted joints.

Two detection strategies-the active and passive linear feature-based methods are firstly adopted to evaluate the tightening status of the joints. In the passive method, intrinsic mode functions (*IMFs*) of acoustic emission (*AE*) signals, are used to evaluate the tightening condition of the joints quantitatively. Experimental results reveal that vibration loosening of composite joints results in an increase in the energy ratios of high-frequency *IMFs*, on which basis the detectability of the *AE*-based evaluation is further improved, making it possible to evaluate the tightening condition of a bolted joint under vibration fatigue. In the active method regarding bolt loosening identification using vibration modal parameters, damping ratio is found more sensitive to bolt loosening compared to resonant frequency. However, these two parameters are not capable of evaluating the residual torque of a loose joint at the early stage. In the acoustic method using linear propagating features of *GUWs*, the defined *WED*-based linear index is comparatively employed to evaluate the residual torque in three types of *Al-Al* joints. As the applied torque increases, such a linear index is found to increase in a single-lap joint while decrease in a cross-lap joint. The defined *WED*-based linear index fails to predict the residual torque of hybrid-lap and composite bolted joints. The detectability of this linear acoustic method in bolt loosening is improved by minimizing the effect of boundary reflection, but still in a limited range.

To circumvent the deficiency of the use of linear signal features of *GUWs*, nonlinear acoustic features, including *SOH*, *TOH* and sidebands, are recalled. The independence of the *CAN*-based nonlinear indices regarding the excitation intensities and their efficiencies in bolt loosening detection including the early stage are investigated through experiments in both *Al-Al* and *C-C* bolted joints. To observe that the sensitivity of the nonlinear index constructed from magnitudes of modulated sidebands persists throughout the whole torque range from fully fastened to fully loose. Moreover, the detectability of such a nonlinear index is found to be independent of joint configurations and joining materials, showing enhanced applicability regarding bolt loosening evaluation compared to the linear index. Nevertheless, nonlinear indices constructed from magnitudes of *SOH* and *TOH*, are found only capable of evaluating the residual torque of joints when the applied torque exceeds certain values.

Last, for facilitating an enhanced comprehending of generation mechanisms for modulated sidebands and of quantitative dependence of sideband magnitudes on the residual torque of the bolt, numerical simulation of the *VAM*-based method regarding detecting bolt loosening in both *Al-Al* and *C-C* single-lap bolted joints is comparatively conducted. Numerical results obtained from the modified contact model is found highly consistent with those of experimental data. Based on this, the occurrence and increase in response magnitudes of modulated sidebands due to deterioration of bolt loosening are theoretically attributed to a decrease in the linear contact stiffness along with an increase in the nonlinear contact stiffness.

Conclusively, through theoretical modeling, numerical simulation, and experimental investigations, a series of *SHM* techniques for identifying bolt loosening in multi-type bolted joints are developed in this thesis based on linear and nonlinear attributes of acousto-ultrasonics. The presented study provides a reliable theoretical foundation, relying on which numerical analysis can be accurately conducted to facilitate the tasks of bolt loosening characterization in a variety of bolted structures.

LIST OF PUBLICATIONS ARISING FROM THIS WORK

Referred Journal Papers

1. Zhang Z, Pan Y, Xiao Y, Zhong Z. Measurement and analysis of laser generated Rayleigh and Lamb waves considering its pulse duration[J]. *Acta Mechanica Solida Sinica*, 2015, 28(5): 441-452.

2. Zhang Z, Xiao Y, Liu Y, Su Z. Preload Relaxation Characteristics in Bolted Composite Joints Based on Vibration Fatigue Test [J]. *Acta Materiae Compositae Sinica*, 2016, 33(1): 163-173.

3. Zhang Z, Xiao Y, Liu Y, Su Z. A quantitative investigation on vibration durability of viscoelastic relaxation in bolted composite joints[J]. *Journal of Composite Materials*, 2016, 50(29): 4041-4056.

4. Zhang Z, Liu M, Su Z, Xiao Y. Quantitative evaluation of residual torque of a loose bolt based on wave energy dissipation and vibro-acoustic modulation: A comparative study[J]. *Journal of Sound and Vibration*, 2016, 383: 156-170.

5. Zhang Z, Xu H, Liao Y, Su Z, Xiao Y. Vibro-acoustic modulation (VAM)-inspired structural integrity monitoring and its applications to bolted composite joints, *Composite Structures* 176 (2017): 505-515.

6. Zhang Z, Liu M, Su Z, Xiao Y. Continuous Monitoring of Residual Torque of Loose Bolt in a Bolted Joint. *Procedia Engineering* 188 (2017): 278-285.

7. Zhang Z, Liu M, Liao Y, Su Z, Xiao Y. Contact acoustic nonlinearity (CAN)-based continuous monitoring of bolt loosening: hybrid use of high-order harmonics and spectral sidebands, *Mechanical Systems and Signal Processing* 103 (2018) 280–294.

8. Zhang Z, Xiao Y, Su Z, Pan Y D. Non-destructive and continuous evaluation of tightening condition of bolted composite joints using intrinsic mode functions of acoustic emission signals, submitted to *Journal of Nondestructive Evaluation*.

Refereed Conference Papers

1. Zhang Z, Pan Y, Xiao Y. Laser-generated Lamb waves inside the aluminum plate: Comparison between theory and experiment [C]. 2013 Symposium on Piezoelectricity, Acoustic Waves, and Device Application (SPAWDA-2013), 25-27 October, 2013, Hunan University, Changsha, China.

2. Zhang Z, Xiao Y. Viscoelastic relaxation in bolted composite joints (part II: vibration damping response) [C]. The 9th Asian-Australasian Conference on Composite Materials (ACCM-9), 15-17 October, 2014, Suzhou, China.

3. Zhang Z, Liu M, Su Z, Xiao Y. Evaluation of Bolt Loosening Based on A Hybrid Approach: Wave Energy Dissipation and Contact Acoustic Nonlinearity [C]. 19th World Conference on Non-Destructive Testing (WCNDT), 13-17 June, 2016, Munich, Germany.

4. Zhang Z, Shen Y, Xiao Y, Su Z. A multiscale model for modal analysis of composite structures with bolted joints [C]. 21st International Conference on Composite Materials (ICCM-21), 20-25 August, 2017, Xi’an, China.

ACKNOWLEDGMENTS

During my study at the Hong Kong Polytechnic University, many teachers inspired me with their vast knowledge and useful advice, to whom I want to express my sincere thanks for their kind help.

Firstly, I would like to express my deep and special gratitude to my chief supervisor at the Hong Kong Polytechnic University, Prof. Zhongqing Su, for his timely offer which admits me to study at PolyU as a joint *Ph.D.* student between the Hong Kong Polytechnic University and Tongji University. I gained a lot during the time spent together with Prof. Su. With his extensive knowledge and research experience, he has been providing valuable advice for my study. My English writing capabilities and presentation skills have been greatly improved with his guidance. Thanks to his full support and thoughtful arrangement, I was able to focus on my study and deepen my research to a large extent in the 21 months at PolyU. What I have learned from him will have a lasting positive impact on my future academic life and beyond. In the meanwhile, I want to express my sincere appreciations to Prof. Li Cheng for his useful guidance. Through his course, advanced vibration analysis, I acquired a more specific theoretical understanding of my *Ph.D.* study.

I would also like to express my thanks to my co-supervisor Prof. Yi Xiao at Tongji University, for his unreserved guidance and support. Prof. Xiao has always tried his best to create valuable opportunities for me to improve my research skill and regulated my academic behavior with his rigorous academic attitude.

During my exchange period at PolyU, I have met and made some great friends in the Department of Mechanical Engineering. Special thanks should be delivered to my colleagues Tuo Liu, Shengbo Shan, Hao Zhang, Lisong Shi, Boyang Li, Jingxuan Sun, Lanlan XIAO and Tianxi Chi in the research office FJ610. They accompanied me to truly integrate into the life of Hong Kong and spend an enjoyable time at PolyU. Also, I want to thank my research fellow Menglong Liu, Hao Xu, Kai Wang, Yaozhong Liao, Jing Liu and Zhibo Wang in the lab DE003. I benefited a lot from their useful advice and timely help.

Finally, I would like to sincerely thank my parents and my girlfriend Qian Li, who accompanied me through all the stages of my *Ph.D.* study. They are always the source of my courage to overcome difficulties. Special thanks go to them for their constant support and encouragement.

TABLE OF CONTENTS

NOMENCLATURE

Acronyms and Initialisms

AE	Acoustic emission
Al-Al	Aluminum-aluminum
AS	Averaged amplitude of sidebands
ASTM	American society for testing materials
CAN	Contact acoustic nonlinearity
C-C	Composite-composite
CFRP	Carbon fiber reinforced plastics
DOF(s)	Degree(s) of freedom
EMD	Empirical mode decomposition
FE	Finite element
FFT	Fast Fourier transform
*GUW*s	Guided ultrasonic waves
HF	High-frequency probing wave
HOH	Third-order harmonics
HT	Hilbert transform
HHT	Hilbert-Huang transform

IMF(s)	Intrinsic mode function(s)
IM	Impact modulation
LS	Left sideband
LF	Low-frequency pumping vibration
LDR	Local defect resonance
M-C	Metal-composite
M-M	Metal-metal
NDE	Nondestructive evaluation
PSD	Power spectral density
PZT	Lead zirconate titanate
RS	Right sideband
SEM	Scanning electron microscopy
STFT	Short-time Fourier transform
SNF	Strongest natural frequency
SOH	Second-order harmonics
SHM	Structural health monitoring
TOF	Time-of-flight
TOH	Third-order harmonics
VAM	Vibro-acoustic modulation
VMP	Vibration modal parameter
WED	Wave energy attenuation

Symbols

$e(t)$	Signal envelope upon processing with Hilbert transform
$\phi(t)$	Instantaneous phase
Υ	Hertzian curvature of asperities in contact
η	Damping ratio
τ	Thread coefficient between the nut and bolt
δ	Total deformation of the two spheres in contact
$\Omega_{transmitted\ in\ I}$	Energy of transmitted guided ultrasonic wave
Ω_{leak}	Energy of leaky guided ultrasonic wave

ε	Strain
σ	Stress
β	First-order classical nonlinearity
β_{SOH}^{theory}	Theoretical nonlinear index making use of the magnitude of *SOH*
β_{TOH}^{theory}	Theoretical nonlinear index making use of the magnitude of *TOH*
β_{VM}^{theory}	Theoretical nonlinear index making use of the magnitude of sidebands
β_{SOH}	Experimental nonlinear index making use of the magnitude of *SOH*
β_{TOH}	Experimental nonlinear index making use of the magnitude of *TOH*
β_{VAM}	Experimental nonlinear index making use of the magnitude of sidebands
β_{VAM}^{M}	Modified experimental nonlinear index making use of the magnitude of sidebands
ϑ	Second-order classical nonlinearity
α	Hysteric nonlinearity
$\dot{\varepsilon}$	strain rate
$\Delta\varepsilon$	Variation of compressive strain
ϕ	Perturbation parameter

ω	Excitation frequency of the harmonic force
ω_1	Excitation frequency of low-frequency pumping vibration
ω_2	Excitation frequency of high-frequency probing wave
$\Omega^{W}_{transimitted}$	Transmitted energy of the whole signal
$\Omega^{S}_{transimitted}$	Transmitted energy of first-arrival guided ultrasonic wave
$\lambda_i^{t/r}\,(i=0,1,2)$	Constants relating to asperity-height distributions along the contact surfaces,
w	Transverse deflection
θ	Rotation angle
$\nu_i\ (i=1,2)$	Poisson's ratio of uniformed spherical asperities on the contact surfaces
ς, χ	Rayleigh damping parameters
c_i	*ith* intrinsic mode function
C_i^T	i^{th} *IMF* of the *AE* signals from a joint under a torque of T
d	Bolt diameter
R_j	energy ratio of *IMF* c_j
$R_{1\text{-}3}$	Summation of energy ratios of first three *IMFs*

$R_{Residual}$	Energy ratio of residual *IMFs*
$\Delta R_{Residual}$	Variation of energy ratios of residual components
f	Resonance frequency
f_r	Fundamental resonance frequency
Δf	Half-power bandwidth
f_{HF}	Frequency of probing wave
f_{LF}	Frequency of pumping vibration
k_L^t	Linear transitional stiffness
k_L^r	Linear rotational stiffness
m_{ik}	Mean of the upper and lower envelopes
h_{ik}	Proto-Intrinsic Mode Function
x_1	Linear response of the bolted joint
x_2	*SOH* response of the bolted joint
x_3	*TOH* response of the bolted joint
x_N	Nonlinear responses of the joint
K_N	Nonlinear contact stiffness matrix
$K_{modified}$	Modified contact stiffness matrix
K_B	Stiffness of the bolted contact interface
K_{eq}	Equivalent stiffness of the bolted joint

K_J	Stiffness of the joining composite material
$K_{H/N}$	Hysteretic and nonlinear stiffness
K_1	Linear contact stiffness
K_2	Nonlinear contact stiffness
M	Mass
N	Total number of asperities in contact
T	Bolt torque
$\dot{U}_{AE}$	Energy release rate
V	Sliding velocity
W	Normal load applied on the asperities
X	Gap distance between contact surfaces
ΔX	A variation in the gap distance
$X(t)$	An original signal to conduct *EMD*
$Z(t)$	Analytic signal

LIST OF FIGURES

LIST OF TABLES

CHAPTER 1

Introduction

1.1. Research Background and Motivations

Bolted joints are ubiquitous in engineering assets, playing a critical role in transferring loads among interconnecting components. The past decades have witnessed an escalation of using bolted joints as a basic building block in complex engineering structures. To meet the demand for design and maintenance, multi-type bolted joints, including cross-lap [1, 2] and single-lap [3], are widely employed to assemble different functional components in the engineering structures. For instance, approximately 3 million fasteners are adopted to assemble more than 130,000 unique engineered parts in a Boeing 777 airplane [4]. Composite material has been used as a new generation of advanced material in varied industrial fields, such as aerospace, automobile and marine engineering, thanks to its various advantageous properties, including the high strength- and stiffness-to-weight ratio, excellent resistance to fatigue and shock, and satisfactory designability [5]. Addressing these merits, there has been an increased preference in assembling composite structural components through bolted joints [6], so as to streamline manufacturing and enhance structural load-carry capability.

Components consisting of metallic and composite materials are assembled together using bolts by the compressive force (the tightening force) produced in the joining materials and by the tensile forces (the bolt axis force) generated due to the elongation of the bolt under external applied torques. The above two forces fastening the components together are generally termed as a *pretension force*. The process in which a decrease occurring in the pretension force due to some certain reason is what so-called *bolt loosening*. Specially, self-loosening can be described as a gradual loss of the pretension force in a bolted joint under a transverse cyclic load [7].

Throughout the service life of a bolted joint, a wide array of diatheses, including mainly cyclic loads, inappropriate manipulation and structural ageing, can initiate and accelerate the process of bolt loosening. The progressive accumulation of bolt loosening can considerably downgrade structural integrity and durability, potentially resulting in bloody loss of life and immense monetary wastage if not duly detected [8-11]. To put it into a perspective, approximately 20% of failure cases of mechanical systems each year worldwide are reported to be caused by the self-loosening of threaded bolts or fasteners. Besides, over 10% of the lifetime of a mechanical system is associated with the detection and rectification of bolt loosening or related risks [12]. Every third week, a dropped object incident caused by bolt failures occurs on Oil &

Gas installations on the Norwegian Continental Shelf, and 25% of these bolted structures are required to be re-tightened every year [13]. In the United States, wheel detachments cause about 20 reported accidents per week and approximately 50% of these failures are found to be caused by loose nuts of wheels. A further survey among the automobile service managers indicated that 23 % of all service problems were attributed to loose fasteners/bolts, with even 12 % of new cars being found to contain loose fasteners/bolts. In 1991, a Continental Express Embraer 120 break up in flight and all 14 people aboard were killed. 47 missing fasteners along the horizontal stabilizer were found to be the reason. In the subsequent inspection, 25 % of 767 model airplanes which had flown more than 25,000 hours were found to have loose or missing fasteners [14]. The train derailing in February 2007 near Lambrigg was reported as a direct consequence of a loose nut of wheel [15]. In July 2013, a metal moved to the middle of the track, caused by a loose connector, preventing the rolling stock from passing through, caused France's worst rail crash [16].

A joint would not lose all the pretension force immediately but with a complicated loosening process manifested as a time-dependent behavior [17]. At the first step, a slow loss of pretension force occurs and vibration gradually increases the degree of bolt loosening through wearing and hammering at the contact interfaces. At the second step, once friction forces between the contact surfaces drop below a critical level, caused by the loss in the pretension force and surface damage, the nut starts to back off, followed by a relative motion between the nut and bolt. Generally speaking, there exist two main types of relative motion during the process of bolt loosening of a joint: one is the relative motion between the nut and bolt, and the other is the one between the fasteners (i.e., nut/bolt) and joining material. Three factors can be responsible for the occurrence of relative motion in a bolted joint [18-21]:

1. Plastic deformation of threads:

A variety of experimental investigation and finite element (*FE*) analysis have been conducted to investigate the mechanisms of self-loosening of a bolted joint at an early stage [7]. The *FE* results indicate that the occurrence of local cyclic plasticity near the roots of threads can lead to cyclic strain ratcheting. The localized cyclic plastic deformation results in a redistribution of stresses in the bolt, and consequently causes a decrease in the pretension force over loading cycles.

2. Interfacial slip induced by dynamic loading: vibration, torsion and impact:

Vibration-induced loosening of a bolted joint can be attributed to a reduction in interfacial friction [22], which results in slip behavior at the interface between the nut thread and bolt head. When a joint is subject to a dynamic loading, during which force transform between assembled components implemented by grip friction, the relative motion between thread flanks and other contact surfaces may exceed the restriction of the friction force between the assembles. The resultant transverse slip at the contact interface drives the bolt to undergo a pendulum movement. Once the magnitude of such movement is large enough, slip of the nut or bolt head occurs. This leads the joint to be free of friction in the circumferential direction and accelerates the process of bolt loosening.

Similarly, loosening of threaded fasteners subject to dynamic loads is reported to result from the occurrence of slip [23]. Localized slip at the contact interfaces is concluded to be responsible for loosening of the fasteners. The minimum shear load, which is required to initiate loosening of fasteners, is significantly lower than that required to cause complete slip of thread head.

Along the same line of thinking, self-loosening of a bolt can also be attributed to microslip occurring at the contact surfaces between the curvic, thread and bolt head [24]. When a joint is subject to cyclic transverse load, rotation of the nut is caused by localized slip without complete slip at the contact interface between the bolt head and thread surface. However, the curvic surface undergoes complete slip under all external loads. The microslip occurring at the contact interfaces is identified to be responsible for self-loosening of a curvic coupling joint.

3. Creep and stress relaxation caused by viscoelasticity of joining materials:

For a bolted composite joint, besides the above two causes, viscoelasticity of polymer should be taken into account when considering the mechanisms of its bolt loosening. Generation of the pretension force in a bolted composite joint is distinct from that in a metallic joint and it is related to the properties in the thickness direction [25, 26]. Due to a lack of reinforcement, polymer matrix, which possesses with viscoelastic behaviors, governs the structural response of a composite joint in the thickness direction. Therefore, composites often exhibit creep and relaxation behaviors (i.e., viscoelastic behaviors) in the thickness direction even at room temperature. From the comparison of preload relaxation between steel and composite joints in a duration of 30 h, about 1/3 of preload relaxation in a composite bolted joint is reported to be caused by viscoelastic behaviors of the polymer matrix. This behavior is magnified when a composite structure with bolted joints is exposed to high level of moisture and/or temperature. For instance, the creep behavior of bolted composite structures in an aircraft caused by aerodynamic heating usually leads to excessive deformation and creep rupture during the intended lifetime of the joints. Relaxation of clamping force in a double-lap graphite/epoxy bolted joint at different steady-state temperatures and moisture conditions for a 100-day duration reveals that the rate of relaxation increases for the joint under high temperature and moisture [27]. Bolt loosening of a composite joint under high temperature is a comprehensive consequence of creep of the gasket and joining materials along with the flange materials [28]. Therefore, determination of allowable bearing strength of a composite joint entails considering the effect of viscoelasticity in the thickness direction of composites, especially for the joints designed for a long-term use.

The various failures caused by bolt loosening, and especially those in critical load-bearing joints [29, 30], have posed an impending need for periodic inspection and continuous surveillance of leftover torque of bolts. Timely inspection and effectual monitoring, not only during installation of bolts or fasteners but also throughout their intended service life, is needed urgently to secure the integrity of the joints, and to drive down the risk of drastic system failure. However, the prevailing inspection and monitoring techniques nowadays to serve this purpose are still restricted by visual, tapping inspection and retightening, which are usually conducted at regularly scheduled intervals. During the visual and tapping inspection, to interrupt the regular operation of the system temporarily, or in some cases to remove the bolted components is usually required. Such interruption or removal processes are usually labor-intensive and time-consuming. In addition, due to the usage of large amount of bolts in engineering structures, retightening process of all the employed bolts requires a frequent periodic maintenance and always involves in a vast number of maintenance personnel, introducing exorbitant cost. On top of this, such a maintenance philosophy is fairly dependent on the experience and knowledge of the maintenance personnel and prone to human error.

In this backdrop, efforts have been cast in developing reliable and cost-friendly methods to detect bolt loosening using nondestructive evaluation (*NDE*) and structural health monitoring (*SHM*) technique. To prevent catastrophic structural failure, *NDE* methods have been widely employed on a routine schedule to detect damage in engineering structures. In conjunction with the use of multi-functional advanced transducers, the detection philosophy of most *NDE* methods is based on comparison of signal characteristics extracted from captured signals, whereby to establish a quantitative relation between changes in signals and occurrence and severity of damage. Nevertheless, as mentioned earlier, most *NDE*-based approaches are intended to be conducted on the routine schedule, disregarding progressive deterioration and changes in working condition of the detected structure (i.e., non-condition-based). For instance, the separation of the vertical stabilizer from Flight TS 961 in 2005 occurred only five days after its latest routine A-check, while the next major C-check was scheduled for one year later [31]. Therefore, non-conditioned-based *NDE* methods are not effectual enough to avoid potential structural failure which may occur without a timely warning.

To circumvent the limitation of traditional *NDE* methods, condition-based *NDE* technique was first proposed at early 1990s. By taking into account actual operational conditions and structural aging, it attempts to provide a more robust solution to structural damage detection. With this, maintenance schedules can be updated over time to secure the most efficient inspection. With development and breakthroughs in signal processing, sensor technology and informatics, *SHM* technique, aimed at implementing an on-line damage detection strategy without terminating normal service of a civil, aerospace and mechanical engineering structure, has been proposed and widely studied. Generally, an *SHM* system consists of a sensor network including both actuators and sensors, a data acquisition system, and a data processing unit. It is noteworthy that a *SHM* technique aims to achieve real-time and condition-based monitoring of the overall integrity of the structures during their normal operation, with the superiority of entailing no operational disruption. It has been demonstrated that an effectual *SHM* system may reduce the overall maintenance cost of an aircraft by over 30% [32]. To best serve the purpose of *SHM*, transducers (i.e., actuators and sensors) should be capable of being permanently embedded in or mounted on the monitored structure.

A *SHM* problem is concluded as a statistical pattern recognition paradigm, which contains four main process [33]: (1) operational evaluation, (2) data acquisition, fusion and cleansing, (3) feature extraction and information condensation, and (4) statistical model development for feature recognition. At a sophisticated level, *SHM* should be hierarchically conducted, with increasing levels of difficulty [34]: (1) qualitatively indicate the occurrence of damage; (2) quantitatively identify the position of damage; (3) quantitatively estimate the severity of damage; and (4) predict residual life of the monitored structure.

During monitoring of an extreme event, such as an earthquake or a fast propagating crack, *SHM* is intended to provide real-time and reliable information about the current performance and to predict the subsequent integrity of the structure. For long-term *SHM* in particular, its output information should be timely updated regarding the durability of the monitored structure including material aging, damage accumulation caused by an external loading and operational environment [35].

Towards the detection of loosening of bolts in jointed structures, both the passive and active acoustic methods using linear features of *GUWs* and vibration signals based on *SHM* and *NDE* techniques, have been developed and deployed by exploring the changes in signal features between the benchmark signal (from healthy condition) and the inspected signal (from current condition). As a representative passive linear acoustic method, acoustic emission (*AE*) is reportedly sensitive to microscopic events presenting in a material, with a widespread application in monitoring engineering structures [36]. The sensors are not required to be arranged closed to the exact location of the source when using the *AE* technique, which facilitates the development of a remote *SHM* system. This outperforms most *NDE* techniques, for instance pulse-echo ultrasonics, radiography, or eddy current, which all require 100% volumetric scanning for damage detection [36]. Therefore, *AE* method is more effectual than these traditional *NDE* techniques in terms of inspection time and preparation, resulting in cost savings. In an active linear acoustic method, wave signal features such as the delay in time-of-flight (*TOF*), wave energy attenuation (*WED*) and mode conversion can be exploited to the detection of bolt loosening. These signal features, to a certain extent, show linear correlation with damage parameters, and are therefore referred to as linear features of acousto-ultrasonics in this study. However, at an embryo stage, bolt loosening is similar with micro-scale cracks and can hardly induce phenomenal changes in linear signal features. One can increase the frequency of incident *GUWs* to reach a higher sensitivity. But this will introduce additional complexity in the appearance of signals due to dispersive properties of *GUWs* at high frequencies. Moreover, *GUWs* propagating in composite structures exhibit complex dispersion behaviors and serious attenuation effect, which leads to further increased difficulty in signal acquisition involving additionally tedious tasks in frequency selection and signal processing, etc. To overcome above deficiencies and achieve an effectual detection, there has been an increased preference to adopt nonlinear acoustic approaches, based on the generation of high-order harmonics (*HOH*) and modulated sidebands. Motivated by this, to reap respective merits and in the meantime circumvent demerits of each method using linear and nonlinear features of acousto-ultrasonics, the present study is dedicated to developing a reliable *SHM* system for the evaluation of tightening status of bolted structures with a combined use of linear and nonlinear acoustic methods.

At this moment, the accuracy of current *NDE* and *SHM* technique regarding bolt loosening detection at an early stage is limited, mainly due to a lack of investigation of generation mechanisms of linear and nonlinear wave features caused by asperity contacts in the mating parts of joints. In this study, the reliance of linear and nonlinear wave features of acousto-ultrasonics on the asperity contacts in the micro perspective at contact surfaces in bolted joints is investigated. On this basis, a quantitative evaluation of residual torque of loose joints with different joint configurations and joining materials, using linear and nonlinear features of acousto-ultrasonics, is proposed in this thesis, featuring a multi-scale analysis with both theoretical and experimental studies. The objectives of this thesis can be concluded as

- Study interaction mechanisms between acousto-ultrasonics and rough contact surfaces of joints;
- Compare performance of linear and nonlinear features of acousto-ultrasonics in continuous monitoring of bolt loosening;
- Develop effective methods for early bolt loosening detection for multi-type joints and propose solutions to bolt loosening detection in real engineering structures.

1.2. Scope of the Thesis

In this *Ph.D.* thesis, a monitoring framework for detecting bolt loosening in a bolted joint, regardless of the material properties and joint configurations of the joint, is developed theoretically and experimentally, with a hybrid use of linear and nonlinear acoustic methods. To facilitate a better comprehending of the detection philosophy of bolt loosening, residual torque of a loose joint is theoretically correlated with the linear and nonlinear features of *GUWs* and vibration signals. Subsequently, bolt loosening-related linear/nonlinear indices are established using the linear and nonlinear features of acousto-ultrasonics. To validate the theoretical development, the proposed indices, using linear and nonlinear features of acousto-ultrasonics, are comparatively adopted to detect bolt loosening in both aluminum-aluminum (*Al-Al*) and composite-composite (*C-C*) bolted joints with different joint configurations.

The chapters are organized in the order of theoretical interpretation and experimental validation. A brief literature review on acousto-ultrasonics for detection of bolt loosening is presented in Chapter 2. Firstly, for the passive linear acoustic method, the mechanism of generation of *AE* and its current applications are introduced. Subsequently, in the active linear acoustic method, a variety of linear signal features extracted from *GUWs* and vibration signals for damage detection, including bolt loosening, are introduced. Emphasis is placed on the nonlinear features, especially *HOH* and modulated sidebands of acousto-ultrasonics, for the identification of small-scale damage, such as early-stage fatigue cracks and bolt loosening. The comparison of sensitivity between linear and nonlinear feature-based methods facilitates the understanding of advantage of the latter one in terms of under-sized damage detection, including early bolt loosening.

Chapter 3 presents theoretical fundamentals for both linear and nonlinear acoustic methods. For the linear passive acoustic method, Hertzian contact theory is used to derive a qualitative relationship between *AE* parameters and contact condition of asperities at the interface of a joint. The effect of sliding speed, contact pressure and surface properties on the generation of *AE* signals is presented and discussed. For the linear active acoustic methods, firstly vibration modal parameters (*VMP*) typified by resonant frequency and damping ratio of a joint are theoretically linked to its residual torque. Subsequently, linear wave features of *GUWs*, i.e., *WED*, is associated with the residual torque of a loose bolt using an analytical model also relying on the Hertzian contact theory. As the counterpart of linear features of acousto-ultrasonics, contact acoustic nonlinearity (*CAN*) engendered at the joining interface is firstly interrogated, and the contact stiffnesses (including both linear and nonlinear components) are described in terms of a Tayler series, on which basis nonlinear indices are constructed to associate nonlinear spectral features (*i.e.,* magnitudes of *HOH* and modulated sidebands) with the residual torque.

To validate the theoretical prediction in Chapter 3, a series of case studies are presented in Chapter 4 using both passive and active linear acousto-ultrasonics. In the passive linear acoustic method, intrinsic mode functions (*IMFs*) of AE signals, obtained by Empirical Mode Decomposition (*EMD*), are used to characterize contact behaviors in a bolted composite joint under different torques when subject to flexural vibration. Composite-composite (*C-C*) friction related *IMFs* are used to investigate the effect of applied torque on contact behaviors at the *C-C* interface. Subsequently, vibration loosening of bolted composite joints under different torques is monitored using the *EMD*-processed signal characteristics of *AE* signal. In the active linear acoustic method using vibration modal parameters, resonance frequency and damping ratio are comparably adopted to characterize residual torque of a joint. In the method using linear features of *GUWs*, the sensitivity of *WED* to bolt loosening is verified by identifying residual torque of loose bolts in both *Al-Al* and *C-C* bolted joints. For the *Al-Al* bolted joints, the dependence of *WED* on joint configurations, namely single-lap, cross-lap and hybrid-lap joints are presented.

The detection of bolt loosening in both *Al-Al* and *C-C* bolted joints, using *HOH* and modulated sidebands residing on *CAN*, are comparably presented in Chapter 5. The theoretically defined damage (bolt loosening)-related nonlinear indices are verified by detecting bolt loosening in both bolted joints. To compare the detectability of *CAN*-based nonlinear feature-based methods with that of *WED*-based linear feature-based method in terms of sensitivity to early bolt loosening, and the dependence on joint configurations and joining materials, nonlinear indices developed from the magnitudes of *HOH* and modulated sidebands are comparatively adopted to evaluate bolt loosening in the same joints as introduced in Chapter 4.

Chapter 6 introduces the method enhancement of *CAN*-based nonlinear feature-based method relying on modulated sidebands through numerical simulation, to facilitate a better comprehending regarding generation mechanism of modulated sidebands and their quantitative dependence on residual torque of a loose bolt. Finite element (*FE*) models of both *Al-Al* and *C-C* single-lap bolted joints are developed and utilized to calculate structural dynamic responses including both linear and nonlinear signatures. The effectiveness and accuracy of the modified model of contact stiffnesses proposed in Chapter 3 are then examined by numerical analysis, where finally, by using the experimental data as reference.

Finally, Chapter 7 serves as the conclusion of the thesis where recommendations for future research are also given.

CHAPTER 2

State of the Art of Methods for Evaluating Bolt Loosening: *From Linear to Nonlinear*

2.1. Introduction

Acousto-ultrasonics, a combination of ultrasonic characterization and *AE* methodology, has attracted a great deal of attention over the years to develop a diversity of *NDE* and *SHM* techniques for monitoring the structural integrity [37], including evaluating bolt loosening.

Conventional *NDE* and *SHM* are based on the linear theory of acousto-ultrasonics, in which the changes in wave signals between the current condition and healthy condition in terms of delay in time-of-flight (i.e., *TOF*), wave energy and mode conversion, are used. The occurrence and deterioration of damage leads to changes in the phase and/or amplitude of the captured signal, however concerned frequency of the captured signal is still the same as the input signal. Since such techniques are based on signal features which show, to some degree, linear correlations with changes in material properties caused by possible damage, they are often termed as linear acoustic techniques. These linear techniques have been proven sensitive to gross defects or open cracks, but lack of detectability to micro cracks or material degradation [37, 38]. The difficulty in extracting unremarkable signal changes from acquired signals has created a bottleneck for the detection philosophy with the use of linear acoustic features.

Alternative techniques to overcome the mentioned deficiencies of linear feature-based methods are so-called nonlinear acousto-ultrasonics methods, in which the occurrence and severity of damage are often correlated to signal characteristics at frequencies distinct from that of the input signal. Without loss of generality, these nonlinear techniques are resided on such a premise that acousto-ultrasonics, when propagating in an elastic medium, can be distorted by both the inherent nonlinearity of material and contact-acoustic-nonlinearity (i.e., *CAN*) induced by the “breathing” motion pattern at the contact interface of a crack or a loose joint. As a result, nonlinear features such as high-order harmonics (i.e., *HOH*) and modulated sidebands are generated and can be associated with health condition of the monitored structure.

In this chapter, both the passive and active linear acoustic approaches along with *CAN*-based nonlinear acoustic methods are comparatively introduced for damage detection including bolt loosening evaluation in the followings.

2.2. Linear Methods: Using Linear Signal Features

Over past decades, a great deal of effort has been directed to develop *NDE* and *SHM* methods for monitoring engineering structures using acousto-ultrasonics, due to the excellent properties of guided ultrasonic wave (i.e., *GUWs*), for instance fast propagation and acceptable attenuation upon propagating a long distance. Amongst them, Lamb waves (one typical type of *GUWs*) have been attracting particular attention of researchers, which propagate inside thin plate- or shell-like structures, of which thickness is on the same order of wavelength. Lamb waves can be characterized into two modes, namely antisymmetric and symmetric modes.

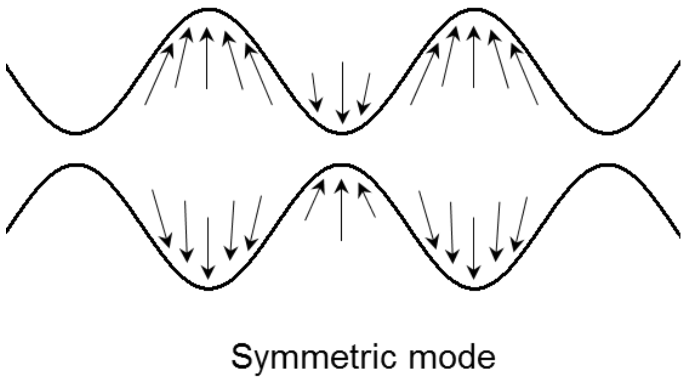

(a)

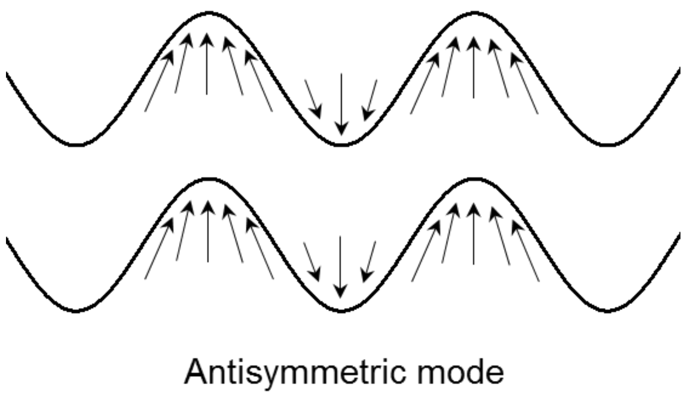

(b)

Figure 2.1 (a) Symmetric; and (b) antisymmetric modes of Lamb waves

Symmetric modes of Lamb waves feature a radial in-plane particle displacement, while antisymmetric modes undergo the mostly out-of-plane displacement, as shown in **Figure 2.1**. The difference in the particle motion patterns of these two modes creates possibilities of Lamb waves regarding identifying a particular type of damage in *NDE* and *SHM* applications using a specific mode, i.e., the symmetric or antisymmetric mode.

However, the highly dispersive behaviors and multiple modes of Lamb waves (see **Figure 2.2**) lead to a complicated representation of Lamb waves in both time and frequency domain [39]. To facilitate meaningful and accurate signal interpretation for damage identification, excitation frequencies of Lamb waves should be prudentially selected to avoid inducing excessive higher-order modes, while ensuring an acceptable sensitivity (determined by wavelength) at the same time.

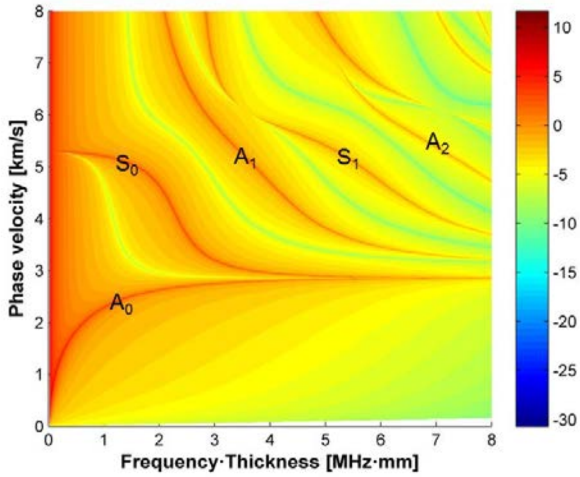

(a)

Figure 2.2 (a) Dispersion curves of phase velocities; and (b) wavenumber *vs.* frequency for an aluminum plate

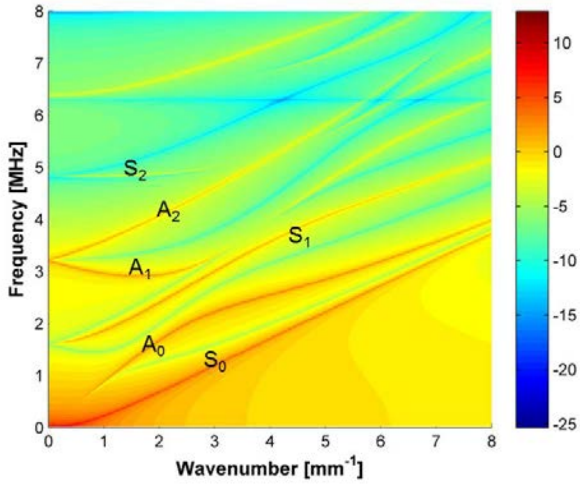

(b)

Figure 2.2 (continued)

GUW (e.g., Lamb wave) -based *SHM* techniques can be conducted in either passive or active ways [40]. In the passive *SHM* techniques, the sensors, which measure temperature, deformation (indicated by strain and stress), and acoustic emission (*AE*) etc., are used to monitor the structure over time. Notably, passive *SHM* techniques, for example using characteristics of *AE* signals, only 'listen' to the structure but do not intend to interact with it. Distinct from passive sensors, active transducers used in an active *SHM* technique, such as lead zirconate titanate (i.e., *PZT*), fiber optic transducers and radiation transducers, are designed to interact directly with the monitored structure and identify the occurrence, extent, and intensity of structural damage [40]. In the active *SHM* technique, active transducers are used for measuring signals transmitted by the sensor with controllable frequencies that are reflected, refracted or scattered by the monitored structure, while in the passive *SHM* technique, passive sensors are designed to receive natural emissions produced by the monitored structure.

Generally speaking, *GUW*-based active linear acoustic method attempts to implement a local detection, which provides diagnosis information in the path between the actuator (to generate *GUWs*) and sensor (to capture *GUWs*), if neglect the boundary reflection used in some special cases. Vibration-based *SHM* techniques in which a global detection using modal parameters, such as resonant frequency, modal shape and damping ratio, is used to evaluate the state of the whole monitored structure. To overcome the limitations of conventional *NDE* techniques as mentioned in Chapter 1, passive linear feature-based method (i.e., AE-based) and active linear acoustic methods (i.e., *GUW*-based and vibration-based) are adopted in this thesis to achieve an on-line detection of bolt loosening.

2.2.1. Passive Linear Philosophy

Acoustic emission (*AE*) describes a rapid release of strain energy (manifested as transient elastic waves) caused by initiation and propagation of a crack or relative motion in the mating parts of a contact configuration such as a loose joint. *AE* signals are widely classified into two categories, namely primary and secondary *AE* [36]. The former is referred to as those generated from within the material of interest such as propagating cracks, while the latter contains all other emissions originating from external sources. A series of parameters defined from characteristics of *AE* signals (i.e., amplitude, energy, rise time, counts and duration, as displayed in **Figure 2.3**), are related to the severity of possible damage in the monitored structure to achieve an on-line passive detection.

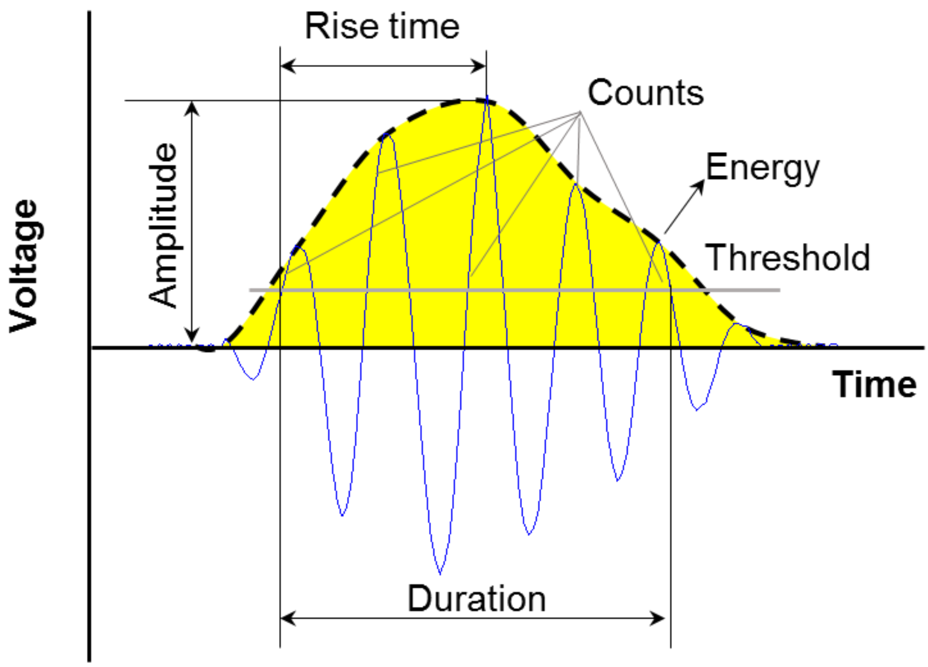

Figure 2.3 Time presentation of a typical *AE* signal

Generally speaking, there are three prevailing signal processing approaches that can be adopted for interpreting *AE* signals [41]:

(i) classification using a single parameter, for instance amplitude, frequency or wavelet level;

(ii) classification using combined parameters in conjunction with pattern recognition techniques; and

(iii) classification with respect to the extensional and flexural mode content.

To achieve a quantitative evaluation of a monitored structure using *AE* signal characteristics, generation mechanism of *AE* signals and their relation with the occurrence and severity of structural damage must be firstly understood. For instance, the onset and growth of cracks in the material under fatigue is a complicated process.

Firstly, cracks initiate and propagate due to shearing force and followed by a tensional loading, during which *AE* generates with distinct signal characteristics [42]. A great amount of studies has been conducted to exhibit the efficiency of *AE* technique in identifying cracks using amplitude (i.e., energy)-based and frequency-based classification [36, 41, 43-46].

Silversides et al. [46] developed an *AE*-based experimental methodology for detecting the onset and propagation of delamination in carbon fiber reinforced plastics (*CFRP*), when the *CFRP* was subject to a fatigue loading. Pattern recognition technique was employed, during a crack opening and closing testing, to recognize *AE* signals emitted by the initiation and growth of cracks from those generated from environment noise. The *AE*-based method was proven to be capable of indicating damage accumulation prior to observable crack propagation, showing a high sensitivity to tiny cracks. Furthermore, the distribution and intensity of *AE* signal energy was quantitatively correlated to the delamination length and growth rate of the cracks. Similarly, Bourchak et al. [43] adopted the *AE* method to monitor the state of *CFRP* subject to static and fatigue loadings. A good correlation between *AE* energy and structural damage was demonstrated by the related results obtained from ultrasonic C-scanning and microscopic inspection. Results from this study indicated *AE* energy can be used as a damage parameter to provide effectual failure criteria for composites under fatigue to avoid potential drastic failures. With development of transducers, piezoelectric sensors were able to be embedded in sandwich composites to detect damage-related *AE* activities when the composites were subject to three-point bending [45]. *AE* signals captured by embedded sensors revealed the failure mechanisms of the sandwich composites: the core damage firstly occurred followed by resin cracking, subsequently interfacial debonding between skin and core, and finally fibers breaking. Compared with the sensors mounted on the surface, the embedded one showed a much higher sensitivity to damage and exhibited great potential as a useful tool for *SHM* in sandwich composites.

On the other hand, using the frequency-based analysis of *AE* signals, classification of failure modes of *CFRP* in a series of standard tensile tests, including matrix cracking, fiber/matrix debonding, and fiber pull-out and fracture, was reported ending up with good results [41].

From above descriptions, it can be concluded that *AE* signals can provide details of physical processes (e.g., initiation and propagation of cracks) in the monitored structures. Along the same line of thinking, contact behaviors in a bolted joint can also be identified by characteristics of *AE* signals. When a joint is subject to a dynamic loading, the mating parts, of which surfaces are uneven with randomly distributed asperities in the micro perspective, undergo a slight relative motion.

Prior to the application of *AE* technique in the detection of bolt loosening in engineering practice, endeavors have been cast in investigating the relation between AE characteristics and contact behaviors at an interface undergoing a relative motion using the primary testing configuration, as shown in **Figure 2.4**.

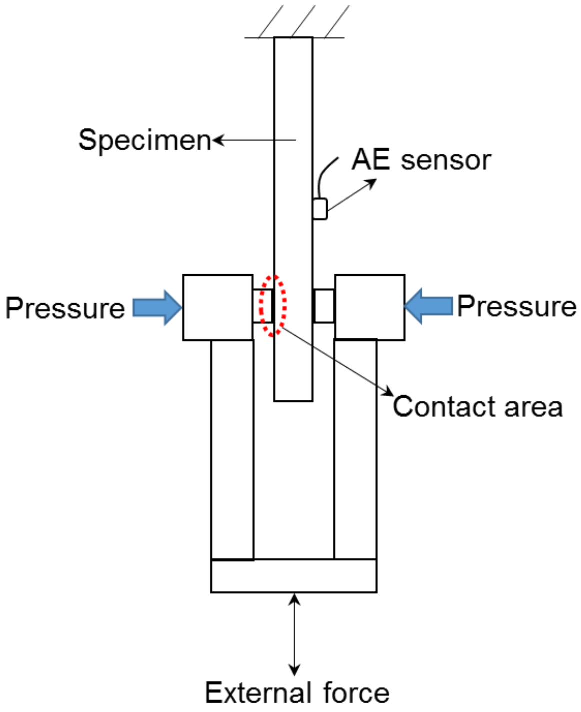

Figure 2.4 Schematic representation of experimental setups for generating friction-related *AE* signals.

Fan et al. [47] developed a theoretical model to study affecting factors of *AE* generation using elastic asperity contact of materials. Sliding speed and distance, number of asperities in contact, loads carried by asperities, and surface properties were identified to impart a direct influence on the energy of *AE* signals. The proposed model provided a theoretical foundation for a quantitative estimation of the contact load at an interface using *AE* signals and facilitated analysis of tribological process at contact interfaces. Asamene and Sundaresan [48] characterized *AE* signals generated from contact surfaces with a series of surface roughness, relative sliding velocities, and normal contact pressures. *AE* features were quantitatively linked to tribological conditions of the contact interface in the experiment, which showed a good agreement with numerical predictions. Moreover, characteristics of friction- and wear- related

AE signals were found distinct from those generated from occurrence and growth of fatigue cracks. To achieve a recognition of wear mechanisms using *AE* technique, Hase et al. [49] comparably investigated the features of *AE* signals generated from adhesive wear and abrasive wear. According to frequency analysis on the *AE* signals generated from these two types of wear, signals from the former presented a large peak in the high-frequency region, while those from the latter contained a series of peaks in the low-frequency region. Therefore, this study verified the application of *AE* technique in the recognition of different wear mechanisms.

To conclude, the pressure applied on a contact interface can affect contact behaviors of the asperities on the surfaces, which can be indicated by characteristics of related *AE* signals. Therefore, it is feasible to identify tightening state of a bolted joint under a dynamic loading (i.e., flexural vibration) with the aid of signal analysis on the *AE* signals. Most failures of bolted joints were reported to be caused by metallurgical fatigue, under-tightening, over-tightening and irregular tightening of bolts [50]. If the applied preload is insufficient, all external loads are to be transferred by the bolt, which results in excessive fluctuating stress when the joint is subject to the dynamic loading. On the other hand, an excessive preload may produce an overlarge and noncyclic tensile load in the bolt, along with a high mean stress in the mating parts of the joint, which may exceed endurance limits of the joining materials [18, 50]. Therefore, an improper preload (i.e., too high or too low) potentially leads to a failure of a bolted joint.

To guarantee the performance of a bolted joint, it is critically important to develop cost-effective detection methods to characterize the contact conditions during assembly and further surveil the tightening condition throughout its service life. In order to serve these purposes, passive acoustic methods using characteristics of *AE* signals have been developed to identify bolt loosening in engineering structures with bolted joints. Alam et al. [51] simulated *AE* signals generated from a series of scenarios of fretting conditions in a bolted joint, such as surface roughness, sliding distances and velocities, and contact pressures. It has been revealed that *AE* signals with a longer duration can be produced when the bolt was loose. In addition, the amplitude and duration along with frequency distribution of *AE* signals generated from a smooth surface were different from those generated from rough surfaces. These findings have demonstrated the potential capability of *AE* technique in quantitative assessment of applied torque of a joint and in continuous monitoring of fatigue performance through an evaluation of fretting wear at contact interfaces of a bolted joint subject to a dynamic loading.

However, currently limited studies are reported to achieve identification of bolt loosening using *AE* technique at a quantitative level. One possible reason is the limitation in the signal processing, typified by traditional frequency-based analysis (e.g., fast Fourier transform, *FFT*), which may result in false information when applied to process non-stationary or nonlinear mechanical fault signals (e.g., *AE* signal). In this backdrop, empirical mode decomposition (i.e., *EMD*) for analyzing nonlinear and nonstationary signals was firstly proposed by Huang [52] and widely applied in various fields (e.g., damage detection [53], pattern recognition [54], system identification [55]). When an *AE* signal is processed with *EMD*, a series of completed and orthogonal "intrinsic mode functions" (*IMFs*) (i.e., components with instantaneous frequencies) are decomposed, which represent the natural oscillatory modes in the original signal and are determined by the characteristics of the signal itself. *IMFs* make it applicable to process nonlinear and non-stationary signals without the need for spurious harmonics. Based on numerical analysis on a white noise [56], the frequency spectra of *IMFs* were found all identical and covering the same area, which proved the accuracy of *EMD*. Therefore, *EMD* is a time-based analysis method that extracts features in the vibratory response of a structure using a set of basic functions [57]. In conjunction with usage of Hilbert transform, Hilbert-Huang transform (*HHT*) spectrum of the signal provide accurate time-frequency signal characteristics and make it possible to monitor the tightening condition of bolted joint using *AE* signals in real practice.

AE signals are nonstationary and nonlinear with unpredictable arrival times and waveforms. One common challenge existing in the processing of *AE* signals is to extract parameters with physical meanings and then to relate them with the state of the monitored structure, using time-based or frequency-based analysis [54]. Some case studies have reported the use of *EMD*-based characteristics of *AE* signals for damage detection, for example extracting natural features of fatigue cracks on rotating shafts [54]. As a representative example, Li and He [58] presented a methodology for fault detection of a rotational machine using *EMD*-processed *AE* signals. Compressed *AE* features were extracted and applied for fault detection, in which a threshold was used to recognize the damaged state from the healthy state of the machine. From the comparison of performance between traditional and *EMD*-based frequency analysis on the gear fault detection, the latter one was found to be more sensitive to gear faults compared to the former one.

To extend the application of *EMD*-processed *AE* signals from gear fault detection to bolt loosening identification, in this study, the effect of applied torque on interfacial contact behaviors and fatigue performance of a bolted composite joint under flexural vibration are studied using *EMD*-based characteristics of *AE* signals. The details will be presented in Chapter 4.

2.2.2. Active Linear Philosophy

Passive acoustic methods are developed to "listen" to the monitored structures and capture damage-related signals, while active acoustic methods are designed to interact with structures with prudentially selected excitations and provide online evaluation without interrupting the normal operation of the inspected structure. Vibration-based and *GUW*-based active linear acoustic methods using modal parameters and linear features of *GUWs*, respectively, are comparably introduced regarding detection of bolt loosening in this section.

2.2.2.1 Using Vibration Modal Parameters

As mentioned in Chapter 1, vibration-based linear active methods are adopted as a global method to identify health state of the entire monitored structure, using modal parameters such as natural frequency, frequency response function, mode shape and damping ratio [59]. The magnitude of changes in modal parameters is a function of the severity and location of damage in a monitored structure. Based on this, the detection philosophy of vibration-based *SHM* is to measure the dynamic characteristic of a structure during its lifetime and then to relate them to the state of the structure [60]. Prior to the implement of detection, a baseline experiment should ideally be conducted before the occurrence of any damage when using such methods. The difference between results of all subsequent experiments and those of baseline experiment is used as a damage index to indicate the onset of structural damage, such as a crack or a loose joint. Moreover, the severity and location of structural damage can be further identified from the mismatch.

A large number of examples have been reported regarding bolt loosening evaluation using the vibration-based methods. Representatively, Eun et al. [61] used an impact test (conducted by a hammer) to track loose bolts in a steel bolted structure. Frequency response functions in the vicinity of the first-order natural frequency were used to extract the proper orthogonal decomposition and orthogonal mode, which were then employed to evaluate the tightening condition of the joint. Similarly, Razi et al. [62] developed a vibration-based *SHM* strategy for detecting bolt loosening in a bolted flange joint. Empirical mode decomposition (*EMD*) was applied to process the vibration signals and construct an energy-based damage indicator to identify the state of the bolted joint. Subsequently, the damage indicator, obtained from various scenarios, verified the accuracy of the proposed methodology for evaluating bolt loosening, through both numerical analysis and experimental investigation. He et al. [63] conducted the vibration-based *SHM* technique to identify the locations and degree of bolt loosening in a bolted connection by detecting changes in natural frequencies. A trust-region search strategy was developed to improve the detection accuracy so that the reliability of such technique can be enhanced regardless of presentation of measurement noise. Caccese et al. [64] employed three different vibration-based techniques, namely low-frequency modal analysis, high-frequency transfer functions and transmittance functions, to detect bolt loosening in a hybrid (metal/composite) joint. From the comparison, transmittance function approach was found to exhibit the highest sensitivity to bolt loosening.

The vibration-based linear method using modal parameters for bolt loosening evaluation is presented in detail in Chapter 4. In addition, the sensitivity of linear response of harmonic forces to bolt loosening is compared with that of nonlinear responses including high-order harmonics and modulated sidebands in Chapter 5.

2.2.2.2 Using Linear Features of *GUWs*

Distinct from vibration-based linear acoustic methods, which attempt to implement a global detection, *GUW*-based linear acoustic methods are usually intended to achieve a local detection grounding on exploring changes in linear features between the benchmark signal (captured from healthy condition) and the inspected signal (captured from current condition).

For instance, a widely adopted linear feature of *GUW*s is time-of-flight (*TOF*), which is referred to as time takes for *GUW*s to travel a certain distance through a solid media. Rhee et al. [65] adopted *TOF*, which can indicate the geometric attenuations caused by structural damage such as a loose bolt, to detect bolt loosening using *PZT* sensors.

Efficiency of such linear features on the detection of bolt loosening in a certain range was validated through both experimental findings and numerical analysis. However, Wang et al. [66] concluded that stress-induced changes in the velocity of *GUW*s were quite slight, which led to an unobservable change in *TOF* and required a relative high sampling rate when collecting wave signals to achieve an effectual detection. In addition, both environmental noise and variation of material thickness had the potential to affect the accuracy of the measured *TOF* and made such detection philosophy challenging. To circumvent the mentioned deficiencies, Jhang et al. [67] measured *TOF* of *GUW*s precisely by using the phase detection method. Case studies were conducted to verify the efficiency of the proposed method regarding bolt loosening evaluation for high-tension bolted joints. A linear relationship between *TOF* and axial stress on the bolt (indicating bolt loosening) was concluded and ultrasonic velocity was found to decrease with an increase in the applied torque. Therefore, the phase detection-based *TOF* method exhibited considerable efficiency in evaluating bolt loosening.

Wave energy is another prevailing linear feature of *GUW*s adopted to identify damage in structures [1-3, 68, 69], for example a crack or a loose bolted joint. Advanced signal processing techniques, such as time reversal and frequency impedance methods are usually adopted to extract the wave energy of *GUWs*. In the time reversal method, the captured original signals are firstly reversed in the time domain and subsequently re-emitted as an excitation signal to obtain the time reversal focused signals. In conjunction with the use of the time reversal method [70], wave energy-based method has been widely studied for active detection of bolted structures. Wang et al. [71]

investigated the relationship between peak amplitude of wave signals, processed with the time reversal-based method, and tightening state of a joint. It was reported that in a certain range the peak amplitude increased with an augment in the applied torque until reaching a saturation. Using an analogous detection philosophy, Ruan et al. [72] obtained a cross-correlation between the loose state and the baseline healthy state of a joint using the peak amplitude of time reversal signals. The efficiency of the proposed method was verified by detecting bolt loosening in both a joint with a single bolt and a large bolted structure with a series of bolts. The correlation process was implemented online without any additional post offline analyses. Yet another wave energy-based *SHM* method, i.e., frequency impedance technique, has also attracted vast attention thanks to its potential for applications in engineering practice [73-75]. In such technique, electrical impedance of the actuator and sensor, which indicates the mechanical impedance of the monitored structure, is used to identify changes in structural properties caused by damage (e.g., a crack or a loose bolted joint) [3, 68, 73, 74, 76]. Ritdumrongkul et al. [68] presented the application of impedance-based technique combined with numerical analysis for quantitative detection of bolt loosening. The bolted joint bonded with lead zirconate titanates (*PZT*s) was modeled using spectral element method, which made it possible to quantitatively correlate the degree of bolt loosening to the change in the structural impedance. The results demonstrated the potential of such method in quantitatively identifying bolt loosening in real-world structures.

However, a high dependence of wave energy on joint configurations regarding bolt loosening evaluation is reported in [77], which introduces additional difficulty in identifying the leftover torque of a loose bolt using the wave energy-based method if the joint configurations are unknown beforehand. Yang and Chang [1, 2] studied wave energy of *GUW*s when interacting with a cross-lap bolted joint in a composite thermal protection. In a certain range of applied torque, the transmitted energy of *GUW*s upon passing through the bolt was reported to decrease with an augment in the residual torque of a loose joint. Estebana and Rogers [3] adopted a similar principle to investigate wave energy of probing waves at a higher frequency upon traversing a loose bolt in a single-lap aluminum bolted joint. An increase in wave energy was observed with an increase in the residual torque was observed, which is contradicting the conclusion from [1, 2]. One possible reason behind is that distinct types/configurations of joints were concerned in these two studies, i.e., a cross-lap joint in [1, 2] and a single-lap joint in [3], as a result an opposite trend of changes of wave energy was reported. Therefore, the mechanisms regarding changes of wave energy of *GUW*s when interacting with loose joints with different joint configurations should be further studied to facilitate its application in real practice.

To conclude, variation of velocity of *GUW*s caused by a loose bolt is at a small extent so that a precise measurement of such velocity (i.e., delay in *TOF*) is at the risk in the *TOF*-based method. In the impedance-based *SHM* method, the selection of excitation frequency plays a critical role in determining the sensitivity of detection, due to that an improper frequency range may provide false damage alarms [73]. In addition, for a wave attenuation-based method, the frequency of an incident wave has to be sufficiently high, so as to reach a small wavelength and guarantee the detection sensitivity and accuracy and this, however, may introduce additional complexity in signal processing, due to the dispersive and multimodal properties of *GUW*s at higher frequencies. Moreover, *GUW*s propagating in composite structures exhibit a much complex dispersion behavior and a serious attenuation effect. This leads to a further increased difficulty in signal acquisition involving additional tedious tasks in frequency selection and signal processing, when such a method is applied to detect bolt loosening in a bolted composite joint. On top of this, bolt loosening at an early stage, like the small-scale damage, is not anticipated to induce evident changes in above linear features to be extracted from *GUW*s.

The detection of bolt loosening in both metallic and composite bolted joints using the wave-energy-dissipation (*WED*)-based linear method is described in Chapter 4. The mentioned limitations of such a method on the detection of early bolt loosening in multi-type metallic bolted joints (i.e., single-lap, cross-lap and hybrid-lap) are to be presented in detail.

2.3. Nonlinear Methods: Using Nonlinear Signal Features

As mentioned in Section 2.2, linear features, under most circumstances, fail to identify small-scale damage. Motivated by this, there has been increased preference in using nonlinear properties of acousto-ultrasonic waves for detecting the small-scale damage, such as generation of *HOH* and modulated sidebands [78-92]. These nonlinear features are introduced by the interaction, termed as contact acoustic nonlinearity (*CAN*), between acoustic waves and contact interfaces of a crack or a loose joint.

When acoustic waves pass through the contact interface, the ‘‘breathing’’ motion pattern between the two surfaces in contact closes the interface during wave compression, while opens the interface in wave tension. As a result, in an ideal case only waves in compression can pass through the interface, as shown in **Figure 2.5**. The asymmetry in the contact restoring forces causes the stiffness parametric modulation, which imposes an additional localized nonlinearity (i.e., *CAN* [81, 83, 93]) to acoustic waves propagating in the medium. Consequently, the magnitudes of *HOH* and modulated sidebands, generated from *CAN*, can be quantitatively correlated to the severity of structural damage.

It is commonly accepted that the sensitivity of nonlinear features of acoustic waves to structural damage (e.g., a crack and a loose bolt) is far greater than that of linear features (e.g., *WED* and *TOF*) [94, 95]. Motivated by this, increasing efforts have been directed to exploit the application of such nonlinear features to identify small-scale damage (e.g., a tiny crack or a loose bolt at its early stage) [93, 96-111]. The current nonlinear acoustic features can be classified into four main categories: *HOH* generation, subharmonics generation, nonlinear resonance, modulated sidebands generation [109]. By such detection principles, it is feasible to predict the behavior of a nonlinear contact configuration as a loose bolt at an early stage, which is undetectable by conventional linear techniques. *HOH* generation and modulated sidebands generation are to be comparatively investigated for bolt loosening evaluation in this *Ph.D.* thesis.

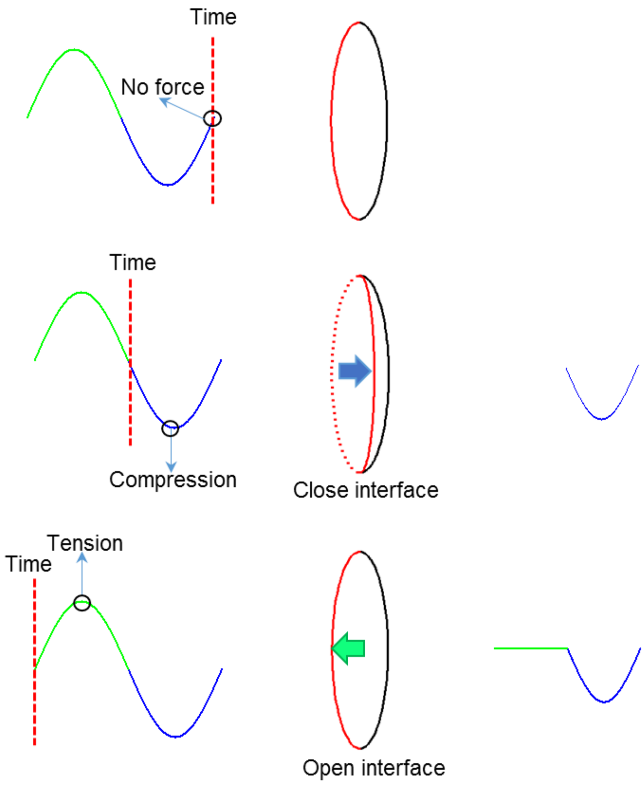

Figure 2.5 *CAN* generated by the interaction between acoustic waves and a contact interface

2.3.1. High-order Harmonic Generation

When acoustic waves, generated from a source with a centered frequency, interact with a contact interface in the process of propagation, a series of harmonic waves (e.g., high-order and sub-harmonics) are generated due to "breathing" effect of the interface (i.e., *CAN*). Specifically, high-order harmonics (*HOH*), including second-order harmonics (*SOH*) and third-order harmonics (*TOH*), are referred to as frequency components at integer multiples of the excitation frequency, while sub-harmonics are nonlinear components with the half frequency of the excitation or alike.

Amongst the mentioned nonlinear features, *SOH* and *TOH* were widely adopted for applications of *SHM*. In most reported studies, nonlinear acoustic methods, using these two nonlinear features of *GUW*s and vibration signals, have been applied to detect fatigue crack or loose bolts in both metallic and composite structures [79-81, 83, 85-92].

(1) *GUW*-based

Matlack and Kim et al. [112] provided a comprehensive summary of theoretical models that correlate the microstructural contributions to the nonlinear parameter defined from *SOH* of *GUWs* and introduced details of different measurements and analysis techniques for *SOH*. As representative results, Kim and Jhang [113] proposed a cumulative nonlinear parameter to develop a one-to-one correspondence between the nonlinear parameter and the thermal degradation of aluminum alloy over the aging time. Seo et al. [114] demonstrated that the variation in the acoustic nonlinearity can indicate the aging level of aluminum alloy upon heat-treated for different durations. Ren et al. [115] developed a new relationship between the second-order and third-order nonlinear parameters for the evaluation of material degradation. Deng and Pei [98] theoretically analyzed the feasibility of nonlinear features (*SOH*) of *GUWs* for evaluating accumulated fatigue damage in an aluminum plate. Nonlinear features of *GUWs* upon interacting with the plate under varied numbers of fatigue cycles were comparably recorded in the experiment. Both theoretical analysis and experimental investigation showed the high sensitivity of *SOH* of *GUWs* to the occurrence and accumulation of fatigue damage in an aluminum plate. Amura et al. [99] predicted crack growth and residual life of metals under fatigue comparably using linear and nonlinear acoustic methods. The third-order harmonic (i.e., *TOH*) was presented without a need to measure two crack conditions to evaluate the absolute residual fatigue life of the metals. A nonlinear index, constructed from the magnitude of *TOH*, was found to be highly sensitive to crack propagation and the experimental results reached a good agreement with the theoretical prediction. Polimeno et al. [103] employed the presence and magnitude of *HOH* to indicate the occurrence and severity of barely visible damage in carbon/epoxy composites after subject to a low-velocity impact. Such a method was proven accurate in identifying the presence and degree of damage and showed the potential for both NDT and *SHM* applications. Mattei [79] presented a strong interaction between nonlinear features of acoustic waves and micro damage in a *CFRP* specimen under a four-point bending fatigue, prior to the occurrence of observable debonding or delamination. Harmonic imaging method, constructed from *SOH* magnitude normalized by fundamental magnitude, exhibited a higher sensitivity than C-scan when applied to detect micro-damage in the *CFRP* specimen at the early stage of fatigue.

The last two decades have witnessed an increasing research interest in the applications of nonlinear features of *GUWs* in the detection of micro-cracks. However, current understanding and modeling of physical mechanisms of *CAN*, presented by bi-linear stiffness, hysteresis, and contact non-classical dissipation [116], is fairly limited. Rare related studies were proven to solve this problem with widely accepted results. Hong et al. [83] developed a modeling technique for investigating nonlinear interaction of ultrasonic waves with a fatigue crack combining an experimental validation. The results showed a satisfactory agreement between the numerical analysis and experimental investigation, which proved that the proposed approach was capable of simulating *CAN* introduced by a fatigue crack. This study facilitated a further development of *SHM* with an ability to identify micro damage and continuously monitor its growth.

With proven efficiency of detecting fatigue crack at the early stage, the *HOH*-based nonlinear methods were extended to the evaluation of early bolt loosening. Amerini et al. [102] developed a theoretical model to predict the pressure-dependent nonlinear stiffness of the contact interface of a joint. The theoretically proposed prediction of *SOH* generation at the contact interface agreed well with the experimental investigation, which showed the potential of *SOH* to be used as an integrity indicator to assess the state of a bolted joint. Shui et al. [88] adopted an acoustic nonlinearity parameter, developed from the magnitude of *SOH*, to evaluate the degradation of an epoxy/resin adhesive joint. The measured acoustic nonlinearity parameter was found to increase with an augment in fatigue cycles of the joint, which was further interpreted by an analytical model. The *SOH*-based nonlinear method was concluded to be efficient in evaluating adhesive strength of adhesive joints. Similarly, Yan et al. [82] presented detection of kissing bonds in an adhesive joint using nonlinear *HOH* features of ultrasonic waves. It was found that the adhesive joint showed a high degree of nonlinearity even when subject to a small compressive load. Shen et al. [107] presented *HOH*-based nonlinear methods for *SHM* of bolted lap joints both numerically and experimentally. The *CAN* generating at the contact interface of a loose joint when interacting with *GUWs*, served as an indicator to evaluate the tightening status of the bolt. Contact finite element models were proposed to investigate the nonlinear contact behavior of the lap joint with experimental verifications. A monotonic relation between the applied torque and the magnitude of *HOH* was proposed by the numerical simulation. However, the experimental investigation failed to reproduce such relation at the late stage of bolt loosening, which called for more studies to discover the possible reason.

(2) Vibration-based

The occurrence of damage (a crack or a loose bolt) was reported not only to introduce detectable *CAN* in *GUWs*, but also to induce generation of *HOH* (due to *CAN*) in the low-frequency vibration [111]. With the development of *HOH*-based methods using *GUWs*, *HOH* of low-frequency vibration have also been extensively studied for possible applications in *SHM* for structural damage.

Pugno et al. [117] reported that occurrence of multiple breathing cracks induces nonlinear dynamic responses (i.e., *HOH*) of a beam, of which the response magnitude was seriously dependent on the severity, number, and location of the cracks. Therefore, the occurrence and evolution of *HOH* can be used as an indicator for damage detection. Bovsunovsky and Surace [118] developed harmonics-based nonlinear methods to detect damage using magnitudes of both sub-harmonics and *HOH*. The sensitivity of such nonlinear feature-based methods was reported to be much higher than those of linear feature-based methods based on measuring changes in natural frequencies and mode shapes. Therefore, the occurrence and magnitude of sub-harmonics and *HOH* can indicate the presence and severity of a crack even at a very early stage. Didenkulov et al. proposed two *HOH*-based nonlinear methods to locate a crack in a beam, based on interaction between vibration and the crack [111], using a single pulse of relative high-frequency vibration and long series of pulse of low-frequency vibration, respectively. Both methods were proven effective for location and identification of the crack. Amerini et al. [102] extended the application of *SOH*-based nonlinear method from crack detection to identifying bolt loosening of a joint, using a nonlinear damage-related index developed from magnitudes of fundamental mode and *SOH*. The comparison between the theoretical prediction and experimental investigation showed the defined nonlinear index was a promising tool to evaluate the loosening state of a bolt including its early stage in the application of both passive and active *SHM*.

To conclude, the presence of “breathing” behavior at the contact interface of a crack or a loose joint introduces detectable *CAN* into *GUWs* or vibration signals. As a result, the generation and magnitude of *HOH*, arising from *CAN*, is capable of indicating the occurrence and severity of damage in the monitored structure. The theoretical interpretation of mechanisms of *HOH* generation in a loose joint is to be described in detail in Chapter 3, supported by experimental validation in Chapter 5 through detecting bolt loosening in multi-type of bolt joints.

2.3.2. Modulated Sideband Generation

Wave modulation-based technique is another prevailing nonlinear acoustic method for damage detection. In this approach, two distinct excitations, namely a low-frequency pumping vibration and another high-frequency probing wave, are introduced in a structure simultaneously. Considering a bolted joint and provided all the bolts are fully fastened in the joint, the acquired signal spectrum of the mixed excitation exhibits two major power concentrations at the two frequencies at which the pumping vibration and probing wave are excited, respectively; or otherwise in the scenario with loose bolts, additional frequency components around the probing signal components are expected to be present in the spectrum – termed as the left sideband (if lower than the frequency of the probing signal) or right sideband (if higher than the frequency of the probing signal) [119-126], as shown in **Figure 2.6**. Consequently, the magnitudes of sidebands can be used to indicate the severity of the monitored structure [94, 95, 127-137].

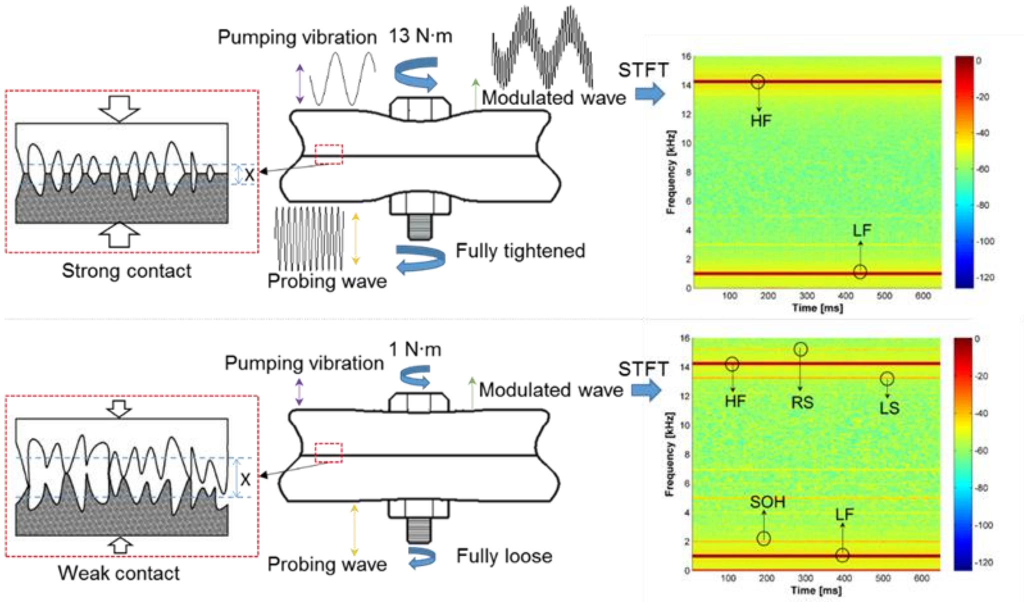

Figure 2.6 Schematic interpretation of *VAM*-based method

To maximize the vibro-acoustic interaction between the mixed excitation and structural damage (i.e., a crack or a loose joint), frequencies of the pumping vibration and probing wave should be selected prudentially to meet the binding conditions (i.e., synchronism, simultaneous arrival, non-zero power flux and nonlinear resonance conditions) for generation of modulated sidebands [100]. In addition, Solodov et al.

[132] reported that local defect resonance (*LDR*) of a structure can be used to magnify the nonlinear interaction between the damage and acoustic waves. Compared with other nonlinear feature-based methods, for example those by exploring the changes in second-order harmonic generation, the acoustic wave-modulation detection philosophy can, by properly selecting the frequency of a mixed excitation, minimize the influence of the nonlinearity contributed by other sources rather than the bolt loosening, such as measurement apparatus and material itself. Thus, the information on bolt loosening can be duly manifested by the acquired *CAN*, reducing the dependence on advanced signal processing.

Impact modulation (*IM*) and vibro-acoustic modulation (*VAM*) are the two major implementation modalities of acoustic wave-modulation, both of which have been demonstrated effective in characterizing various types of structural damage and fatigue cracks in particular [92, 127, 128, 136]. An *IM* method relies on the use of an impact excitation to generate signals under the natural vibration modes of an inspected structure. Representatively, Meyer and Adams [136] extended the application of *IM* to the identification of bolt loosening in an aluminum joint, and experimental data showed reasonable consistency with theoretical results. However, in an *IM* method, the signals captured under natural modes excited by an impact force are usually vulnerable to the contamination of measurement noise and uncertainties, leading to inaccurate identification results. On the other hand, a *VAM* method adopts stable vibration signals generated by a harmonic excitation with a much lower level of measurement noise involved, and therefore the nonlinear responses (*i.e.*, sidebands) can be manifested explicitly in signal spectra.

The wave modulation-based method has been applied to detect fatigue crack and impact damage in both metallic and composite material. Sohn et al. [133] adopted nonlinear wave modulation method to identify fatigue cracks in a metallic plate with a complex geometry configuration. The excitation frequencies of pumping and probing waves were selected by sweeping these two wave signals via *PZT* wafers over certain frequency ranges. The proposed wave modulation method successfully evaluated the occurrence and growth of fatigue cracks in the specimen. Aymerich et al. [126] adopted the *VAM* method to detect damage in composite laminates upon subject to a low-velocity impact. The pumping vibration and probing wave, excited at resonant frequencies of the plate, were introduced by a shaker and a low-profile *PZT* transducer, respectively. Magnitudes of sidebands were found able to quantitatively indicate the severity of impact damage. Similarly, Klepka et al. [127, 128, 131] presented damage detection in a composite sandwich panel using the *VAM* method but adopted non-contact laser vibrometry for ultrasonic sensing. The experimental results showed the sensitivity of modulated sidebands to the undersized impact damage in the composite chiral sandwich panel.

The application of *VAM* method has been extended from crack identification to bolt loosening detection in bolted metallic structures with the premise that both contain contact interfaces exhibiting similar “breathing” behavior when the interfaces interact with acoustic waves. Zhou et al. [120] investigated the detectability of *VAM* method to early bolt loosening with both theoretical analysis and experimental validation. The damage (bolt loosening)- related indicator was defined from the modulated components (i.e., intrinsic mode functions, *IMFs*) processed by *EMD*. The results showed that the proposed nonlinear index accurately indicated bolt loosening even including its embryo stage. Amerini and Meo [138] adopted both linear and nonlinear feature-based methods to identify the state of a bolted structure using first-order acoustic moment (i.e., a linear index), *SOH* and modulated sidebands (i.e., nonlinear indices). A good agreement between the analytical prediction and experimental results was presented. In addition, the fully tightened state of a bolted joint can be clearly identified by the occurrence of plateau region in the nonlinear indices. However, quantitative comparison of sensitivity between linear and nonlinear feature-based methods to bolt loosening was not involved in this study.

To summarize, *VAM*-based nonlinear method has been successfully developed for the detection of fatigue cracks and impact damage in both metallic and composite structures. Some scholars even extended its application to detect bolt loosening in metallic structures. It is important to notice that most existing studies in bolt loosening identification based on nonlinear dynamic responses (i.e., generation of sidebands) were conducted relying on empirical knowledge, whereas theoretical investigations regarding of mechanisms of nonlinear feature generation such as *HOH* and modulated sidebands are far from sufficient. In this backdrop, the development of numerical studies is crucial in facilitating actual bolt loosening identification in different joints, which, however, is hampered to a large extent.

The theoretical modeling of *CAN* in a loose joint will be presented in Chapter 3, where the magnitudes of modulated sidebands are theoretically correlated with the degree of residual torque of a loose bolt. To verify the theoretical prediction, experimental investigation of detecting bolt loosening in multiple types of bolted joints using the *VAM*-based method will be presented in Chapter 5. Especially, a numerical study, where finite element (*FE*) models of both *Al-Al* and *C-C* single-lap bolted joints are proposed and utilized to calculate structural dynamic responses including both linear and nonlinear signatures, is described in Chapter 6 to facilitate a better understanding of mechanisms of generation of modulated sidebands and their quantitative relation with the degree of bolt loosening.

2.4. Summary

In this chapter, the prevailing methods on the detection of bolt loosening are briefly reviewed. Using linear features of *GUWs*, passive *AE* method is reported to exhibit its efficiency in qualitative detection of sudden changes (e.g., the occurrence and propagation of a crack) in a structure and fretting wear between contact surfaces. However, quantitative identification of bolt loosening using *AE* technique is rarely presented, due to the limitation existing in the current signal processing. *EMD* method, which is capable of processing non-stationary or nonlinear mechanical fault signals (e.g., *AE* signal), is found as a promising tool to characterize *AE* signals generated from contact surfaces in a bolted joint under vibration. In the active acoustic method using vibration modal parameters, resonant frequency and damping ratio in the application of damage detection with respect to cracks and loose bolts are presented. However, such methods can be only used to detect gross damage, for instance a visible crack or bolt loosening at a serious stage. In the active acoustic method using linear features of *GUWs*, *TOF* and wave energy are discussed as two representative parameters employed for the detection of a crack and bolt loosening. Due to the wavelength-dependent sensitivity of these two parameters, excitation frequency of probing *GUWs* is usually increased to obtain a reduced wavelength. Consequently, this introduces the presence of multiple modes of *GUWs* and resultant complicate signal appearance, caused by multi-modal and complex dispersion characteristics of *GUWs* at high frequencies. Therefore, when applied to identify micro damage (including early bolt loosening) in a structure, *GUW*-based linear active acoustic method may compromise its efficacy. Realizing the limitation of linear acoustic techniques in the detection of early bolt loosening, nonlinear acoustic features introduced by *CAN*, including generation of *HOH* and modulated sidebands are introduced in parallel. In the *HOH*-based nonlinear methods, *SOH* of *GUWs* and vibration signals have been successfully employed to quantitatively evaluate fatigue cracks or impact damage. Whereas, *TOH* of acoustic waves is seldom reported being adopted to indicate the structure damage. In addition, when employing *HOH* of *GUWs* to conduct the detection, nonlinearity from the experimental devices (e.g., signal generator and *PZT*) should be carefully treated to obtain the direct damage-related nonlinearity. Noticing successful applications of *VAM*-based method in detecting undersize cracks, in this study emphases are placed on the prevailing use of nonlinear modulated sidebands. Efforts are directed to extend its application from crack identification to quantitative evaluation of early bolt loosening in both *Al-Al* and *C-C* bolted joints with different joint configurations. Both theoretical analysis and experimental investigations are conducted to facilitate the understanding of mechanisms of generation of modulated sidebands along with its dependence on residual torque of a loose bolt.

CHAPTER 3

Theoretical Fundamentals: *From Linear to Nonlinear*

3.1. Introduction

As mentioned in previous two chapters, linear and nonlinear features of acousto-ultrasonics have emerged as promising tools in the applications of *SHM* for on-line and continuous detection of structural damage, which is difficult to fulfil by conventional off-line *NDT* techniques. In Chapter 2, a variety of literatures regarding usage of linear and nonlinear features of *GUWs* and vibration for damage identification are reviewed. Current research strengths in these fields are found restricted to the implementation of experimental investigation. There exist very limited studies concerning the development of theoretical analysis or numerical simulation to reveal the mechanism of generation of nonlinear features of acousto-ultrasonics when interacting with a loose joint.

Generally speaking, a paramount challenge in the theoretical modeling of the interaction between acousto-ultrasonics and a loose joint (i.e., contact interfaces in the mating parts) is to develop a quantitative relation between the contact condition at the interface from the microscopic-perspective and signal features of acousto-ultrasonics in the frequency domain. In this chapter:

(1) for the passive acoustic method, an acoustic emission (*AE*) model involving in elastic asperity contacts is introduced to derive factors affecting the energy of *AE* signals. In particular, the effect of pressure (induced by applied torque) on the contact condition of the interface (i.e., the mating parts of a joint) undergone a slight relative motion is discussed;

(2) for the modal parameter-based linear acoustic method, resonant frequency and damping ratio are theoretically correlated to the applied torque of a joint. For the wave-energy-dissipation (*WED*)-based active acoustic method using linear features of *GUWs*, an analytical model residing on Hertzian contact theory is established, whereby *WED* is quantitatively linked to the residual torque of a loose bolt. In addition, the reliance of *WED* on the joint configurations (i.e., lap types) is presented to facilitate a better comprehending of limitations of such linear feature-based method in evaluating tightening condition of bolted structures with multi-type joint configurations;

(3) for the nonlinear acoustic methods using *HOH* and modulated sidebands, the loose bolt is considered as damage taking nonlinear behaviors. *CAN*, engendered

at the interface of a loose joint, is characterized by establishing a modified theoretical model with pressure-dependent contact stiffness including both linear and nonlinear parts. Subsequently, the nonlinear contact stiffness is linked to nonlinear spectral features (i.e., *HOH* and modulated sidebands) of the response of a loose joint using a single-degree-of-freedom system. Based on this, a qualitative relation between applied torque of the joint and nonlinear features of acousto-ultrasonics is developed theoretically.

3.2. Linear Feature-based Methods

The surfaces of the assemblies (i.e., joining materials) of a joint are rough and cratered with randomly distributed asperities from a microscopic perspective. When the bolt is fastened to introduce clamping force on these two assemblies, the interface between them features a partial contact, as illustrated schematically in **Figure 3.1**.

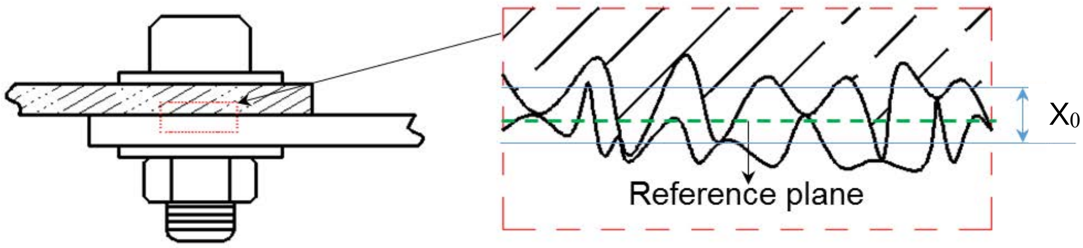

Figure 3.1 Rough surfaces in contact

The loads carried by asperities on the surfaces, which are introduced by applying a torque on the bolt, have a direct influence on the contact condition of the interface. When a bolted joint is subject to vibration, a relative motion between the two contact surfaces consequently produces *AE* signals arising from contacts of asperities at the interface. Therefore, characteristics of *AE* signals can be related to the contact condition of the interface, and further indicate the applied torque once the related mechanism of *AE* generation is ascertained. Along the same line of thinking, in the vibration-based linear acoustic method, contacts of asperities at the interface which determine the local stiffness and energy dissipation, are quantitatively associated with modal parameters of a joint, including the natural (resonant) frequency and damping ratio. On the other hand, in the active linear acoustic method, when *GUWs* interact with contact interfaces of a joint, *WED* of *GUWs* is also decided by contact condition (i.e., asperity contacts) of the interfaces and can be further correlated to the tightening condition of the joint. Based on these, detection philosophy for both passive and active linear acoustic methods using linear features of *GUWs* and vibration are presented in what follows.

3.2.1. Passive Philosophy

Provided two assemblies of a joint come into contact, due to surface roughness (i.e., manifested as randomly distributed asperities with different sizes), the real contact area at the interface only takes a small portion of the nominal contact area. The loads induced by applied torque on the bolt is mainly carried by asperities with larger heights on the contact surfaces of the composite assemblies. When a relative motion between the two contact surfaces occurs due to an external load such as vibration and shock, contacts of asperities release energy through varied contact behaviors including collision, friction, and wear. The energy release rate ($\dot{U}_{AE}$) of *AE* signals generated from asperity contacts at the interface can be given as [47, 139]

$$\dot{U}_{AE} \propto NWV\Upsilon^{-0.5}, \tag{3.1}$$

where W signifies the normal load applied on the asperities, V is the sliding velocity, and Υ and N denote Hertzian curvature and total number of asperities in contact, respectively. It can be seen that the surface properties (typified by Υ, N), applied torque (represented by W) and external dynamic load (reflected by V) jointly influence the energy generation of *AE* signals. From **Equation (3.1)**, it can also be predicted that characteristics of *AE* signals are associated with the contact traits of the interfaces with different surface properties in a bolted joint. When the applied torque on the bolt increases, a larger pressure is introduced to the contact surfaces and consequently more asperities come into contact, leading to an increase in N. Whereas interfacial friction increases due to the augment in the contact pressure, as a result, a decrease in the sliding velocity V of two contact surfaces occurs. These two resultant outcomes, due to the increase of applied torque, lead to a contradicting change in the energy of *AE* signals.

In practice, the mechanisms of generation of *AE* signals in a bolted joint subject to vibration are complex due to the existence of multi-source and varied affecting factors. In a bolted composite joint, there exists a series of contact interfaces (e.g., metal-composite contacts between metallic fasteners and composite beams and composite-composite contacts between composite beams, as shown in **Figure 3.2** (a)), of which surfaces are rough with randomly distributed asperities. For instance, the microstructure of the surface of the composite specimen was obtained by scanning electron microscopy (*SEM*) and displayed in **Figure 3.2** (b). To observe that asperities of different sizes distribute on the nominally flat surface. In practice, asperity contacts present at both the *M-C* and *C-C* interfaces in the joint introducing acoustic emission

(*AE*) signals with specific signal characteristics, when the joint is subject to the dynamic loading.

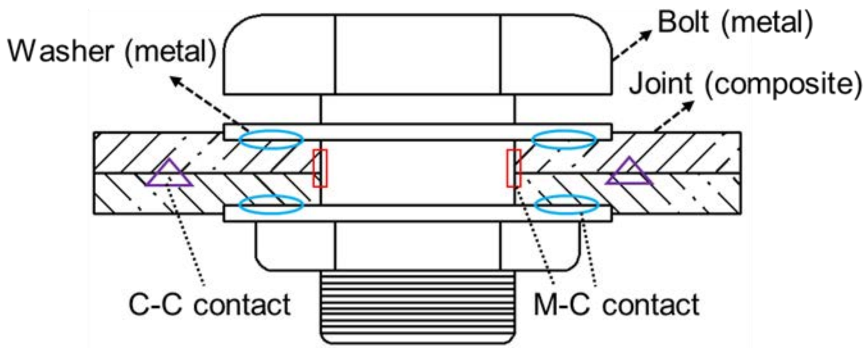

(a)

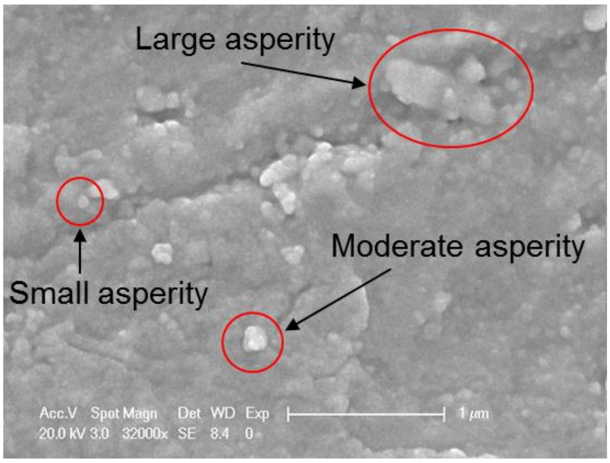

(b)

Figure 3.2 (a) *M-C* and *C-C* contacts in a bolted composite joint; (b) asperities on the composite surface obtained by *SEM*

Consequently, captured *AE* signals contain mixed features arising from asperity contacts at these two interfaces with distinct surface properties. From the above analysis, it can be argued that energy-based methods have the potential to recognize *AE* signals generated from contact interfaces with different applied torques. In addition, due to different surface properties of these two materials, e.g., metal and composite, *AE* signals produced by contacts of asperities with different sizes on the two surfaces exhibit different time durations (i.e., with different centered frequencies). Therefore, in conjunction with energy-based methods, frequency-based pattern recognition can be used to characterize *AE* signals from these two contact interfaces.

However, even at the single-type contact interface, different contact behaviors produce between asperities in different sizes, as shown in **Figure 3.3**. Take the *C-C* interface as an example, three representative types of asperity contacts are discussed to facilitate the understanding of generation mechanisms of *AE* signals in a bolted composite joint and the influence of residual torque on the signal characteristics.

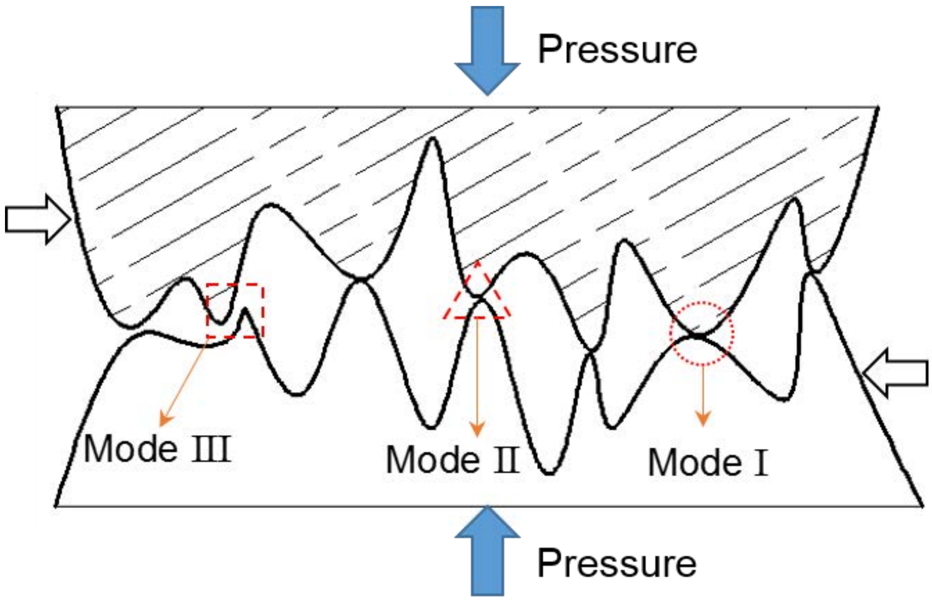

Figure 3.3 Different contact modes of asperities at the *C-C* interface of a composite joint

When the bolt of a joint is fastened, the largest asperities (Mode Ⅰ) on the surfaces firstly come into contact and undergo intensive deformation, the moderate asperities (Mode Ⅱ) are in a weak contact and slight gaps exists between the smallest asperities

(Mode III). Once a relative motion between the contact surfaces presents, sliding friction occurs between both the Mode II and Mode I asperities but with different contact durations, which are determined by the real contact area of the asperities. The Mode I asperities carry a larger contact force and consequently a higher degree of deformation presents, leading to a larger real contact area. As a result, *AE* signals with a longer duration (i.e., a lower centered frequency) are generated. Conversely, shorter-duration *AE* signals (i.e., with a higher centered frequency) generate from the contacts between the Mode II asperities. If sliding distance of the two surfaces exceeds the gap between the Mode III asperities, Mode III asperities on one contact surface attempt to slide past those on the opposite surface, which results in the collision contact behavior and generates *AE* signals with the shortest duration. Based on these, frequency-based analysis should be capable of characterizing *AE* signals generated from asperities with different sizes.

Meanwhile when the bolt is tightened with augmenting torques, higher pressure is induced at the interface and consequently sliding friction at different stages present between the contact asperities, as shown in **Figure 3.4**. With an increase in the applied torque, the elastic and plastic friction occurs sequentially. Once the asperities are overloaded, the wear produces consequently at the contact interface. To conclude, the contacts between the three types of asperities naturally generate AE signals with distinct characteristics in terms of time durations and centered frequencies. Upon the occurrence of bolt loosening in a bolted composite joint, a reduce in contact area between asperities, caused by the decrease in contact pressure, results in more frequency components with higher centered frequencies in the AE signals.

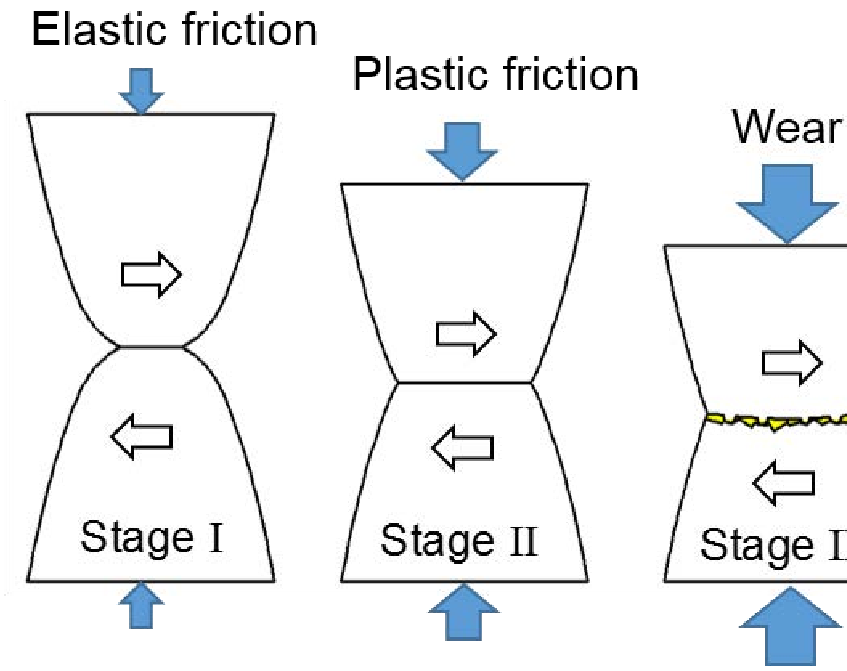

Figure 3.4 Different contact stages of asperities at the *C-C* interface of a composite joint under increasing applied torques

From above descriptions, it can be inferred that with energy-based and frequency-based analysis, characteristics of *AE* signals can be quantitatively linked to the applied torque on the bolt of a joint, which is to be presented in detail in Chapter 4.

3.2.2. Active Philosophy

The detection philosophy of bolt loosening using vibration modal parameters and wave energy dissipation (*WED*) of *GUWs* are presented in this section.

3.2.2.1 Modal Parameters-based

As mentioned in Section 3.2.1, asperity contacts occur at the interface of a joint when an external load introduces a relative motion between the two contact surfaces. Contact behaviors between asperities in the mating parts of a joint dissipate parts of energy induced by the external load and generate *AE* signals, which also lead to changes in the structural modal parameters, for instance resonant frequency and damping ratio.

To interrogate the effect of applied torque on the vibration modal parameters of a bolted composite joint, a single-degree-of-freedom system is developed based on viscoelastic modal and vibration theory (see **Figure 3.5**).

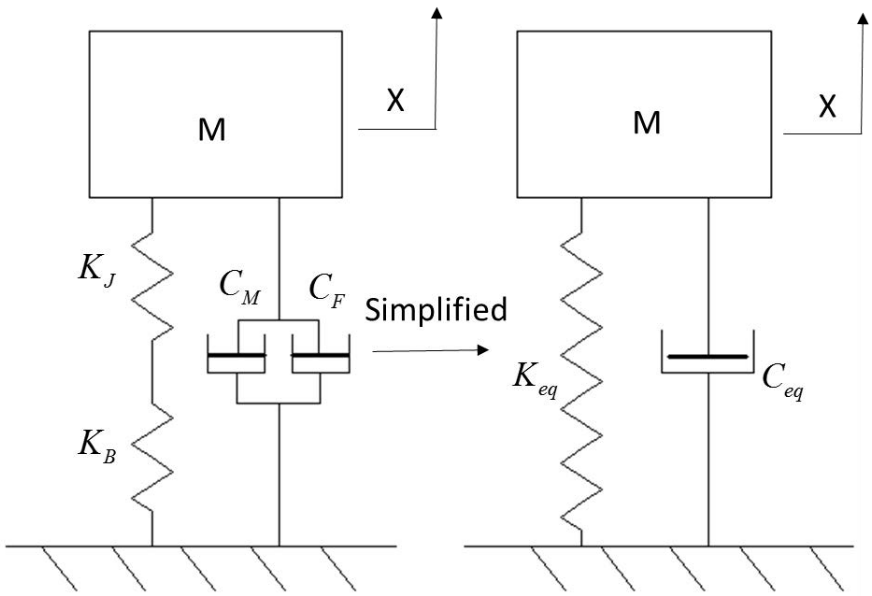

Figure 3.5 Simplified model of a bolted composite joint

where K_J and K_B are the stiffness of the joining composite material and contact interface, respectively. K_{eq} denotes the equivalent stiffness of the bolted joint. C_M and C_F represent material internal damping and interface friction damping, respectively. Similarly, C_{eq} signifies the equivalent damping of the joint. It is noteworthy that C_M and K_J remain constant regardless of changes in the applied torque on the bolt, while C_F and K_B are determined by contact condition of asperities at the interface and subject to functions of applied torque, which can be expressed as

$$C_F = f(\mathrm{T}) \text{ and } K_B = G(\mathrm{T}). \qquad \textbf{(3.2)}$$

In engineering practice, it is challenging to directly measure the contact stiffness or damping of a joint. The alternative solution is to obtain modal parameters (i.e., resonance frequency and damping ratio), which have quantitative relations with K_B and C_F, respectively. The correlation between the equivalent damping C_{eq} of a joint and the damping ratio η obtained from the modal testing on the joint can be written as

$$\eta = \frac{C_{eq}}{C_c}, \qquad \textbf{(3.3)}$$

where C_c is the critical damping of the joint (a constant) and

$$C_{eq} = C_M + C_F. \qquad \textbf{(3.4)}$$

The dependence of resonant frequency and response magnitude of a joint on the contact condition at the interface (determined by applied torque) is derived in what follows.

The equation of motion of the joint subject to a harmonic force ($F\sin(\omega t)$) can be written as:

$$M\ddot{x} + C_{eq}\dot{x} + K_{eq}x = F\sin(\omega t), \qquad \textbf{(3.5)}$$

where

$$K_{eq} = \frac{K_B K_J}{K_B + K_J}. \tag{3.6}$$

Solve **Equation (3.5)** to obtain the resonant frequency f as

$$f = \frac{1}{2\pi}\sqrt{1-\eta^2}\sqrt{\frac{K_{eq}}{M}}. \tag{3.7}$$

Then, the response magnitude A of the joint under the harmonic excitation can be deduced as

$$A = \frac{r^2}{\sqrt{(1-r^2)^2 + (2\eta r)^2}}\frac{F}{M}, \tag{3.8}$$

where

$$\eta = \frac{C_{\mathrm{eq}}}{2\sqrt{K_{eq}M}} \text{ and } r = \omega\sqrt{\frac{M}{K_{eq}}}. \tag{3.9}$$

From the above analysis, it can be concluded that contact stiffness and damping at the interface, subject to an applied torque on the bolt, influence the modal parameters (i.e., damping ratio and resonance frequency) of a joint. In addition, according to **Equations (3.2)** and **(3.8)**, it can also be predicted that the response magnitude of a joint subject to a harmonic excitation is determined by η and r, which are associated with the applied torque. The detection of bolt loosening using modal parameters and response amplitude are presented in Chapters 4 and 5, respectively. In particular, in Chapter 5, the sensitivity of linear response magnitude of pumping vibration and probing wave to the residual torque remained on the loose bolt will be comparatively presented with those of nonlinear harmonics of pumping vibration.

3.2.2.2 *WED*-based

In the active acoustic method using linear features of acoustic waves, i.e., wave-energy-dissipation (*WED*) of *GUWs*, two lead zirconate titanate (*PZT*) wafers are usually pasted on the two sides of the bolt, as shown in **Figure 3.6**. One is used as an actuator to generate *GUWs* interacting with the mating parts of the joint, and the other studies as a sensor to capture wave signals, of which the energy is adopted to construct a linear index to indicate the residual torque of the bolt. Due to difference in the joint configurations (i.e., lap types) between the single-lap and cross-lap bolted joints as shown in **Figure 3.6**, *GUWs* captured in these two joints propagate along different paths. In the single-lap joint, *GUWs* traverse the interface from one beam to another beam, therefore the energy of captured *GUWs* is termed as leak energy. While in the cross-lap bolted joint, *GUWs* pass through the interface propagating in only one beam, of which energy is named as transmitted energy in what follows. A simplified theoretical model, as shown in **Figure 3.6**, is employed to correlate these two energies to the degree of applied torque.

Provided the bolt is fastened, the relation between the preload P of the bolt and the torque T applied on the bolt can be described, in an elastic regime, as [140]

$$P = \frac{T}{\tau d}, \tag{3.10}$$

where d signifies the bolt diameter and τ a thread coefficient subject to the friction between the nut and bolt. As mentioned, the surfaces of two assemblies of the joint are rough, as shown in **Figure 3.6**. The preload relaxation of a bolt (a reduction occurs in the applied torque), can result in the decrease in the pressure at the contact interface and consequently the real contact area. To theoretically derive a qualitative relation between the residual torque and the real contact area, a simplified model for both single-lap and cross-lap bolted joints consisting of two joining components (Assembly I and II) is developed as exhibited in **Figure 3.6**. Within a small amount of real contact area at the interface, the simplified model assumes that the two interacting assemblies consist of uniformed spherical asperities on the contact surfaces, with radii of R_1 and R_2, respectively.

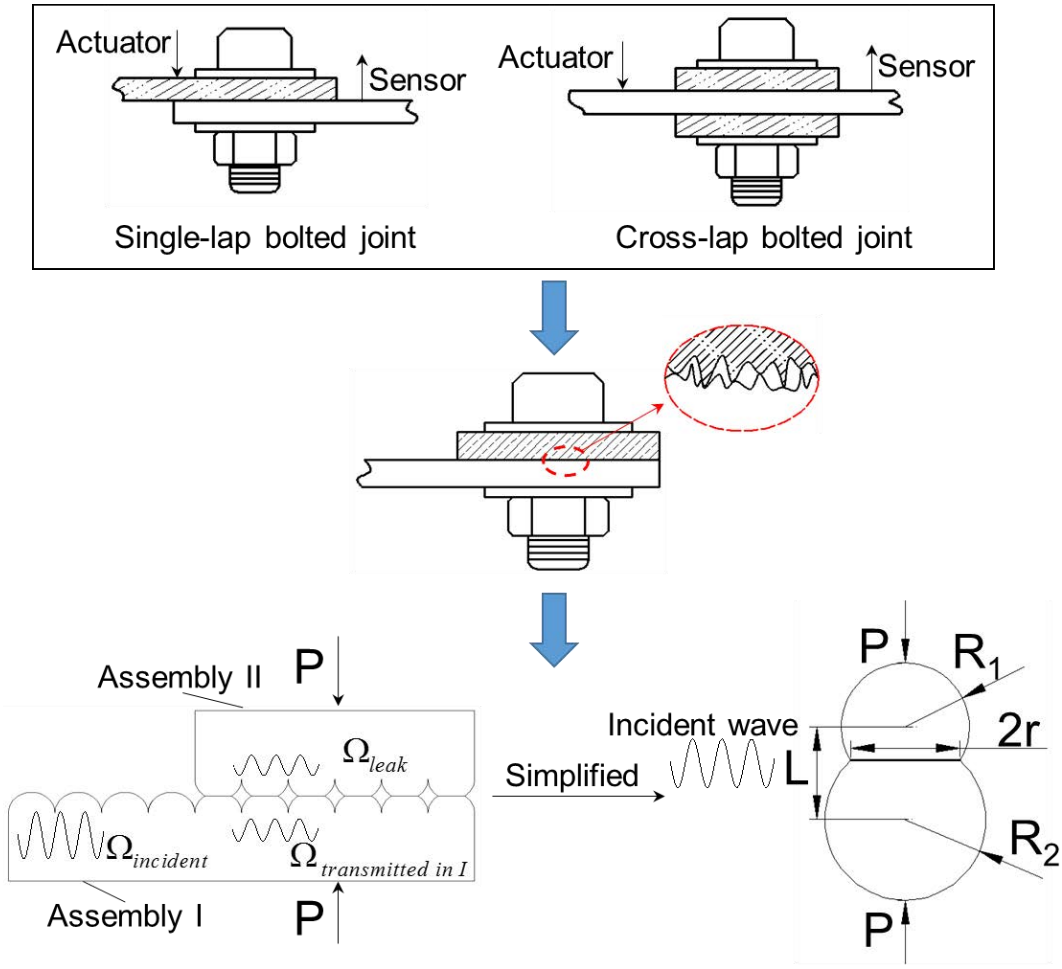

Figure 3.6 Simplified models of single-lap and cross-lap bolted joints

To simplify the solution, a model of the two spheres with the two radii in contact interacting with incident *GUWs* is recalled to derive the relation between applied torque of the bolt and leak/transmitted energy of *GUWs* upon traversing the bolt. According to Hertzian contact theory, the radius r of the real contact area when two spheres come in contact is expressed, as [141]

$$r = [\frac{3}{4}\pi(\gamma_1 + \gamma_2)\frac{R_1 R_2}{R_1 + R_2}]^{1/3} P^{1/3}, \quad \textbf{(3.11)}$$

where

$$\gamma_1 = \frac{1 - \nu_1^2}{\pi E_1} \text{ and } \gamma_2 = \frac{1 - \nu_2^2}{\pi E_2}, \quad \textbf{(3.12)}$$

where E signifies the Young's modulus and v is the Poisson's ratio, where components with subscripts *1* for Assembly I and those with subscripts *2* for Assembly II. The real contact area S can subsequently be obtained by

$$S = \pi r^2 = [\frac{3}{4}\pi^{5/2}(\gamma_1 + \gamma_2)\frac{R_1 R_2}{R_1 + R_2}]^{2/3} P^{2/3}. \quad \textbf{(3.13)}$$

At a given preload P, the total deformation (δ) of these two spheres (in the direction of P) in an elastic region, can be calculated by [141]

$$\delta = [\frac{9}{16}\pi^2(\gamma_1 + \gamma_2)^2 \frac{R_1 + R_2}{R_1 R_2}]^{1/3} P^{2/3}. \quad \textbf{(3.14)}$$

Therefore, the distance L between the centers of two spheres is yielded as

$$L = R_1 + R_2 - \delta. \quad \textbf{(3.15)}$$

Equation (3.15) indicates the dependence of the contact stiffness at the interface on L and P, which infers the extent to which the interface resists deformation when subject to a contact force.

Now consider incident *GUWs* (simplified as a harmonic wave in **Figure 3.6**) interacting with the above joint. Upon traversing the mating parts of the joint, the incident *GUWs* in Assembly I are divided into four kinds of components:

(i) the waves to be dissipated, due to friction at the contact interface (i.e., evanescent waves decaying quickly);

(ii) the waves to be reflected by the interface and subsequently propagate in Assembly I but in an opposite direction compared to incident wave;

(iii) the waves to continue propagating in Assembly I in the same direction as incident wave after transmitting the bolt, and carry wave energy $\Omega_{transmitted\ in\ I}$; and

(iv) the remaining *GUWs* to be leaked to Assembly II via the interface, carrying wave energy Ω_{leak}, and then continue the propagation in Assembly II.

It should be pointed out that $\Omega_{transmitted\ in\ I}$ and Ω_{leak} are the wave energy of captured signals for the single-lap and cross-lap bolted joint in engineering practice, respectively, as shown in **Figure 3.6**. **Equation (3.13)** indicates that the real contact area S is proportional to $P^{2/3}$. With an assumption that the amount of leak energy of *GUWs* is proportional to S and it has

$$\Omega_{leak} \propto S \propto P^{2/3} \propto T^{2/3}. \tag{3.16}$$

From **Equation (3.16)**, it is axiomatic that Ω_{leak} tends to increase with an augment in applied torque T, and meanwhile $\Omega_{transmitted\ in\ I}$ decreases given the incident energy remains constant. Based on these, Ω_{leak} and $\Omega_{transmitted\ in\ I}$ can serve as two damage indices for quantitative detection of bolt loosening for the single-lap and cross-lap bolted joints, respectively. The efficiencies of these two linear indices in evaluating bolt loosening are to be validated by identifying the residual torque of both *Al-Al* and *C-C* bolted joints in Chapter 4.

3.3. Nonlinear Feature-based Methods

It has been demonstrated that the sensitivity of nonlinear feature-based methods in the identification of under-sized damage including early bolt loosening is usually higher compared to linear feature-based approaches [37]. Realizing limitations of linear features of acousto-ultrasonics to bolt loosening at an early stage, endeavors have been cast to develop nonlinear acoustic methods residing on contact-acoustic-nonlinearity (*CAN*) at the contact interface of a loose joint to achieve an effectual monitoring. However, at this moment, the understanding of mechanisms associated with nonlinear interaction between acoustic waves and damage (e.g., a crack or a loose joint) in the physical sense is still limited without an ideal model gaining a wide acceptance [38].

Motivated by this, to facilitate a better comprehending of detection philosophy of nonlinear acoustic methods, the theoretical modeling of *CAN* and its dependence on applied torque in a loose joint is studied and detailed in this section.

3.3.1. Modeling of *CAN* in a Loose Joint

As introduced in Section 2.3, when interacting with acoustic waves, the interface of a crack or a loose joint opens and closes if it undergoes certain extent of tension and compression, respectively. The contact stiffness of the interface under compression is higher than that under a tensile stress due to the fact that the latter is accompanied by weakening of the contact interface. In addition, the closing/opening behaviors at the interface of a joint are often involved in friction, clapping and kissing, thermo-elasticity, and varied other nonlinear wave-interaction effects, which make it challenging to perfectly model *CAN* of the contact interface. Generally, the one-dimensional (1-D) constitutive relation between the strain (ε) the stress (σ) considering first-order (β) and second-order (ϑ) classical nonlinearity along with hysteric nonlinearity (α), which are adopted to model nonlinear dynamic response of a structure, can be given as [94, 95]

$$\sigma = \int K_{H/N}(\varepsilon, \dot{\varepsilon}) d\varepsilon, \tag{3.17}$$

where $\dot{\varepsilon}$ is strain rate and *K* denotes the hysteretic and nonlinear stiffness which can be given as

$$K_{H/N}(\varepsilon, \dot{\varepsilon}) = K_1 \left\{ 1 - \beta\varepsilon - \vartheta\varepsilon^2 - \alpha[\Delta\varepsilon + \varepsilon(t) sign(\dot{\varepsilon})] + \cdots \right\}, \tag{3.18}$$

where K_1 signifies the linear stiffness, *t* is the time and

$$sign(\dot{\varepsilon}) = \begin{cases} 1, \dot{\varepsilon} > 0 \\ -1, \dot{\varepsilon} < 0 \end{cases}. \tag{3.19}$$

When different sources of nonlinearities are considered, distinct nonlinear features are presented in the theoretical frequency spectra, as shown in **Figure 3.7**(a)-(d). From **Figure 3.7**(a)-(d), it can be concluded that in the theoretical modeling when only the linear contact stiffness at the interface is considered, no harmonics occur in the corresponding frequency spectrum.

With the use of first-order classical nonlinearity (i.e., β in **Equation (3.18)**), every high-order harmonic presents. When taking into account the second-order classical nonlinearity (i.e., δ in **Equation (3.18)**) or hysteretic nonlinearity (i.e., α in **Equation (3.18)**), only the odd harmonics can be modeled. In addition, for *VAM*-based method, when β is involved, sidebands occur at the frequency of probing wave plus and minus the integrate times of frequencies of pumping vibration. Otherwise, when other nonlinearities are considered, the sidebands only present at the frequency of probing wave plus and minus the even times of frequencies of pumping vibration [137]. Therefore, the selection of proper type of nonlinearity plays a critical role in modeling *CAN* at the contact interface of a loose joint.

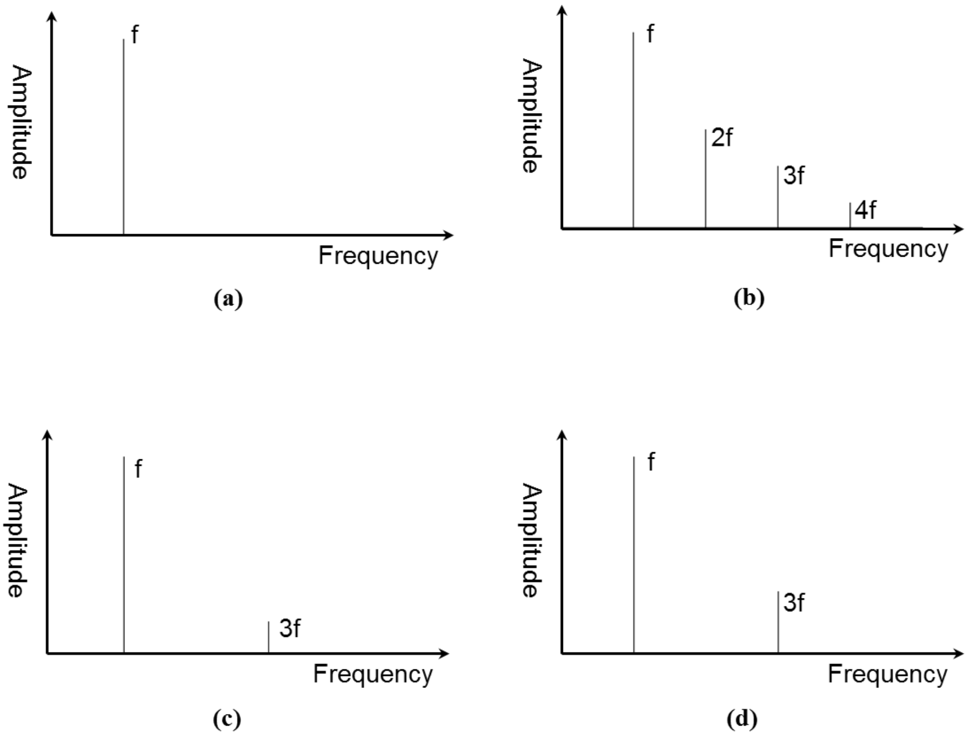

Figure 3.7 Frequency spectra of structural responses involved in varies types of nonlinearity: (a) linear stiffness; (b) first-order classical nonlinearity; (c) second-order classical nonlinearity; and (d) hysteretic nonlinearity

From the experimental observation (to be presented in Chapter 5), both even and odd high-order harmonics (*HOH*) of pumping vibration are found in the related spectra. Besides, the modulated sidebands occur at the frequency of probing wave plus and minus the integrate times of frequencies of pumping vibration. Physically, the application of the first-order classical nonlinearity introduces a softening effect when the relative motion between the two contact surfaces of a joint is positive (i.e., to open the interface) and a stiffening effect when the relative displacement is negative (i.e., to close the interface). Combining the experimental observation and physical interpretation of nonlinearities in distinct types, the first-order classical nonlinearity will be used for the theoretical modeling in the followings.

In the absence of acoustic waves, the two contact surfaces of a joint are assumed to be at an equilibrium gap distance X_0, as shown in **Figure 3.1**. The gap distance X will change periodically with a variation of ΔX when acoustic waves passing through, which leads to a slight change in the pressure P_X applied on the contact surfaces, induced by applied torque. Subsequently the contact pressure P_X can be expressed by its Taylor series expansion near the $X = X_0$ up to its second-order term to obtain the first-order classical nonlinearity [90] as

$$P_X = P(X_0 + \Delta X) = P_0 - K_1 \Delta X + K_2 \Delta X^2. \quad \textbf{(3.20)}$$

Then stiffness of the contact surface can be written as [90]

$$K_1 = -\left.\frac{dP}{dX}\right|_{X=X_0} = CP^m \propto T^m, \quad \textbf{(3.21)}$$

$$K_2 = \frac{1}{2}\frac{d^2P}{dX^2}\bigg|_{X=X_0} = 0.5mC^2P^{2m-1} \propto T^{2m-1}, \quad \textbf{(3.22)}$$

where K_1 is the linear stiffness and K_2 the nonlinear stiffness of the contact interface. C and m are associated with the surface properties of the material in contact. It is noteworthy that the value of m should not be more than 0.5, so in most cases, K_1 increases while K_2 decreases with increasing pressure. Based on this model, contact stiffness at the interface, including linear and nonlinear parts, is related to the applied torque of the bolt. In the following section, the contact stiffness is quantitatively linked to the nonlinear responses (i.e., *HOH* and modulated sidebands) of a loose joint.

3.3.2. *CAN*-based Bolt Loosening-related Nonlinear Indices

As mentioned in Chapter 2, nonlinear responses including *HOH* and modulated sidebands are two direct consequences of *CAN* at the contact interface due to a crack or a loose joint. In the previous section, *CAN* in a loose joint has been modeled and quantitatively linked to the degree of the residual torque of the bolt. In this section, the nonlinear responses (i.e., *HOH* and sidebands) of a loose joint are theoretically correlated with the residual torque by using the nonlinear stiffness derived in the previous section. Furthermore, the nonlinear damage (bolt loosening)-related indices for the evaluation of bolt loosening will be constructed from the nonlinear responses.

3.3.2.1 *HOH*-based

A single-degree-of-freedom system, as shown schematically in **Figure 3.8**, is considered to link the nonlinear contact stiffness to the nonlinear harmonic responses of a loose joint when subject to a harmonic force (with an equivalent force $F\cos\omega t$).

The equation of motion of the joint can be defined as

$$M\ddot{x}+K_1x-\phi K_2x^2=F\cos\omega t, \tag{3.23}$$

where ω signifies the excitation frequency of the harmonic force. *M* donates the mass and *t* is the time. The term with K_2 represents a nonlinear perturbation in which ϕ is a small quantity to scale the perturbation to be minute. According to the perturbation theory [142], to obtain the nonlinear responses of *SOH* and *TOH*, the solution to **Equation (3.23)** takes the form as following

$$x=x_1+\phi x_2+\phi^2x_3, \tag{3.24}$$

where x_1 represents the linear response, x_2 denotes the *SOH* response, and x_3 contains the *TOH* response of the bolted joint.

Substituting **Equations (3.24)** to **(3.23)** and forcing the coefficients of ϕ-related terms to be identical on the left and right sides of the equation, one has

$$M\ddot{x}_1+K_1x_1=F\cos\omega t, \tag{3.25}$$

$$M\ddot{x}_2+K_1x_2=K_2x_1^2, \tag{3.26}$$

$$M\ddot{x}_3+K_1x_3=2K_2x_1x_2. \tag{3.27}$$

Further, neglecting the transient component, the linear and nonlinear responses can be obtained as

$$x_1=\frac{F}{K_1-M\omega^2}\cos\omega t=B_1\cos\omega t, \tag{3.28}$$

$$x_2 = \frac{0.5K_2}{K_1 - 4M\omega^2} B_1^2 \cos 2\omega t, \tag{3.29}$$

$$x_3 = \frac{K_2^2}{2(K_1 - 9M\omega^2)(K_1 - 4M\omega^2)} B_1^3 \cos 3\omega t + \frac{K_2^2}{2(K_1 - 4M\omega^2)(K_1 - M\omega^2)} B_1^3 \cos \omega t. \tag{3.30}$$

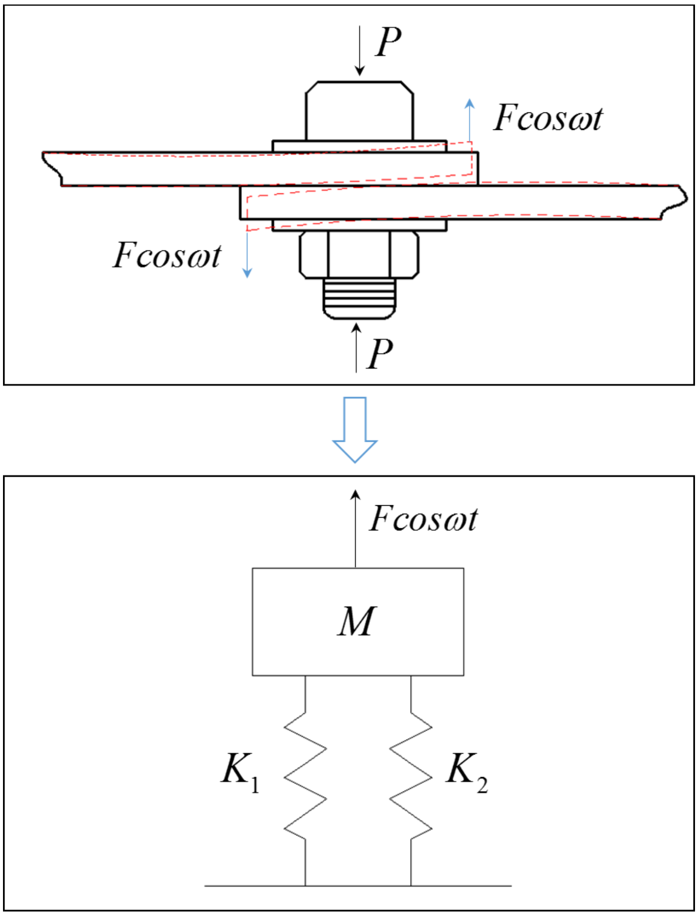

Figure 3.8 Simplified model of a joint subject to one harmonic force

In **Equations (3.28)** and **(3.30)**, those terms involving ω concern the linear response of the joint in the fundamental mode and the terms 2ω and 3ω in **Equations (3.29)** and **(3.30)** regulate characteristics of *SOH* and *TOH*, respectively. Considering the nonlinear responses are much weaker compared to the linear one, which leads to

$x_3 << x_1$, the magnitude of the linear (A_{LF}) can be expressed as

$$A_{LF} = \frac{K_2^2}{2(K_1 - 4M\omega^2)(K_1 - M\omega^2)} B_1^3 + B_1 \approx \frac{F}{K_1 - M\omega^2} \quad \textbf{(3.31)}$$

Then magnitudes of *SOH* (A_{SOH}) and *TOH* (A_{TOH}) responses can be written as

$$A_{SOH} = \frac{0.5K_2}{K_1 - 4M\omega^2} A_{LF}^2, \quad \textbf{(3.32)}$$

$$A_{TOH} = \frac{0.5K_2^2}{(K_1 - 9M\omega^2)(K_1 - 4M\omega^2)} A_{LF}^3. \quad \textbf{(3.33)}$$

From **Equations (3.32)** and **(3.33)**, it can be noted that the magnitude of nonlinear responses (i.e., *SOH* and *TOH*) is proportional to the nonlinear contact stiffness K_2, which is dependent on the contact properties (i.e., C and *m*) at the contact interface, along with the residual torque T applied on the bolt. Subsequently, two nonlinear indices β_{SOH}^{theory} and β_{TOH}^{theory}, making use of the magnitude of *SOH* and *TOH*, respectively, are defined to indicate the residual torque T, as

$$\beta_{SOH}^{theory} = \frac{A_{SOH}}{A_{LF}^2} = \frac{0.5K_2}{K_1 - 4M\omega^2}, \quad \textbf{(3.34)}$$

$$\beta_{TOH}^{theory} = \frac{A_{TOH}}{A_{LF}^3} = \frac{0.5K_2}{K_1 - 4M\omega^2} \frac{K_2}{K_1 - 9M\omega^2}. \quad \textbf{(3.35)}$$

3.3.2.2 *VAM*-based

In the *VAM*-based method, the loose joint is subject to a mixed excitation from a low-frequency pumping vibration (with an equivalent force $F_1 \cos \omega_1 t$) and a high-frequency probing wave (with an equivalent force $F_2 \cos \omega_2 t$), which are independent of each other, as exhibited in **Figure 3.9**.

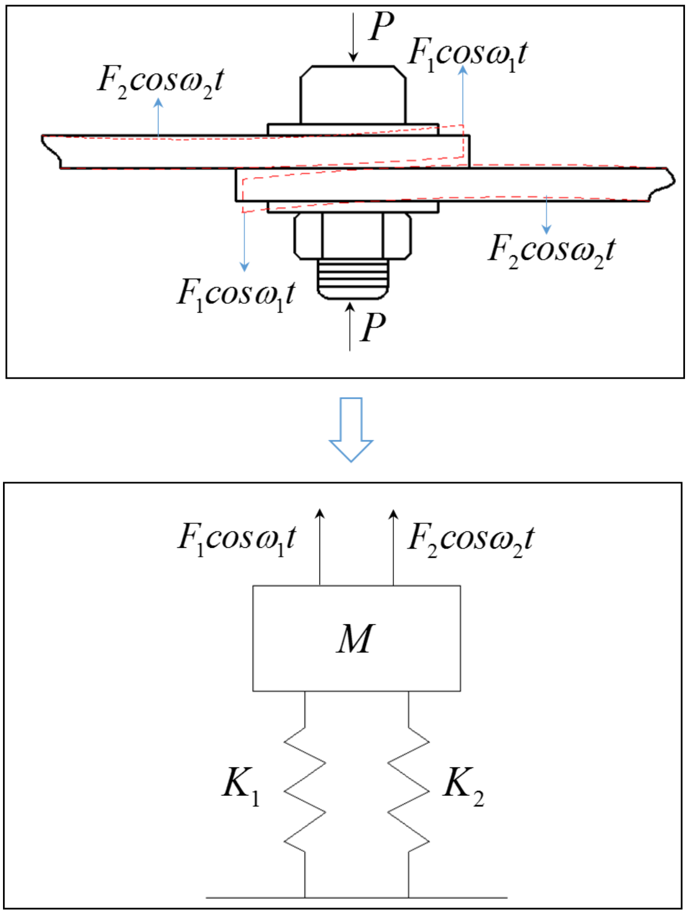

Figure 3.9 Simplified model of a joint subject to two harmonic forces

The equation of motion of the joint can be described as

$$M\ddot{x} + K_1 x - \phi K_2 x^2 = F_1 \cos\omega_1 t + F_2 \cos\omega_2 t, \tag{3.36}$$

where ω_1 and ω_2 are the frequencies of the pumping vibration and probing wave, respectively.

Using the analogous method based on perturbation theory, the solution to **Equation (3.36)** takes the following form

$$x = x_1 + \phi x_N, \tag{3.37}$$

x_1 represents the linear dynamic responses of the joint to the mixed excitation at frequencies of ω_1 (pumping vibration) and ω_2 (probing wave). x_N signifies the nonlinear responses of the joint, as manifested as a series of sidebands and second-order harmonics.

Substituting **Equations (3.37)** to **(3.36)** to and forcing the coefficients of ϕ-related terms to be identical on the left and right sides of the equation, one then has

$$M\ddot{x}_1 + K_1 x_1 = F_1 \cos\omega_1 t + F_2 \cos\omega_2 t, \tag{3.38}$$

$$M\ddot{x}_N + K_1 x_N = K_2 x_1^2. \tag{3.39}$$

Further, upon neglecting the transient components which are independent of the magnitudes of the linear and nonlinear responses, x_1 can be obtained as

$$x_1 = G_1 \cos\omega_1 t + G_2 \cos\omega_2 t, \tag{3.40}$$

where $G_1 = \dfrac{F_1}{K_1 - M\omega_1^{\,2}}$ and $G_2 = \dfrac{F_2}{K_1 - M\omega_2^{\,2}}$. Solving **Equation (3.39)** yields

$$x_N = x_{sidebands} + x_2, \tag{3.41}$$

where

$$x_{sidebands} = \frac{G_1 G_2}{K_1 - M(\omega_1 + \omega_2)^2} K_2 \cos(\omega_1 + \omega_2)t + \frac{G_1 G_2}{K_1 - M(\omega_1 - \omega_2)^2} K_2 \cos(\omega_1 - \omega_2)t, \tag{3.42}$$

$$x_2 = \frac{0.5G_1^2}{K_1 - 4M\omega_1^2} K_2 \cos(2\omega_1 t) + \frac{0.5G_2^2}{K_1 - 4M\omega_2^2} K_2 \cos(2\omega_2 t). \tag{3.43}$$

In **Equation (3.42)**, the terms $(\omega_1 + \omega_2)$ and $(\omega_1 - \omega_2)$ jointly regulate characteristics of the sidebands in the spectrum, and in **Equation (3.43)**, those terms involving $2\omega_1$ and $2\omega_2$ concern the *SOH* responses of the joint subject to the pumping vibration and probing wave, respectively.

From **Equation (3.42)**, it can be noted that the magnitude of a sideband in the spectrum is proportional linearly to the nonlinear contact stiffness K_2, which is dependent on the contact properties at the contact interface under the mixed excitation, as well as the residual torque T of the bolt. Consequently, based on **Equation (3.42)**, another nonlinear index, β_{VAM}^{theory}, embracing the magnitudes of the left (A_L), right (A_R) sidebands, probing wave (A_{HF}) and pumping vibration (A_{LF}) in the spectrum is defined in this study, as

$$\beta_{VAM}^{theory} = \frac{(A_L + A_R)}{2A_{HF}A_{LF}} = \frac{0.5K_2}{K_1 - M(\omega_1 - \omega_2)^2} + \frac{0.5K_2}{K_1 - M(\omega_1 + \omega_2)^2}. \quad \textbf{(3.44)}$$

It is noteworthy that the above derivations are not restricted by joint configurations, and therefore these nonlinear indices are applicable to any joint type, outperforming linear index with a high dependence on joint type.

Integrating the defined linear and nonlinear indices, an inspection framework is further developed for detecting bolt loosening and evaluating the residual torque of loose bolts in both *Al-Al* and *C-C* bolted joints in Chapters 4 and 5, respectively.

3.4. Summary

To facilitate an understanding of detection philosophy of bolt loosening using linear and nonlinear features of acousto-ultrasonics, dedicated modeling for deriving both linear and nonlinear damage (bolt loosening)-related indices is established in this chapter.

For the passive linear acoustic method, the affecting factors (i.e., the normal load, number of asperities in contact, surface properties and sliding velocity of the contact surfaces) of *AE* generation are theoretically defined. The energy-based and frequency-based analyses are predicted capable of characterizing *AE* signals generated from different contact interfaces (i.e., *C-C* and *M-C* contact), and further link the signal characteristics to the degree of applied torque. For the active linear acoustic method using vibration modal parameters, resonant frequency and damping ratio are proven being able to indicate the tightening state of a joint. For the active acoustic method using linear features of *GUWs*, based on Hertzian contact theory, a linear index, developed from *WED*, is quantitatively linked to the residual torque of the bolt. However, such an index is found with a high dependence on the joint configurations (lap types).

Given the necessity of evaluating small-scale (i.e., early bolt loosening) damage, using nonlinear features (i.e., *HOH* and modulated sidebands) of acoustic waves, a theoretical model to describe *CAN*, which is associated with the interaction between the contact interface of a loose joint and the acoustic waves, is presented. With a single-degree-freedom system, nonlinear responses, i.e., *HOH* and modulated sidebands, of a bolted joint subject to one harmonic excitation and two mixed excitations (i.e., low-frequency pumping vibration and high-frequency probing wave) are theoretically correlated with the nonlinear contact stiffness (determined by applied torque). Based on this, three nonlinear indices (i.e., *SOH*-based, *TOH*-based and *VAM*-based) are constructed from the magnitude of *SOH*, *TOH* and modulated sidebands for the evaluation of residual torque of loose bolts regardless of joint type.

Up to this point, both the linear and nonlinear features are theoretically related to the residual torque of loose joints, next two chapters (Chapter 4 and 5) will focus on experimental validation of the proposed linear and nonlinear indices, respectively. In particular, the limitations of *WED*-based linear index on the detection of bolt loosening in multi-type of bolted joints are exhibited in Chapter 4, and the advantages of nonlinear indices in detecting early bolt loosening in both *Al-Al* and *C-C* bolted joints are comparably presented in Chapter 5.

CHAPTER 4

Implementation of Methods Using Linear Features of Acousto-ultrasonics

4.1. Introduction

In Chapter 3, based on a contact theory, the generation of *AE* signals is physically linked to the contacts of asperities at the interface of a joint. From the theoretical derivation, amplitude (energy)-based and frequency-based analyses are predicted capable of characterizing *AE* signals generated at different contact interfaces (i.e., *C-C* and *M-C* interfaces) and further indicating the tightening state of a joint. As a global linear acoustic method, modal parameters, including resonant frequency and damping ratio, are found able to identify the health state of a bolted joint. As a local linear acoustic method, *WED* of *GUWs*, when interacting with the contact interface of a joint, is correlated to the residual torque of the loose bolt using an analytical model residing on Hertzian contact theory.

In this chapter, the proposed linear indices, constructed from extracted *AE* signal characteristics, vibration modal parameters and *WED* of *GUWs*, respectively, are verified by a series of case studies. In particular, the intrinsic mode functions (*IMFs*) of acoustic emission (*AE*) signals, extracted from signals using an empirical mode decomposition (*EMD*), are used to characterize the contact conditions (e.g., sliding friction or collision) of asperities in the mating parts of bolted composite joints undergone flexural vibration, whereby to evaluate the tightening condition of the joints quantitatively. Specifically, the sliding friction-related *IMFs*, generated in the mating parts of the two joining composite components (i.e., composite-composite contact, termed as *C-C* contact for short) are ascertained from those generated from the contacts between the joining composite components and the metallic fasteners (i.e., metal-composite contact, termed as *M-C* contact for short), via a Hilbert-Huang transform (*HHT*). Subsequently, the *C-C* contact-related *IMFs* are linked to the contact behaviors of asperities at the joining interface, reflecting quantitatively the degree of the residual torque of the bolted joints. The fatigue performance of the joints is further evaluated according to the changes in the energy ratios of the *C-C* contact-related *IMFs*. Resonant frequency and damping ratio obtained from modal testing are comparatively adopted to present their dependence on the residual torque of a bolted composite joint. Finally, detection of bolt loosening in both *Al-Al* and *C-C* bolted joints using *WED* of *GUWs* is introduced. Three types of *Al-Al* bolted joints, namely single-lap, cross-lap and hybrid-lap, are comparably used to exhibit the dependence of *WED*-based method on the joint configurations (i.e., lap types). Furthermore, to investigate the influence of boundary reflection on the sensitivity of *WED*-based method to bolt loosening, the transmitted energy of first-arrival wave packet of *GUWs*, calculated by Hilbert Transform (*HT*), is intercepted and comparably applied to assess the residual torque of a loose bolt in the cross-lap *Al-Al* bolted joint. In addition, the performance of *WED*-based method in the evaluation of loose bolts in both single-lap *Al-Al* and *C-C* bolted joints is compared with the limitations of such a linear index when applied to detect bolted structures consisting of high-attenuation materials (i.e., composite materials).

This chapter emphasizes on improvements of conventional linear acoustic methods in aspect of signal processing and interpreting. Time domain and frequency domain along with time-frequency methods are comparatively adopted to process both *GUWs* and vibration signals.

4.2. Passive Linear Method: *AE*-based

Empirical mode decomposition (*EMD*), which has been widely studied and used in various fields (e.g., damage detection, pattern recognition and system identification) demonstrating a high-frequency resolution, is introduced and further employed to extract characteristics of *AE* signals for the detection of bolt loosening in the followings.

4.2.1. Empirical Mode Decomposition

When a signal is processed with *EMD*, a set of complete and almost orthogonal components (i.e., *IMFs*) can be obtained from the signal, each of which represents a natural oscillatory mode of the original signal, and is determined by characteristics of the signal itself. To facilitate a better understanding of procedure of *EMD* method, its flowchart is exhibited in **Figure 4.1**.

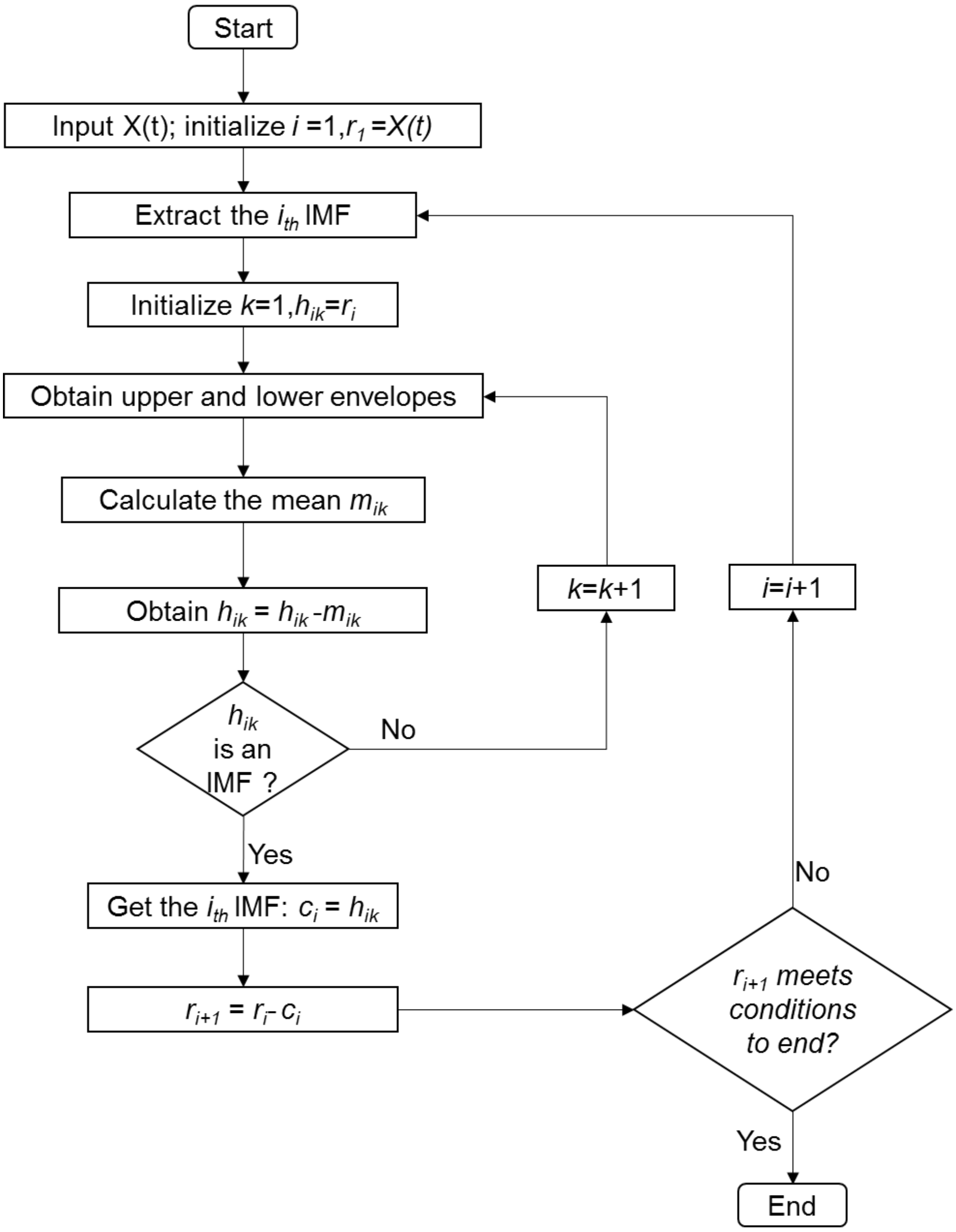

Figure 4.1 Flowchart of *EMD*

To conduct *EMD* on a signal $X(t)$, the upper and lower envelops of the signal are first obtained by connecting local maxima and minima using a cubic spline function, respectively, as schematically illustrated in **Figure 4.2**.

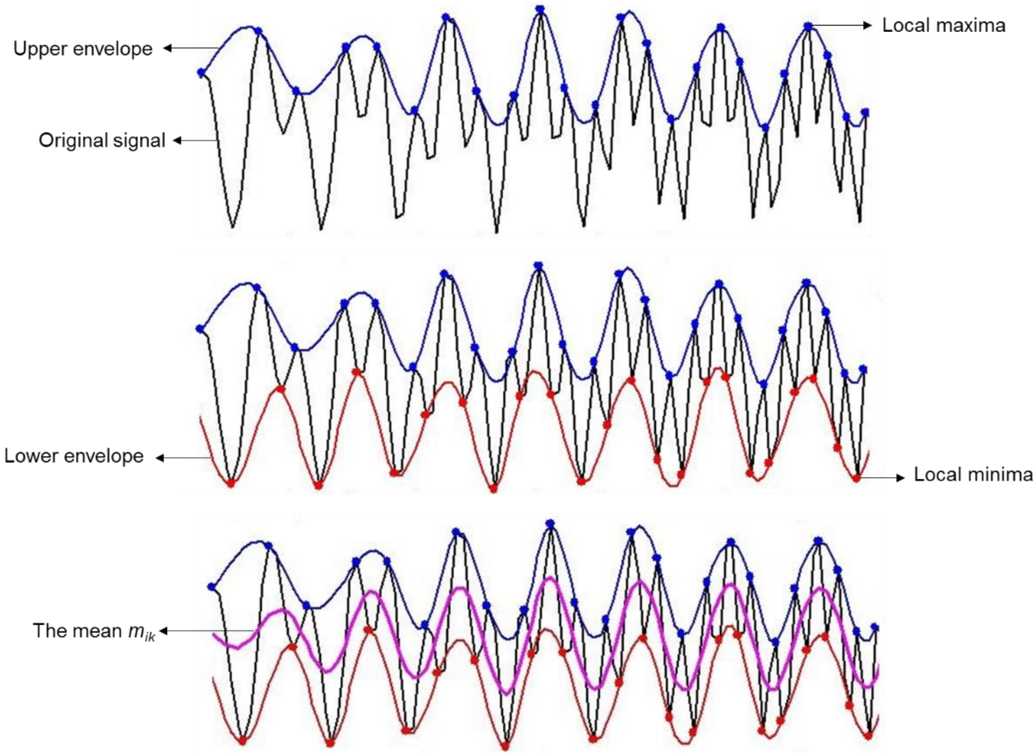

Figure 4.2 Sifting process of *EMD*

The mean of the upper and lower envelopes is then obtained and signified as m_{11}, and the first "Proto-Intrinsic Mode Function", h_{11} is defined as

$$X(t) - m_{11} = h_{11}. \quad \textbf{(4.1)}$$

In the subsequent processes, h_{11} is treated as a new original signal and m_{12} is obtained by averaging the upper and lower envelopes of h_{11}. Then the second "Proto-Intrinsic Mode Function" h_{12} is obtained as

$$h_{11} - m_{12} = h_{12}. \quad \textbf{(4.2)}$$

The above process (i.e., sifting process) is repeated k times until h_{1k} becomes the first *IMF* c_1, which satisfies two conditions: (1) in the whole data set, the number of extrema and the number of zero crossings must either equal or differ at most by one; and (2) at any point, the mean value of the envelope fitted by the local maxima and the envelope fitted by the local minima is zero [52].

$$c_1 = h_{1k}. \tag{4.3}$$

According to the above description of the generation mechanisms of *AE* signals, the first *IMF* (c_1) is deduced to be associated with asperity contacts with the shortest contact duration (*i.e.,* the highest centered frequency).

Then difference between *X(t)* and c_1 is defined as the first residue r_1

$$X(t) - \mathrm{c}_1 = r_1. \tag{4.4}$$

The sifting process is repeated until all *IMFs* of the original signal are obtained.

$$r_1 - \mathrm{c}_2 = r_2, \tag{4.5}$$

$$\cdots$$

$$r_{n\text{-}1} - \mathrm{c}_n = r_n. \tag{4.6}$$

The decomposition process is terminated until the residue r_n becomes a constant, a monotonic function, or a function with only one maximum and one minimum.

Finally, the signal *X(t)* can be expressed with the sum of decomposed *IMFs* and the residue as

$$X(t) = \sum_{j=1}^{n} c_j + r_n. \tag{4.7}$$

It is noteworthy that the decomposed *IMFs* with decreasing centered frequencies are usually physically meaningful, which will be used to recognize contact behaviors of asperities at the interface in the following case studies.

4.2.2. Case Study I: Effect of Applied Torque on Contact Behaviors of a Joint

In this section, *EMD*-extracted characteristics of *AE* signals are used to evaluate the applied torque of a bolted joint consisting of two composite beams assembled by an M6 bolt. The beam specimens were cut from a composite laminated T700/7901 carbon-fiber-reinforced epoxy, obtained using hot pressing with a stacking sequence [90, 0, 90, 0]s. Specimens were 1mm thick and 30 mm wide. Three sets of experimental setups were used to capture *AE* signals generated from contacts of asperities at the single-type interface (i.e., *C-C* contact in two assembled composite beams as displayed in **Figure 4.3** (a) and *M-C* contact in a bolted beam as shown in **Figure 4.3** (b)) and mixing-type contact interfaces (including both *C-C* and *M-C* interfaces in a bolted composite joint as exhibited in **Figure 4.3** (c)). Insulation tape was used on the tip of the free end of different specimens to adjust the structural mass and further keep their resonant frequencies consistent.

In **Figure 4.3** (a), two composite beams, with lengths of 100 mm and 190 mm, respectively, were assembled with an overlap length of 20 mm by using insulation tape. One end of the beam was secured to the moving element (i.e., excitation part) of a vibration table (ES-3-150) with an M8 bolt. Sealant was used to avoid *AE* source from contacts between the M8 bolt and other components. The specimens were excited using a vertical force with a displacement of 0.6 mm at a frequency of 22.3 Hz through the sinusoidal motion of the moving element, and were monitored with an acceleration sensor. A four-channel SAEU2S *AE* system (Soundwel Co.) was employed to capture *AE* signals generated from the two assembled composite beams (i.e., *C-C* contact) subject to vibration in a short time (i.e., 8 seconds), using an SR 150M sensor with a wide resonant frequency range between 10 and 160 kHz, as displayed in **Figure 4.4**. The *AE* signals were recorded at a sampling frequency of 2 MHz. A threshold of 40 dB was used to avoid involvement of environment noise in the captured signals.

In **Figure 4.3** (b), an intact beam with a length of 270 mm was drilled to bear a thread hole and assembled with an M6 bolt. The M6 bolt was tightened from 1 to 9 N·m, with an increasing step of 1 N·m, so as to collect *AE* signals generated from the *M-C* contact (i.e., contact between the metallic fasteners and the composite beam) in each scenario. The *AE* signals were collected when the specimens were under the same excitation condition as those shown in **Figure 4.3** (a).

In **Figure 4.3** (c), the same beams as those shown in **Figure 4.3** (a) were assembled with an M6 bolt to form a bolted composite joint. To remove the sharp asperities on the rough surface and minimize thread gap between the nut and bolt, pre-loading was repeated before the experiment. Then, the joint was tightened from 1 to 9 N·m and excited under each torque in a short time (i.e., 8 seconds) to obtain the *AE* signals generated from the mixing-type contact (including both *C-C* and *M-C* contacts).

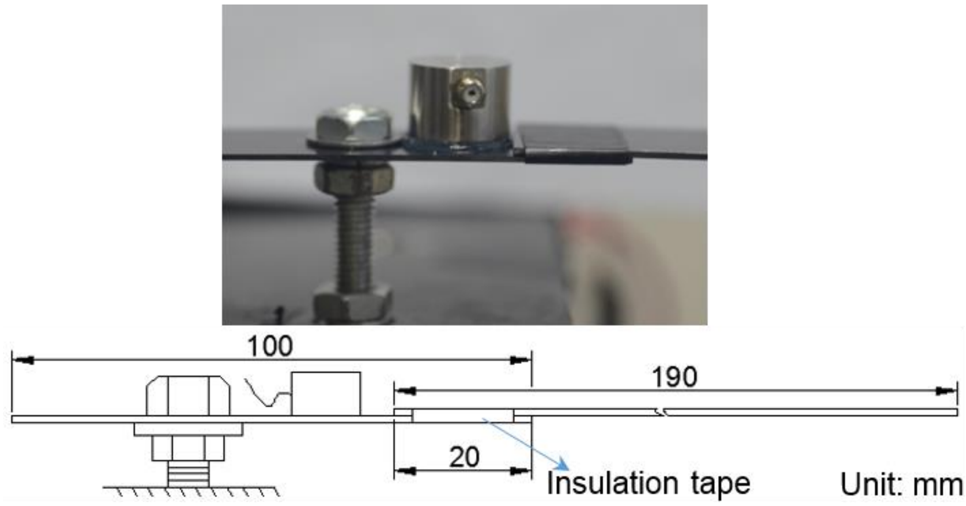

(a)

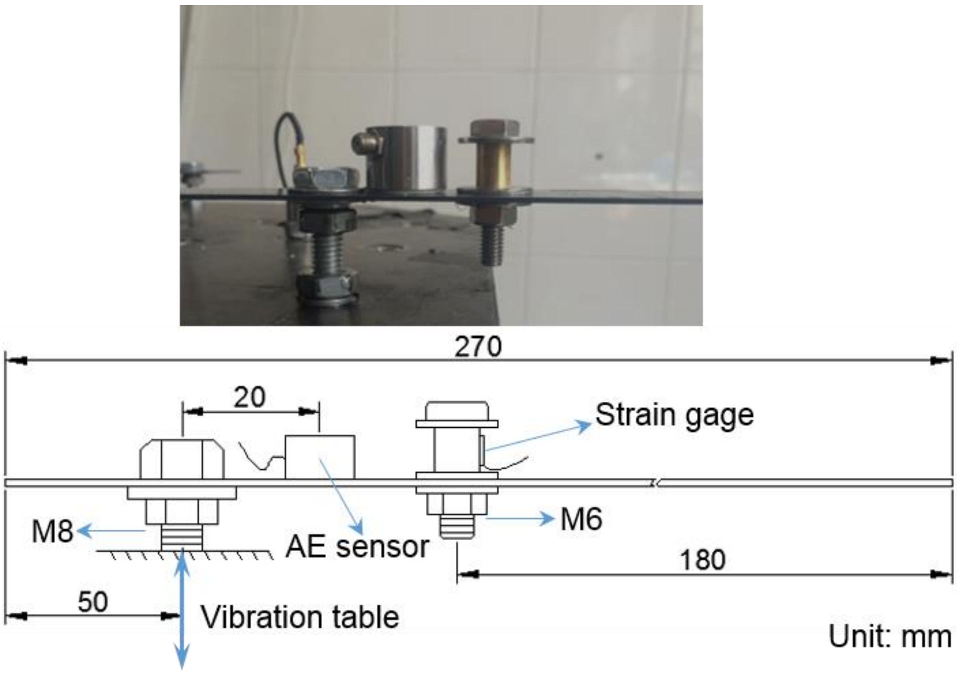

(b)

Figure 4.3 Experimental set-ups for collecting *AE* signals (a) in two beams assembled by insulation tape; (b) in a bolted beam; (c) in a bolted joint

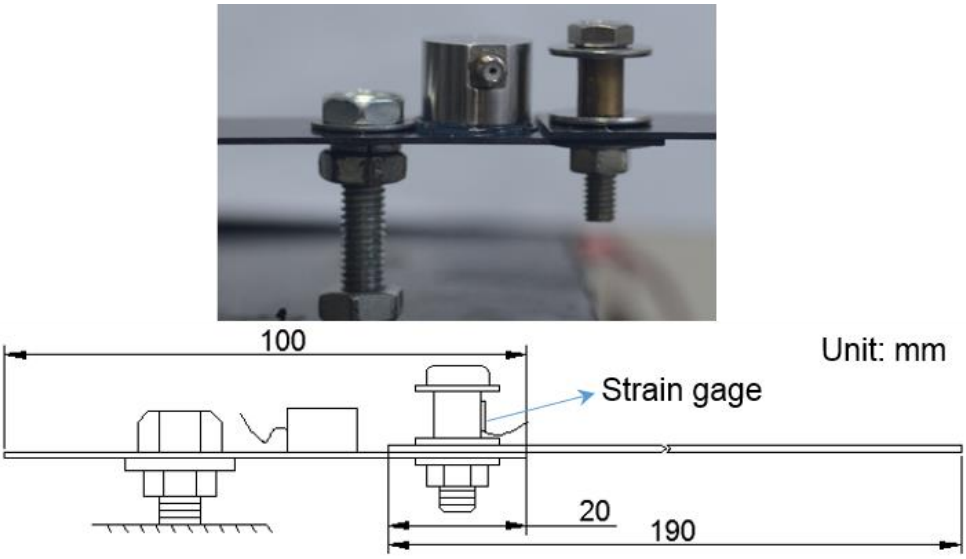

(c)

Figure 4.3 (continued)

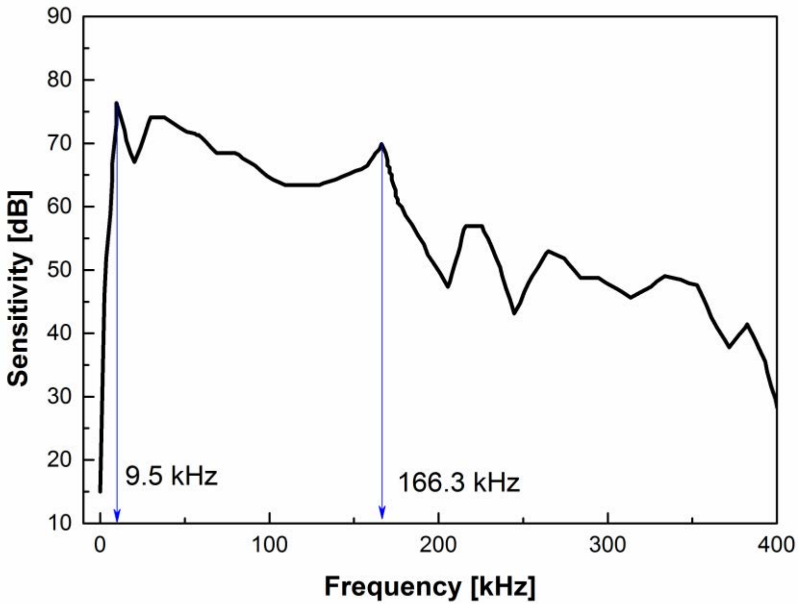

Figure 4.4 Resonant frequency range of the *AE* sensor

This study is dedicated to investigating the contact behaviors between joining materials (i.e., *C*-*C* contact) in a bolted composite joint under vibration. To achieve quantitative monitoring of bolt torque using the *AE* signals generated from the *C*-*C* and *M-C* contacts, their unique characteristics and quantitative dependence on the applied torque must be firstly understood. The *AE* signals generated at the single-type contact interface (i.e., *C-C* contact as shown in **Figure 4.3** (a) and *M-C* contact as shown in **Figure 4.3** (b)) are processed with *HHT* and the decomposed *IMFs* are comparably studied to ascertain their distinct characteristics in this section.

The original *AE* signal (the average of 300 signals) and its first four *IMFs*, generated from the *C-C* contact between the two composite beams assembled by insulation tape are displayed in **Figure 4.5** and **4.6**, respectively. The first four *IMFs* in **Figure** 4.6 are observed to possess increasing periods.

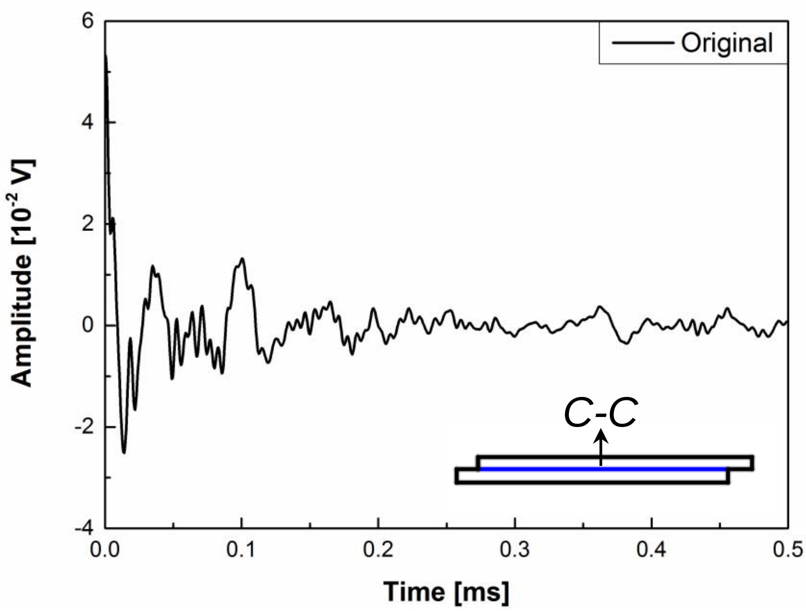

Figure 4.5 Time presentation of the original *AE* signal captured from the two beams assembled by insulation tape

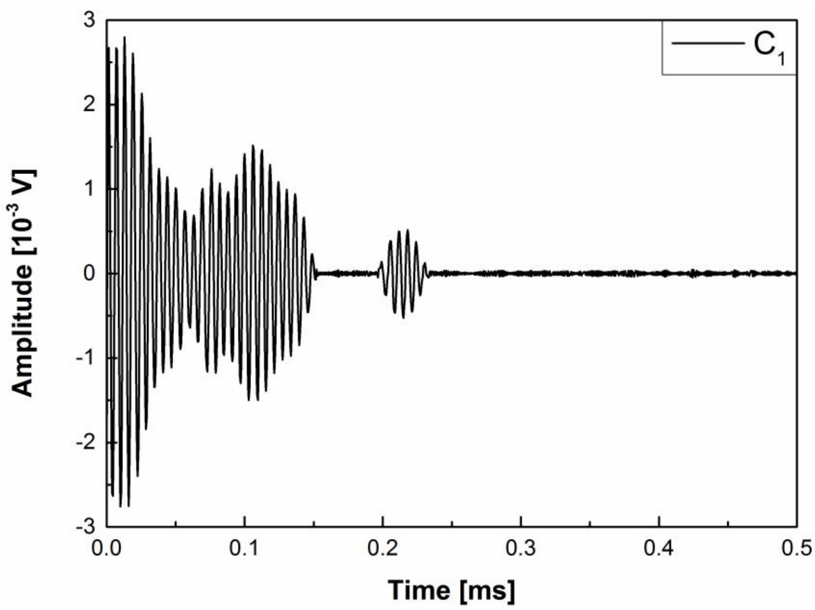

(a)

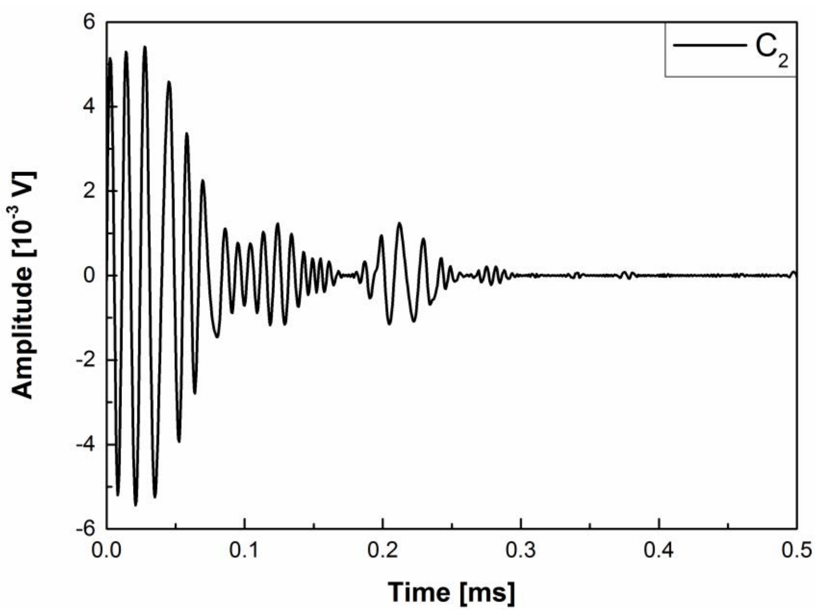

(b)

Figure 4.6 Time presentations of first four *IMFs* of the *AE* signal in Figure 4.5: (a) C_1; (b) C_2; (c) C_3; and (d) C_4

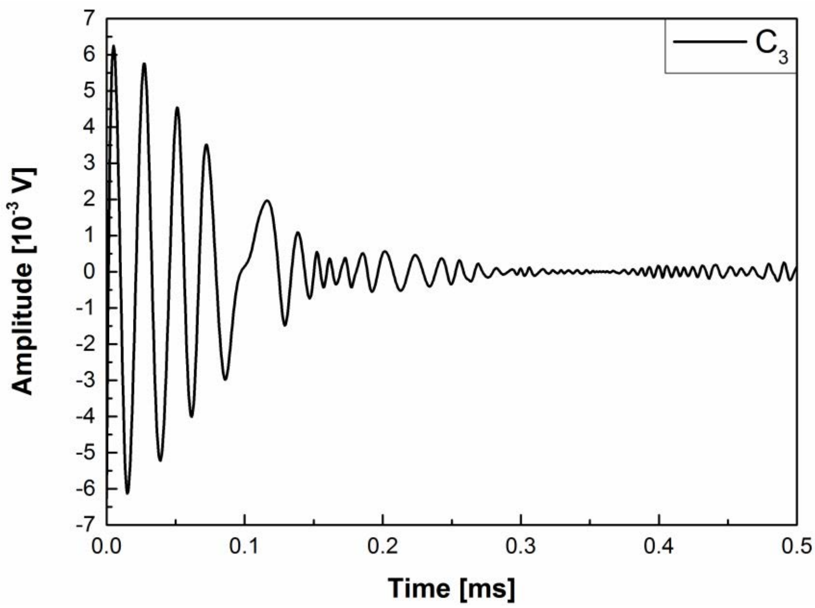

(c)

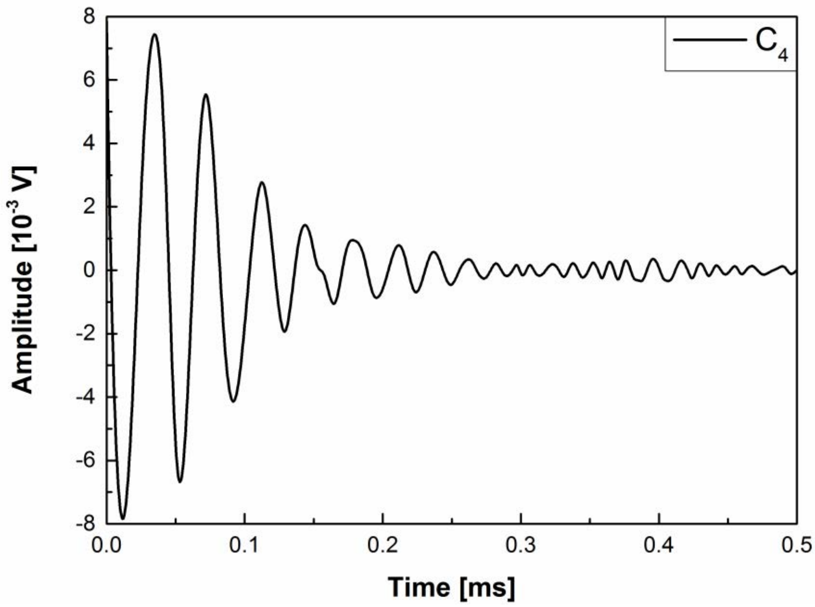

(d)

Figure 4.6 (continued)

Time frequency analysis on the original signal was comparably conducted by using short-time Fourier transform and Hilbert-Huang transform and the corresponding spectra are displayed in **Figure 4.7** (a) and (b), respectively. A higher time-frequency resolution is observed in the *HHT* spectrum presented with normalized energy compared to the former one. In addition, the main energy of the *AE* signal is observed to distribute in the frequency range between 20 and 200 kHz.

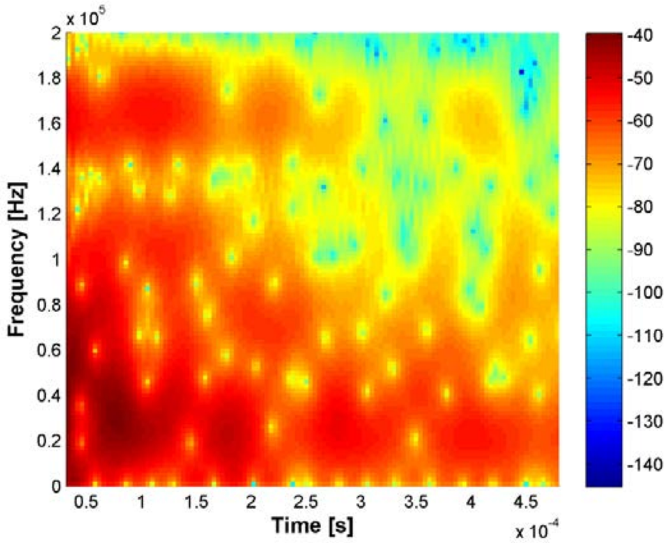

(a)

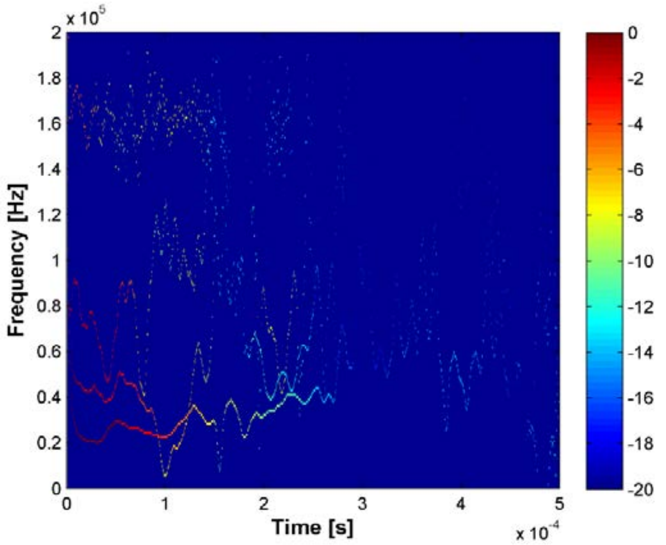

(b)

Figure 4.7 (a) Short-time Fourier transform; and (b) Hilbert-Huang transform spectra of the signal in Figure 4.5

Figure 4.8 (a) and (b) show the time-presentation of the original *AE* signal (the average of 300 signals) and its first *IMF* generated from the bolted beam (i.e., *M-C* contact) under 1 and 7 N·m, respectively. Noted that C_i^T denotes the i^{th} *IMF* of the *AE* signals generated from specimens under a torque of T. From the comparison regarding signal envelopes in the time domain, a high similarity can be found between the original signal and its first *IMF*, which means the first *IMF* dominates the energy of the original signal.

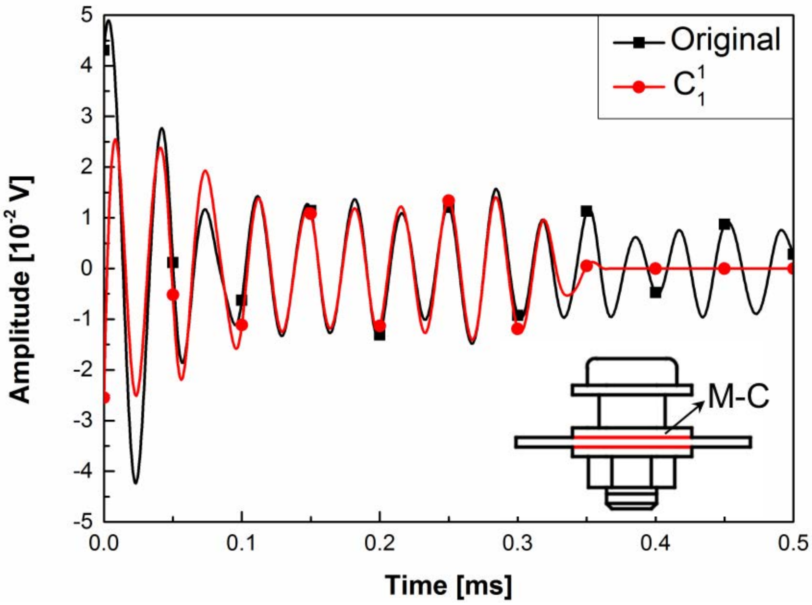

(a)

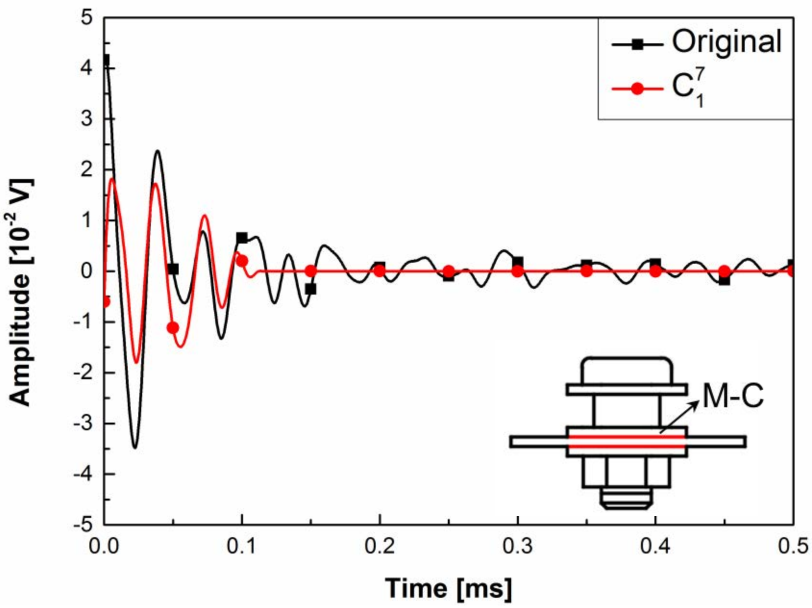

(b)

Figure 4.8 Time presentations of the original *AE* signal and its first *IMF* captured from the bolted beam under (a) 1 N·m; and (b) 7 N·m

The *HHT* spectra presented with normalized energy of the two signals in **Figure 4.8** (a) and (b) are comparatively shown in **Figure 4.9** (a) and (b).

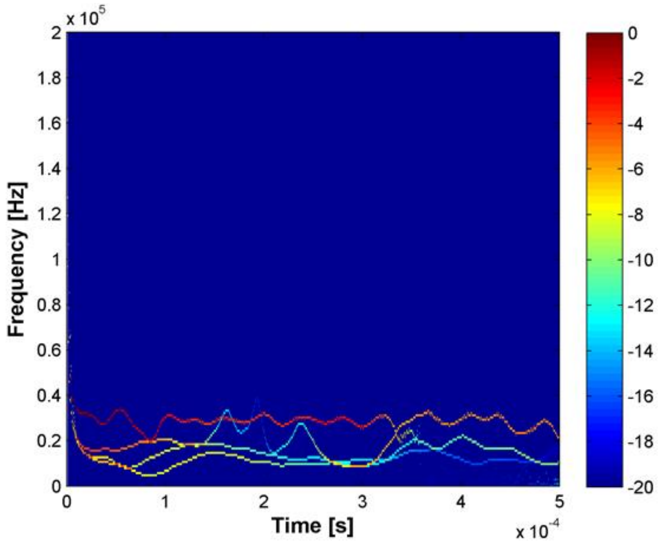

(a)

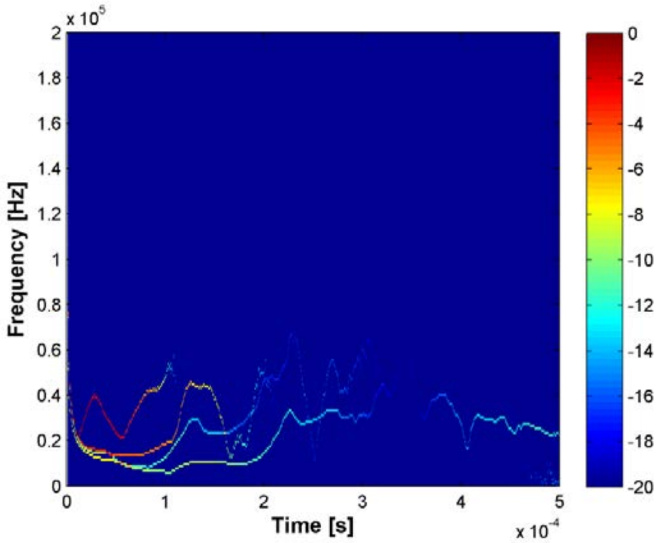

(b)

Figure 4.9 Hilbert-Huang transform spectra of the *AE* signals (a) in Figure 4.8 (a); (b) in Figure 4.8 (b); and (c) marginal spectra of the *AE* signals captured from the bolted beam under different torques

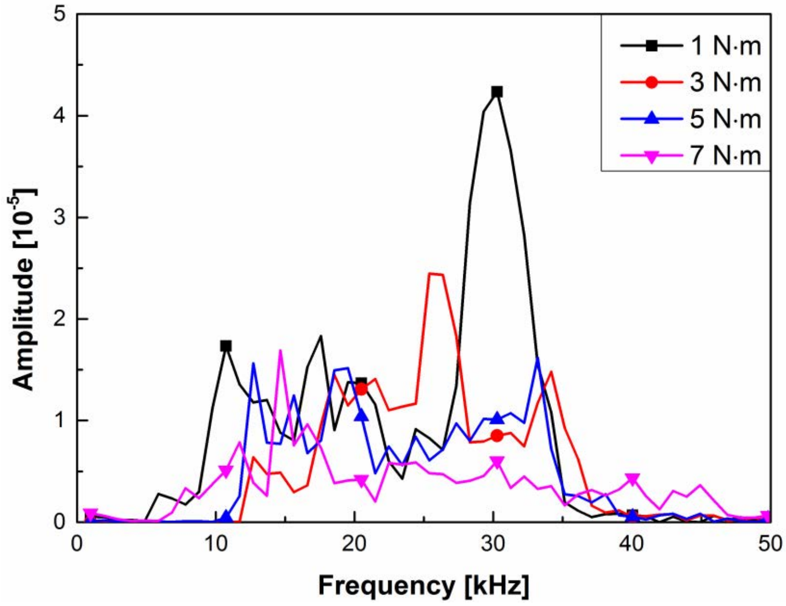

(c)

Figure 4.9 (continued)

To observe the main frequency components of the *AE* signals generated from the *M-C* contact distribute between 10 and 40 kHz, regardless of the applied torque. Marginal spectra of the *AE* signals captured from the bolted beam under different torques are shown in **Figure 4.9** (c), in which the energy ratio of low-frequency components (below 25 kHz) becomes larger with the increase of applied torque. This phenomenon is consistent with previous analysis in terms of the influence of applied torque on the asperity contacts and resultant *AE* signal characteristics. To be more specially, a high pressure increases the contact area of asperities and consequently more *IMFs* with longer durations (i.e., low centered frequencies) occurs. It is noteworthy that when the bolt was tightened to 8 N·m or more, no *AE* signals were captured. This is because that no obvious relative motion at the *M-C* interface occurs when the applied torque reaches 8 N·m, which introduces a high pressure at the interface between the metallic washer and the composite beam (i.e., *M-C* interface). It also indicates that *AE* source from the contacts between the M8 bolt and other components was circumvented.

Comparing the *AE* signals generated from the *M-C* contact to those generated from the *C-C* contact, it is found that the *M-C* contact generates the *AE* signals dominating the frequency range between 10 and 40 kHz, while the *AE* signals induced by the *C-C* contact mainly distribute between 20 and 200 kHz. The difference in roughness and hardness between metal and resin is responsible for the diversity of their frequency distribution. Therefore, the first three *IMFs* with centered frequencies higher than 40 kHz, decomposed from the *AE* signals produced by the *C-C* contact, are identified and can be further used to indicate contact conditions of a bolted composite joint.

In order to identify asperity contacts in a bolted composite joint undergone vibration using the *HHT*-based characteristics of *AE* signals, the bolted joint, shown in **Figure 4.3** (c), was tightened with increasing torques and vibrated with a displacement of 0.6 mm at 22.3 Hz, which is closed to its first-order resonant frequency (*i.e.,* 22.0 Hz). The typical amplitude distribution of the *AE* signals recorded during vibration is shown in **Figure 4.10** (a), and **Figure 4.10** (b) is the averaged results of three repeated tests.

To observe that in **Figure 4.10** (a) when the applied torque is 3 N·m, the amplitude of the *AE* signals distributes over a wide range, which indicates uncontrolled contact behaviors in the bolted joint, due to a lack of sufficient pressure on the contact surfaces. Similar phenomena present when the torque is 1 and 2 N·m, which are not to be discussed in detail. When the applied torque continues increasing, the amplitude of the *AE* signals reaches a steady value, especially for the joint under 7 N·m.

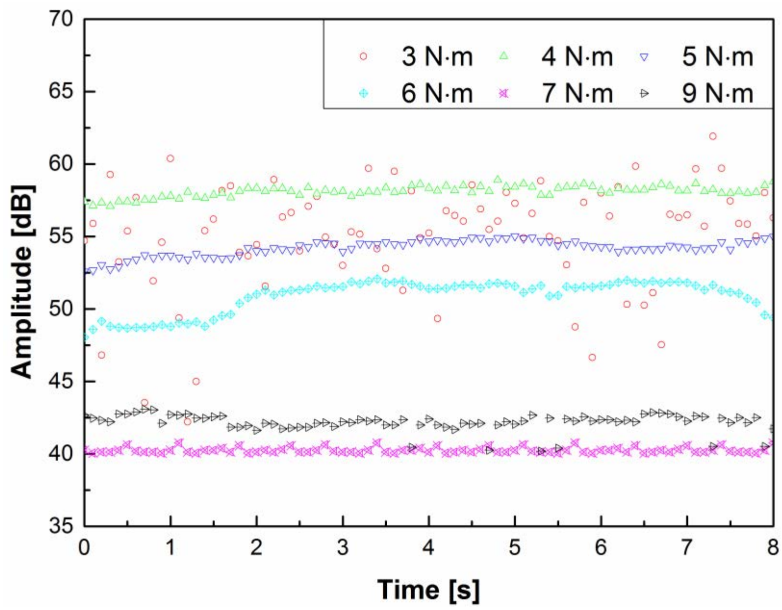

(a)

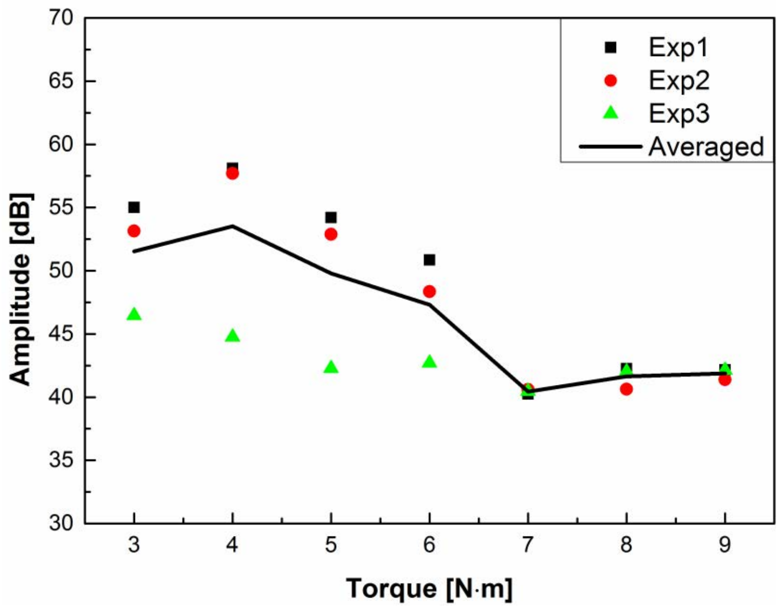

(b)

Figure 4.10 (a) Typical amplitude distribution; and (b) averaged amplitude of the *AE* signals captured from the bolted joint under different torques in three tests

From the averaged results as displayed in **Figure 4.10 (b)**, a monotonic decrease in the signal amplitude is observed until the applied torque reaches 7 N·m. After then, it increases slightly until 9 N·m. Damage caused by fretting wear on the composite surface below the outer border of the washer was found in the further observation. Therefore, *AE* signals induced by the surface damage are inferred to cause the increase of signal amplitude (i.e., gross energy) after the torque exceeds 7 N·m. To conclude, with usage of gross energy of *AE* signals, the detectable range regarding bolt loosening is limited from 4 to 7 N·m.

The *AE* signals (averages of 300 signals) generated in the bolted joint under 3, 7 and 9 N·m were further processed with *HHT* and their *IMFs* (C_i^T) in time-domain are shown in **Figure 4.11**, **4.12** and **4.13**, respectively.

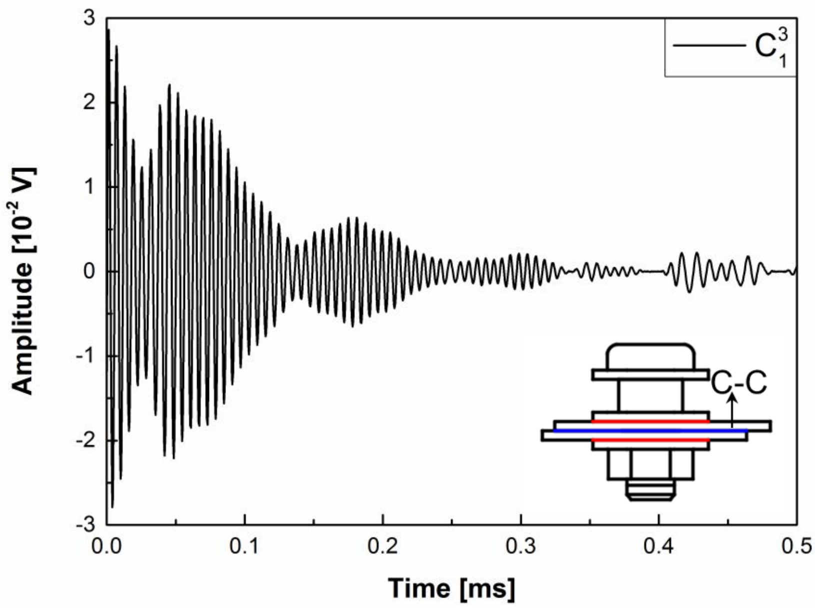

(a)

Figure 4.11 Time presentations of the first three *IMFs* of the *AE* signal acquired from the bolted joint under 3 N·m: (a) C_1^3; (b) C_2^3; and (c) C_3^3

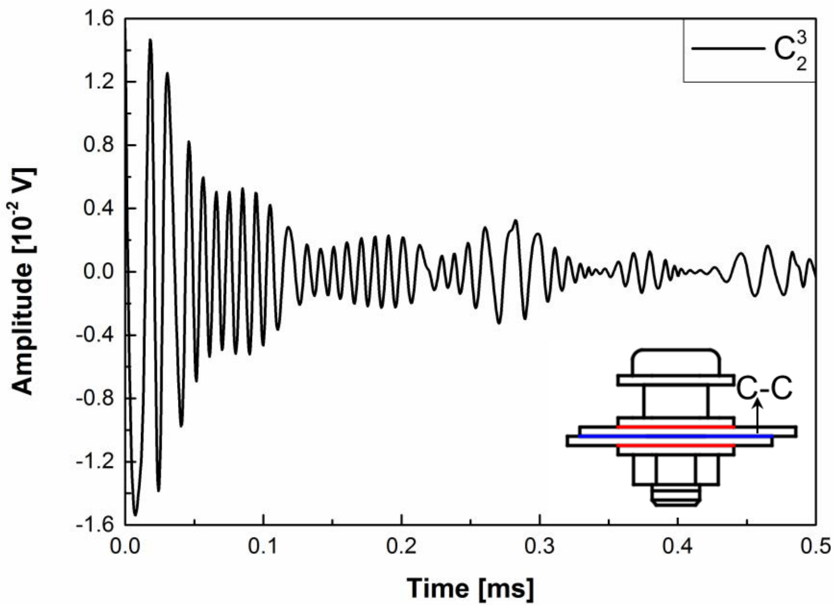

(b)

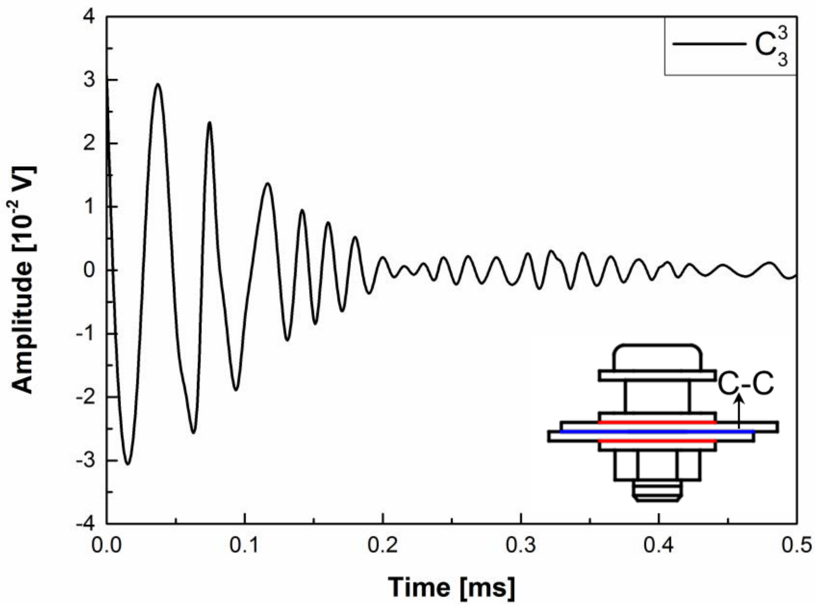

(c)

Figure 4.11 (continued)

In **Figure 4.11**, the first three *IMFs* (*i.e.*, C_1^3, C_2^3 and C_3^3) decomposed from the *AE* signal generated from the bolted joint under a torque of 3 N·m, are found to be similar with C_1, C_2 and C_3 in **Figure 4.6**. In addition, from further observation on the results from joint under 7 and 9 N·m, the periods of the *IMFs* are observed to increase when the joint was applied with augmenting torques.

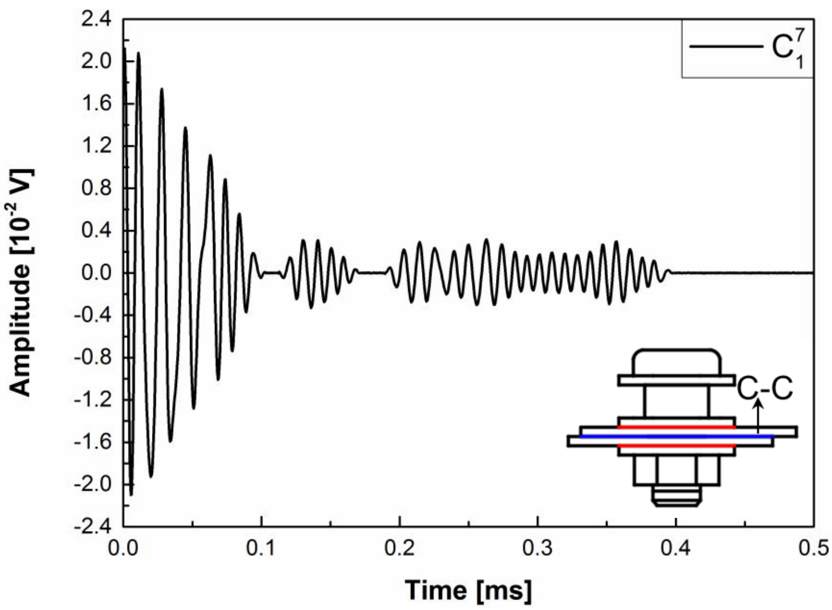

(a)

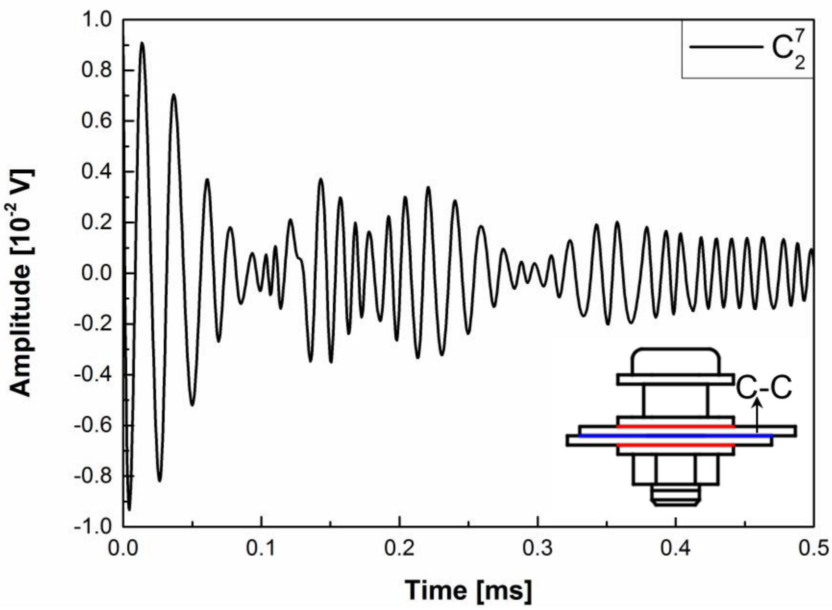

(b)

Figure 4.12 Time presentations of the first two *IMFs* of the *AE* signal acquired from the bolted joint under 7 N·m: (a) C_1^7; and (b) C_2^7

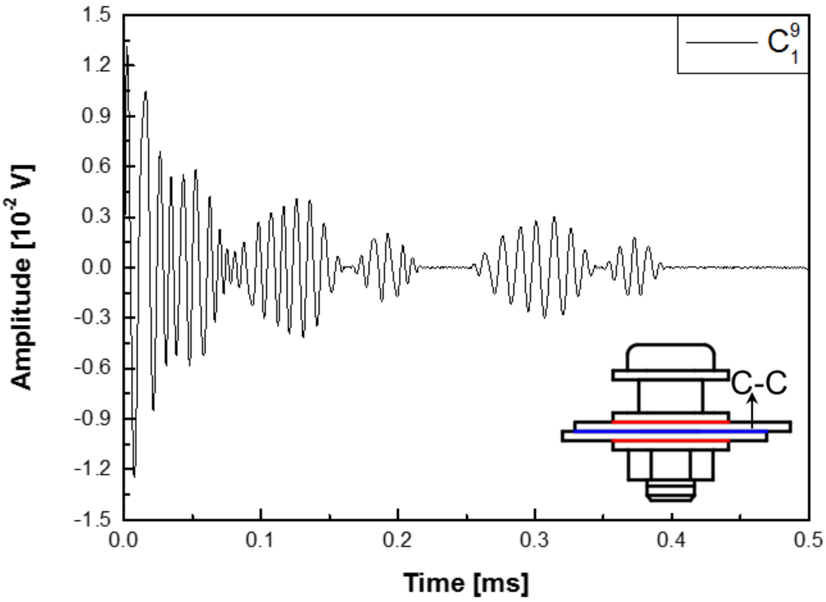

(a)

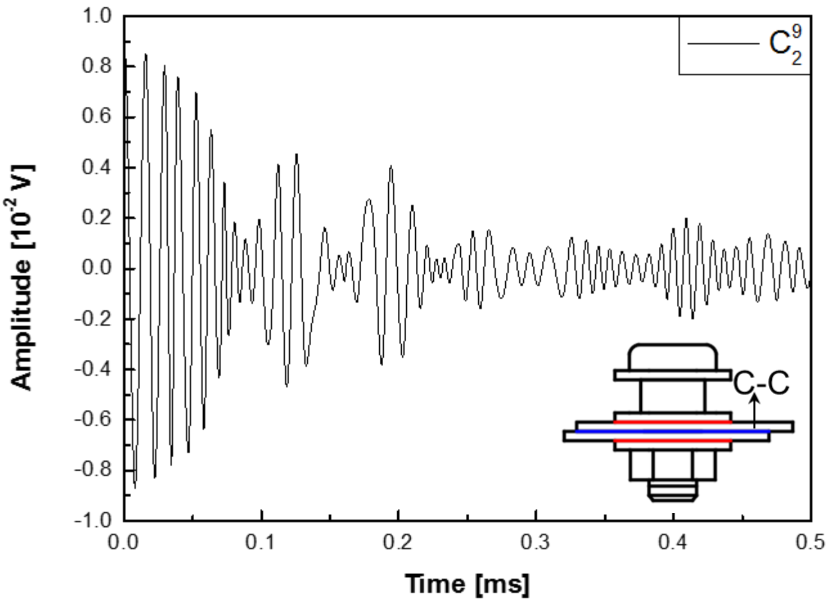

(b)

Figure 4.13 Time presentations of the first two *IMFs* of the *AE* signal acquired from the bolted joint under 9 N·m: (a) C_1^9; and (b) C_2^9

To investigate energy shift in the signals generated from the joint under increasing torques, *HHT* spectra of the signals (first four *IMFs*) are comparably displayed in **Figure 4.14**. The first three *IMFs* are observed to possess main frequency components higher than 40 kHz and show a high sensitivity to changes in the applied torque. The energy ratios of these high-frequency *IMFs* (indicated by the normalized energy) decrease with the increasing torque applied on the joint, which is similar with results in the bolted beam. Through the comparison with signals generated from the *C-C* and *M-C* contacts in terms of *HHT* spectra, the first three *IMFs* of the signals captured from the bolted composite joint are inferred to be produced by the *C-C* contact.

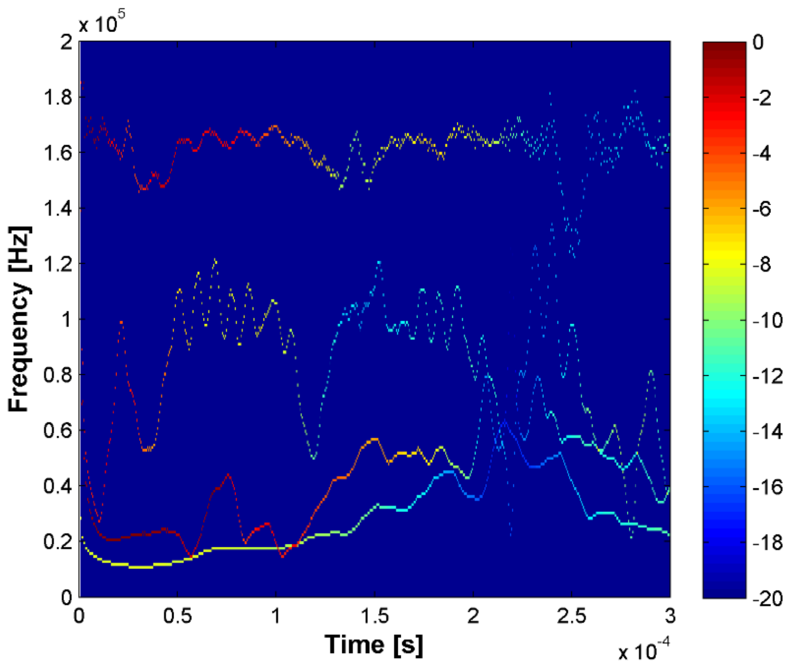

(a)

Figure 4.14 Hilbert-Huang transform spectra of the *AE* signals from the joint under (a)3 N·m; (b) 5 N·m; (c) 7 N·m; and (d) 9 N·m

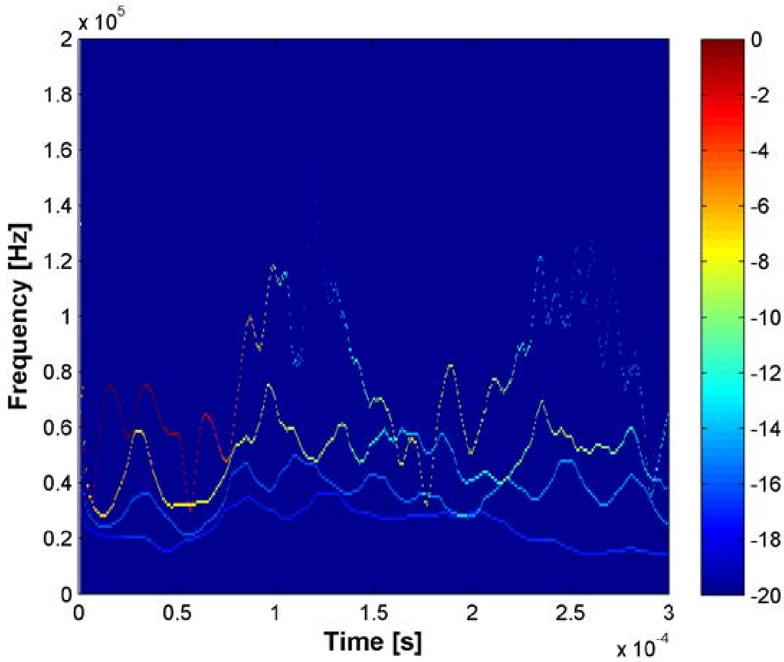

(b)

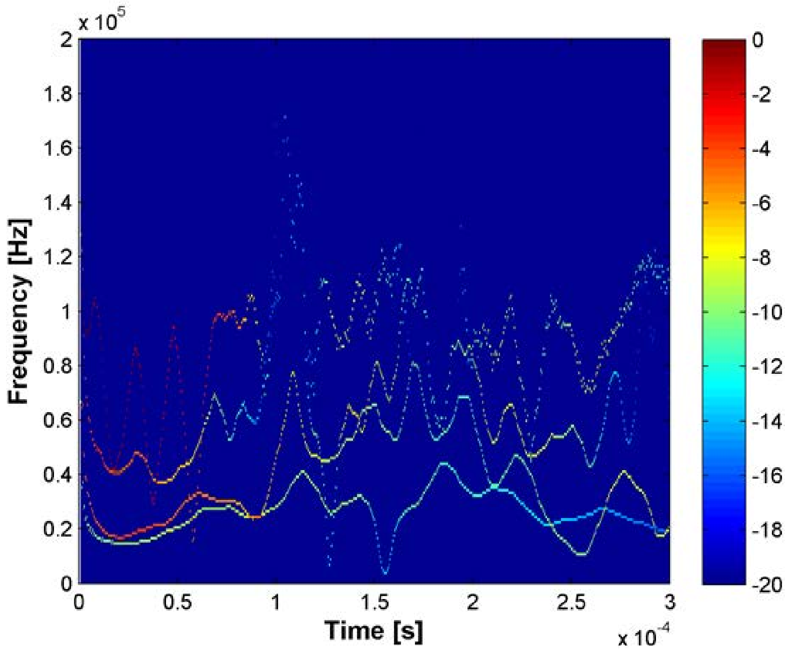

(c)

Figure 4.14 (continued)

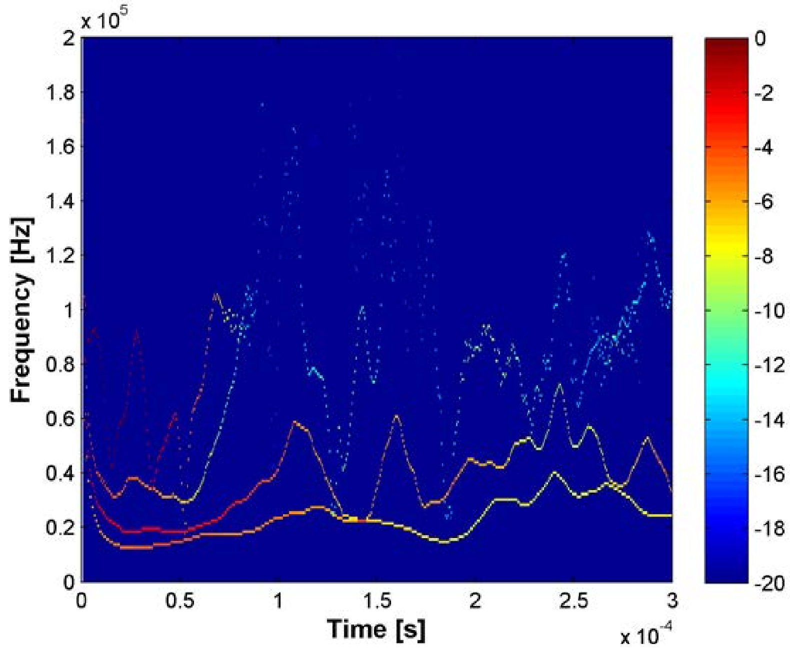

(d)

Figure 4.14 (continued)

To achieve a quantitative analysis, energy ratio (R_j) of each *IMF* c_j is calculated using the following equation

$$R_j = E(\mathrm{c}_j) / \sum_{j=1}^{n} E(c_j) \times 100\%, \tag{4.8}$$

where $E(\mathrm{c}_j)$ is the equivalent energy of *IMF* c_j, obtained by accumulating the squares of signal amplitudes of c_j in the time domain. The energy ratios of first three *IMFs* and their summation ($R_{1\text{-}3}$) along with the ratio of residual *IMFs* ($R_{Residual}$) are obtained and displayed in **Figure 4.15**.

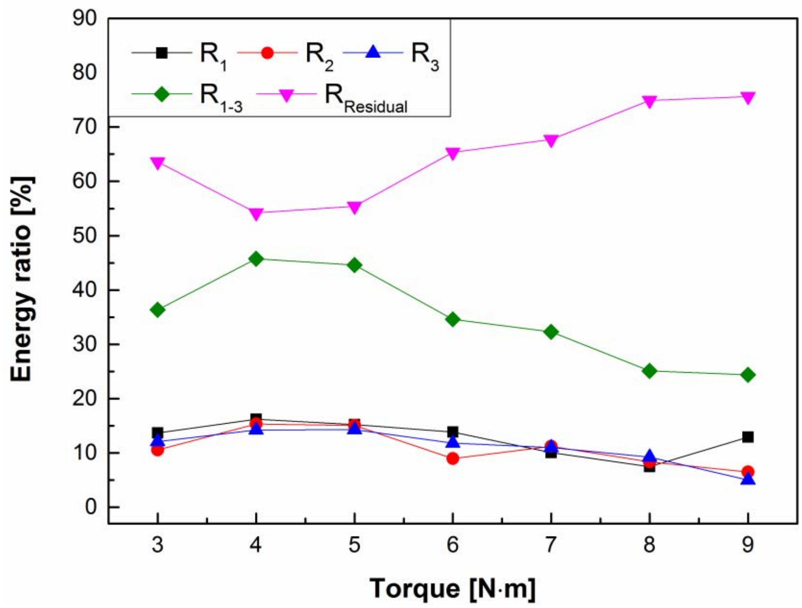

Figure 4.15 Energy ratios of *IMF* components decomposed from the *AE* signals from joints under different torques

R_2 and R_3 are found to decrease when the torque applied on the bolt increases from 4 to 9 N·m, while an observable increase presents in R_1 when the torque increases to 9 N·m, which is inferred to be correlated to the surface damage as mentioned above. With usage of $R_{Residual}$ and $R_{1\text{-}3}$, changes of bolt torque in the range between 4 and 9 N·m can be detected. The *HHT*-processed characteristics of signal show a better sensitivity to early bolt loosening compared to amplitude-dependent technology as shown in **Figure 4.10**.

4.2.3. Case Study II: Effect of Applied Torque on Fatigue Performance of Joints

From previous analysis, it can be concluded that the decrease in bolt torque results in a reduce in the interfacial pressure and an augment in the sliding distance between contact surface. As a consequence, more asperities with relative small sizes feature weak contacts and produce more high-frequency *IMFs* in the *AE* signals. To validate the efficiency of proposed *AE* method in the continuous monitoring of bolt loosening, in this section, four bolted composite joints (see **Figure 4.16**) under 3, 5, 7 and 9 N·m are fatigued for 2 hours simultaneously and monitored by using the *HHT*-based characteristics of *AE* signals.

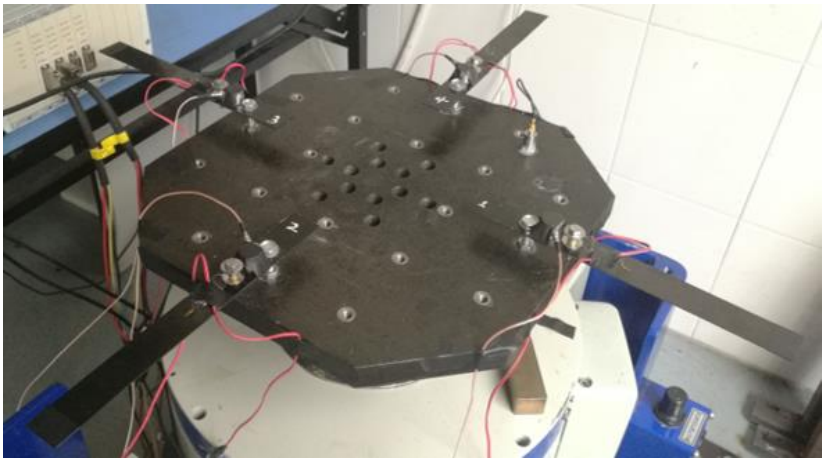

Figure 4.16 Experimental set-ups for collecting *AE* signals in four bolted joints under fatigue

During the vibration fatigue, the *AE* signals and compressive strain of the bolt (indicating the residual torque), are continuously registered in the *AE* device and strain indicator, respectively. The accumulated energy of the original *AE* signals generated in the four joints and the changes in the compressive strain of the bolts are plotted over time in **Figure 4.17** (a) and (b), respectively. The slope of the energy curves represents energy release rate of asperity contacts, which can be used to indicate the stability of the bolted joints under fatigue. From **Figure 4.17**(a), it can be found that the *AE* signals generated in the bolted joint under 3 N·m exhibit most frequent changes in the energy release rate. While the *AE* signals generated in the bolted joint under 7

N·m exhibit a relative low energy release rate, which indicates a stable contact condition of the bolted joint under this torque. However, cumulative energies of the *AE* signals from the joints under torques of 7 N·m and 9 N·m are similar during the fatigue process and such similarity also occurs in the curves for the joints under torques of 3 N·m and 5 N·m in the first fatigue hour.

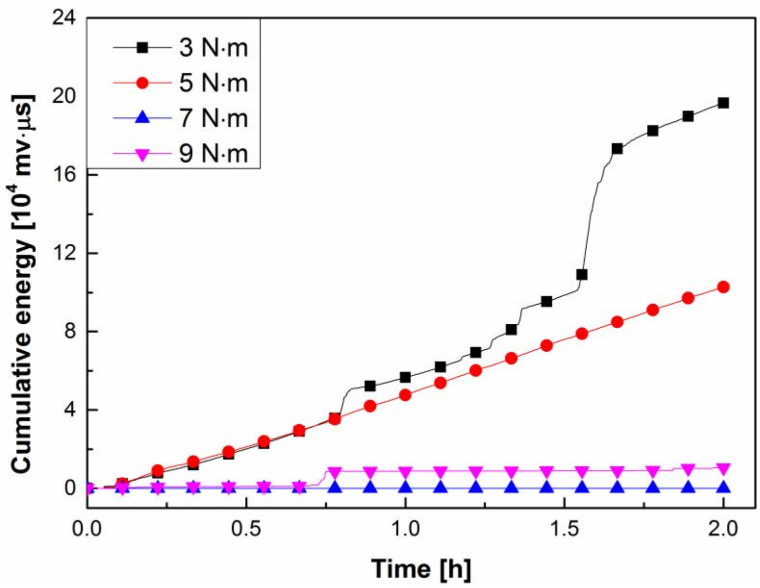

(a)

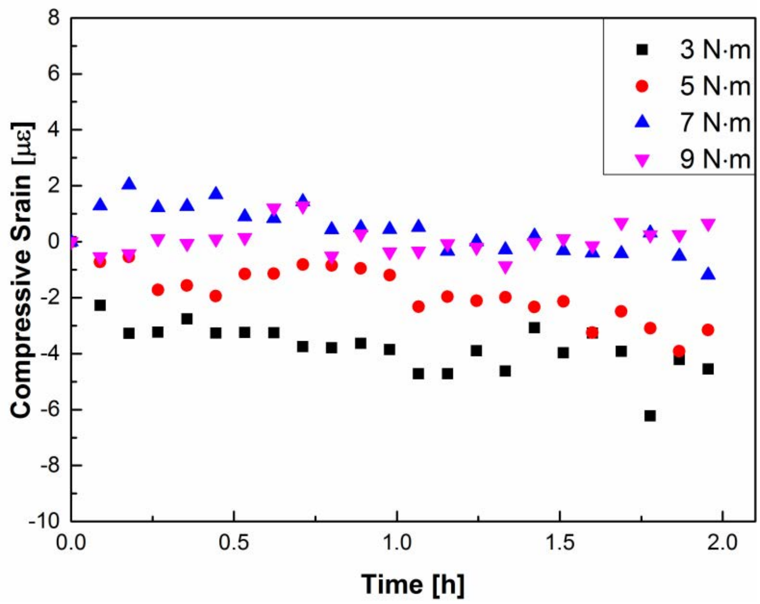

(b)

Figure 4.17 (a) Cumulative energy of the *AE* signals captured from the bolted joints under fatigue; and (b) reductions in the compressive strain of related bolts

In **Figure 4.17** (b), the degree of bolt loosening, evaluated by the decrease in the compressive strain, is found to decrease with an increase in the applied torque when it is not larger than 7 N·m. From the comparison between **Figure 4.17** (a) and (b), the released energy of the *AE* signals, to some extent, is found to be capable of qualitatively detecting the state of a bolted joint under vibration fatigue, but not capable of identifying the influence of applied torque on the fatigue process of bolted joints under vibration.

To further quantitatively detect tightening condition of the bolted joints under different torques when subject to vibration fatigue using the *AE* technology, *HHT*-processed *AE* signals regarding time-frequency characteristics are to be discussed in what follows. *HHT* spectra of the *AE* signals (average of 300 signals) from the joints under 3 N·m and 7 N·m over fatigue are comparatively shown in **Figure 4.18** (a)-(d).

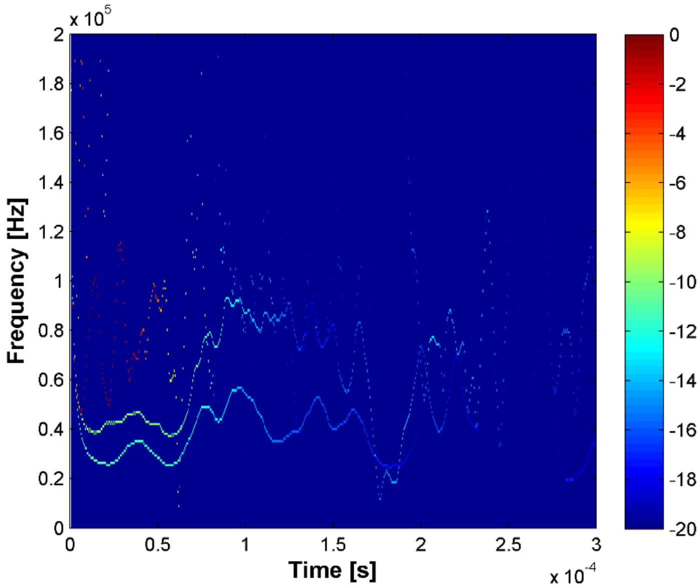

(a)

Figure 4.18 Hilbert-Huang spectra of the *AE* signals from the joint under 3 N·m before (a) and after (b) fatigue; from the joint under 7 N·m before (c) and after (d) fatigue

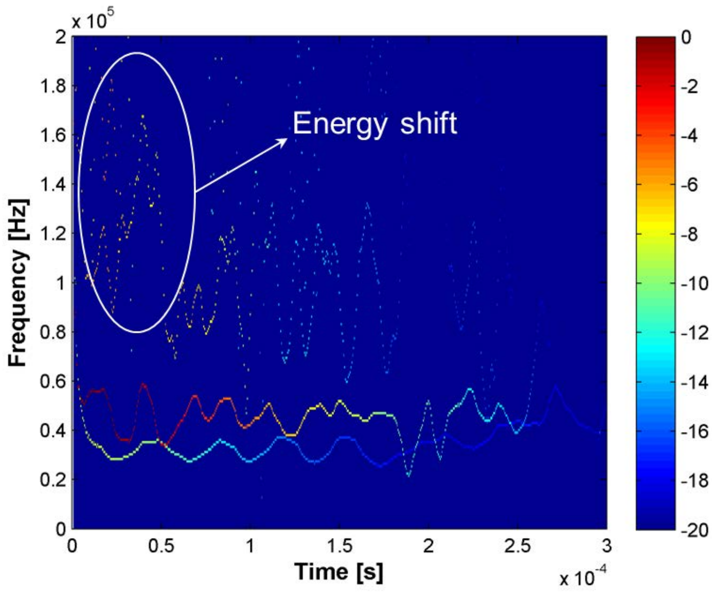

(b)

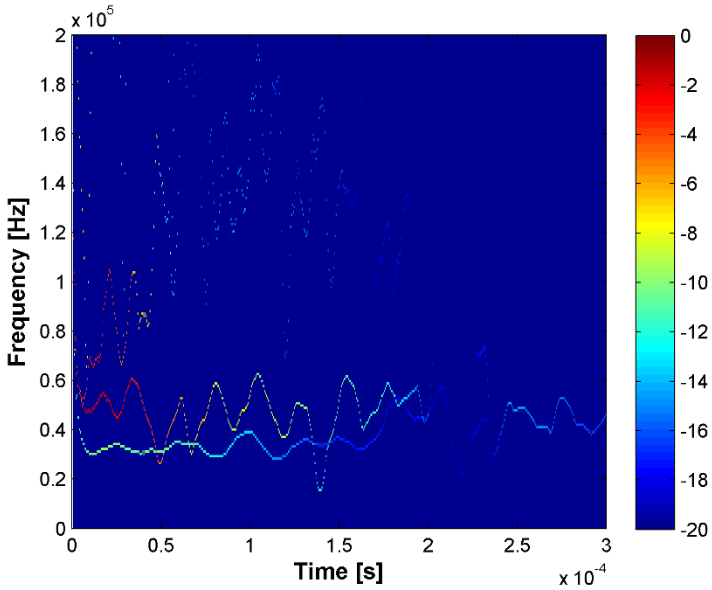

(c)

Figure 4.18 (continued)

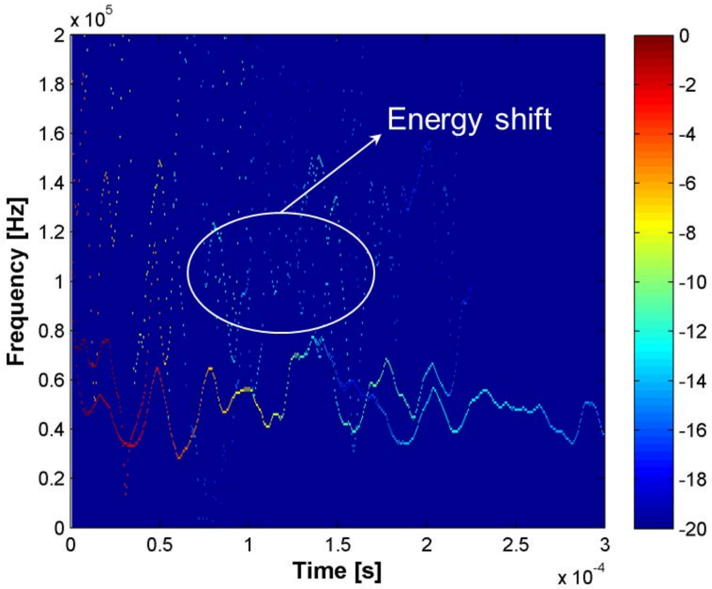

(d)

Figure 4.18 (continued)

To observe that *C-C* contact-related (i.e., high-frequency) *IMFs* become stronger and distribute in a wider time range after fatigue.

The evolution of energy ratios of first three *IMF* components of the *AE* signals generated from the bolted joints under different torques over fatigue is exhibited in **Table 4. 1**. For the joints under 3, 5 and 7 N·m, the energy ratios of residual *IMFs* decrease with some fluctuations over fatigue time, which indicates the high-frequency *IMFs* become more intensive after fatigue and is consistent with results as shown in **Figure 4.18**. While for the joint under 9 N·m, the energy ratio of residual *IMFs* firstly decreases in the first hour and after then it increases.

Table 4. 1 Evolution of energy ratios of *IMF* components decomposed from the *AE* signals from the bolted joints under different torques over fatigue (unit: %)

	3 N·m				**5 N·m**			
Time/h	R_1	R_2	R_3	$R_{Residual}$	R_1	R_2	R_3	$R_{Residual}$
0	23.68	15.44	06.32	54.56	12.07	5.44	4.96	77.53
0.5	11.11	10.78	09.72	68.39	11.00	6.66	4.63	77.71
1.0	26.41	17.06	11.93	44.60	15.11	9.32	9.44	66.13
1.5	28.93	20.95	16.33	33.79	11.13	0.94	8.14	79.79
2.0	29.54	19.80	14.06	36.60	16.34	9.77	6.61	67.28
	7 N·m				**9 N·m**			
Time/h	R_1	R_2	R_3	$R_{Residual}$	R_1	R_2	R_3	$R_{Residual}$
0	14.69	8.77	5.33	71.21	12.31	6.85	2.22	78.62
0.5	9.89	6.22	4.28	79.61	11.81	8.07	6.31	73.81
1.0	9.49	4.33	2.78	83.40	14.29	9.71	6.59	69.41
1.5	10.82	3.81	1.53	83.84	10.60	8.07	6.55	74.78
2.0	10.68	9.13	9.03	71.16	9.73	4.01	3.05	83.21

Upon further comparison between variation of compressive strain of the bolts and changes in the energy ratios of residual *IMFs*, as shown in **Table 4. 2**, a considerable consistency in between can be concluded.

Table 4. 2 Variation of compressive strain ($\Delta\varepsilon$, unit: $\mu\varepsilon$) and energy ratios of residual components ($\Delta R_{Residual}$, unit: %) over fatigue

	3 N·m		**5 N·m**	
Time/h	$\Delta\varepsilon$	$\Delta R_{Residual}$	$\Delta\varepsilon$	$\Delta R_{Residual}$
0	0	0	0	0
0.5	-3.72	13.83	-1.48	0.18
1.0	-2.34	-9.96	-1.27	-11.4
1.5	-5.4	-20.77	-2.2	2.26
2.0	-5.36	-17.96	-3.02	-10.25
	7 N·m		**9 N·m**	
Time/h	$\Delta\varepsilon$	$\Delta R_{Residual}$	$\Delta\varepsilon$	$\Delta R_{Residual}$
0	0	0	0	0
0.5	0.74	8.4	-0.56	-4.81
1.0	0.41	12.19	-1	-9.21
1.5	-0.69	12.63	-0.01	-3.84
2.0	-0.88	-0.05	0.98	4.59

As representative results, tightening torque of the joint under 9 N·m decreases in the first 1.5 h and increases after then. Such a change trend presents in the energy ratio of residual *IMFs*. Therefore, the *HHT*-based characteristics of *AE* signals outperform the amplitude (energy)-based *AE* method in the continuous evaluation of tightening condition of the bolted composite joints under vibration fatigue.

To conclude, evaluation of tightening condition of bolted composite joints subject to vibration is attempted by directly analyzing the asperity contacts at the *C-C* interface using the *HHT*-based characteristics of *AE* signals in this study. The following conclusions can be drawn according to the experimental findings.

(1) *HHT* shows a higher time-frequency resolution when processing bolt loosening-induced *AE* signals, which possess non-stationary characteristics, compared to *STFT*;

(2) *AE* signals induced by asperity contacts at different contact interfaces (i.e., *C-C* and *M-C* contacts) in bolted composite joints can be discriminated by comparing the time-presentation envelopes and the time-frequency distribution of the *IMFs* in the *HHT* spectrum;

(3) The gross energy of *AE* signals shows a considerable sensitivity to changes in the residual torque of a bolted composite joint in a limited range. Such method fails to quantitatively detect the tightening condition of joints under vibration fatigue. With usage of *HHT*-based signal characteristics, energy ratios of high-

frequency *IMFs* induced by the *C-C* contact achieve an enhanced sensitivity to the decrease in bolt torque. Bolt loosening results in increases in the energy-ratios of the *C-C* contact-related *IMFs*. Based on this, vibration loosening of bolted composite joints under different torques is quantitatively correlated to the increase of energy ratios of *C-C* contact related *IMFs*. On this basis, continuous evaluation of bolted composite joints under vibration fatigue is achieved by the *HHT*-processed characteristics of *AE* signals.

4.3. Active Linear Method: Modal Parameters-based

In this section, vibration modal parameters, including both resonant frequency and damping ratio are comparatively adopted to evaluate the residual torque of the bolted composite joint. The beam specimens were cut from sheets of laminated T700/7901 carbon-fiber-reinforced epoxy, obtained using hot pressing with a stacking sequence $[90, 0]_{4s}$. Specimens were 2 mm thick and 30 mm wide. A beam with a length of 50 mm was assembled with another beam with lengths of 70, 100, 150 mm to form three types of bolted joints, termed as L70, L100 and L150, respectively. The setup as shown in **Figure 4.19**, used to obtain modal parameters of the joint under different torques, consists of test specimens, fixtures, a displacement sensor (Donghua 5E106) and a dynamic strain indicator (Donghua 5923N). The joint was clamped vertically with one end fixed (i.e., the beam with a length of 50 mm) by the fixtures. During the modal test, impact forces were applied at different points of the specimen and the displacement meter was used to measure the displacement response at a sampling frequency of 10 kHz.

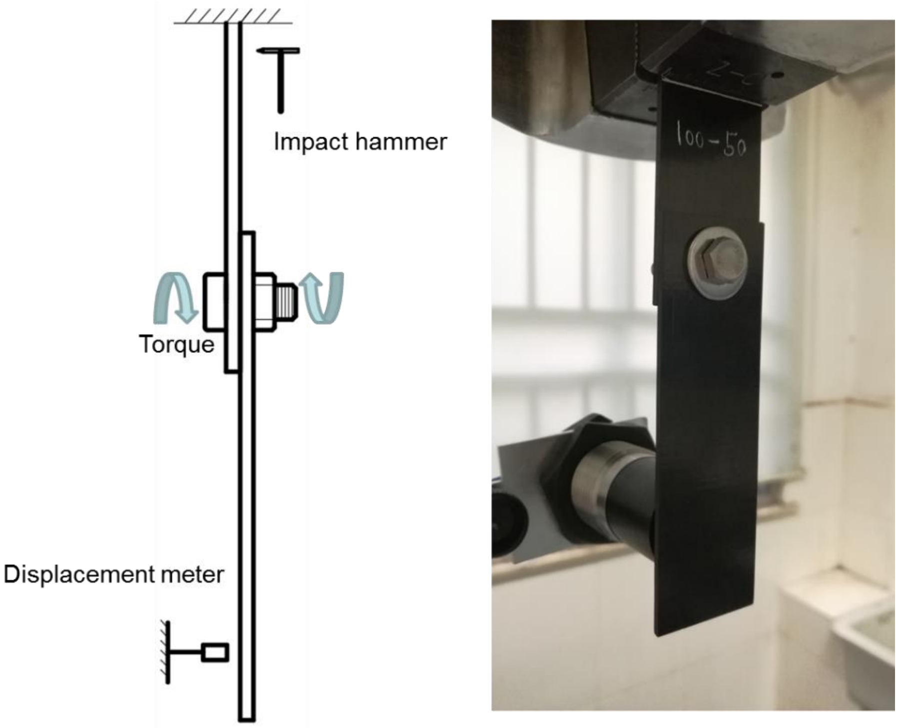

Figure 4.19 Experimental setups of impact testing for bolted composite joints

A typical displacement response of a specimen subject to an impact force is shown in **Figure 4.20** and damping ratio (η) of the specimen is calculated by fitting the envelope of free decay curve with the following equation

$$y = Ae^{2\pi\eta t}. \tag{4.9}$$

On the other hand, resonant frequency of the specimen is ascertained in the frequency spectrum obtained by applying *FFT* on the displacement response, as shown in **Figure 4.21**. For three types of joints, a torque of 13 N·m guarantees a full tightness of the bolt. Making reference to the state of full tightness, a series of 13 scenarios was considered, with the residual torque remained on the bolt varying from 1 (fully loosened) to 13 N·m (fully tightened) at an increment of 1 N·m. Under each scenario, signal acquisition was repeated three times and averaged to minimize operational errors and measurement uncertainties.

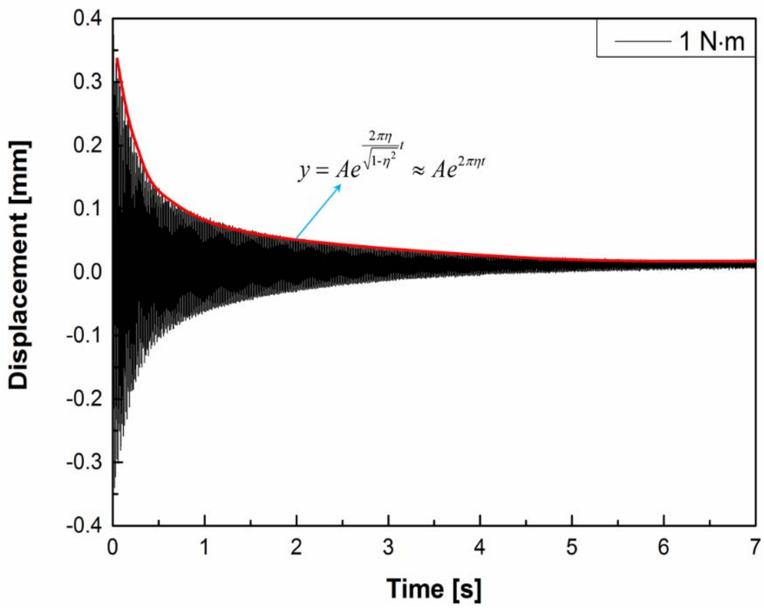

Figure 4.20 Free decay curve regarding response displacement of a joint subject to an impact force

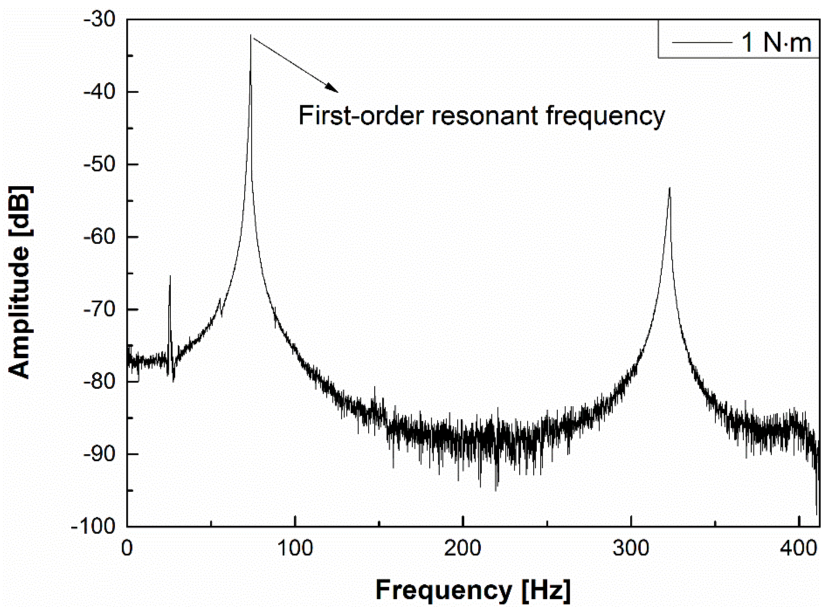

Figure 4.21 Typical frequency response function of a joint subject to an impact force

For the sake of avoiding involvement of air damping, which is linearly dependent on the excitation magnitude, damping ratio of the three joints subject to varied excitation intensity are obtained, as shown in **Figure 4.22**, **4.24** and **4.26**, respectively. Subsequently, the intercept of the curve, which represents damping ratio of a joint measured from a "zero" excitation magnitude, is taken as damping ratio of the joint in this thesis.

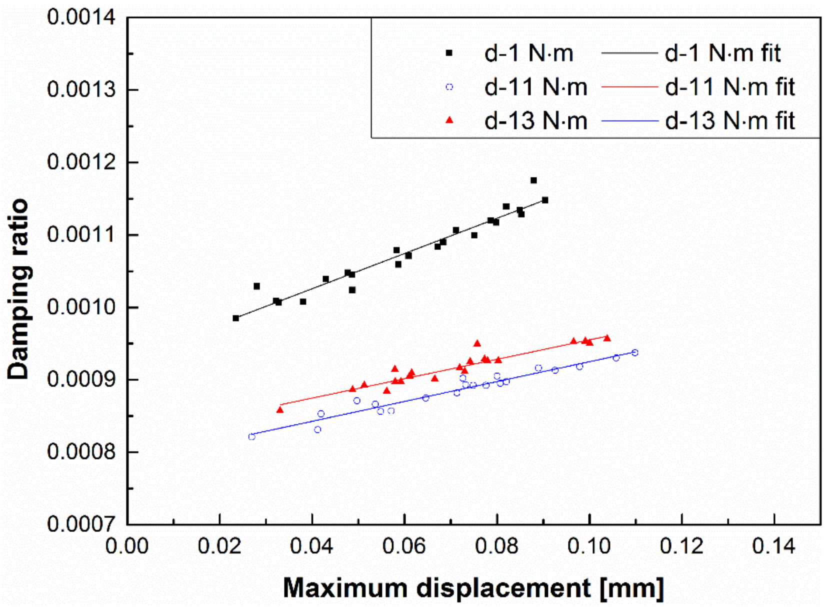

Figure 4.22 Dependence of damping ratio of the joint (L150) on the excitation intensity

From the results in terms of damping ratio and resonant frequency of the three types of joints under increasing torques, as displayed in **Figure 4.23**, **4.25** and **4.27**, respectively, it can be concluded that in a certain torque range damping ratio increases while resonant frequency decreases with an augment in the applied torque. Take the L150 joint as a representative result, damping ratio decreases starting at 1 N·m until the applied torque reaches 11 N·m, after which it presents an increasing trend.

Whereas, resonant frequency increases starting from 1 N·m until a preload of 9 N·m is reached, after which it stabilizes with increase in preload. This implies that pressure applied on the joining material induced by a torque of 9 N·m is close to or exceeds the compressive yield strength of connecting material in the thickness direction.

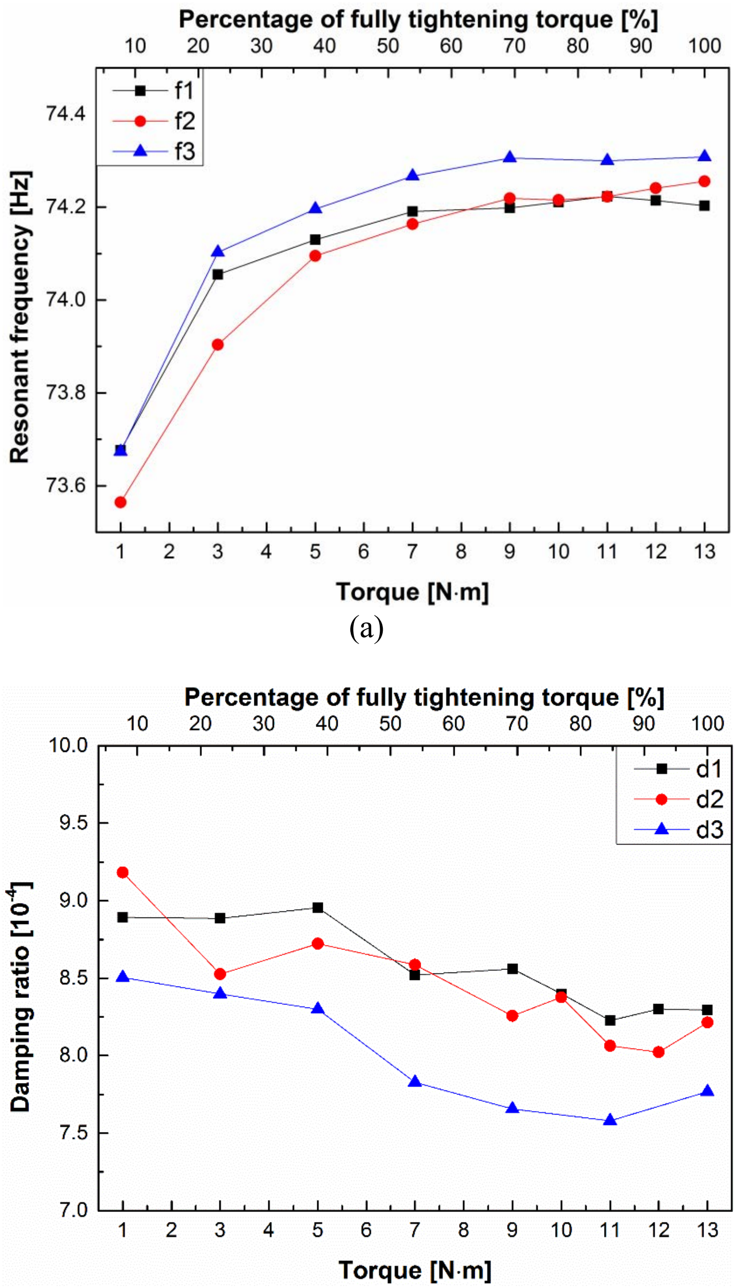

(a)

(b)

Figure 4.23 Reliance of modal parameters of the joint (L150) on the applied torque:(a) resonant frequency; and (b) damping ratio

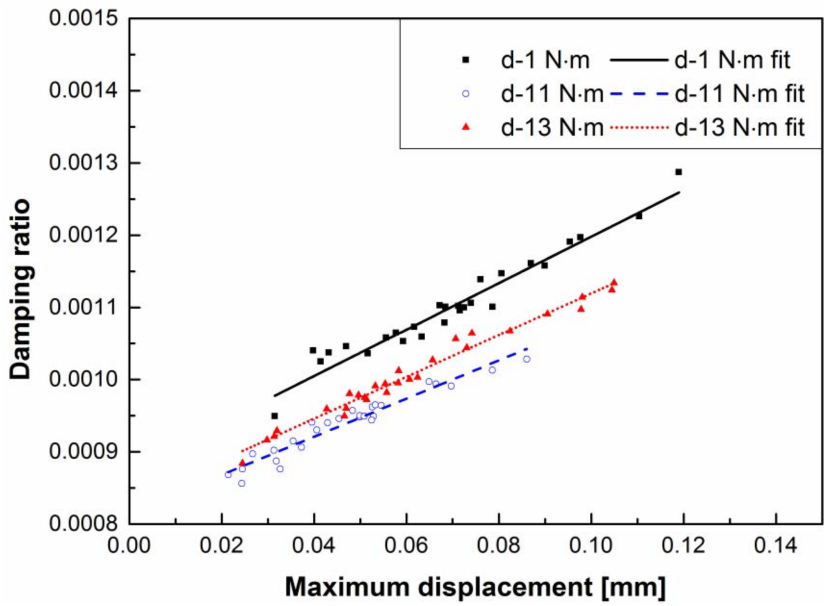

Figure 4.24 Dependence of damping ratio of the joint (L100) on the excitation intensity

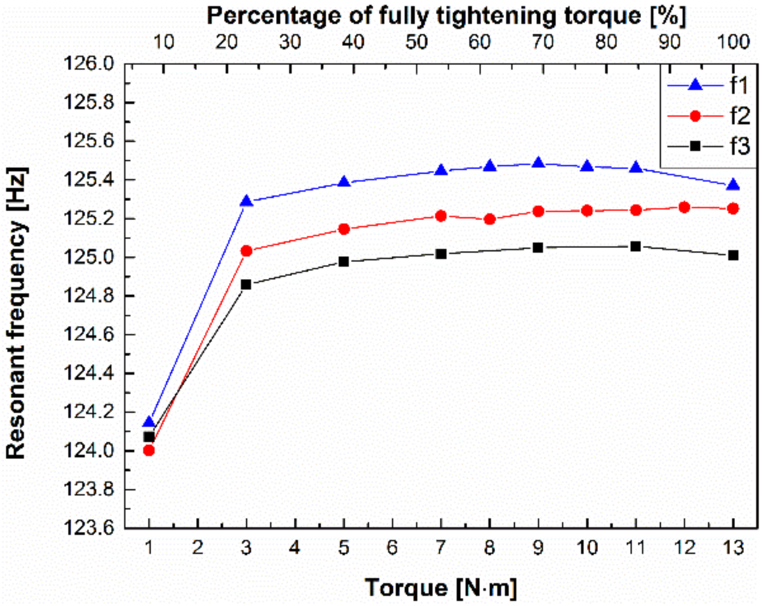

(a)

Figure 4.25 Reliance of modal parameters of the joint (L100) on the applied torque:(a) resonant frequency; and (b) damping ratio

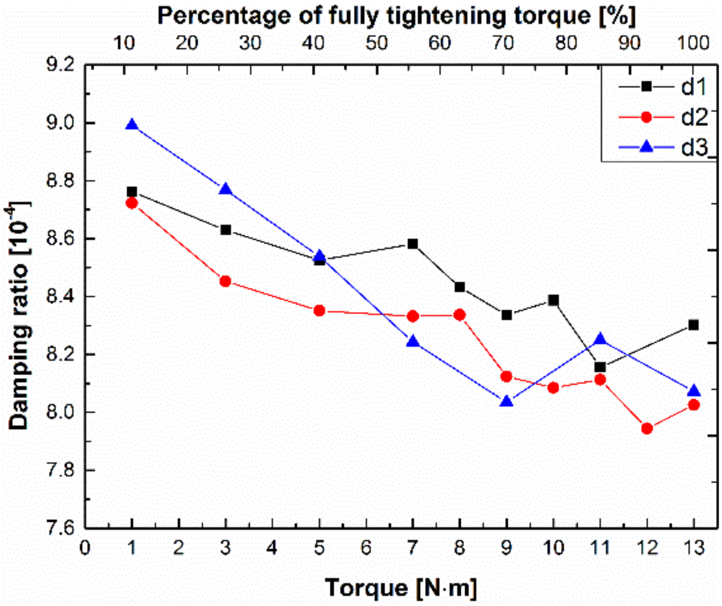

(b)

Figure 4.25 (continued)

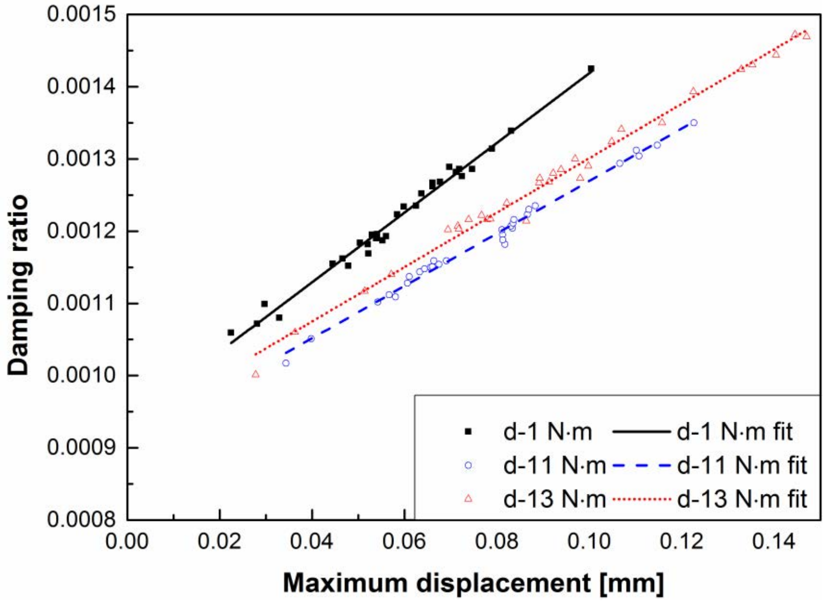

Figure 4.26 Dependence of damping ratio of the joint (L70) on the excitation intensity

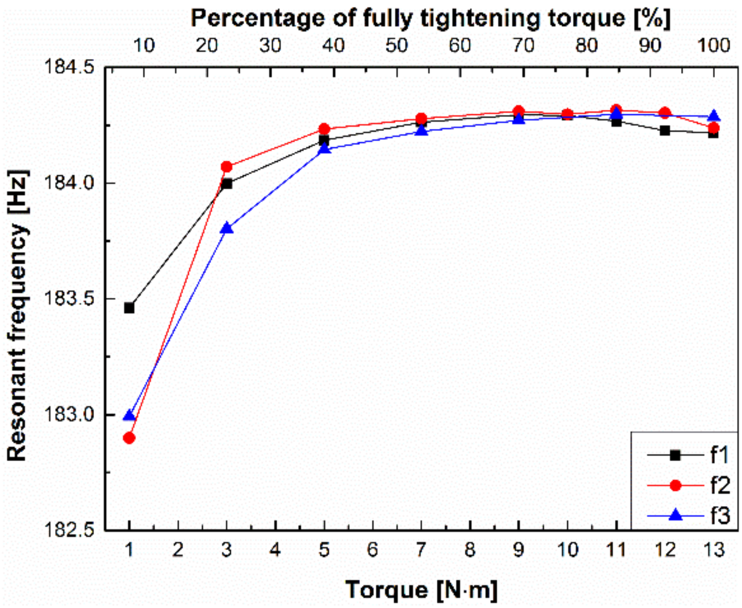

(a)

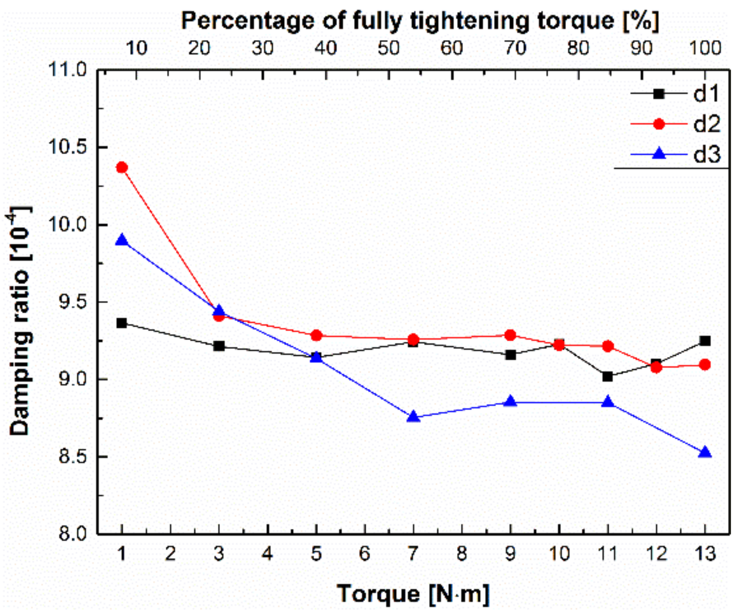

(b)

Figure 4.27 Reliance of modal parameters of the joint (L70) on the applied torque:(a) resonant frequency; and (b) damping ratio

To sum up that damping ratio is found more sensitive to preload changes in comparison to resonant frequency. However, such a method using damping ratio is not capable of evaluating the early bolt loosening with a satisfactory stability, which is critically important to avoid drastic failure of bolted structures in real practice.

4.4. Active Linear Method: *WED*-based

In this section, *WED*-based method using linear features of *GUWs* is comparably employed to characterize bolt loosening for both *Al-Al* and *C-C* bolted joints. The dependence of *WED*-based method on joint configurations will be presented through comparisons of performance with respect to bolt loosening evaluation in multi-type *Al-Al* joints, namely single-lap, cross-lap and hybrid-lap. In addition, limitation of this method in the application of identifying loose bolts in the composite structures with bolted joints are to be discussed through observations on the detectability in both single-lap *Al-Al* and *C-C* bolted joints.

4.4.1. Case Study I: Detection of Bolt Loosening in Multi-type *Al-Al* Bolted Joints

In Chapter 3, *WED* of *GUWs* is quantitatively linked to the residual torque of a loose bolt as

$$\Omega_{leak} \propto T^{2/3} \text{ and } \Omega_{transmitted\ in\ I} \propto -T^{2/3}. \qquad \textbf{(4.10)}$$

The proposed inspection framework is validated experimentally in this section. Three types of *Al-Al* bolted joints, including a single-lap (Type I), a cross-lap (Type II) and a hybrid (comprising both single- and cross- laps) (Type III) bolted aluminum alloy joints, were considered, as shown in **Figure 28**. (a)-(c), respectively. In particular, the hybrid joint (Type III) was aimed at testifying the performance of such linear acoustic method towards multi-type joints. Dimensions of each joint are indicated in **Figure 4.28** (a)-(c). The right end of each joint was fixed to form a cantilever. M6 bolts were used in all the three connections. The experimental set-ups for the three types of joints are photographed in **Figure 4.29** (a)-(c), respectively.

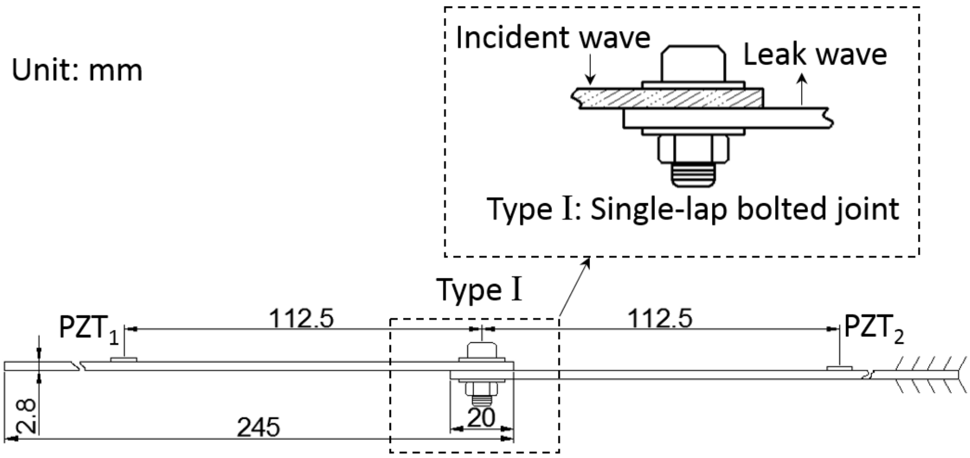

(a)

Figure 4.28 Specimen configurations for *WED*-based linear method: (a) single-lap (Type I); (b) cross-lap (Type II); and (c) hybrid-lap (Type III)

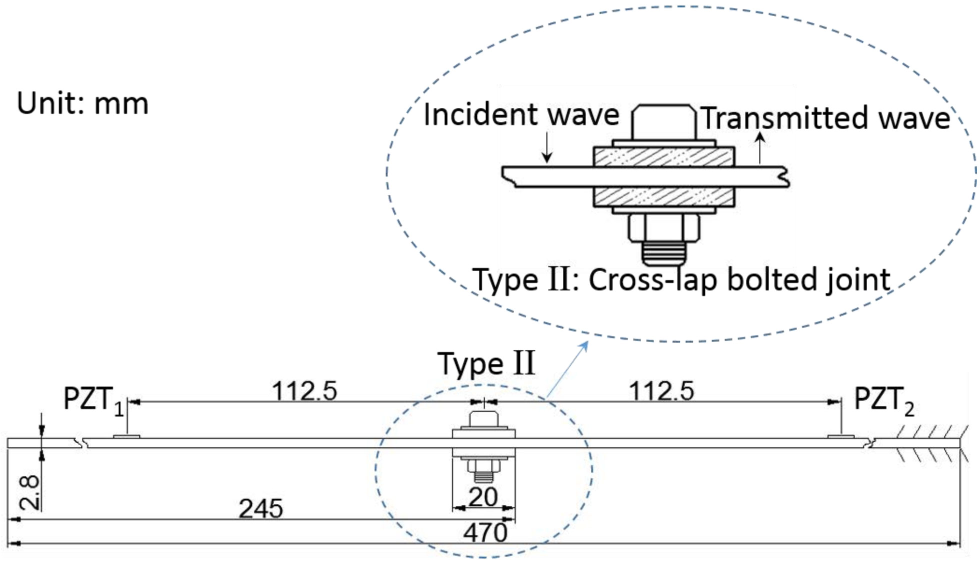

(b)

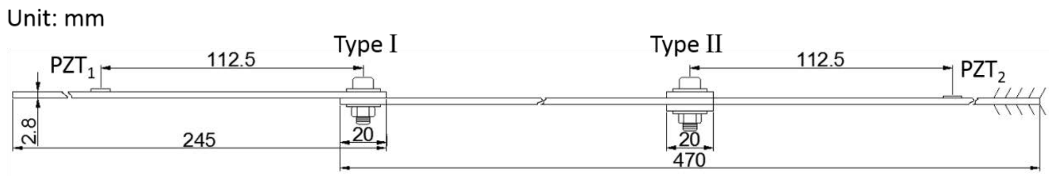

(c)

Figure 4.28 Specimen configurations for *WED*-based linear method: (a) single-lap (Type I); (b) cross-lap (Type II); and (c) hybrid-lap (Type III)(continued)

Two PZT wafers were surface-mounted on each joint, 112.5 mm from the bolt, one serving as the actuator (PZT_1) and the other as the sensor (PZT_2). A 14-cycle Hanning window-modulated sinusoidal tone-burst signal at a central frequency of 310 kHz was generated using a signal generator (NI® PXIe-1071), amplified with a high-frequency power amplifier (Ciprian® US-TXP-3) to 200 V (peek-to-peak), and then applied on PZT_1, to introduce *GUWs* into the joint. At the frequency of 310 kHz, *GUWs* with a strongest response magnitude were excited, which was subsequently chosen as the excitation frequency. Wave propagation, upon traversing the bolt, was monitored by

PZT2 using an oscilloscope (Agilent® DSO9064A) at a sampling frequency of 20 MHz. Captured *GUWs* were averaged 64 times to remove random measurement noise.

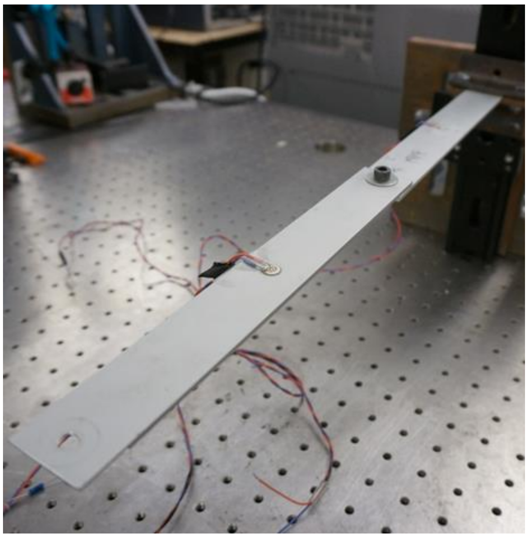

(a)

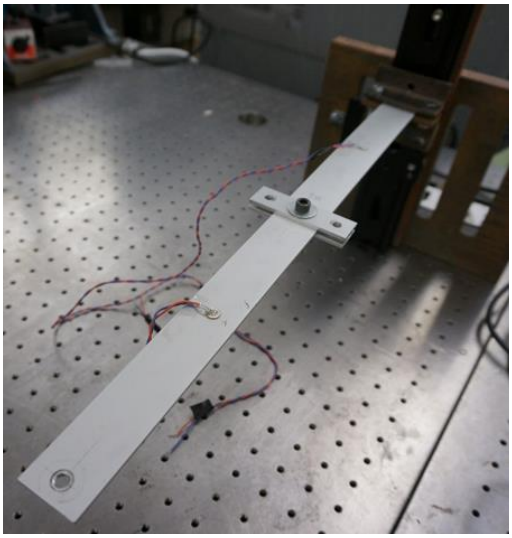

(b)

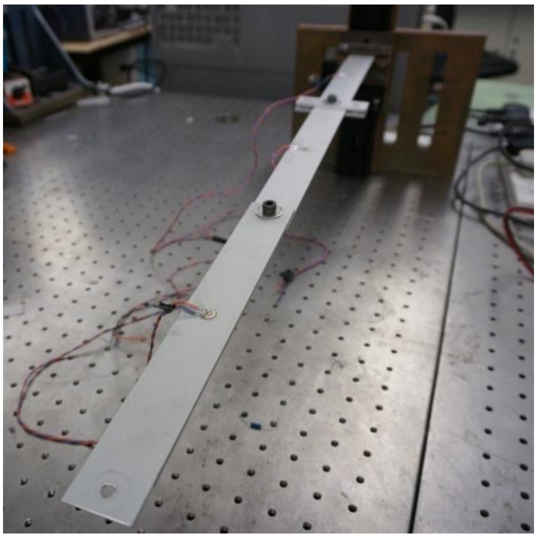

(c)

Figure 4.29 Photographed experimental set-ups for *WED*-based linear method: (a) single-lap (Type I); (b) cross-lap (Type II); and (c) hybrid-lap (Type III)

FFT was performed on captured signals, to ascertain distribution of wave energy in the frequency domain. As representative results, **Figure 4.30** (a) shows a raw signal captured from Type I joint, when T was 1 N·m under which the bolt was fully loose, and **Figure 4.30** (b) is the *FFT*-processed spectrum of the signal in (a).

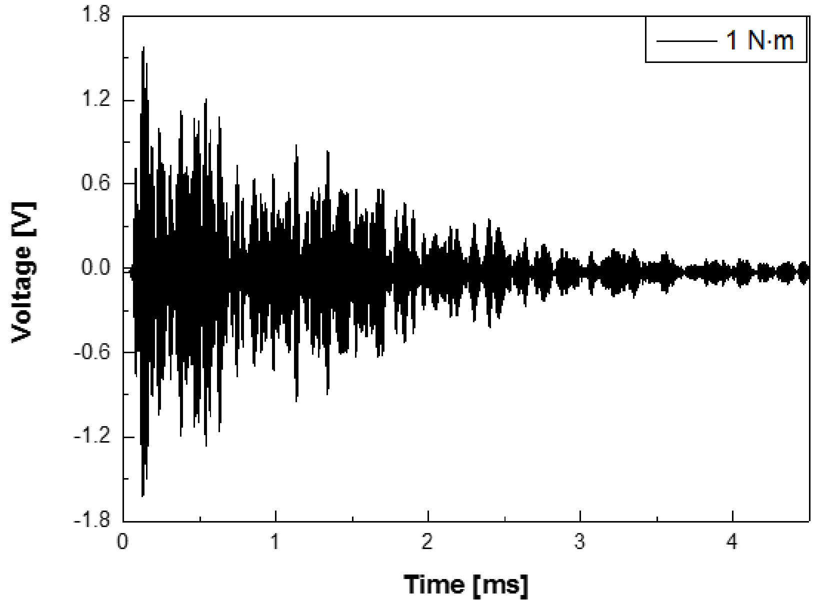

(a)

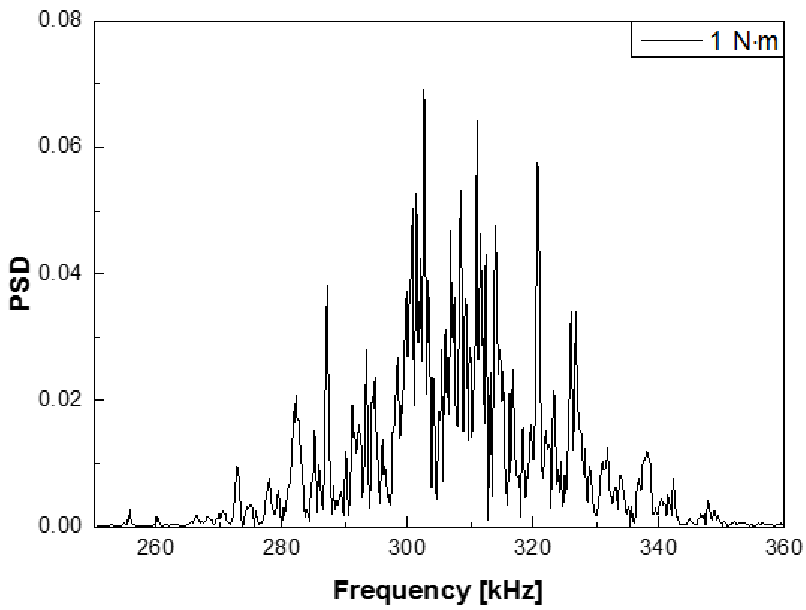

(b)

Figure 4.30 (a) Acquired *GUWs* upon traversing the matting part of the single-lap bolted joint; and (b) spectrum of the signal shown in (a)

A wide range of the energy distribution can be observed in the spectrum which can be attributed to the dispersive and multi-modal traits of *GUWs* propagating in the joint. The majority of the wave energy is observed to be in a range from 270 to 350 kHz.

To establish Ω_{leak} and $\Omega_{transmitted\ in\ I}$ (i.e., the linear index based on *WED*), the power spectral density (*PSD*) of each signal in the spectrum (denoted by $W(f)$), where f signifies frequency) was integrated within a frequency range [f_1, f_2] over which the signal possesses the majority of its energy (in this case, $f_1 = 270\ kHz$ and $f_2 = 350\ kHz$ as mentioned in the above), as

$$\Omega_{leak} = \int_{f1}^{f2} W(f) \cdot df, \text{ (for single-lap joint)} \quad \textbf{(4.11)}$$

or

$$\Omega_{transmitted\ in\ I} = \int_{f1}^{f2} W(f) \cdot df. \text{ (for cross-lap joint)} \quad \textbf{(4.12)}$$

Taking into account the yielding strength of the selected aluminum alloy and the allowable tensile load of the bolt, it was calculated that a torque (T) of 13 N·m, at which a compressive stress of about 300 MPa would be applied on the bolt, guarantees a full tightening of the bolt. Based on this, a series of scenarios were considered in experiment, with the residual torque T varying from 1 (full loosening) to 13 N·m (full tightening) with a step of 1 N·m. Note that in Type III (hybrid joint), the torque values applied on both bolts were identical for the convenience of discussion.

For Type I joint, the obtained correlation between the linear index (i.e., Ω_{leak} defined by **Equation (4.11)**) and the degree of bolt loosening (represented by T) is shown in

Figure 4.31(a), from which it is noticed that the linear index Ω_{leak} increases drastically when T augmenting from 1 (full loosening) to 3 N·m, followed with a moderate increase until T reaches 7 N·m and then a saturation afterwards. Such a monotonic relationship can be attributable to the fact a tighter bolting naturally leads to a greater interfacial area at the interface, and consequently a greater amount of leak of incident wave energy from Assembly I to II that is then captured by PZT_2; when T continues the increase to 7 N·m afterwards, no further increase in the real contact area could be created, echoing the observed saturation of the index beyond 7 N·m. This experimental observation well matches the tendency in the variation of transmitted wave energy as predicted theoretically by **Equation (4.10)**.

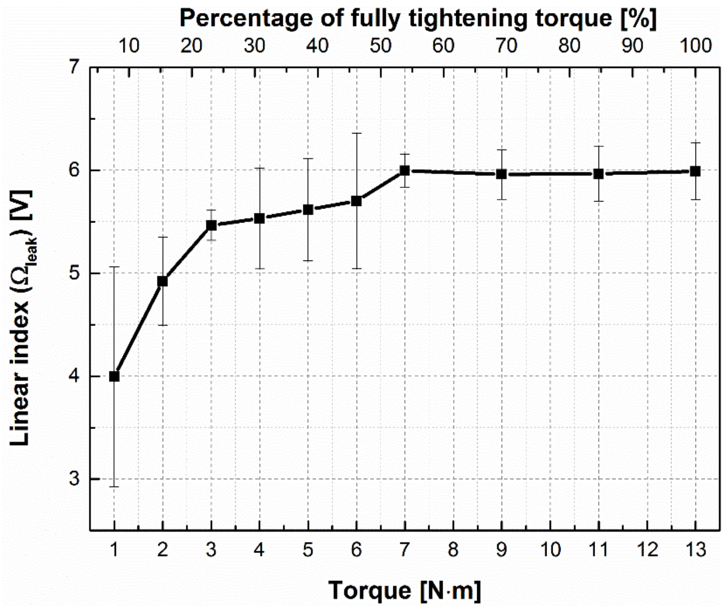

(a)

Figure 4.31 Linear index *vs.* residual torque T for different joints: (a) single-lap;(b) cross-lap; and (c) hybrid-lap

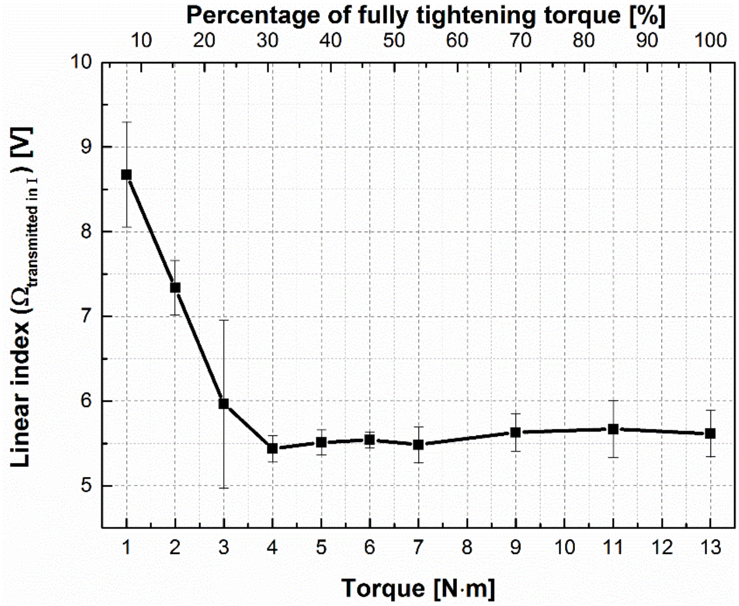

(b)

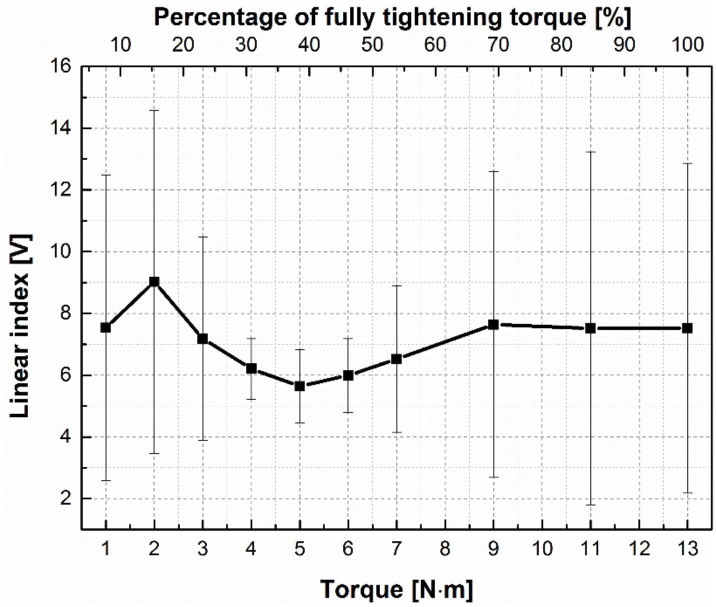

(c)

Figure 4.31 (continued)

For Type II joint, an opposite tendency in the linear index ($\Omega_{transmitted\ in\ I}$ defined by

Equation (4.12) subject to T , is found, shown in **Figure 4.31** (b). This observation is also coincident with the theoretical prediction in **Equation (4.10)** It is interesting to note that the results in **Figure 4.31** (a) and (b) indeed corroborate, respectively, the conclusions drawn from previous studies [1, 2] and [3] as detailed Chapter 2, in which an opposite trend in variation of *WED* had been observed for different types of joints.

For Type III joint, the trend of the linear index is displayed in **Figure 4.31** (c), revealing a non-monotonic change which fluctuates against T . This is a consequence of the mixture of the variation of Ω_{leak} in the single-lap joint (Type I) and the variation of $\Omega_{transmitted\ in\ I}$ in the cross-lap joint (Type II), which are contrary to one another.

Conclusion can thus be drawn that evaluation of bolt loosening, purely based on the *WED*-based linear method, may present good results only if a single type of joint is involved; it may not show consistent prediction provided multi-type joints are concerned – highlighting a bottleneck of the linear approach. In addition, it can be found that the linear index shows the best sensitivity to the bolt loosening in a limited range. For example, for Type I, this range is from 7 N·m down to 1 N·m (reflected as the steepest slope of the index in this range), and from 4 N·m down to 1 N·m for the cross-lap joint. To further extend its detectability, some improvements in *WED*-based method for the detection of bolt loosening, by using first-arrival wave packet of *GUWs* to avoid boundary reflection, are presented in what follows.

To fully understand the energy dissipation of *GUWs* when traversing the mating parts of a joint, the intact beam firstly went through a threaded hole drilling, and then was attached with two mass blocks to form a cross-lap bolted joint. These three statuses were comparably studied, as shown in **Figure 4.32**.

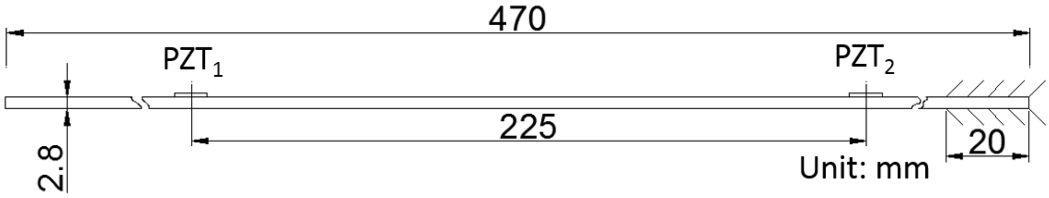

(a)

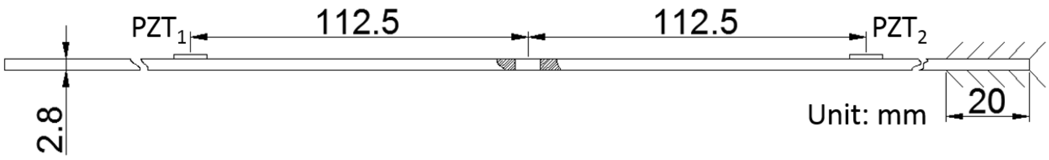

(b)

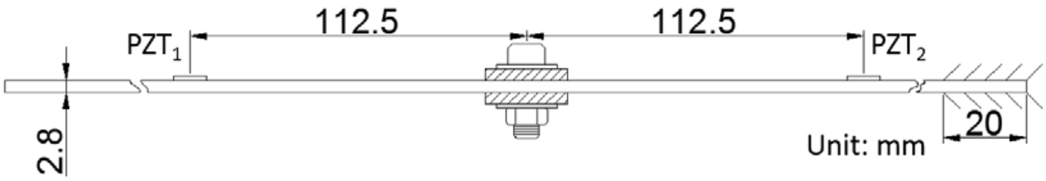

(c)

Figure 4.32 Specimen configurations for improved *WED*-based linear method: (a) an intact beam; (b) a beam with a thread hole; and (c) a cross-lap bolted joint

To reduce the complexity of signal appearance, low-frequency *GUWs* were selected to analyze their interaction with the mating parts of a joint [143]. Therefore, first-arrival wave packet of *GUWs* was selected for analysis of interaction with the cross-lap bolted joint under different applied torques.

HT was performed on captured signals to obtain the energy envelope of the signal. For an arbitrary time series *Y*(*t*), the *HT* is defined as [143]

$$H(t)=\frac{1}{\pi}\int_{-\infty}^{+\infty}\frac{Y(t^{'})}{t-t^{'}}dt^{'}. \tag{4.13}$$

Then analytic signal *Z*(*t*), of which the real part is the original signal *Y*(*t*) and the imaginary part is its *HT* *H*(*t*), can be constructed as

$$Z(t)=Y(t)+iH(t)=e(t)e^{i\phi(t)}. \tag{4.14}$$

The envelope *e*(*t*) and instantaneous phase $\phi(t)$ can be written as

$$e(t)=\sqrt{Y^{2}(t)+H^{2}(t)}\ \text{and}\ \ \phi(t)=\arctan\frac{H(t)}{Y(t)}. \tag{4.15}$$

Using **Equation (4.15)**, the transmitted energy was calculated by integrating the energy envelope in the time domain with different intervals, to ascertain the effect of boundary reflection. As representative results, the energy envelope of a complete signal traversing the mating parts of the cross-lap joint under a torque of 7 N·m (see **Figure 4.33** (a)) was obtained and shown in **Figure 4.33** (b)

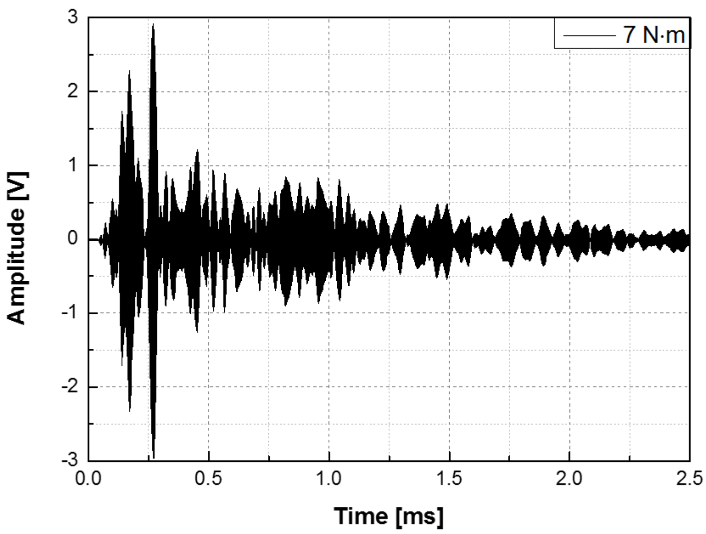

(a)

Figure 4.33 (a) Acquired *GUWs* upon traversing the mating part of the cross-lap bolted joint under 7 N·m and (b) energy envelope of the signal shown in (a)

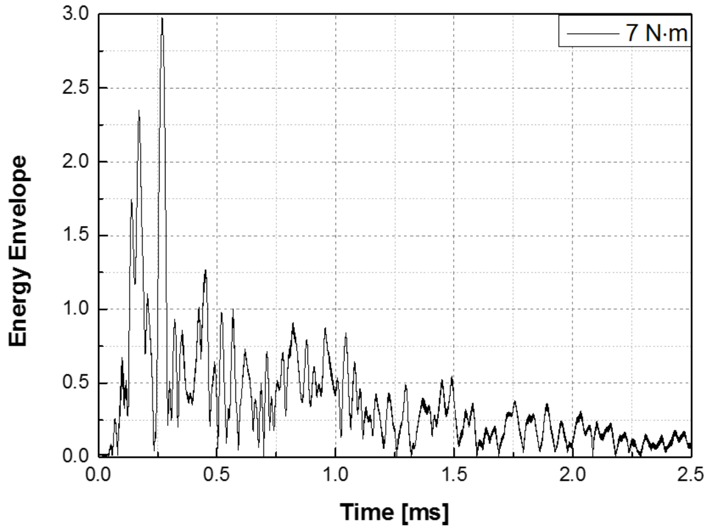

(b)

Figure 4.33 (continued)

It can be found that the energy envelope obtained by *HT* agrees well with the envelope of the original signal in the time domain. In addition, strong reflection can be observed in **Figure 4.33** (b). To avoid the effect of boundary reflection, proper time interval was intercepted to integrate the equivalent transmitted energy using the first-arrival wave packet of *GUWs*, through the comparative experiments on the three statuses in **Figure 4.32** (a)-(c).

In **Figure 4.34** (a)-(c), it is found that the first-arrival wave packet of *GUWs*, mainly distribute between 40 and 80 μs. From **Figure 4.34** (a), the energy of transmitted *GUWs* is found to decrease upon the drilling of the thread hole, which scatters the incident wave. After the beam was attached with the two mass blocks with increasing torques, the transmitted energy of first-arrival wave packet of *GUWs* continues decreasing (see **Figure 4.34** (b)). The corresponding energy envelopes shown in

Figure 4.34 (c) clearly show the mentioned reduction in the energy of first-arrival wave packet of *GUWs* due to the presence of thread hole and the increase in applied torque.

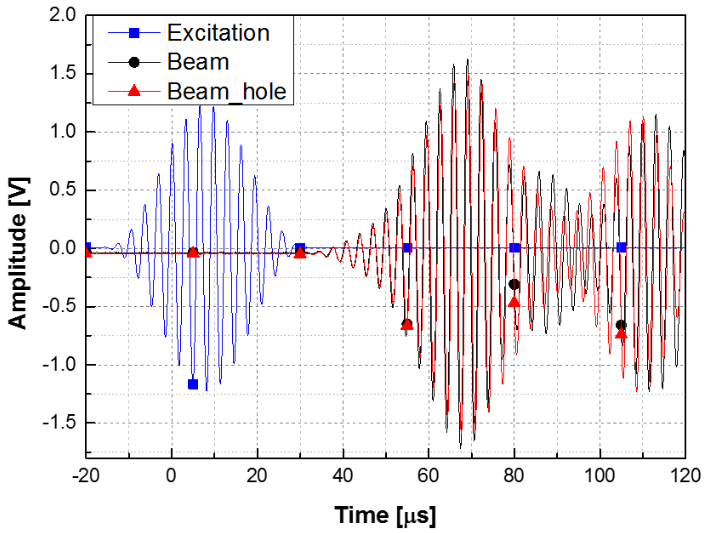

(a)

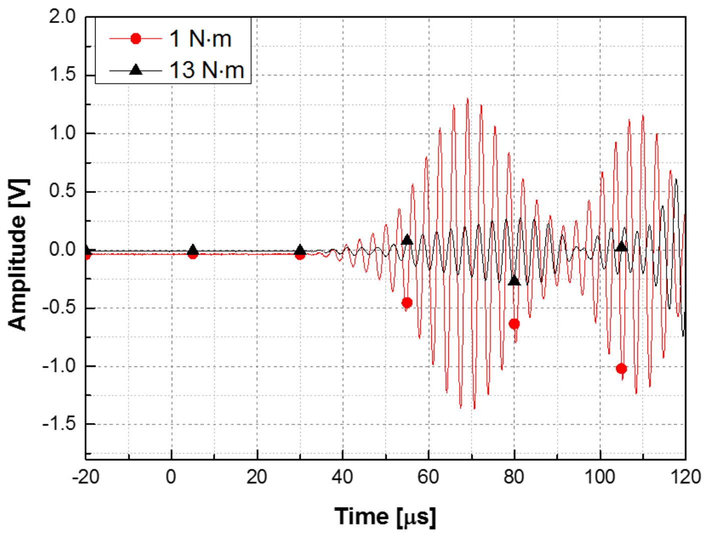

(b)

Figure 4.34 Acquired *GUWs* upon traversing (a) the beam; (b) the mating part of the cross-lap bolted joint; and (c) energy envelopes of the signals shown in (a) and (b)

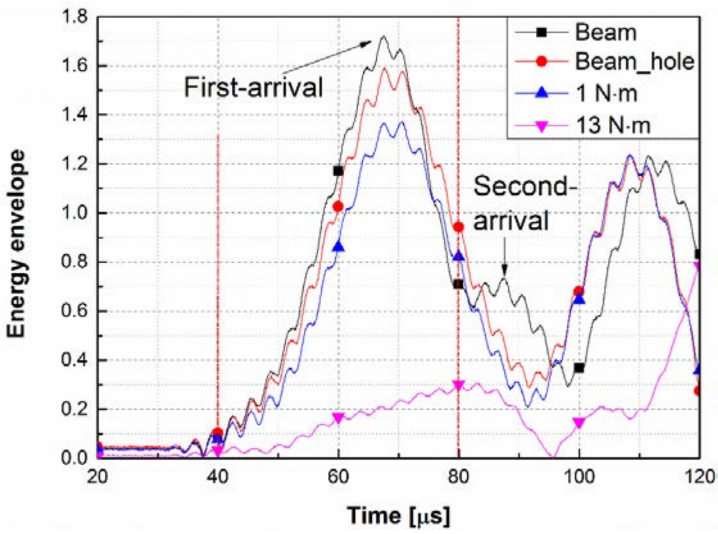

(c)

Figure 4.34 (continued)

In addition, the second-arrival wave packet of *GUWs* almost disappears once the beam was drilled a hole, while first-arrival wave packet of *GUWs* just undergoes acceptable attenuation, which exhibits the potential of the latter in the application of identifying bolt loosening in the cross-lap bolt joint.

To quantitatively link the energy of transmitted *GUWs* to the degree of the residual torque, the transmitted energy of *GUWs* traversing the bolt under different applied torques were quantified by integrating the related energy envelopes. The transmitted energy of the whole signal ($\Omega^{W}_{transimitted}$) and first-arrival wave packet of *GUWs* ($\Omega^{S}_{transimitted}$) in the time range 40-80 μs, were comparably calculated using the same experimental data, and are shown in **Figure 4.35** (a) and (b), respectively. The solid points and the curve denote the experimental data and the averaged results of three repeated experiments, respectively.

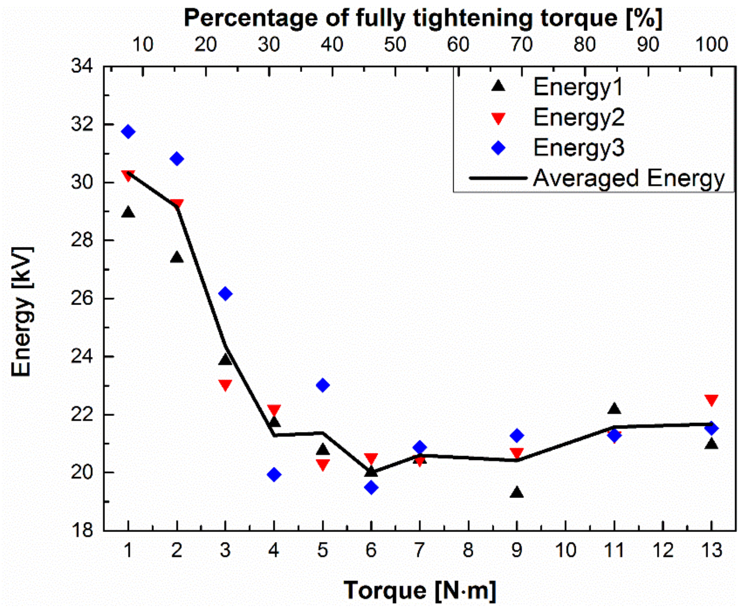

(a)

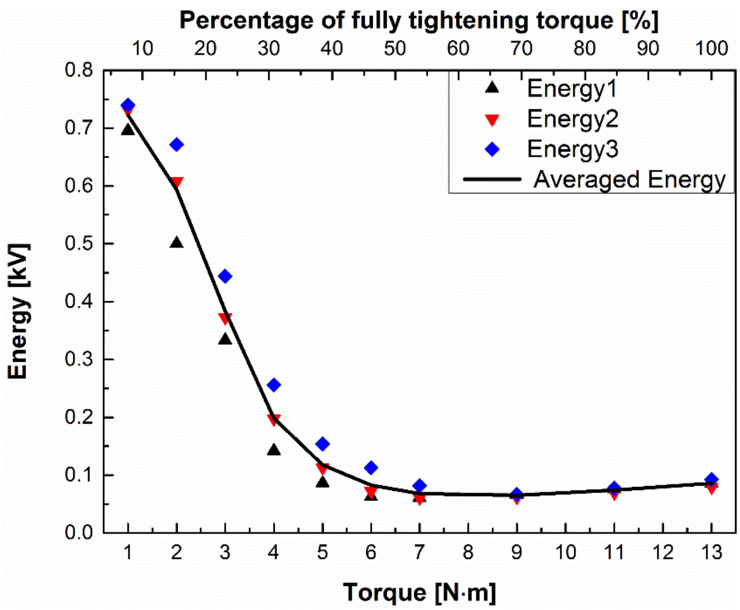

(b)

Figure 4.35 Linear index *vs.* residual torque T for the cross-lap bolted joint (a) original *WED*-based linear method; and (b) improved *WED*-based linear method

In **Figure 4.35** (a), it can be observed that $\Omega^{W}_{transimitted}$ decreases drastically from 1 N·m to 4 N·m, then it stabilizes with some fluctuations before the torque reaches 9 N·m, subsequently it increases slightly until 13 N·m. On the other hand, $\Omega^{S}_{transimitted}$ decreases drastically from 1 to 4 N·m and subsequently reduces slightly until the preload reaches 7 N·m, over which it stabilizes despite the increase in the applied torque. Such a monotonic trend can be attributed to the fact that a stronger clamping force results in a larger interfacial area at the interface, and consequently a greater amount of incident wave leaks from beam I to attached components. Over the torque of 7 N·m, the contact area undergoes little change, due to the occurrence of plastic deformation of contact surfaces, regardless of the further increase in the applied torque [1]. As a result, the energy of *GUWs* passing through the mating parts of the joint remains stable. From the comparison between **Figure 4.35** (a) and (b), it can be concluded that boundary reflection introduces unexpected fluctuations in the data and limits the detection range.

4.4.2. Case Study II: Detection of Bolt Loosening in Single-lap *C-C* Bolted Joint

The proposed *WED*-based method is comparably adopted to evaluate the residual torque of a single-lap bolted composite joint in this section. The specimen configuration (same as that of the single-lap *Al-Al* bolted joint except the thickness) and arrangement of transducers (same as that of the *Al-Al* joint) are shown in **Figure 4.36** (a). The photographic illustration of the setups is comparatively exhibited in **Figure 4.36** (b).

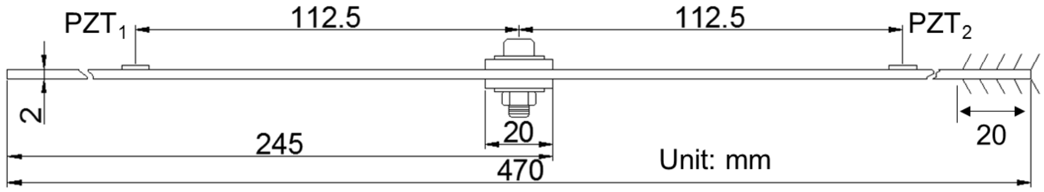

(a)

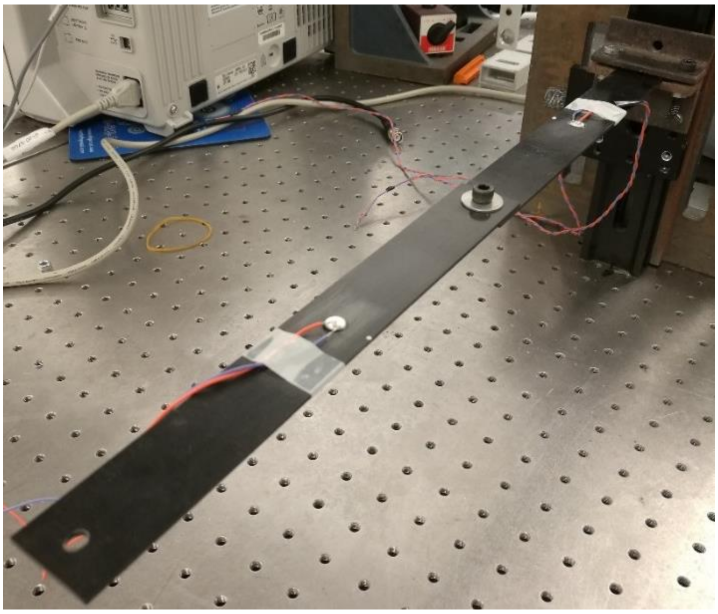

(b)

Figure 4.36 (a) Schematic; and (b) photographic illustrations of the experimental set-ups of *WED*-based method for the single-lap *C-C* joint

After a series of trails, a 7-cycle Hanning window-modulated sinusoidal tone-burst signal at a central frequency of 270 kHz with an amplified voltage of 200 V (peek-to-peak) was used to generate *GUWs* to interact with the joint. The time presentation and frequency spectrum of the excitation signal are shown in **Figure 4.37** (a) and (b), respectively. The *C-C* joint was tightened (same as *Al-Al* joint) with increasing torques from 1 to 13 N·m and tested in each scenario. Wave signals were captured at a sampling frequency of 20 MHz and averaged 64 times to remove random measurement noise.

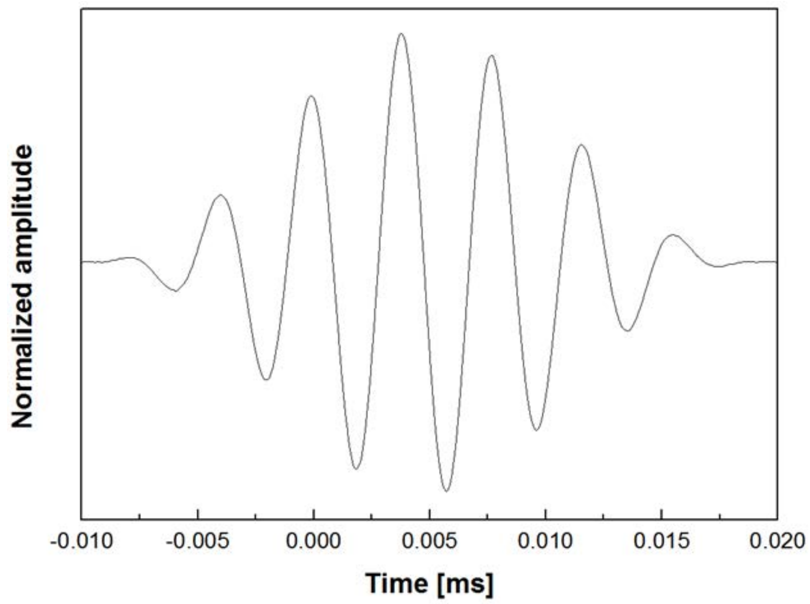

(a)

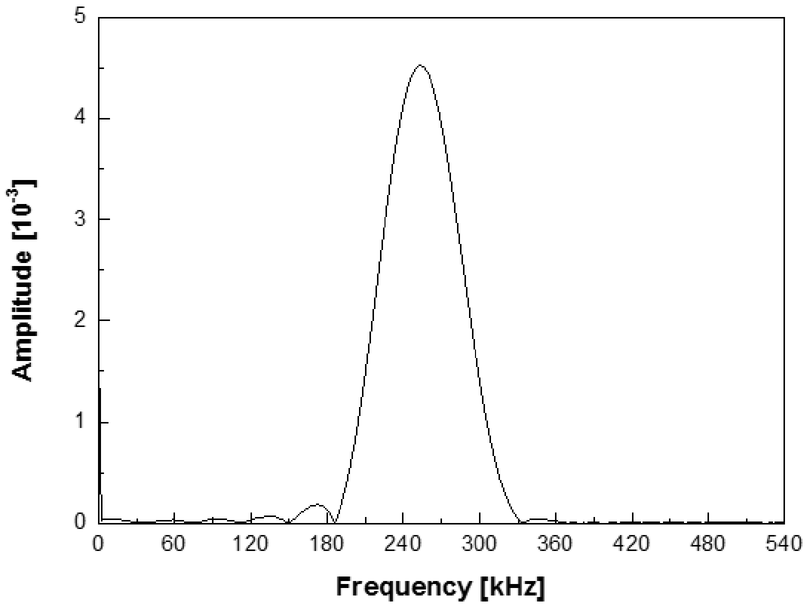

(b)

Figure 4.37 (a) Time presentation; and (b) corresponding frequency spectrum of the excitation signal

The typical time presentation of captured *GUWs* in the *C-C* joint under 7 N·m is shown in **Figure 4.38** (a), which exhibits a more severe attenuation compared to that propagating in the *Al-Al* joint as shown in **Figure 4.33** (a).

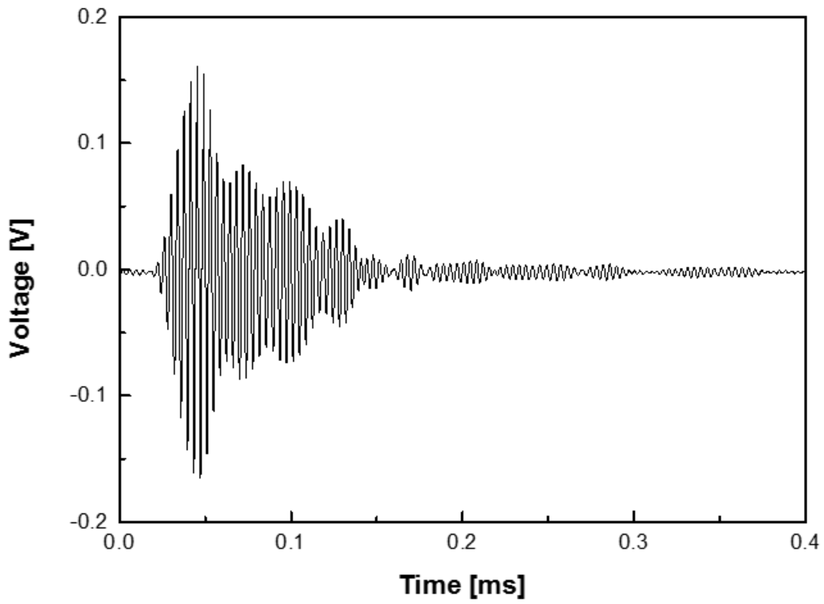

(a)

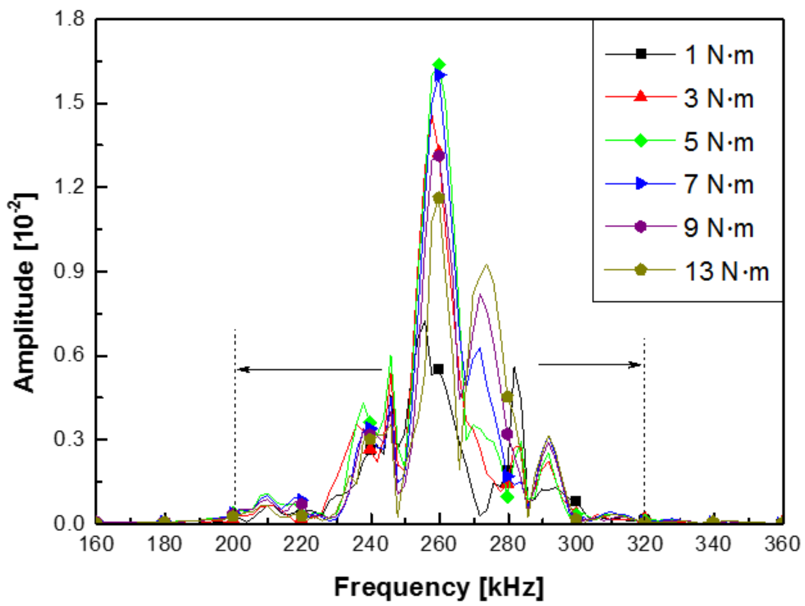

(b)

Figure 4.38 (a) Time presentation of captured *GUWs* from the joint under 7 N·m; (b) the dependence of (b) frequency spectra; and (c) leak energy of the captured *GUWs* on the applied torque

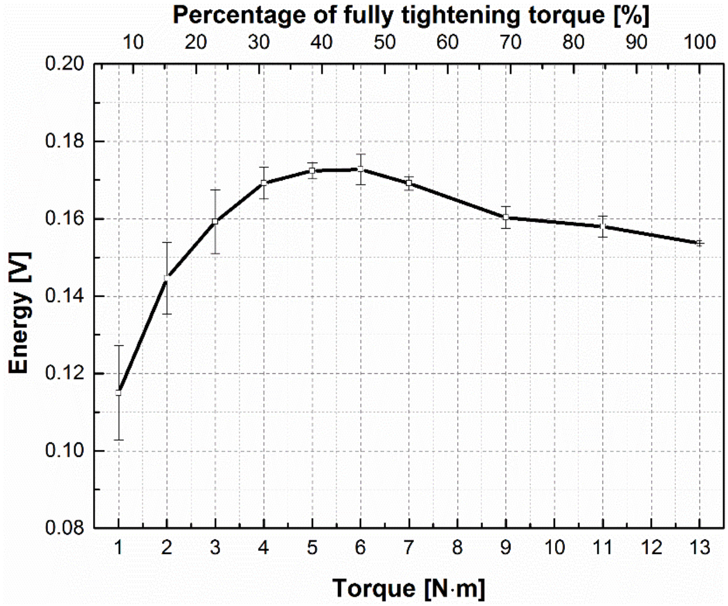

(c)

Figure 4.38 (continued)

To ascertain the distribution of wave energy in the frequency domain, frequency spectra of *GUWs* passing through the mating parts of the joint under different torques were obtained and exhibited in **Figure 4.38** (b). A similar wide range of the energy distribution presents in the spectra with the majority of the wave energy distributed in the range from 270 to 320 kHz. Therefore, leak energy of captured *GUWs* was integrated according to **Equation (4.11)** within the range from 200 to 320 kHz.

The averaged results are shown **Figure 4.38** (c). From the observations in **Figure 4.38** (c), it can be concluded that leak energy augments drastically when the applied torque increases from 1 to 4 N·m, followed by a moderate increase until 6 N·m. A slight decrease occurs in the leak energy when the torque continues increasing to 9 N·m. After then, the leak energy remains almost the same regardless of the increase in the applied torque. When the applied torque is larger than 6 N·m, no further increase in the real contact area in the mating parts of a joint can be created. In addition, serious stress concentration within the region of washer damages the surface of joint (polymer) and produces buckling of the washer, and consequently leads to a slight reduction in leak energy. To conclude, such method exhibits its efficiency to evaluate the residual torque in a limited range but not including early bolt loosening.

4.5. Summary

In this chapter, the efficiency of linear indices proposed in Chapter 3 in the detection of bolt loosening for both *Al-Al* and *C-C* bolted joints is validated by a series of case studies.

In the passive acoustic method, *IMFs* of *AE* signals, obtained by *EMD*, are employed to characterize contact behaviors in a bolted composite joint under different torques. The *C-C* contact related *IMFs* are recognized from those with respect to the *M-C* contact by using frequency-based analysis. Based on micro contact theory, decomposed *IMFs* are linked to different contact behaviors of asperities with different sizes at the *C-C* interface and subsequently employed to indicate the degree of applied torque of the bolted joint. Gross energy of *AE* signals is capable of evaluating the residual torque of the joints within a limited range. Vibration loosening of composite joints was found to result in an increase in the energy ratios of *C-C* contact-related *IMFs*, on which basis the detectability of the *AE*-based non-destructive evaluation is further improved, making it possible to evaluate the tightening condition of a bolted joint when the joint undergoes vibration fatigue. This study provides a feasible method to accurately evaluate the contact conditions of bolted composite joints during assembly and to continuously monitor the tightening condition throughout the service life of the joints using the *AE* technique.

In the modal parameters-based method, resonant frequency and damping ratio are comparatively adopted to evaluate the residual torque of a bolted composite joint. From the comparison, damping ratio is found significantly more sensitive to preload changes in comparison to resonant frequency.

In the *WED*-based linear method, three types of *Al-Al* bolted joints, namely single-lap, cross-lap and hybrid-lap are firstly tested to exhibit the dependence of such method on the joint configurations (i.e., lap types) of joints. To observe *WED*, indicated by leak energy and transmitted energy, presents a monotonic tendency, subject to the residual torque, for the single-lap and cross-lap joints, respectively. However, such a monotonic tendency does not exist for this linear index (defined based on *WED* of *GUWs*) when applied to a hybrid-lap joint, showing its dependence on joint configuration of a joint. Subsequently, to investigate the influence of boundary reflection on the *WED*-based method, the transmitted energy of first-arrival wave packet of *GUWs*, calculated by *HT*, is intercepted and comparably applied to assess the residual torque of a loose bolt in the cross-lap *Al-Al* bolted joint. The modified *WED*-based method using the transmitted energy of first-arrival wave packet of *GUWs* successfully improves the stability of acquired data and extends its detectable range. In addition, the performance of *WED*-based method in the identification of bolt loosening in both single-lap *Al-Al* and *C-C* bolted joints are compared to show serious attenuation of *GUWs* when propagating in composites. This may further limit the application of such method for the detection of bolt loosening in bolted composite structures.

Some improvements in conventional linear feature-based methods in aspect of signal processing and interpreting are presented in this chapter. However, the detection of early bolt loosening is still hard to fulfill by these linear techniques. Next chapter will move to the application of *CAN*-based nonlinear acoustic methods in the detection of bolt loosening including its early stage.

CHAPTER 5

Implementation of Methods Using Nonlinear Features of Acousto-ultrasonics

5.1. Introduction

The preceding chapters have presented that both the theoretical analysis and experimental validation of the linear acoustic methods for the detection of bolt loosening in both aluminum-aluminum (*Al-Al*) and composite-composite (*C-C*) bolted joints. Such linear acoustic techniques are found not capable of achieving a satisfactory evaluation of early bolt loosening. With safety a paramount priority, reliability, integrity and durability criteria must be strictly met for bolted joints, and this entails early awareness of bolt loosening and continuous monitoring of bolt tightness. As opposed to the use of linear signal features, there has been an increased preference in exploiting nonlinear acoustic properties, represented by those using high-order harmonics (particularly the second-order harmonic (*SOH*)) or vibro-acoustic modulation (*VAM*). It is widely accepted that the sensitivity of nonlinear feature-based methods to undersized damage, including material degradation, micro cracks and early bolt loosening, is much higher than that of conventional linear feature-based methods. Thanks to endeavors from a vast of scholars, nonlinear acoustic methods have demonstrated their detectability of material degradation and early fatigue cracks. In Chapter 3, the magnitudes of nonlinear responses (i.e., *HOH* and modulated sidebands) have been theoretically linked with the residual torque of a loose joint regardless of joining materials and lap/joint configurations. Motivated by these, contact acoustic nonlinearity (*CAN*)-based nonlinear methods for the detection of early bolt loosening are presented using a variety of case studies in this chapter. Firstly, to verify the accuracy of the theoretical model proposed in Chapter 3, the reliance of defined nonlinear indices on the mixed excitation from a low-frequency pumping vibration and a high-frequency probing wave are presented in both *Al-Al* and *C-C* single-lap bolted joints. Subsequently, three nonlinear indices, defined from *SOH*, *TOH* and modulated sidebands, respectively, are comparatively adopted to evaluate the residual torque of loose bolts in both *Al-Al* and *C-C* bolted joints. To compare with the *WED*-based linear method, which exhibits a high dependence on lap/joint configurations, *CAN*-based nonlinear acoustic methods are employed for the three types of *Al-Al* bolted joints, namely single-lap, cross-lap and hybrid lap in the following case studies.

5.2. Dependence of Nonlinear Indices on Excitations

As derived in Section 3.3.2, the relation between the excitation force of the low-frequency pumping vibration (F_{LF}) and induced linear structural response (A_{LF}) can be written as

$$A_{LF} \propto F_{LF}. \tag{5.1}$$

Similarly, the dependence of response magnitude of the high-frequency probing wave (A_{HF}) on the intensity of its input force (F_{HF}) can be given as

$$A_{HF} \propto F_{HF}. \tag{5.2}$$

The reliance of nonlinear responses, namely *SOH* (A_{SOH}) and *TOH* (A_{TOH}) on the linear responses can be further expressed as

$$A_{SOH} \propto \beta_{SOH}^{theory} A_{LF}^{2}, \tag{5.3}$$

$$A_{TOH} \propto \beta_{TOH}^{theory} A_{LF}^{3}. \tag{5.4}$$

When a joint is subject to the mixed excitation, the response magnitudes of left (A_{LS}) and right (A_{RS}) sidebands can be expressed with the response magnitudes of pumping vibration and probing wave, as

$$A_{LS} \; or \; A_{RS} \propto \beta_{VAM}^{theory} A_{LF} A_{HF}. \tag{5.5}$$

Based on these, three nonlinear indices (i.e., β_{SOH} , β_{TOH} and β_{VAM}^{M}), defined in the unit of dB, using magnitudes of *SOH*, *TOH* and sidebands (*LS*, *RS*), respectively, are defined as

$$\beta_{SOH} = SOH - 2 * LF, \tag{5.6}$$

$$\beta_{TOH} = TOH - 3 * LF, \tag{5.7}$$

$$\beta_{VAM}^{M} = (LS + RS)/2 - LF - HF, \tag{5.8}$$

Here, $LF = 20\log(A_{LF})$ and so on. The nonlinear index constructed from the sideband response was found being defined neglecting the influence of pumping vibration in some reported studies [77], as

$$\beta_{VAM} = (LS + RS)/2 - HF. \tag{5.9}$$

To validate the accuracy of these four nonlinear damage (bolt loosening)-related indices, their independence on the intensity of excitations, predicted by the theoretical analysis, is presented for both *Al-Al* and *C-C* single-lap bolted joints in what follows. Two beam-like specimens were assembled by an M6 bolt, then clamped as a cantilever system. To indicate material properties, the aluminum and composites joints were hereinafter denoted by *Al-Al* and *C-C* joints, respectively. For *Al-Al* joint, the two joining aluminum components of the same geometric dimension of 245×30×2.8 mm^3 were assembled with a lap length of 20 mm (bolt was positioned in the middle of the lap area) and a clamped length of 10 mm. For *C-C* joint, the two composite joining components, both measuring 245×30×2.0 mm^3, were assembled with the same lap and clamped length as those used in *Al-Al* joint. Particularly, the composite specimen is a zero-degree unidirectional laminate fabricated in accordance with a standard hot-press process. For both joints, a piezo stack actuator (PI®, P-885.11) was surface-mounted on each joint to generate high-frequency probing waves, while a shaker (B&K®, Model type: 4809) was used to introduce a point-force-like low-frequency pumping vibration to the joint. The stack actuator was 39.2 mm from the bolt and shaker was 39.2 mm from the free end. Two sinusoidal signals at different frequencies were generated by a waveform generator (HIOKI®, Model Type: 7075), to supply the stack actuator and the shaker, respectively. A power amplifier (B&K®, Model Type: 2706) intensified the pumping vibration. The response signal of the joint under the mixed excitation was captured with an accelerometer (B&K®, Model Type: 4393), 35.8 mm from the bolt, and saved using an oscilloscope (Agilent® DSO9064A) at a sampling frequency of 200 kHz. The schematic illustration of setups and surface properties of the composite specimen are displayed in **Figure 5.1**.

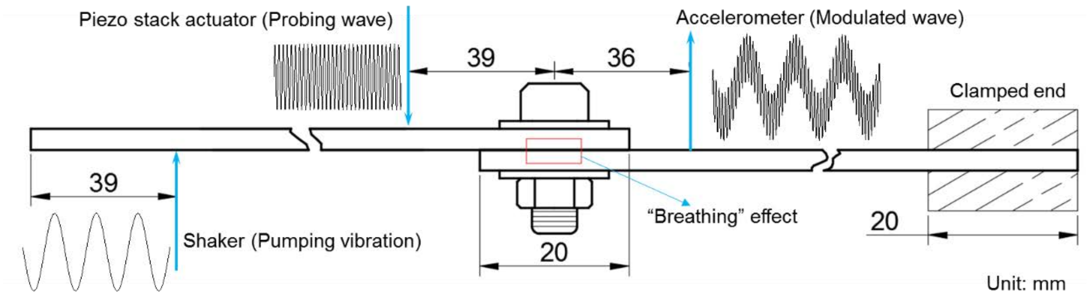

(a)

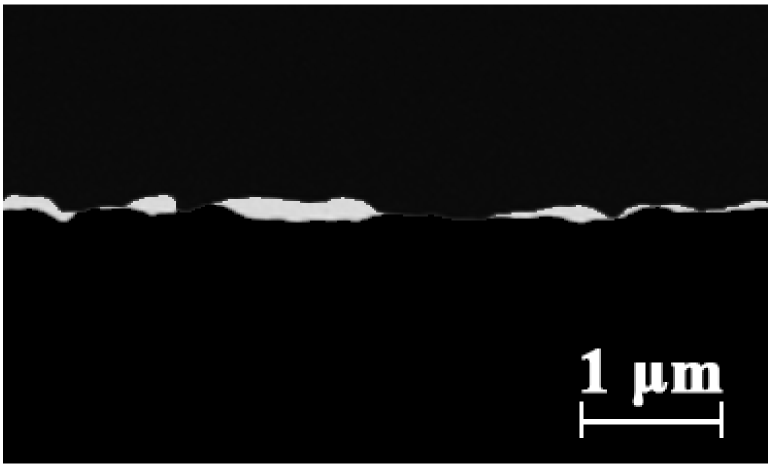

(b)

Figure 5.1 (a) Specimen configurations of the *Al-Al* and *C-C* single-lap bolted joints for *VAM*-based nonlinear method; and (b) two rough surfaces in contact

5.2.1. Selections of Excitation Frequencies

To enhance the intensity of *CAN* at the interface of a loose joint when it interacts with acoustic waves, excitation frequencies of pumping vibration were selected from the low-order natural frequencies, which were ascertained by an impact force (see **Figure 5.2** (a) and **Figure** 5.3 (a)). Subsequently, the magnitudes of *SOH* in the response to the pumping vibration, under the identified natural frequencies of each joint, was obtained from the spectra. In **Figure 5.2** (b), for the *Al-Al* joint, the natural frequency of 992 Hz was found to produces the *SOH* with the strongest magnitude, indicating a high degree of nonlinearity (i.e., *CAN*) in structural responses at this particular frequency. It is therefore 992 Hz was selected as the excitation frequency of pumping vibration for the *Al-Al* bolted joint. In an analogous manner, 758 Hz was selected for the *C-C* bolted joint as the excitation frequency of pumping vibration, as displayed in **Figure 5.3** (b). To determine excitation frequencies of the probing wave, a white noise excitation was generated via the piezo stack actuator. The frequency responses of the joint were captured in a range between 9 and 16 kHz, and the frequency with the strongest response, termed as the *strongest natural frequency* (*SNF*) in this study, was ascertained. At *SNF*, *CAN* (*i.e.,* response magnitudes of sidebands) reaches its local maximum. As shown in **Figure 5.2** (c) and **5.3** (c), the identified frequencies at 14.24 kHz for the *Al-Al* bolted joint and 14.99 kHz for the *C-C* bolted joint were selected as excitation frequencies of probing wave, respectively.

Now that excitation frequencies of pumping vibration and probing wave are selected, the dependence of structural responses on the intensity of these two excitations is to be discussed in the following two sections.

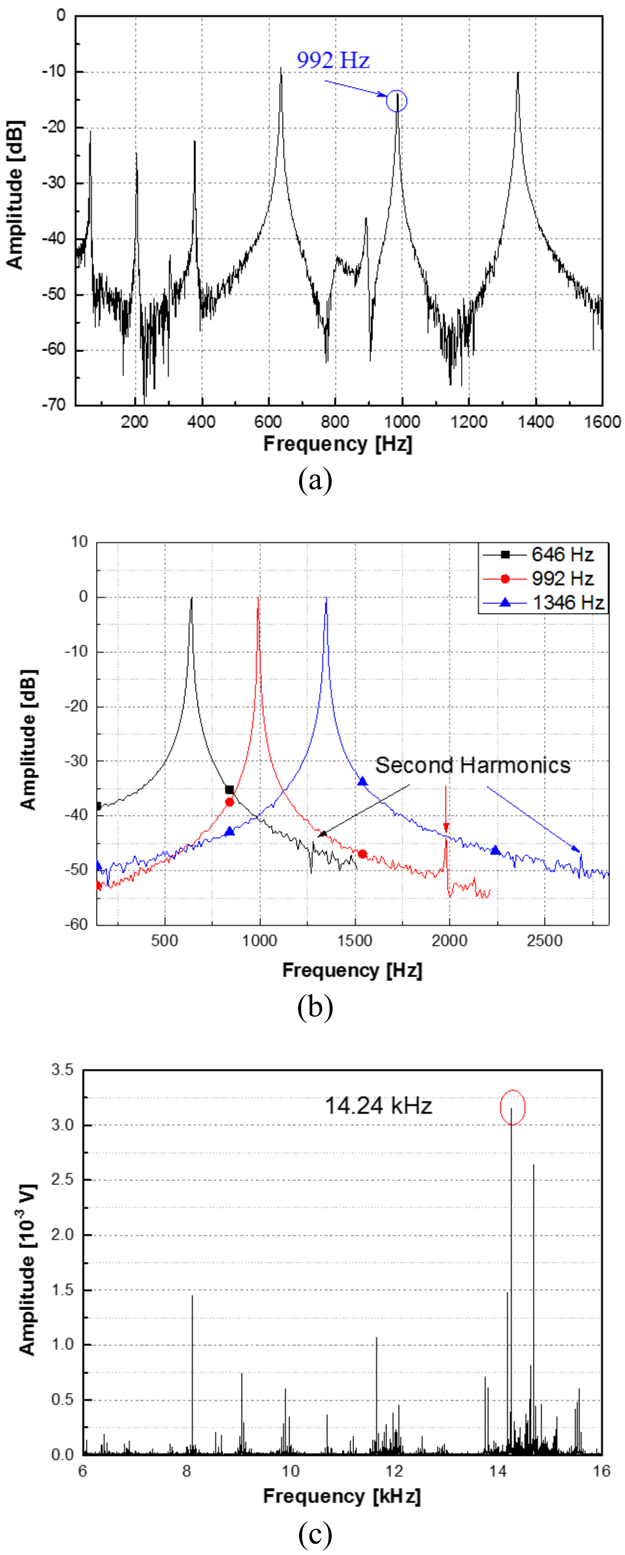

Figure 5.2 Spectra of response of the single-lap *Al-Al* bolted joint (when *T*=1 N·m): (a) under an impact force; (b) under a harmonic force; and (c) under white noise

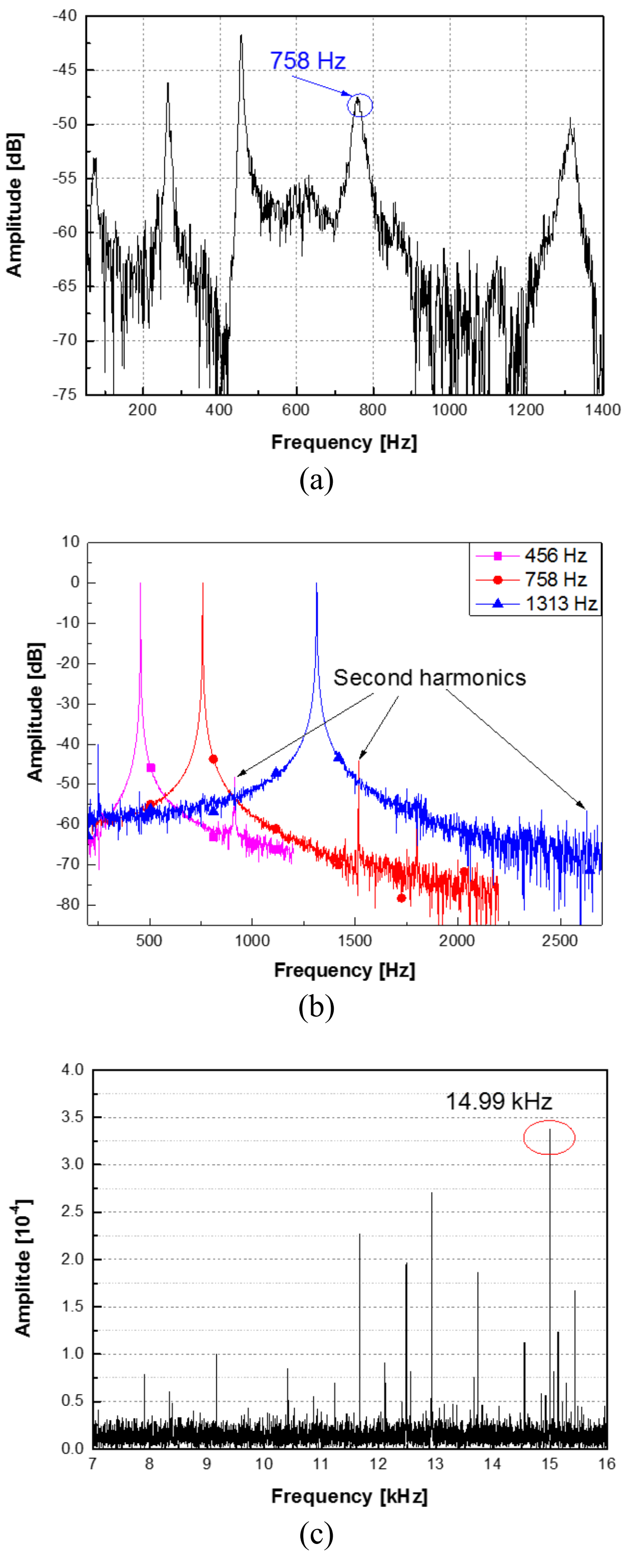

Figure 5.3 Spectra of response of the single-lap *C-C* bolted joint (when *T*=1 N·m): (a) under an impact force; (b) under a harmonic force; and (c) under white noise

5.2.2. *Al-Al* Single-lap Bolted Joint

For the single-lap *Al-Al* bolted joint under a torque of 5 N·m, the input magnitude of pumping vibration varied from 3 to 13 V and meanwhile the input voltage of probing wave kept consistent at 10 V. The accordingly obtained linear (i.e., responses to low-frequency pumping vibration (*LF*) and high-frequency probing wave (*HF*)) and nonlinear (i.e., *SOH* response of pumping vibration, *TOH* response of pumping vibration, left (LS) and right (*RS*) sidebands) structural responses are displayed in **Figure 5.4** (a)-(d).

From **Figure 5.4** (a)-(d), it can be observed that no phenomenal nonlinear responses occur when the input magnitude for the pumping vibration is 3 V. When the input magnitude continues increasing, response magnitudes of *LF* and its harmonics (i.e., *SOH* and *TOH*) along with modulated sidebands (i.e., *LS* and *RS*) present and increase. While response magnitude of *HF* exhibits an independence on the input magnitude of pumping vibration. Subsequently, the input magnitude of probing wave was increased from 7 to 16 V and in the meanwhile the input magnitude of pumping vibration was set consistent at 10 V. The typical related linear and nonlinear structural responses are displayed in **Figure 5.5** (a)-(c). To observe that the magnitudes of *HF*, *LS* and *RS* increase as the input magnitude of probing wave increasing, whereas the magnitude of *LF* remains almost unchanged.

To quantitatively investigate the reliance of the linear and nonlinear structural responses on the input magnitudes of the two excitations, their relation in between is shown in **Figure 5.6** (a) and (b).

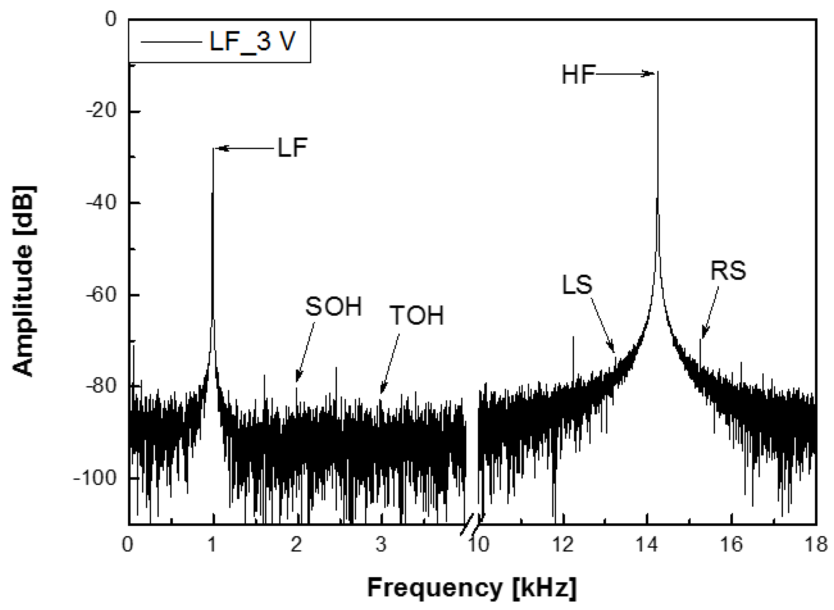

(a)

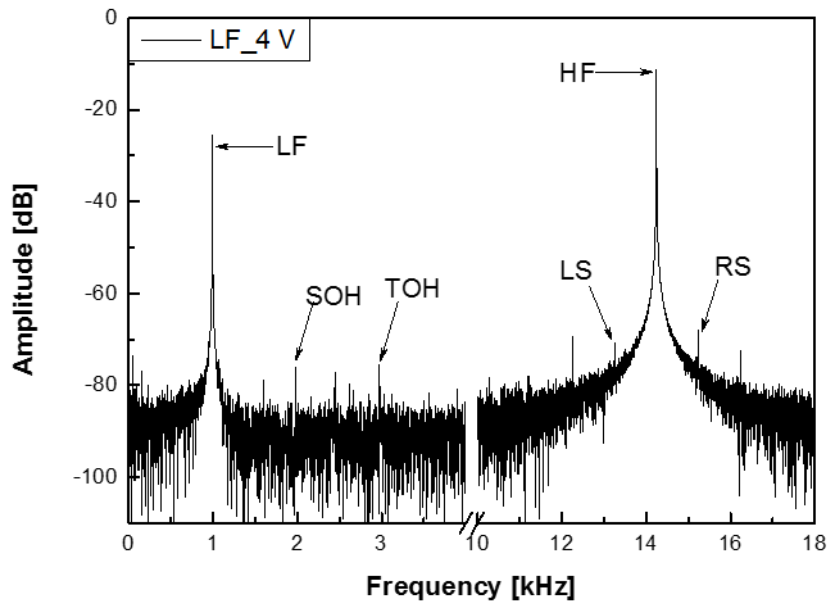

(b)

Figure 5.4 Frequency spectra *vs.* intensity(voltage) of low-frequency pumping vibration for the single-lap *Al-Al* bolted joint: (a)3 V; (b)4 V; (c)10 V; and (d)13 V

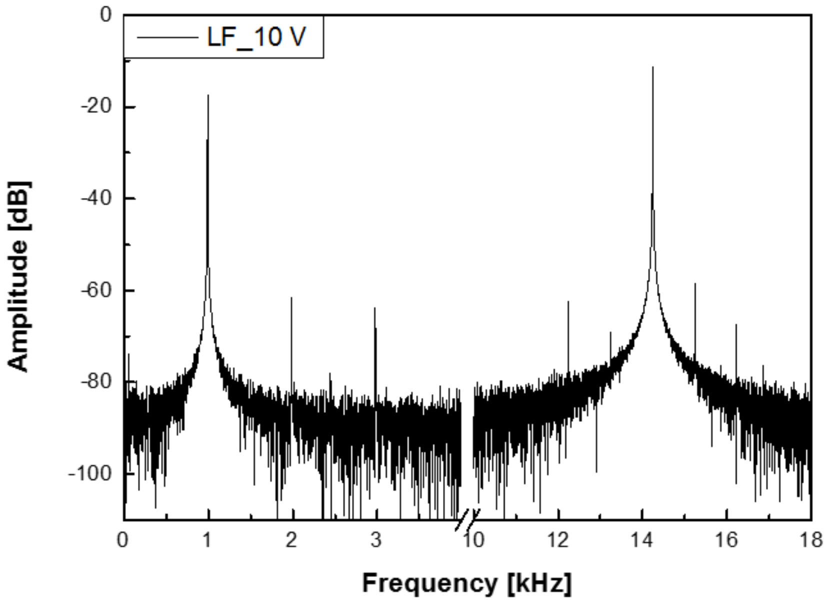

(c)

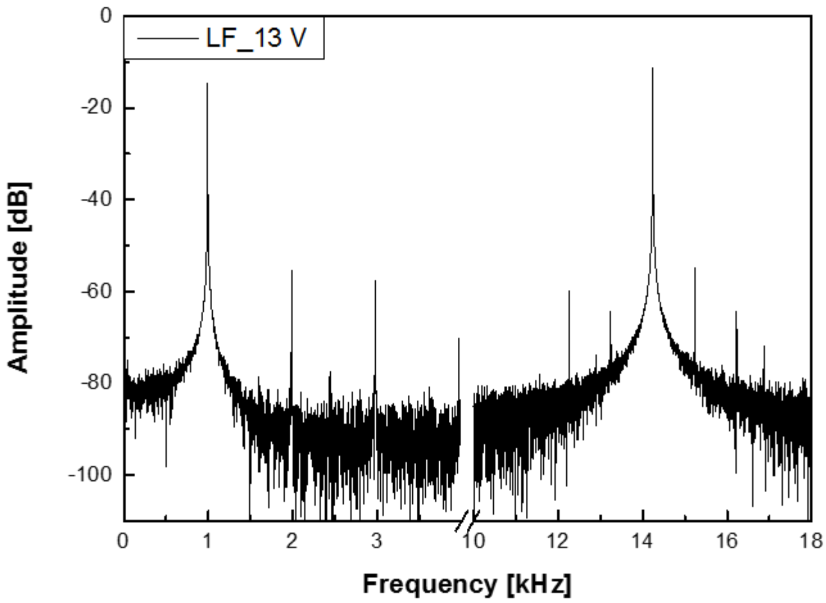

(d)

Figure 5.4 (continued)

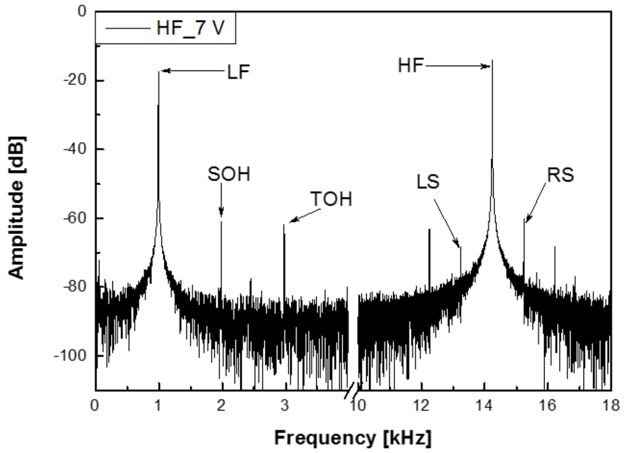

(a)

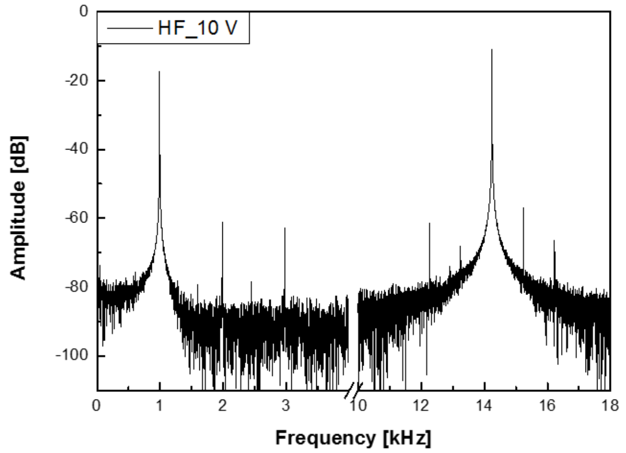

(b)

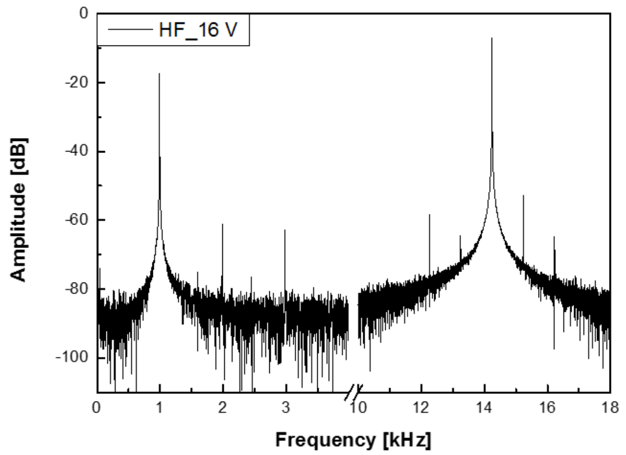

(c)

Figure 5.5 Frequency spectra *vs.* intensity (voltage) of high-frequency probing wave for the single-lap *Al-Al* bolted joint: (a)7 V; (b)10 V; and (c)16 V

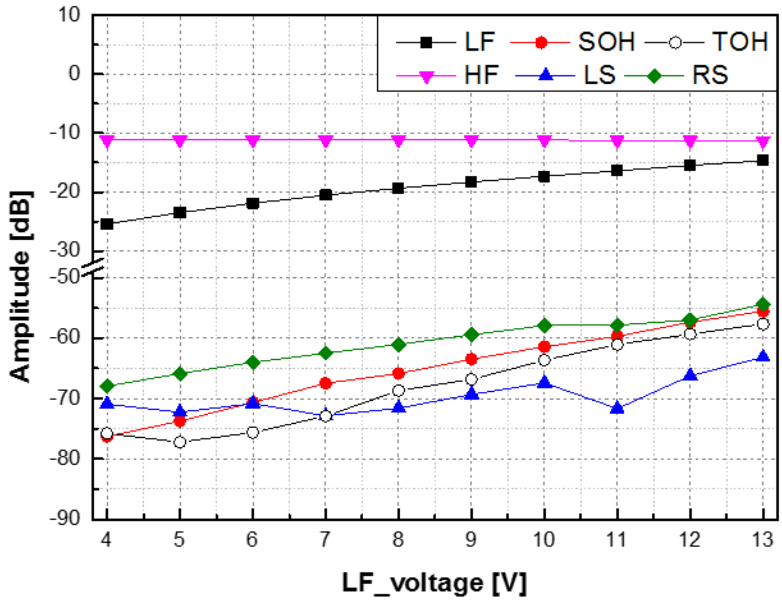

(a)

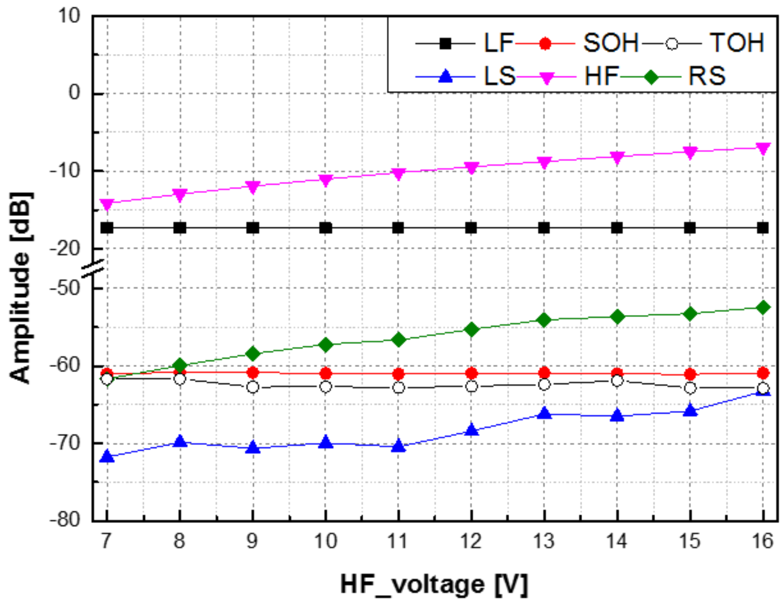

(b)

Figure 5.6 Linear and nonlinear responses vs. magnitudes of (a) pumping vibration; and (b) probing wave for the *Al-Al* single-lap bolted joint (when *T*=5 N·m)

As it can be observed that *LF* and *HF* exhibit a linear dependence on the input magnitude (i.e., input force) of pumping vibration and probing wave, respectively, which agrees with the theoretical predictions by **Equations (5.1)** and **(5.2)**. In the meanwhile, nonlinear responses (i.e., *SOH*, *TOH*, *LS* and *RS*) also increase linearly with an augment in the input magnitudes of pumping vibration and probing wave, which confirms the validity of **Equations (5.3)- (5.5)**.

To verify the rationality of the defined damage-related nonlinear indices in **Equations (5.6)- (5.9)**, the dependence of β_{SOH} , β_{TOH} , β_{VAM}^{M} and β_{VAM} on the magnitudes of pumping vibration (*LF*) and probing wave (*HF*) is displayed in **Figure 5.7** (a) and (b), respectively, where the scattered points are the experimental results and the solid lines are the fitting curves. From **Figure 5.7** (a), it can be found that β_{SOH} and β_{VAM}^{M} are independent of the magnitude of *LF*, while β_{VAM} shows a linear correlation with the magnitude of *LF*. The dependence of *TOH* response on *LF* magnitude can be divided into two stages. Before the response magnitude of *LF* reaches -22 dB, β_{TOH} decreases with an increase in *LF* and after then it remains almost unchanged regardless of an augment in *LF*. In **Figure 5.7** (b), a clear independence of all nonlinear indices on the intensity of *HF* presents. From above experimental observations, the accuracy of theoretical predictions in **Equations (5.1)- (5.9)** is verified. In addition, the utilization of β_{VAM} for damage detection must reside on a premise that the response magnitude of *LF* remains the same during the testing. Besides, a proper intensity of *LF* should be secured to achieve an effectual detection when using β_{TOH} for *SHM*.

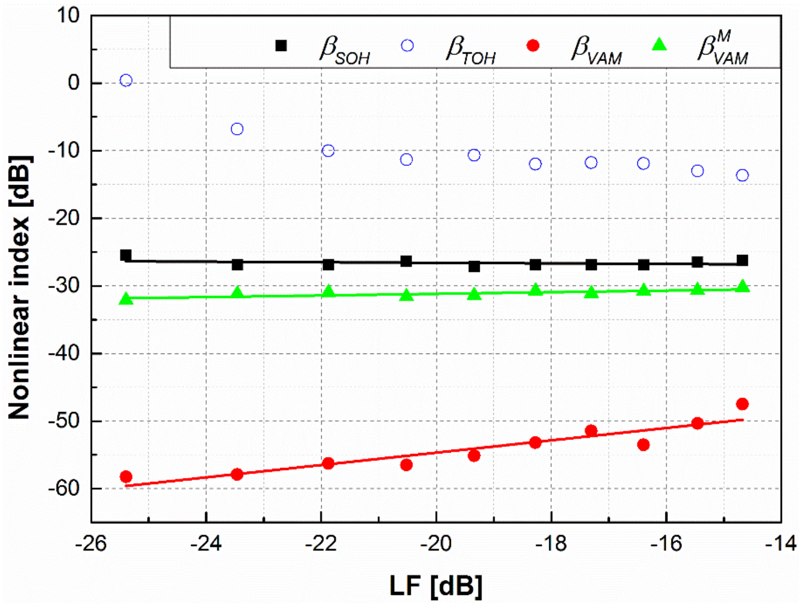

(a)

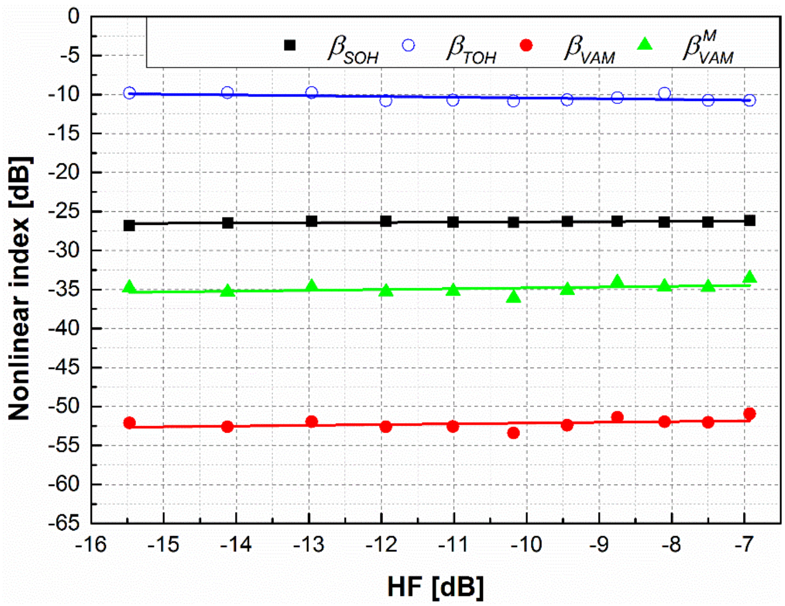

(b)

Figure 5.7 Different nonlinear indices *vs.* magnitudes of (a) pumping vibration; and (b) probing wave for the *Al-Al* single-lap bolted joint (when T= 5 N·m)

5.2.3. *C-C* Single-lap Bolted Joint

To study the effect of joining materials on the relation between the structural responses and the intensity of the two excitations, the above theoretical predictions are comparatively verified in a *C-C* single-lap bolted joint.

During the testing, to study the influence of the intensity of pumping vibration on the structural responses, the input magnitude of probing wave was set consistent at 10 V and that of pumping vibration varied from 2 to 10 V. Subsequently, the input magnitude of probing wave increased from 10 to 20 V to investigate the related effect of probing wave. The typical frequency spectra of the joint subject to different input voltages of pumping vibration and probing wave are exhibited in **Figure 5.8** and **5.9**, respectively. Similar with the observations in the *Al-Al* single-lap bolted joint, the magnitudes of *LF*, *SOH*, *TOH*, *LS* and *RS* increase when the input magnitude of pumping vibration increasing, and the magnitudes of *HF*, *LS* and *RS* are observed to increase as input magnitude of probing wave increases. The quantitative dependence of structural responses (both linear and nonlinear parts) on the input magnitudes of pumping vibration and probing wave are shown in **Figure 5.10** (a) and (b), respectively. A good agreement between theoretical predictions and experimental investigation is found. It is noteworthy that there exists a slight difference between *LS* and *RS* regarding the reliance on the intensity of pumping vibration. In addition, *TOH* exhibits a linear dependence on the intensity of pumping vibration only when the input magnitude reaches over 6.5 V. The mechanisms of these phenomena are not clear, but it may associate with varied sources of *CAN* at the interface of a loose joint, which is to be discussed later.

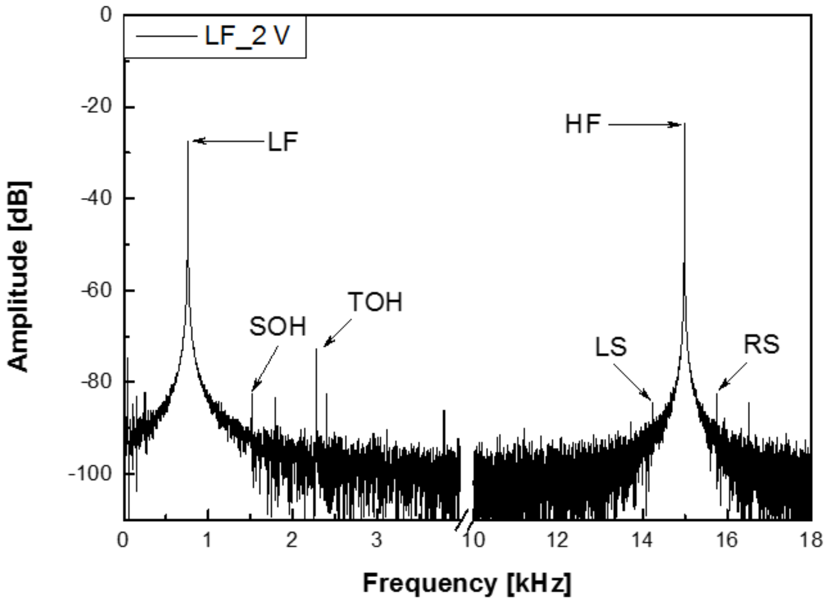

(a)

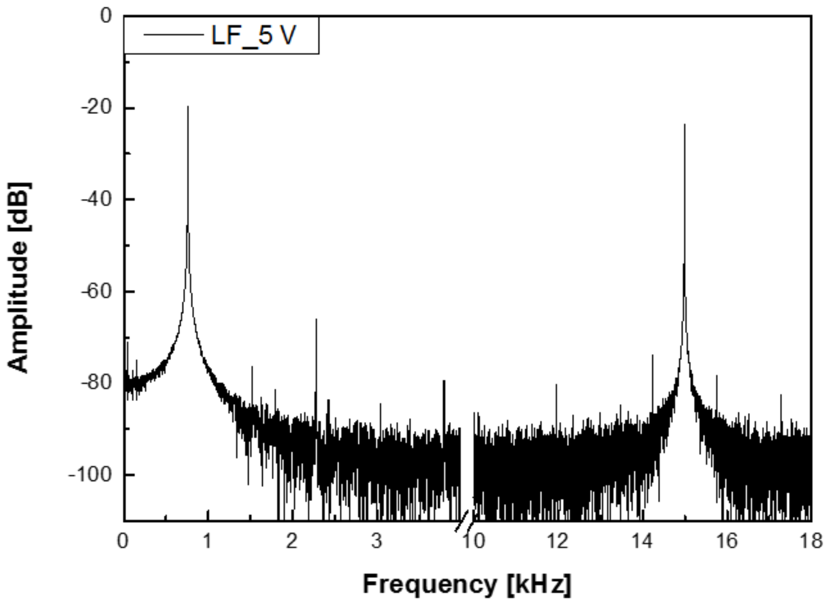

(b)

Figure 5.8 Frequency spectra *vs.* intensity (voltage) of low-frequency pumping vibration for the single-lap *C-C* bolted joint: (a)2 V; (b)5 V; (c)8 V; and (d)10 V

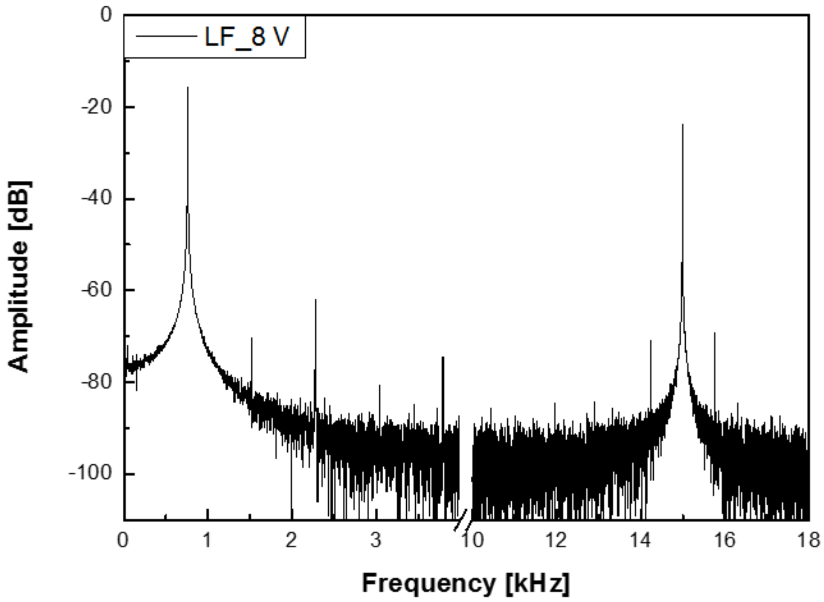

(c)

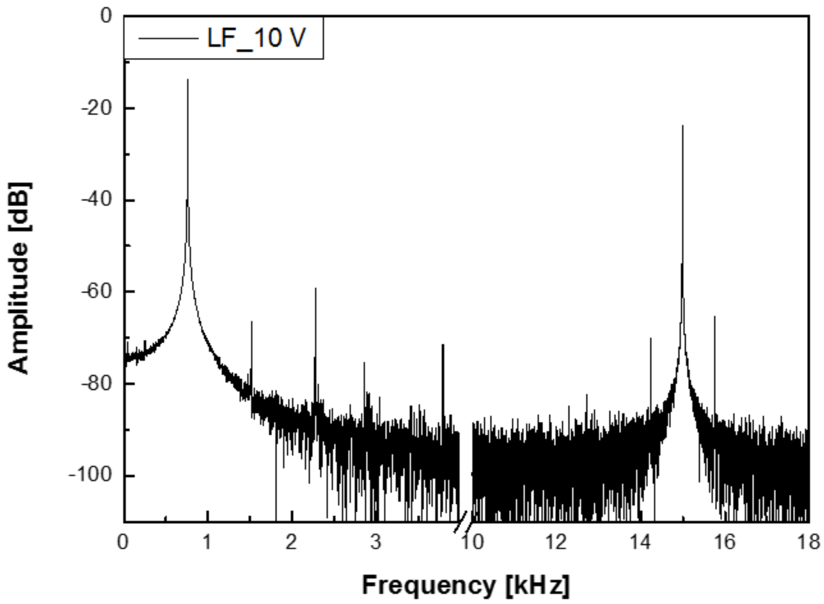

(d)

Figure 5.8 (continued)

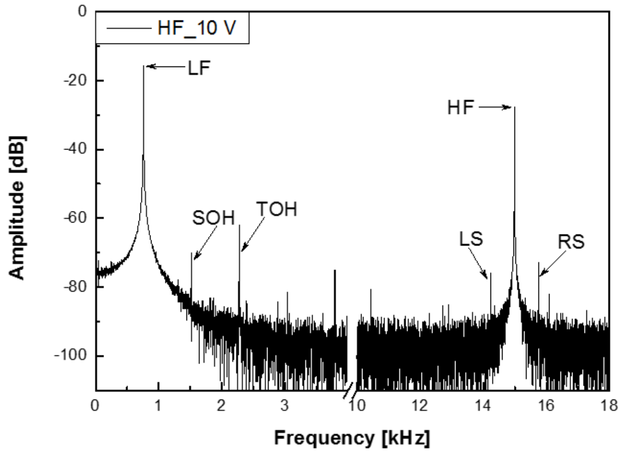

(a)

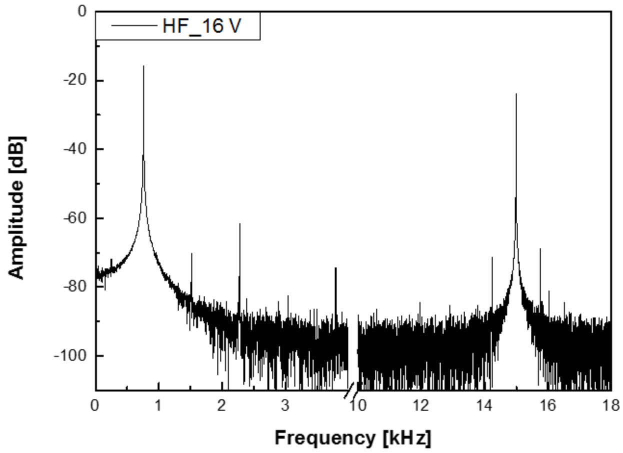

(b)

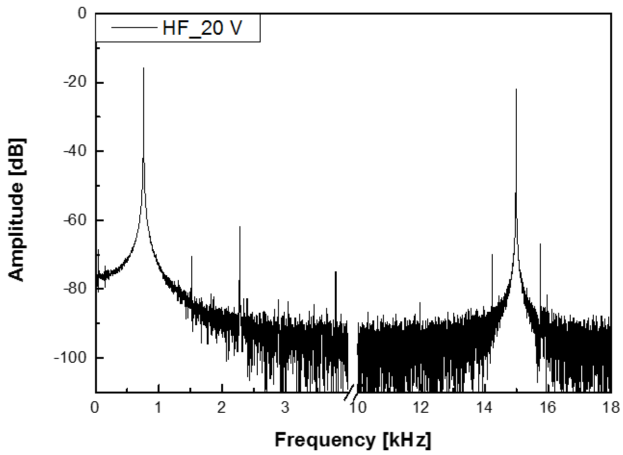

(c)

Figure 5.9 Frequency spectra *vs.* intensity (voltage) of high-frequency probing wave for the single-lap *C-C* bolted joint: (a)10 V; (b)16 V; and (c)20 V

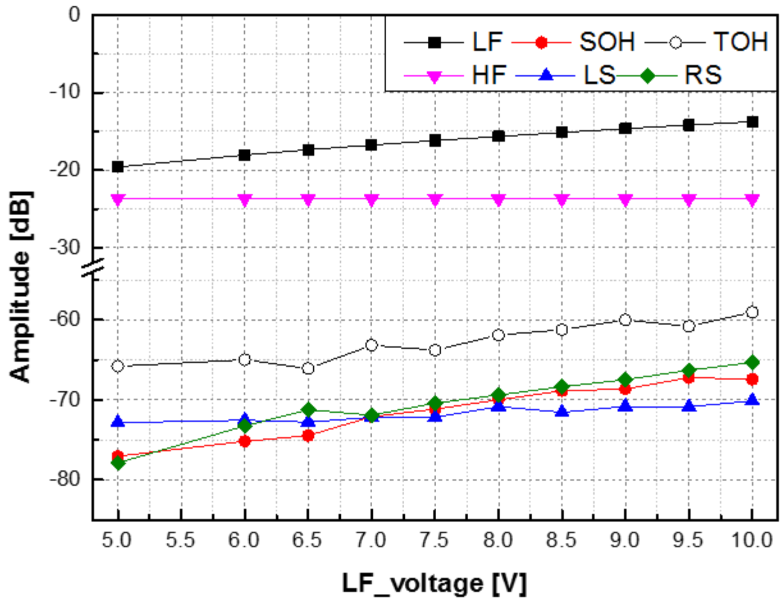

(a)

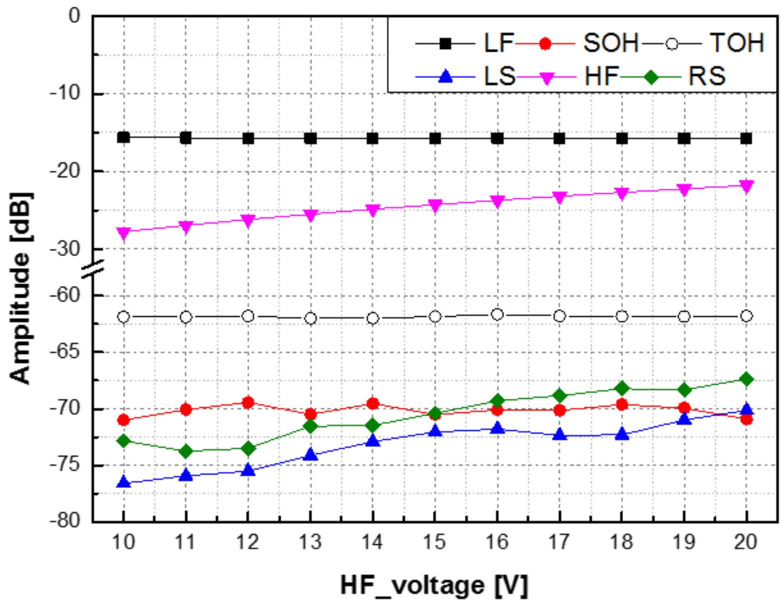

(b)

Figure 5.10 Linear and nonlinear responses *vs.* magnitudes of (a) pumping vibration; and (b) probing wave for the *C*-*C* single-lap bolted joint (when *T*=5 N·m)

The dependence of defined nonlinear indices in **Equations (5.6)- (5.9)**, on the excitation magnitudes is displayed in **Figure 5.11** (a) and (b). Similar with results of the *Al-Al* joint, a good consistency between theoretical analysis and experimental findings presents.

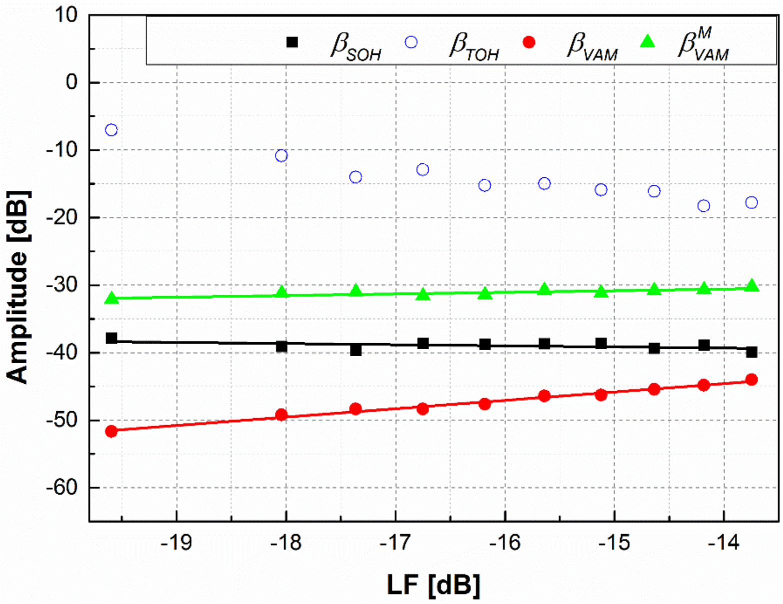

(a)

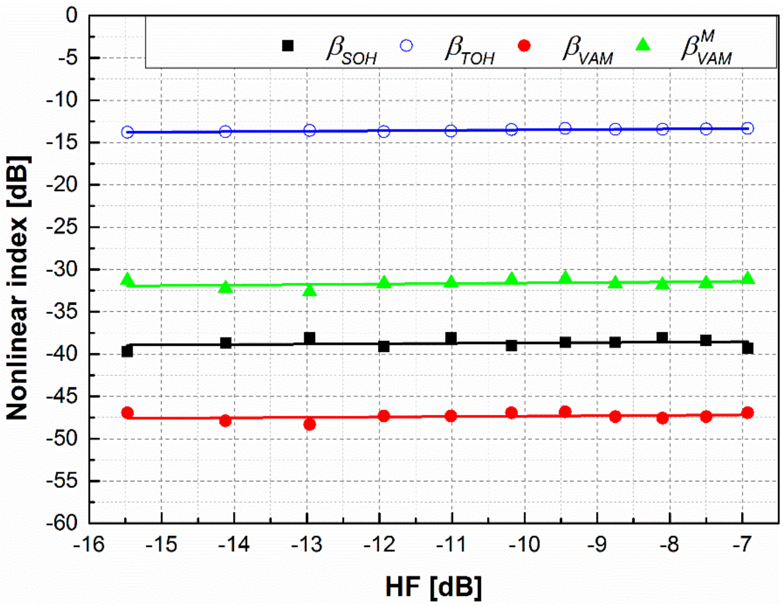

(b)

Figure 5.11 Different nonlinear indices *vs.* magnitudes of (a) pumping vibration; and (b) probing wave for the *C-C* single-lap bolted joint (when T= 5 N·m)

To verify their efficiencies in terms of bolt loosening evaluation, these four nonlinear indices will be comparably employed to identify the residual torque of loose bolts for both *Al-Al* and *C-C* bolted joints in the following sections.

5.3. Case Study I: Detection of Bolt Loosening in Multi-type *Al-Al* Bolted Joints

The proposed detection framework in Chapter 3 based on the defined nonlinear indices are validated by identifying bolt loosening in three types of *Al-Al* bolted joints, namely single-lap, cross-lap and hybrid-lap joints.

5.3.1. Single-lap

The same specimens of the *Al-Al* single-lap bolted joint with unchanged boundary conditions as those used in the *WED*-based linear method in Chapter 4 were recalled, as illustrated in **Figure 5.12**, to validate the *CAN*-based nonlinear approaches.

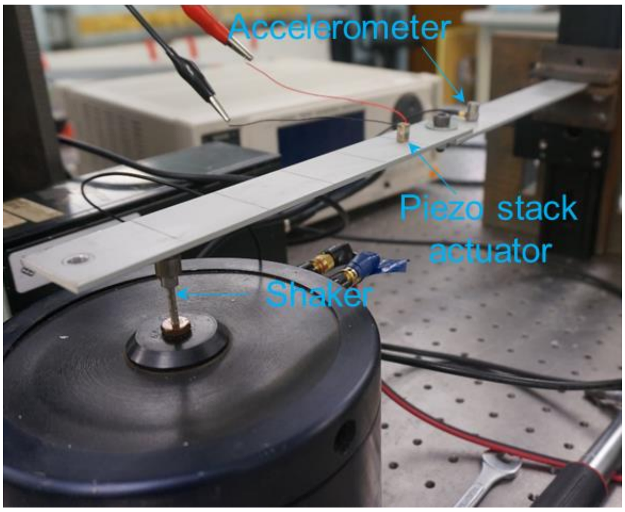

Figure 5.12 Experimental setups for the *Al-Al* single-lap bolted joint using *CAN*-based nonlinear methods

Similar with the scenarios adopted in the *WED*-based linear method, the applied torque on the bolt of the joint was increased from 1 to 13 N·m. Structural responses of the joint upon subject to the mixed excitation were captured at each scenario. As mentioned, the excitation frequencies of the pumping vibration and probing wave were selected as 992 Hz and 14.24 kHz, respectively. Note that the input magnitudes of two excitations were both set as 10 V for all the three types of *Al*-*Al* bolted joints.

Frequency spectra of the joint under three representative torques are shown in **Figure 5.13** (a)-(c), to obverse the occurrence of strong nonlinear responses (i.e., *SOH*, *TOH*, *LS* and *RS*) when the bolt is fully loose (under 1 N·m), while fairly weak nonlinear responses present when the bolt is fully fastened (under 13 N·m).

To put the analysis into a quantitative manner, correlation between the magnitudes of *CAN*-induced nonlinear responses (i.e., *SOH*, *TOH*, *LS* and *RS*) and the degree of bolt loosening is established and shown in **Figure 5.14** (a). Whereby AS is the averaged magnitude of left (A_{LS}) right (A_{RS}) sidebands defined as

$$AS = (A_{LS} + A_{RS}) / 2. \qquad \textbf{(5.10)}$$

In **Figure 5.14** (a), a consistent, monotonic tendency for AS can be clearly noted, which decreases rapidly when the applied torque T of bolt reaches 2 N·m from the fully loose condition (T=1 N·m) and after then a moderate decrease presents until the bolt is fully tightened (T=13 N·m). In the meanwhile, nonlinear harmonics (i.e., *SOH* and *TOH*) decrease clearly with an increase in the applied torque once it reaches threshold values (5 N·m for *SOH* and 4 N·m for *TOH*). At the late stage of bolt loosening, when the applied torque is less than the mentioned threshold values, the dependence of *HOH* on the residual torque of a loose joint is not clear. On the other hand, the magnitude of *LF* remains almost the same regardless of an increase in the applied torque. The magnitude of *HF* decreases slightly in the torque range between 2 and 7 N·m and keeps unchanged at the early stage of bolt loosening (when *T* is over 7 N·m). These experimental findings agree well with conclusions drawn in reported papers which are reviewed in Chapter 2. The linear acoustic features (i.e., response magnitudes of pumping vibration (*LF*) and probing wave (*HF*)) are not able to characterize undersized damage, including early bolt loosening, while nonlinear acoustic features such as *SOH*, *TOH* and sidebands show a high sensitivity to bolt loosening even at the early stage.

Subsequently, the four nonlinear indices for the *Al-Al* single-lap bolted joint under different applied torques were obtained, using **Equations (5.6)- (5.9)**, respectively, and displayed in **Figure 5.14** (b). At the early stage of bolt loosening, when *T* is no less than 5 N·m, these four nonlinear indices show a similar dependence on the applied torque. At the late stage, *HOH*-based nonlinear methods fail to identify the state of the loose bolt, during which nonlinear indices developed from the magnitudes of *HOH* show an unclear dependence on the residual torque remained on the bolt. It should be pointed out that the similarity in the change trends between β_{VAM} and β_{VAM}^{M} is due to that *LF* response changes slightly subject to different degrees of bolt loosening. From the comparison, it can be concluded that the *VAM*-based method using modulated sidebands shows the best detectability of bolt loosening with an excellent sensitivity through the whole detection range.

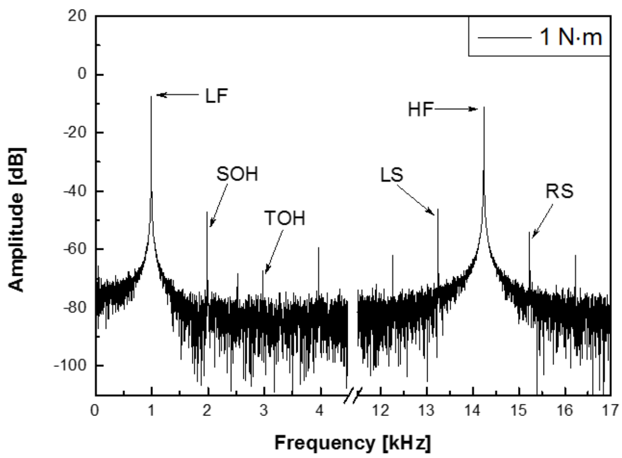

(a)

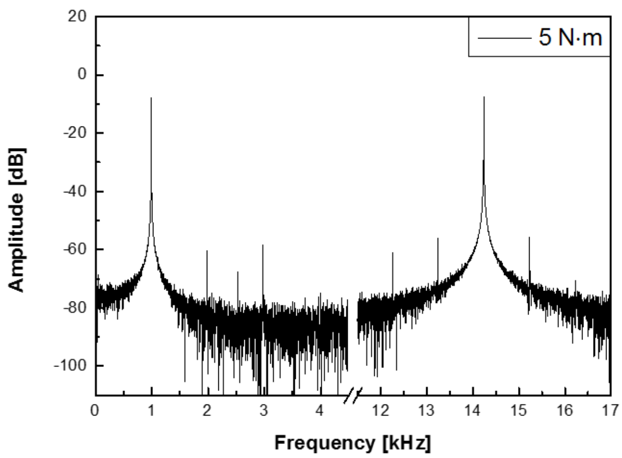

(b)

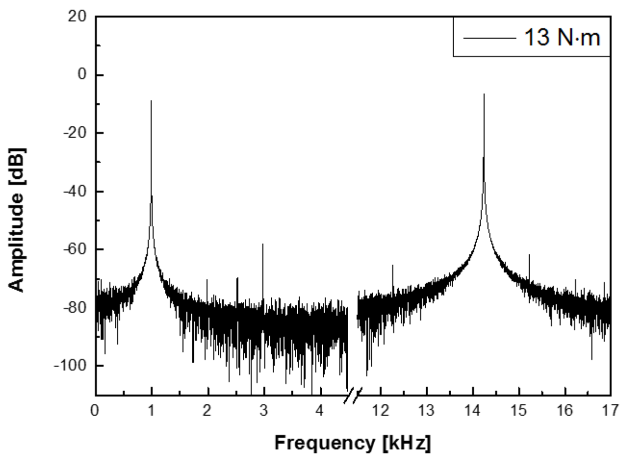

(c)

Figure 5.13 Spectra of the *Al-Al* single-lap joint with different degrees of residual torque remained on the bolt when the joint is subject to a mixed excitation: (a) 1 N·m (fully tightened); (b) 5 N·m (intermediately tightened); and (c) 13 N·m (fully loosened)

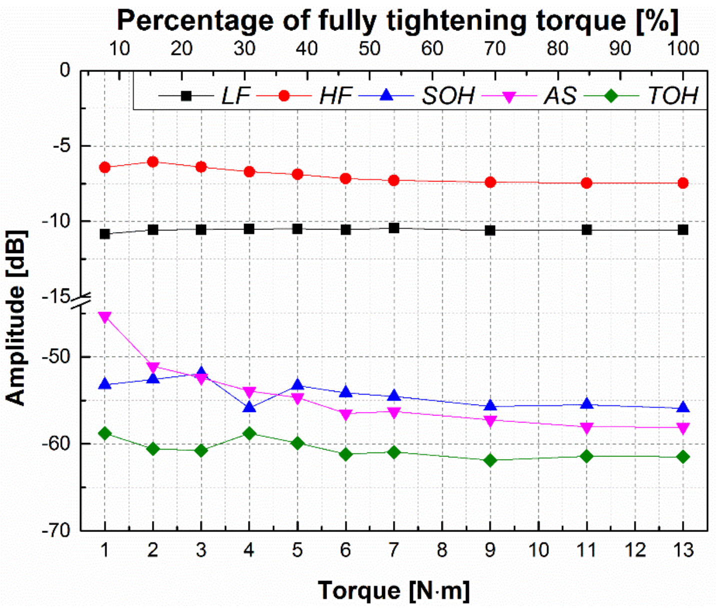

(a)

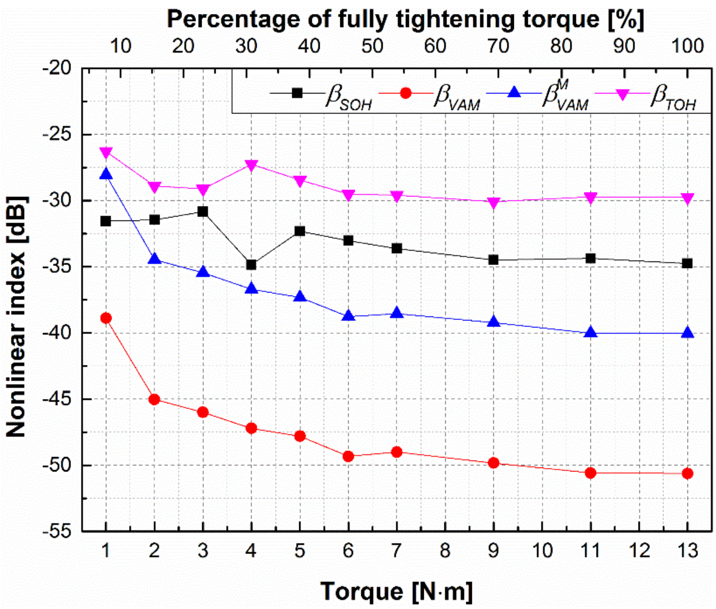

(b)

Figure 5.14 (a) Linear and nonlinear responses *vs.* residual torque; and (b) nonlinear indices *vs.* residual torque T for the *Al-Al* single-lap bolted joint

5.3.2. Cross-lap

The efficiency of the proposed nonlinear indices is further validated by detecting bolt loosening in the *Al-Al* cross-lap bolt joint. The experimental setup and specimen configurations are shown in **Figure 5.15** (a) and (b), respectively.

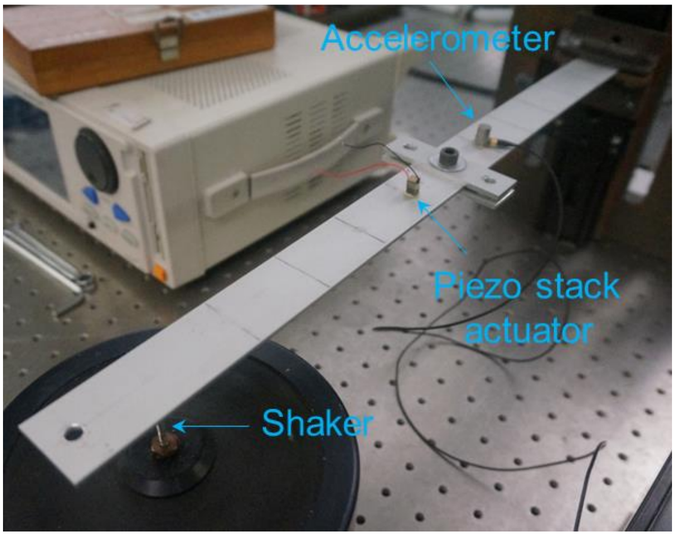

(a)

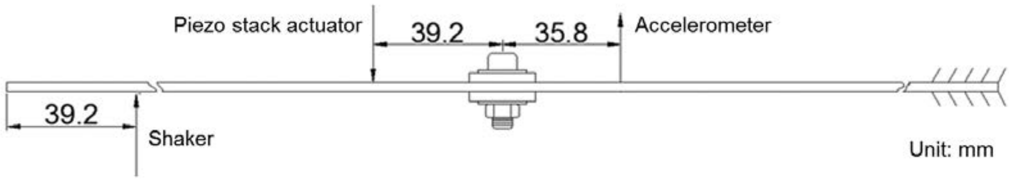

(b)

Figure 5.15 (a) Experimental setups; and (b) specimen configurations for the *Al-Al* cross-lap bolted joint using *CAN*-based nonlinear methods

The excitation frequencies of pumping vibration and probing wave for the *Al-Al* cross-lap bolted joints were selected following the similar principles with those for the *Al-Al* single-lap bolted joint according to the related spectral responses as shown in **Figure 5.16** (a)-(c). After then, 860 Hz and 14.77 kHz were selected as the excitation frequencies of pumping vibration and probing wave, respectively.

Upon conducting tests on the cross-lap bolted joint, three typical frequency spectra are displayed in **Figure 5.17** (a)-(c), for the joint with torques of 1, 5 and 13 N·m remained on the bolt. The nonlinear responses are observed to decrease with an increase in the applied torque. It is noteworthy that even at the fully tightened state of the joint (with a leftover torque of 13 N·m on the bolt) strong responses of *SOH* and *TOH* present, which indicates a high degree of *CAN* in the joint. From the comparison of excitation conditions between the *Al-Al* single-lap and cross-lap bolted joints, the intensity of pumping vibration (indicated by the response magnitude of *LF*) is found almost the same for these two joints. Therefore, the difference in the degree of *CAN* between them is caused by the diversity of natural frequencies selected for the pumping vibration and difference of joint configurations. To quantitatively identify the severity of bolt loosening using the nonlinear features, the reliance of linear responses and *CAN*-induced nonlinear responses on the residual torque is shown in **Figure 5.18** (a). The nonlinear indices for the *Al-Al* cross-lap bolted joint subject to different applied torques were calculated using **Equations (5.6)- (5.9)**, respectively, and displayed in **Figure 5.18** (b). From the observation, conclusions can be drawn that linear responses (i.e., *LF* and *HF*) change slightly regardless of the increase in the applied torque, while nonlinear responses (i.e., *SOH*, *TOH* and *AS*) show a high sensitivity to bolt loosening. Therefore, the magnitudes of sidebands can serve as an indicator to calibrate the degree of bolt loosening, including its early stage. Distinct from the performance of detecting bolt loosening in the single-lap joint, *TOH* presents a monotonic relation with the residual torque for the *Al-Al* cross-lap joint. Whereas, the dependence of *SOH* on the leftover torque of the joint occurs only when the applied torque exceeds 3 N·m.

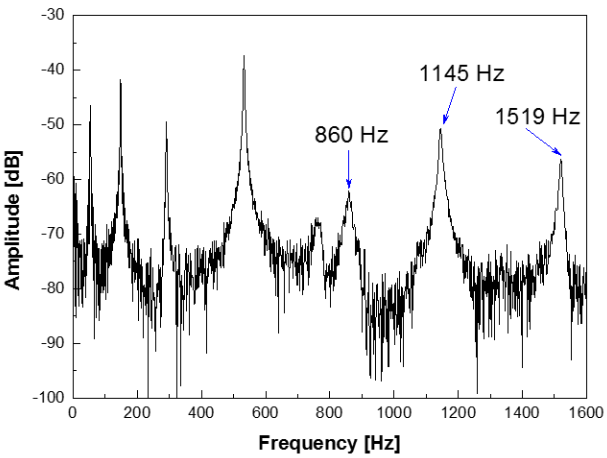

(a)

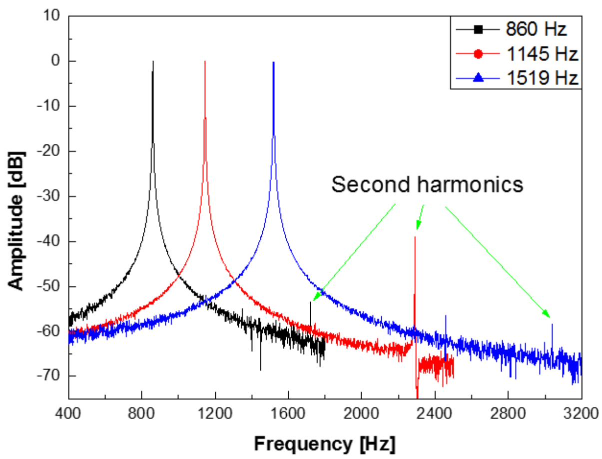

(b)

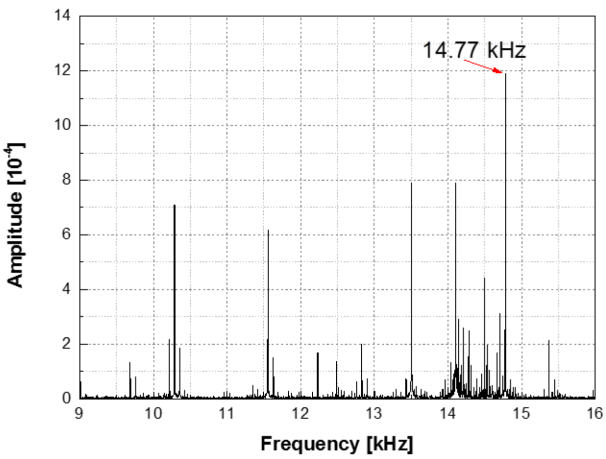

(c)

Figure 5.16 Spectra of response of the *Al-Al* cross-lap bolted joint (when T=1 N·m): (a) under an impact force; (b) under a harmonic force; and (c) under white noise

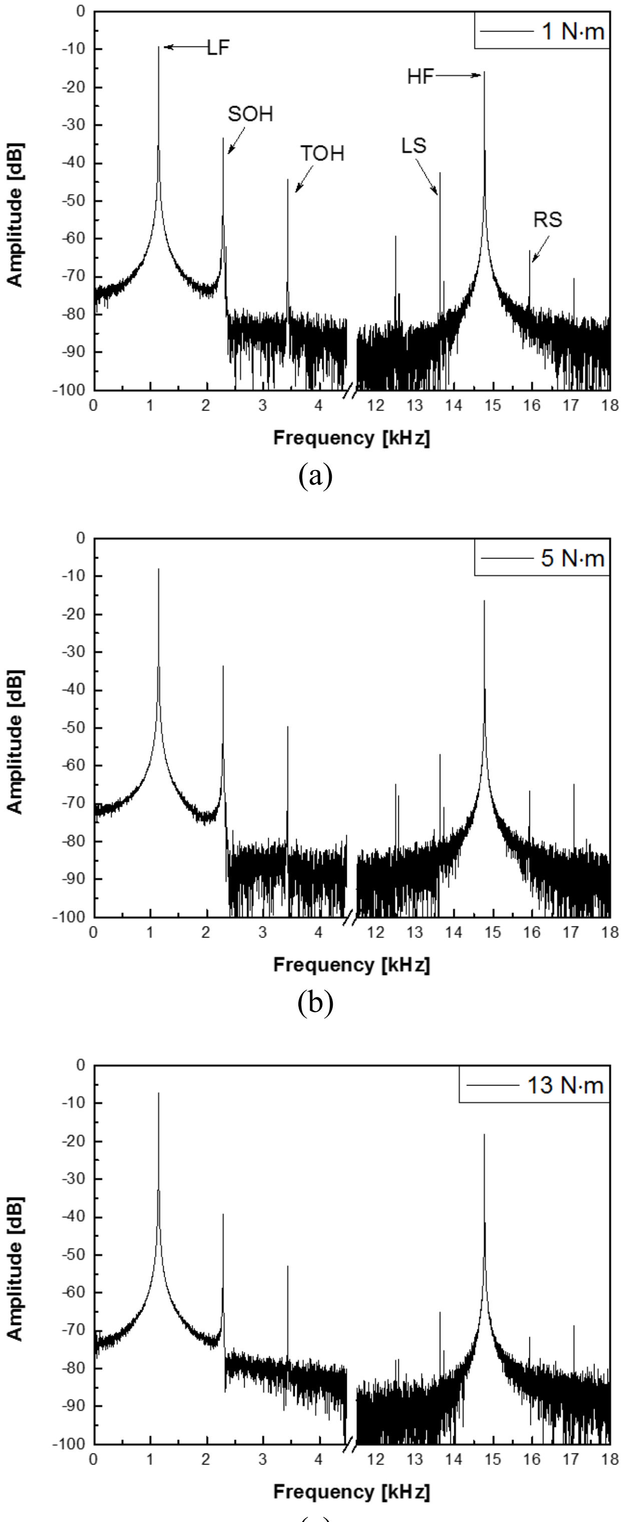

(c)

Figure 5.17 Spectra of the *Al-Al* cross-lap bolted joint with different degrees of residual torque remained on the bolt when the joint is subject to a mixed excitation: (a) 1 N·m (fully tightened); (b) 5 N·m (intermediately tightened); and (c) 13 N·m (fully loosened)

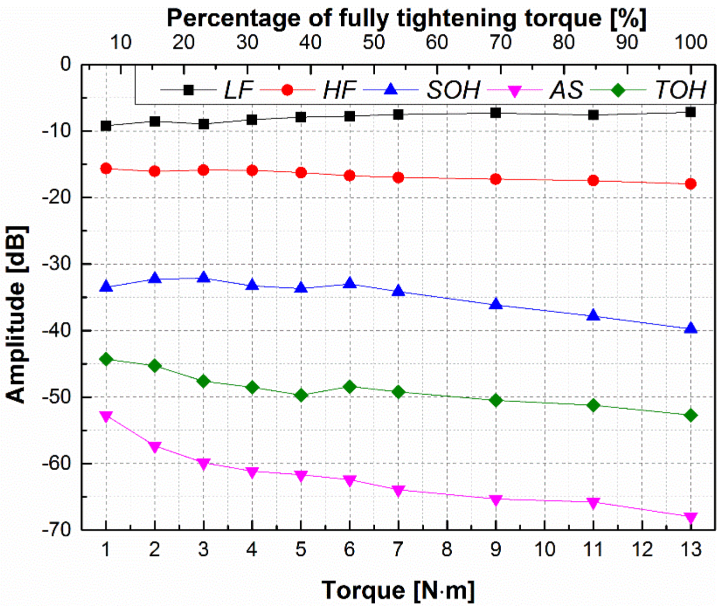

(a)

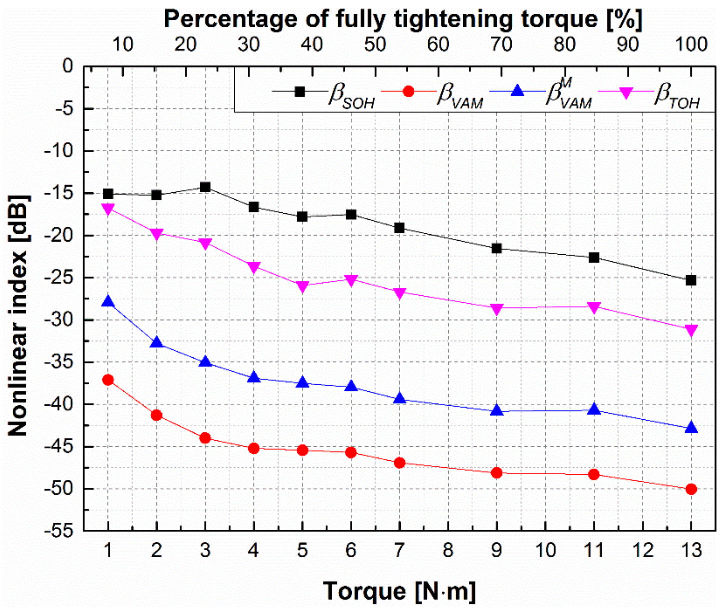

(b)

Figure 5.18 Linear and nonlinear responses *vs.* residual torque; and (b) nonlinear indices *vs.* residual torque for the *Al-Al* cross-lap bolted joint

5.3.3. Hybrid-lap

The proposed detection framework using nonlinear features is further adopted to identify the residual torque of loose bolts in the *Al-Al* hybrid-lap joint. The experimental setup and specimen configurations are shown in **Figure 5.19** (a) and (b), respectively.

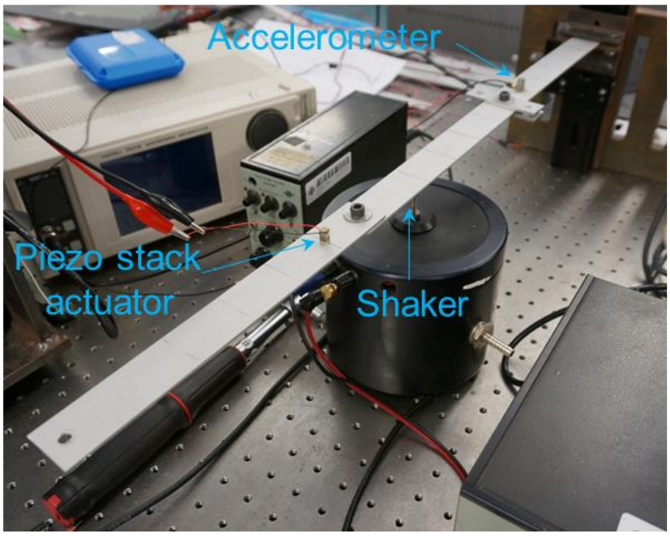

(a)

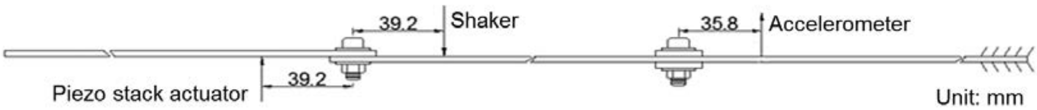

(b)

Figure 5.19 (a) Experimental setups; and (b) specimen configurations for the *Al-Al* hybrid-lap bolted joint using *CAN*-based nonlinear methods

In particular, the hybrid-lap bolted joint consists of both a single-lap and a cross-lap bolted joints, which is used to testify the performance of nonlinear indices towards multi-type joints widely adopted in the real engineering structures. It should be pointed out that for the hybrid-lap bolted joint, the torque values applied on both bolts were identical for the convenience of discussion and increased gradually from 1 N·m to 13 N·m.

Frequency spectra of the hybrid joint under three typical applied torques (i.e., 1, 5 and 13 N·m) are shown in **Figure 5.20** (a)-(c), to observe the occurrence of strong modulated sidebands when the bolt is fully loose (under 1 N·m), while fairly weak nonlinear responses present when the bolt is fully fastened (under 13 N·m). However, both *SOH* and *TOH* persist their strong response magnitudes despite the augment in the applied torque. As a result, they show a conditional sensitivity to changes in the applied torque compared to the modulated sidebands. Note that magnitude of *TOH* is even larger than that of *SOH* in some scenarios, which disagrees with the theoretical predictions by the first-order classical nonlinearity as proposed in Chapter 3 and to be discussed in detail later.

To achieve a quantitative analysis, correlation between the structural responses and the residual torque of the two bolts is established and shown in **Figure 5.21** (a). To observe a monotonic decrease in the magnitudes of sidebands due to the increase in the applied torque of the bolts. The magnitude of *SOH* decreases as the applied torque increasing after it is over 5 N·m. However, the dependence of *TOH* on the applied torque is not clear. On the other hand, linear responses (i.e., both *LF* and *HF*) present an independence on the applied torque. From the comparison in terms of efficiency of these four nonlinear indices in characterizing bolt loosening as shown in **Figure 5.21** (b), conclusions can be drawn that only *VAM*-based nonlinear index β_{VAM} and β_{VAM}^{M} are capable of identifying bolt loosening for such a hybrid-lap bolted joint.

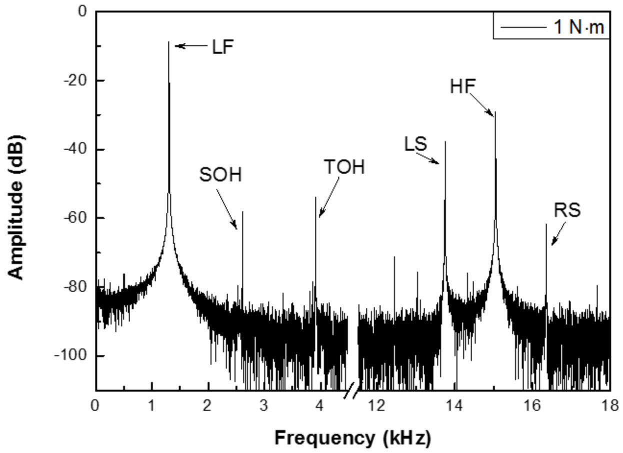

(a)

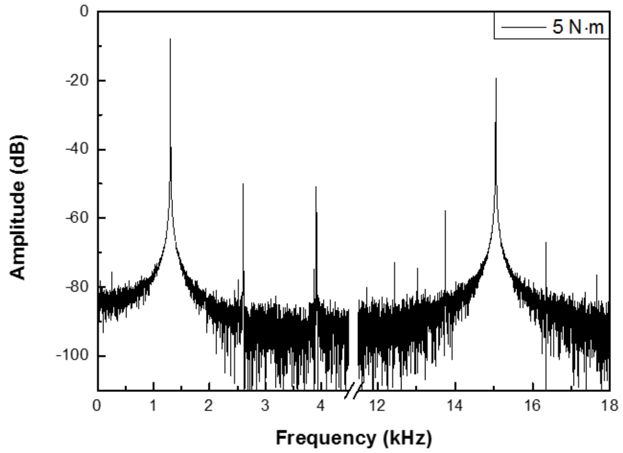

(b)

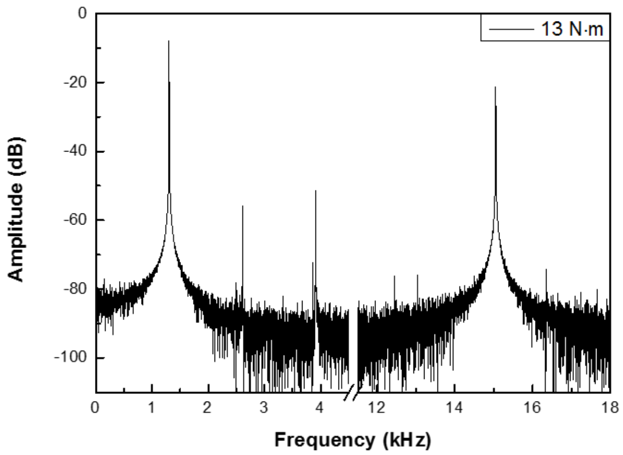

(c)

Figure 5.20 Spectra of the *Al-Al* hybrid-lap bolted join with different degrees of residual torque remained on the bolt when the joint is subject to a mixed excitation: (a) 1 N·m (fully tightened); (b) 5 N·m (intermediately tightened); and (c) 13 N·m (fully loosened)

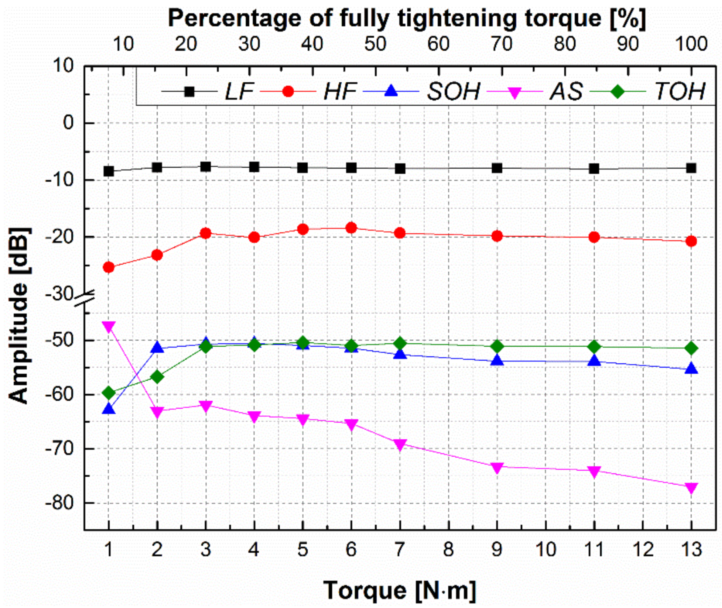

(a)

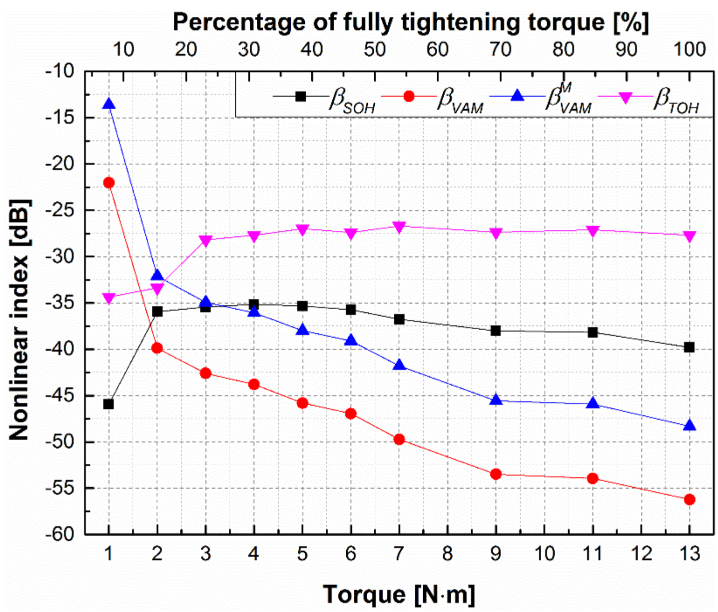

(b)

Figure 5.21 (a) Linear and nonlinear responses *vs.* residual torque; and (b) Nonlinear indices *vs.* residual torque T for the *Al-Al* hybrid-lap bolted joint

5.4. Case Study II: Detection of Bolt Loosening in a Single-lap *C-C* Bolted Joint

In most reported studies, *CAN*-based nonlinear methods are mainly used to detect loose bolts in metallic structures. Advanced composite materials, which offer unique advantages such as high specific stiffness and strength, have been designed as a new generation of structural materials, of which assemble also relies on the use of bolted joints. However, there are rather limited studies devoted to identifying bolt loosening in bolted composite structures. With the utilization of low-frequency excitations, arising from which acoustic waves exhibit a lower degree of attenuation, the *VAM*-based method has the potential to be employed to monitor large composite structures with bolted joints. Having demonstrated the efficiency in identifying the residual torque of loose bolts in the multi-type *Al-Al* joints in previous sections, the proposed detection framework using nonlinear features of acoustic waves is comparably adopted to detect bolt loosening in the *C-C* single-lap bolted joint.

The experimental setup for the *C-C* single-lap bolted joint using the *CAN*-based nonlinear methods is displayed in **Figure 5.22**. The applied torque on the bolt was increased from 1 to 13 N·m and structural responses were captured at each scenario. As mentioned in Section 5.2.1, excitation frequencies of pumping vibration and probing wave for the *C-C* joint were selected as 758 Hz and 14.9 kHz, respectively, of which the input magnitudes were set as 8 V and 16 V, respectively.

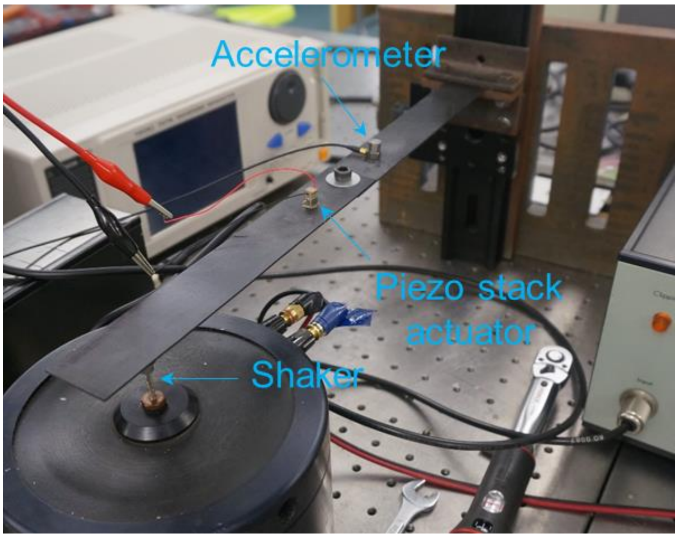

Figure 5.22 Experimental setups for the *C-C* single-lap bolted joint using *CAN*-based nonlinear methods

Upon conducting tests on the *C-C* joint under different degrees of bolt loosening, frequency spectra of the joint applied with three representative torques are shown in **Figure 5.23** (a)-(c). By comparing **Figure 5.23** (b) with (c), to observe when the applied torque is in the range between 5 and 13 N·m, the variation in the magnitudes of *LF* and *HF*, those are mainly associated with the change in linear dynamic responses, is deemed as negligible. On the contrary, the variation of nonlinear responses, e.g., changes in the magnitudes of sidebands, is considered capable of distinguishing changes in the bolt loosening degree even at the embryo stage. In addition, *SOH* and *TOH* show a relative lower sensitivity to bolt loosening at its early stage. Furthermore, a comparison between **Figure 5.23** (a) and (b) shows that much sharper variations of both linear (signal magnitudes of the *LF* and *HF*) and nonlinear (signal magnitudes of the sidebands) responses can be easily induced at a serious bolt loosening stage (i.e., in the bolt torque range between 5 and 1 N·m).

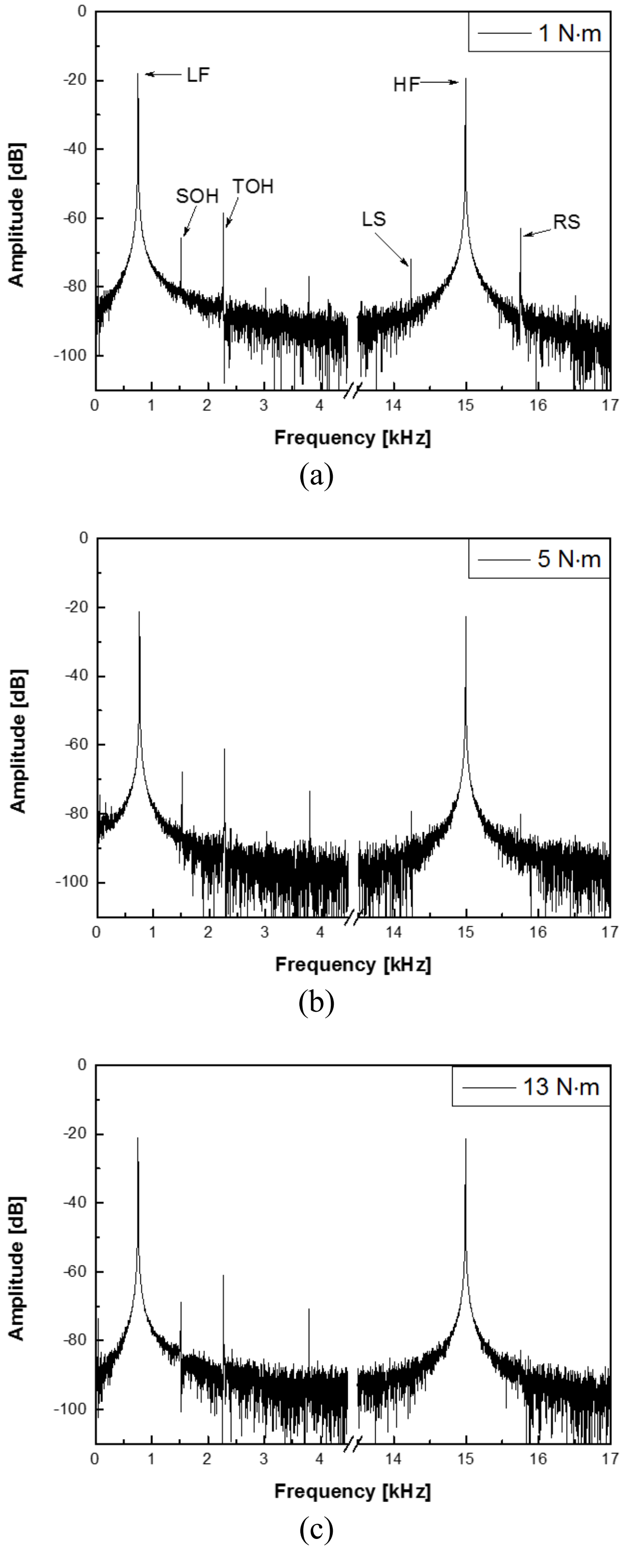

Figure 5.23 Spectra of the *C-C* single-lap bolted joint with different degrees of residual torque remained on the bolt when the joint is subject to a mixed excitation: (a) 1 N·m (fully tightened); (b) 5 N·m (intermediately tightened); and (c) 13 N·m (fully loosened)

Within the entire range of bolt torques from 1 to 13 N·m, linear and nonlinear responses of the joint at ten different bolt torque levels are displayed in **Figure 5.24** (a). The linear response, manifested as magnitude of *LF*, is observed to remain unchanged regardless of the variation of the applied torque, whereas the magnitude of *HF* changes phenomenally. As introduced in Chapter 3, the pressure-dependent damping and contact stiffness at the interface is responsible for the change in the linear response at the high frequency, i.e., *HF* magnitude. As a consequence, some fluctuations present in the change trend of *AS* (considering $AS \propto \beta_{VAM}^{theory} A_{LF} A_{HF}$.), which states the necessity of application of damage (bolt loosening)-related indices for the detection. The nonlinear indices, subject to the increasing residual torque of the bolt, are shown in **Figure 5.24** (b). It can be clearly identified that an obvious change of curve tendency of both β_{VAM} and β_{VAM}^{M} takes place at a certain point, probably between 6 and 7 N·m, below which sensitivity of these nonlinear indices to bolt loosening degree is much higher than that achieved beyond the point. Such an observation is consistent with the specific cases as presented in **Figure 5.23** (a)-(c), implying that bolt loosening at an early stage is of much higher difficulty to be quantified than that at a serious stage. By further scrutinizing the data distribution, and also by taking into account the unavoidable interference of measurement noise that leads to some disturbed data needing certain extent of tolerance, such as the one at 6 N·m, a conclusion can be made that the overall decreasing tendency of the curve sustains up to a considerably large level of bolt torque around 11 N·m, which means that the sensitivity of β_{VAM} and β_{VAM}^{M} is possible to be guaranteed in practical application at a quite early stage of bolt loosening. While *HOH*-based nonlinear indices demonstrate their detectability of bolt loosening in a limited range.

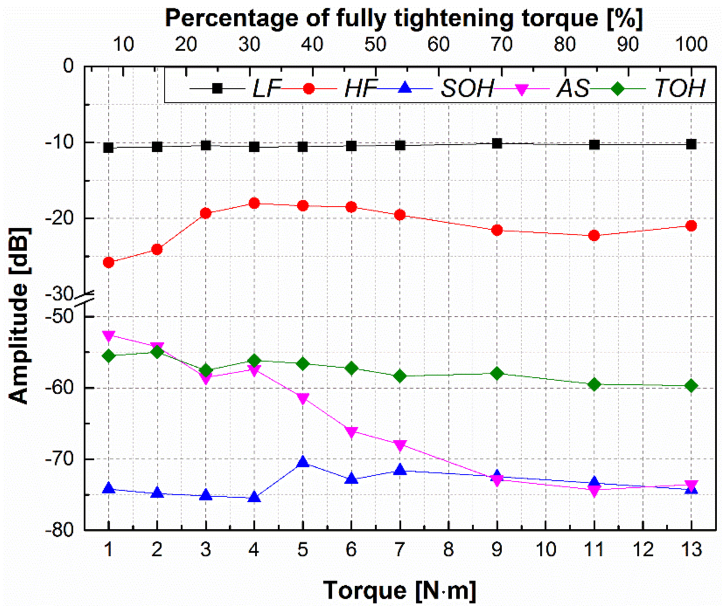

(a)

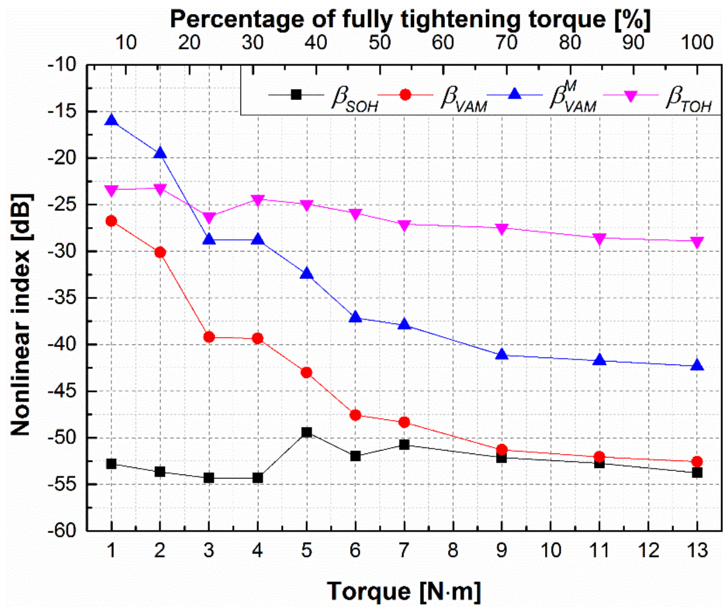

(b)

Figure 5.24 (a) Linear and nonlinear responses *vs.* residual torque; and (b) nonlinear indices *vs.* residual torque T for the *C-C* single-lap bolted joint

5.5. Discussions

From above experimental observations, some interesting phenomena present. For example, in some cases (i.e., for the *Al-Al* hybrid-lap and *C-C* single-lap bolted joints) the magnitude of *TOH* is even larger than that of *SOH*, which is not consistent with the theoretical prediction by using the first-order classical nonlinearity. Furthermore, the similar dependence on the residual torque (predicted by the theoretical model in Chapter 3) between *HOH* and modulated sidebands presents only when the applied torque is over certain value, for instance 5 N·m. These disagreements between the theoretical predictions and the experimental observations can be attributed to varied mechanisms of nonlinearity in real practice. In the macroscopic scale of material, local variation of stiffness due to the occurrence of loose bolts in a structure, produced by either hysteretic or pure elastic nonlinearity, amplitude-dependent dissipation or stick-slip friction at the contact interface, introduces different types of nonlinearity, for example first-order and second-order classical nonlinearity along with hysteretic nonlinearity. As mentioned in Chapter 3, application of the first-order classical nonlinearity introduces both even and odd *HOH* and every order sidebands at the frequencies of $f_{HF} \pm f_{LF}$ and $f_{HF} \pm 2f_{LF}$, as shown in **Figure 5.25**, while the other two introduce only odd *HOH* and second sidebands at the frequencies of $f_{HF} \pm 2f_{LF}$. Based on these, it can be inferred that when the applied torque is relative small, varied sources of nonlinearity produce simultaneously at the contact interface, due to a lack of efficient restriction pressure. This uncontrolled contact condition generates nonlinear features which cannot perfectly be described by using the theoretical model proposed in Chapter 3, based on the first-order classical nonlinearity. However, at the early stage of bolt loosening, the theoretical model provides predictions with an acceptable consistency with experimental results, which means the first-order classical nonlinearity dominants the nonlinear sources at the contact interface at this stage.

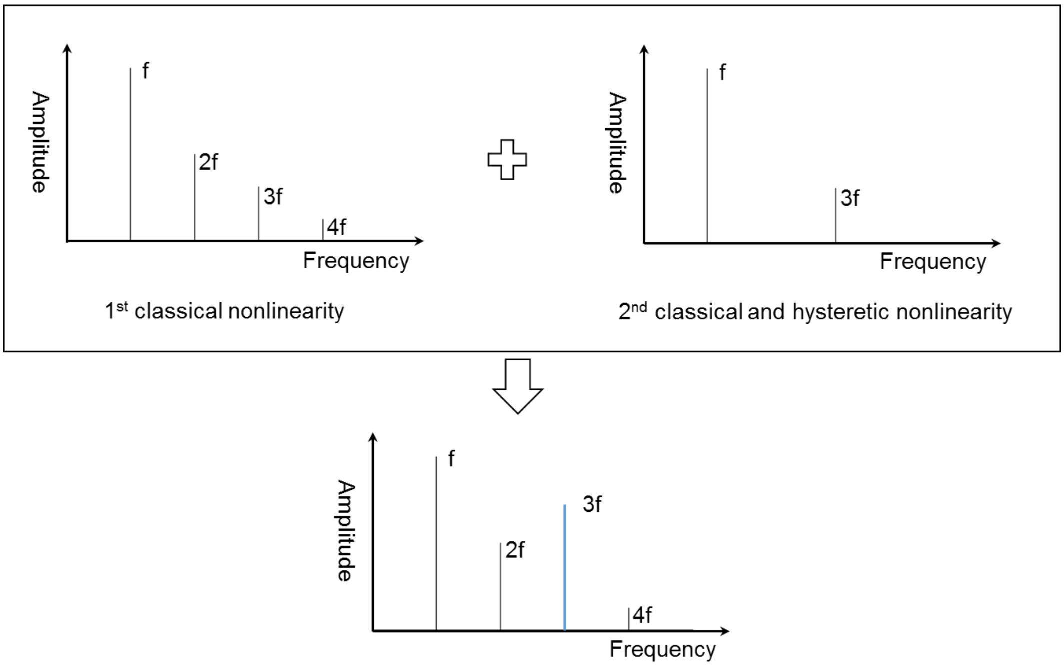

Figure 5.25 Varied mechanisms of nonlinearity at the contact interface of a loose joint

5.6. *WED*-based Linear Index *vs.* *CAN*-based Nonlinear Indices

To further compare the sensitivity of linear and nonlinear indices to bolt loosening for both the *Al-Al* and *C-C* bolted joints. In particular, the dependence of these indices on joint configurations and joining materials of are to be discussed in what follows.

5.6.1. Dependence on Joint Configurations

The relation between the linear/nonlinear indices and the residual torque of the bolt is exhibited in **Figure 5.26** (a)-(d). In **Figure 5.26** (a), the *WED*-based linear index, defined in terms of leaked or transmitted energy of incident waves upon passing through the bolt, is found to increase as the applied torque increases in a single-lap bolted joint, but decreases in a cross-lap bolted joint, showing a high dependence on the joint type. As it can be seen in **Figure 5.26** (a) that this linear index fails to identify the residual torque of the hybrid-lap bolted joint due to its serious dependence on joint configurations. In addition, bolt loosening at the early stage would not introduce a phenomenal change in the real contact area, as a result, the detectability is limited when using such a linear acoustic method for bolt loosening evaluation. The dependence of *SOH*-based and *TOH*-based nonlinear indices on the applied torque of the three types of *Al-Al* joints are displayed in **Figure 5.26** (b) and (c), respectively. To observe that over certain torque values, a monotonic decrease occurs in both nonlinear indices with an increase in the applied torque. Such nonlinear indices show a better detectability for the cross-lap bolted joint, compared to that for the other two joints. As displayed in **Figure 5.26** (d), for all the three types of joints, a consistent and monotonic tendency in the *VAM*-based nonlinear index can be clearly noted, which decreases rapidly when the bolt is tightened from fully loose (T=1 N·m) to a transit condition (T=2 N·m). After then a moderate decrease presents in the nonlinear index until the bolt is fully applied with a torque of 13 N·m. To conclude, the sensitivity of the *VAM*-based nonlinear index persists throughout the whole range, showing enhanced sensitivity than *HOH*-based indices. Such a nonlinear index thus renders a capability of quantitatively evaluating the residual torque of a loose bolt, including its early stage, in spite of joint types.

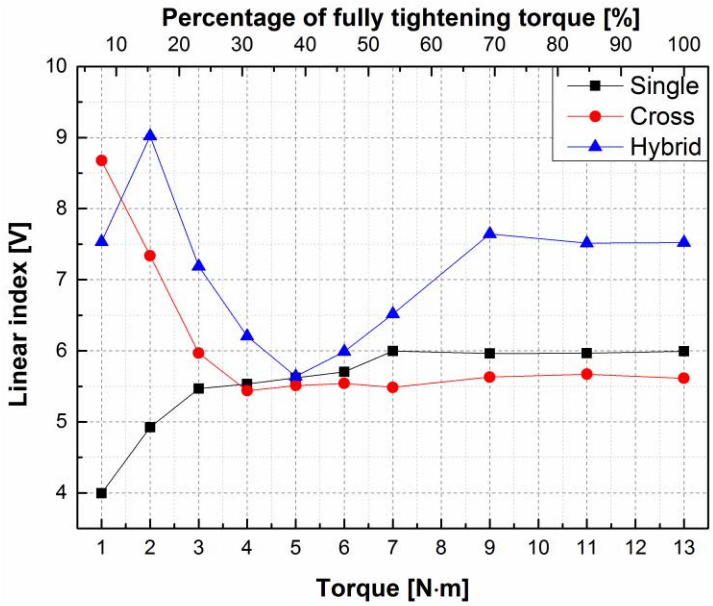

(a)

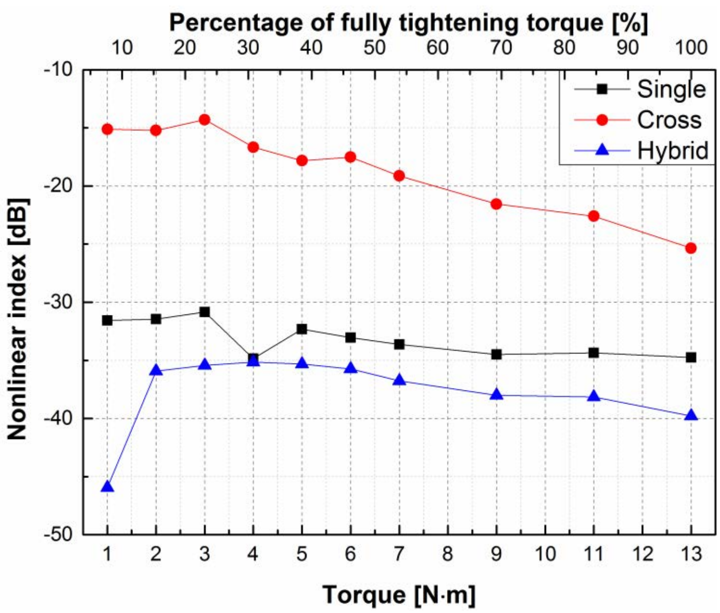

(b)

Figure 5.26 Linear and nonlinear indices *vs*. residual torque for multi-type *Al-Al* joints: (a) *WED*-based; (b) *SOH*-based; (c) *TOH*-based; and (d) *VAM*-based

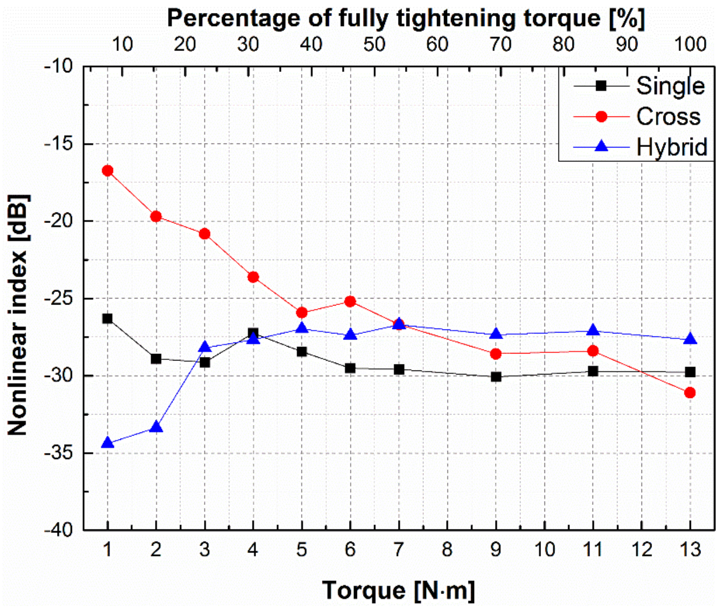

(c)

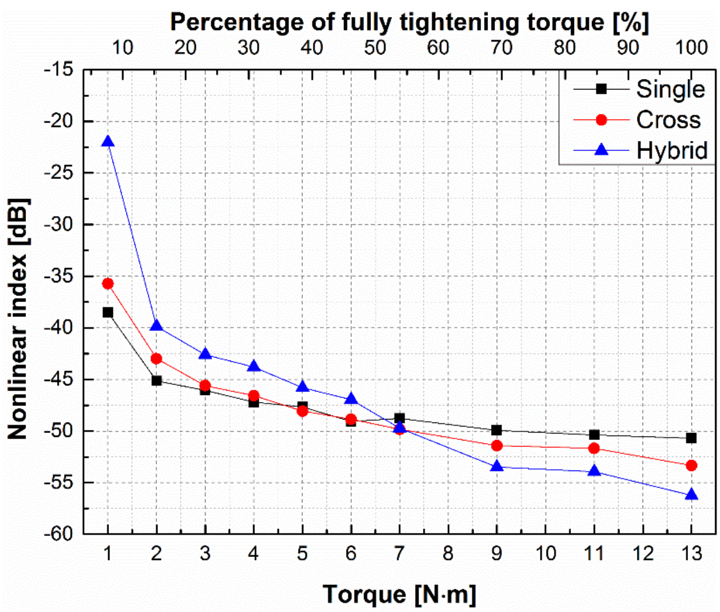

(d)

Figure 5.26 (continued)

5.6.2. Dependence on Joining Materials

The dependence of linear and nonlinear indices on joining materials are comparably exhibited in **Figure 5.27** (a)-(d). To observe that the detectability of the *WED*-based linear index is rather limited in terms of detectable range for the single-lap *C-C* bolted joint, which is caused by serious attention of *GUWs* propagating in composites. This problem may also present when such a linear feature-based method is employed to detect bolt loosening in large and complex structures. On the other hand, Both *SOH*-based and *TOH*-based nonlinear indices exhibit a similar dependence on the residual torque for the *Al-Al* and *C-C* bolted joints. Finally, the *VAM*-based nonlinear index even shows a better detectability for the *C-C* joint compared to the *Al-Al* joint.

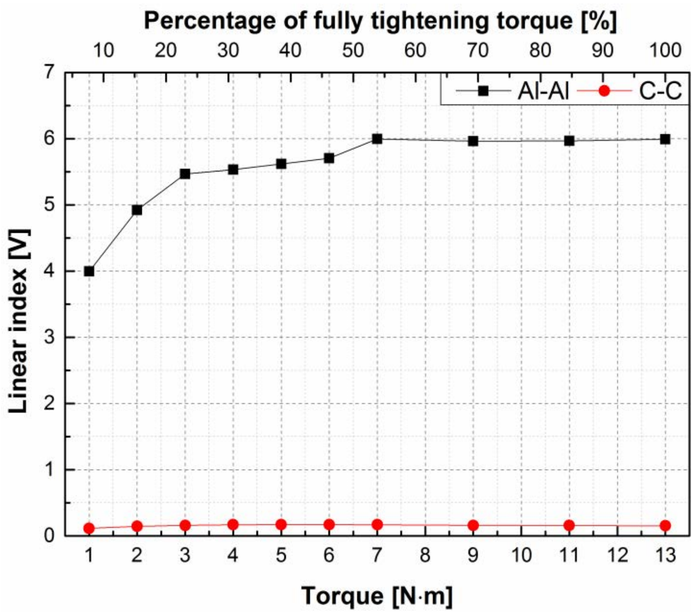

(a)

Figure 5.27 Linear and nonlinear indices *vs*. residual torque for the single-lap *Al-Al* and *C-C* joints: (a) *WED*-based; (b)*SOH*-based; (c) *TOH*-based; and (d) *VAM*-based

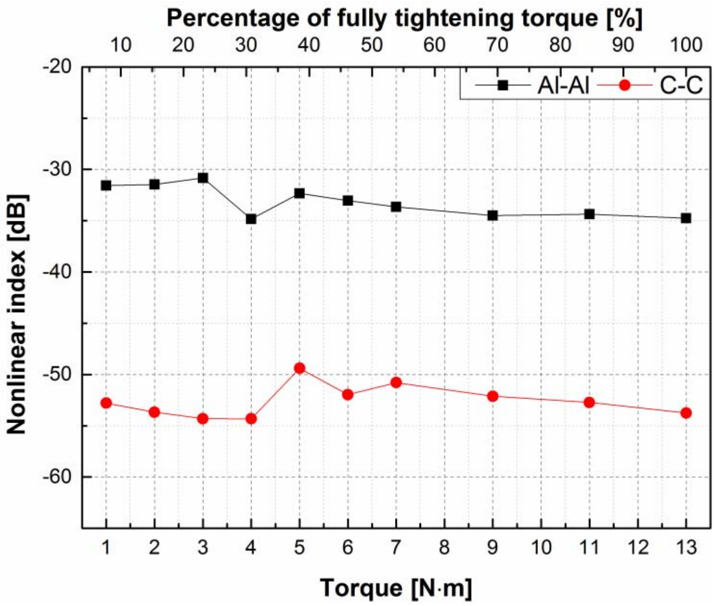

(b)

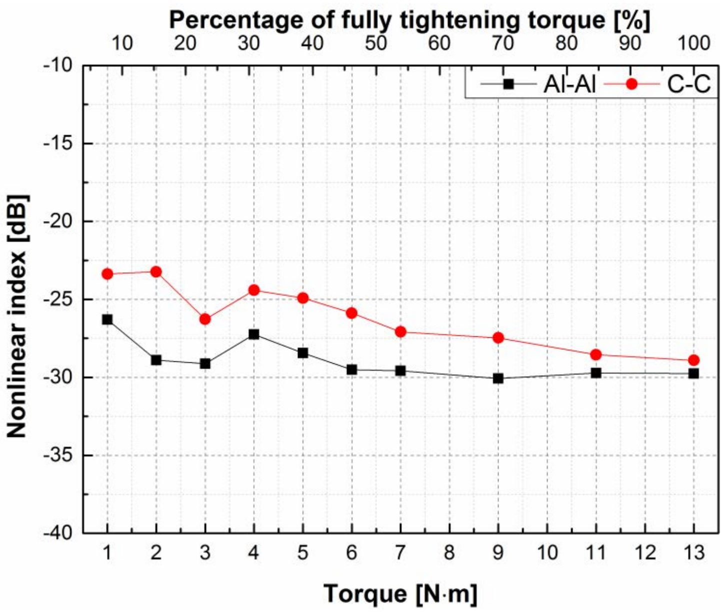

(c)

Figure 5.27 (continued)

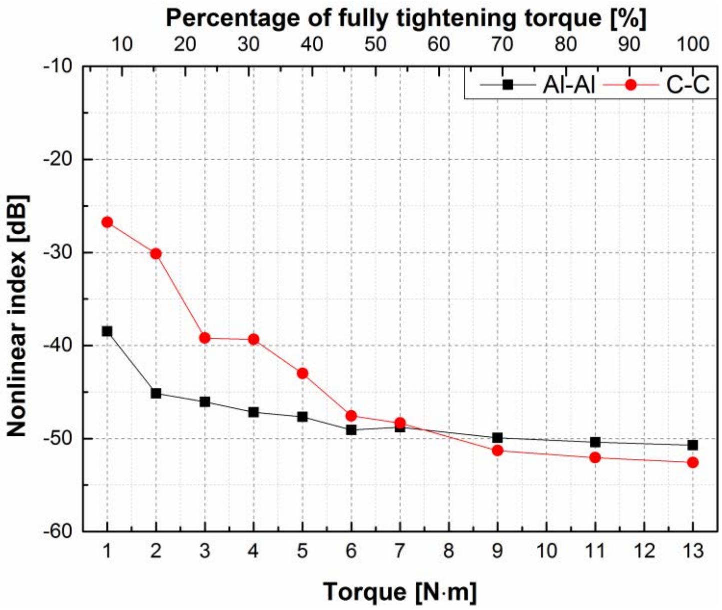

(d)

Figure 5.27 (continued)

To sum up, nonlinear indices, especially the *VAM*-based nonlinear index, show a high sensitivity to bolt loosening in both joints regardless of joining materials. Whereas, the *WED*-based linear index is only capable of evaluating the residual torque of the *Al-Al* joint at the late stage of bolt loosening. In addition, serious attenuation characteristic of *GUWs* when propagating in the composites should be carefully treated when applying such a linear feature-based method to detect bolt loosening in the *C-C* joint.

5.7. Summary

To sum up, in this chapter the accuracy of the theoretical model proposed in Chapter 3 is firstly verified by investigating the dependence of nonlinear indices on intensities of both pumping vibration and probing wave in both the *Al-Al* and *C-C* single-lap bolted joints. The linear responses of *LF* and *HF* exhibit a linear correlation with according input forces of pumping vibration and probing wave, respectively, which agrees with the theoretical predictions by **Equations (5.1)- (5.2).** In the meanwhile, nonlinear responses (i.e., *SOH*, *LS* and *RS*) also increase linearly as the input magnitudes of the pumping vibration and probing wave increase, which confirms the validity of **Equations (5.3)- (5.5)**. β_{SOH} and β_{VAM}^{M} are found being independent of the magnitude of *LF*, while β_{VAM} shows a linear correlation with *LF* magnitude. The dependence of *TOH* on *LF* can be divided into two stages. Before the response magnitude of *LF* reaches a certain value, β_{TOH} decreases with an increase in *LF* and after then it remains almost unchanged regardless of an augment in *LF*. On the other hand, a clear independence of all nonlinear indices on the intensity of *HF* presents. Thus, the utilization of β_{VAM} for damage detection must reside on a premise that the response magnitude of *LF* remains the same during the testing. A proper intensity of *LF* should be secured to achieve an effectual detection when using β_{TOH} .

Subsequently, to further verify the efficiencies of the proposed linear and nonlinear feature-based methods, these four nonlinear indices are comparably adopted to identify the residual torque of loose bolts for both the *Al-Al* and *C-C* bolted joints. To observe that linear responses (i.e., *LF* and *HF*) are not capable of indicating the state of loose joints at the early stage, while the sensitivity of nonlinear indices β_{VAM} and β_{VAM}^{M} , proposed from the magnitudes of modulated sidebands, persist their efficiency throughout the whole range from fully fastened to fully loose, regardless of joint configurations and joining materials, showing enhanced sensitivity than the linear counterpart. β_{TOH} presents its efficiency throughout the whole range only for the *Al-Al* cross-lap bolted joint. In most scenarios, β_{TOH} and β_{SOH} are able to identify the tightening state of loose joints when the leftover torque is over certain value. Otherwise, due to the mixed mechanisms of nonlinearity, *HOH*-based nonlinear indices fail to identify the state of loose joints at the late stage of bolt loosening. Therefore, the *VAM*-based nonlinear method shows the highest potential in the application of *SHM* for bolt loosening in real engineering structures while more studies are required to further improve the detectability of the *HOH*-based methods.

CHAPTER 6

Enhancement of Vibro-acoustic Modulation

6.1. Introduction

In Chapter 5, vibro-acoustic modulation (*VAM*)-based and high-order harmonics (*HOH*)-based nonlinear indices are comparably examined to evaluate the residual torque of loose bolts in both *Al-Al* and *C-C* bolted joints. Nonlinear indices β_{SOH} and β_{TOH}, developed from the magnitudes of *SOH* and *TOH*, respectively, are observed capable of identifying bolt loosening at the early stage but not including the late stage, during which varied nonlinearity sources synergistically determine the response magnitudes of nonlinear harmonics. As a result, the theoretical scenario proposed in Chapter 3 fails to accurately predict the dependence of *HOH* on the residual torque of the bolt. On the other hand, *VAM*-based nonlinear indices β_{VAM}^{M} and β_{VAM} successfully characterize bolt loosening throughout the whole torque range from fully loose to fully tightened in both *Al-Al* and *C-C* bolted joints, without a dependence on joint configurations or joining materials.

Given that the simplified scenario proposed in Chapter 3 only builds a qualitative relation between nonlinear responses and the residual torque of a joint. To gain a theoretical insight into the essence of generation of nonlinear dynamic responses (i.e., sidebands), an enhanced theoretical scenario of interfacial contact stiffness is established, facilitating defining the dependence of contact-acoustic-nonlinearity (*CAN*) on the contact pressure at a solid-solid interface. Numerical simulation based on the theoretical scenario with structural nonlinear contact stiffness is implemented, to achieve insight into *CAN* induced by a loose bolt in the joint under *VAM*, and a quantitative correlation between vibro-acoustic nonlinear distortions (manifested as sidebands in signal spectrum) and the degree of bolt loosening is ascertained.

As the essential cause to introduce nonlinear dynamic signatures such as sideband responses, *CAN* is firstly characterized by establishing a modified theoretical scenario of interfacial contact stiffness. In this scenario, similar with those in Chapter 3, a linear term increasing and a nonlinear term decreasing exponentially with the increase of bolt torque are contained to theoretically describe changes in the applied torque of a joint. Based on the numerical results, a *VAM*-inspired framework is developed for monitoring structural integrity of single-lap *Al-Al* and *C-C* bolted joints, which is experimentally validated by evaluating different degrees of leftover torques on loose bolts in these two joints. The effectiveness and accuracy of the modified scenario are then examined by numerical study, where *FE* scenarios of the *C-C* and *Al-Al* joints are developed and utilized to calculate structural dynamic responses including both linear and nonlinear signatures. The numerical results obtained without/with nonlinear contact stiffness are comparatively presented to reveal the relation between the degree of *CAN* and response magnitudes of modulated sidebands.

6.2. An Enhanced Theoretical Model of Interfacial Contact Stiffness

In Chapter 3, a simplified contact scenario is adopted to describe the relation between the applied torque and contact stiffness at the interface of a joint (including both linear and nonlinear parts, subject to a power-law). A single-degree-freedom system successfully links the contact stiffness of loose joints to the response magnitudes of nonlinear features (i.e., modulated sidebands), which has been validated by subsequent experimental observations. To build a quantitative correlation between the magnitudes of modulated sidebands and the residual torque of loose joints, numerical simulation of the *VAM*-based method using a two-degree-freedom system is presented in the followings.

As mentioned in Chapter 2, currently there exist no perfect scenarios, gaining a wide acceptance, to describe *CAN* when acoustic waves interact with the interface of a crack or a loose joint. From our experimental observations, multiple sources of nonlinearity at the contact interface of a joint are inferred to affect the generation and intensity of the nonlinear responses. To take the theoretical analysis a step further and simplify the calculation, the first-order classical nonlinearity is still adopted in the numerical simulation, although it may not be capable of involving in all mechanisms of *CAN*.

The surface of a solid is rough with randomly distributed asperities, and consequently the solid-solid interface features partial contact when two solids come into contact. It can be inferred that the real contact area of the interface increases with an augment of the contact pressure. Earlier studies [1] have confirmed that linear interfacial contact stiffness is proportional to the real contact area at the interface, which is synergistically determined by the contact pressure and surface roughness. Along the same line of thinking, when two structural components are assembled via a bolt, a partial contact occurs at the interface, even when the bolt is fully fastened.

Provided that the bolt is loose to a certain extent, the accordingly reduced contact pressure at the interface induces "breathing" effect (i.e., *CAN*) when the joint is subject to a harmonic vibration. The local nonlinear contact stiffness in the mating parts (i.e., *CAN*) of the loose joint, which is associated with the residual torque remained on the bolt, dominates both the structural nonlinear stiffness and resultant nonlinear response of the joint. To facilitate comprehending of the mechanism of nonlinear distortion generation in the modulated waves (manifested as sideband magnitudes in signal spectra) when the joint is subject to a mixed excitation, it is of vital importance to ascertain the reliance of interfacial contact stiffness on the residual torque on the loose bolt. To this end, a power-law relation between the linear contact stiffness, K_L, and interfacial pressure, *P*, at the solid-to-solid interface can be given by [90]

$$K_L = \begin{Bmatrix} k_L^t \\ k_L^r \end{Bmatrix} = \begin{Bmatrix} \lambda_0^t \\ \lambda_0^r \end{Bmatrix} P^m, \tag{6.1}$$

where k_L^t and k_L^r are the linear transitional and rotational stiffness, respectively; λ_0^t, λ_0^r and m are constants relating to asperity-height distributions along the contact surfaces, which can be used to characterize the degree of surface roughness.

However, in experiment, the utilization of **Equation (6.1)** is fairly restricted because it is a challenging task to measure the interfacial pressure. Considering that P is approximately proportional to the interfacial preload, F, and a linear relationship between F and the applied bolt torque, T, exists (according to $F = T / \tau d$, where d and τ are the bolt diameter and friction coefficient between the nut and bolt, respectively), K_L in **Equation (6.1)** can thus be linked directly with T, in terms of

$$K_L = \begin{Bmatrix} \lambda_1^t \\ \lambda_1^r \end{Bmatrix} T^m, \qquad \textbf{(6.2)}$$

where λ_1^t and λ_1^r are the modified surface-roughness-related constants proportional to λ_0^t and λ_0^r in **Equation (6.1)**, respectively. The inclusion of T in **Equation (6.2)** makes it possible to indicate quantitatively the bolt loosening, as T is a parameter that can be acquired via measurement. Under most circumstances, most asperities on the contact surfaces in the mating parts of a composite joint feature comparable and similar heights and curvatures, which leads to a quantitative correlation between the real contact area (A) and contact pressure as $A \propto P^{0.5}$. Given that $K_L \propto A$ and $P \propto T$, m in **Equation (6.2)** is estimated to be 0.5.

As mentioned earlier, a typical interfacial "breathing" effect is induced into a loose joint when the joint is subject to *VAM*, where a rapid and periodical variation in the contact area occurs. Such a phenomenon results in generation of *CAN*, which, however, cannot be reflected by merely using K_L in **Equation (6.2)**, because K_L is the linear contact stiffness and independent of *CAN*.

To circumvent the above deficiency, a nonlinear contact stiffness, K_N, is introduced to scenario the bolted joint, which reads

$$K_N = \begin{Bmatrix} k_N^t \\ k_N^r \end{Bmatrix}, \tag{6.3}$$

where k_N^t and k_N^r are the nonlinear transitional and rotational stiffness, respectively. For simplicity, k_N^t and k_N^r were set to be constant values in [136] to introduce nonlinear dynamic responses. However, a constant K_N obviously implies that the bolt loosening-induced *CAN* is a constant, regardless of the residual torque on the bolt and the degree of bolt loosening, restricting the detection of bolt loosening from extending to a quantitative manner. In this scenario, K_N is re-defined to include both the linear and nonlinear contact stiffness, as

$$K_{enhanced} = \begin{Bmatrix} K_L \\ K_N \end{Bmatrix} = \begin{Bmatrix} \lambda_1^t T^m \\ \lambda_1^r T^m \\ \lambda_2^t T^n \\ \lambda_2^r T^n \end{Bmatrix}, \tag{6.4}$$

where $K_{enhanced}$ is the re-defined contact stiffness. λ_2^t, λ_2^r and *n* are three constants related to the surface roughness and actual contact area. In particular, the case in which $n = 0$ in **Equation (6.4)** actually corresponds to a constant K_N as assumed elsewhere [136]. In the enhanced scenario, the terms in K_N are assumed to vary inversely with the real contact area, as demonstrated elsewhere, by setting $n = -0.5$ in **Equation (6.4)**. The enhanced scenario implies that when bolt loosening initiates and progresses, K_N increases in magnitude and augments the extent of *CAN*; and in the meantime, K_L decreases due to the reduction in the interfacial pressure and actual contact area. Therefore, $K_{enhanced}$ is linked, quantitatively, to the residual torque remained on the loose bolt. It is noteworthy that the above discussion and scenario is independent of the types of joining material and it is therefore applicable to describe the interfacial contact behaviors of both a composite and a metallic joint. This is to be proven using numerical simulation in the sequent session using a single-lap composite-composite (*C*-*C*) and aluminum-aluminum(*Al*-*Al*) bolted connection.

6.3. Numerical Simulation

Now that the quantitative dependence of linear and nonlinear contact stiffness at the contact interface on the residual torque of a loose joint is developed based on micro contact theory. The accuracy of the enhanced contact scenario is to be examined by numerical study, where *FE* scenarios of the single-lap *C-C* and *Al-Al* joints are developed and employed to calculate both linear and nonlinear structural dynamic responses when they are subject to two excitations at distinct frequencies in what follows.

6.3.1. Numerical Analysis of Bolted Joints Using the Enhanced Theoretical Model

Based on the analytical scenario of interfacial contact stiffness of a bolted joint with a loose bolt, as described by **Equation (6.4)**, the analysis of a bolted joint is achieved, in conjunction with the use of a finite element (*FE*) method. The *FE* scenarios of the *C-C* and *Al-Al* joints as tested in the experiment are developed, as shown in **Figure 6.1**.

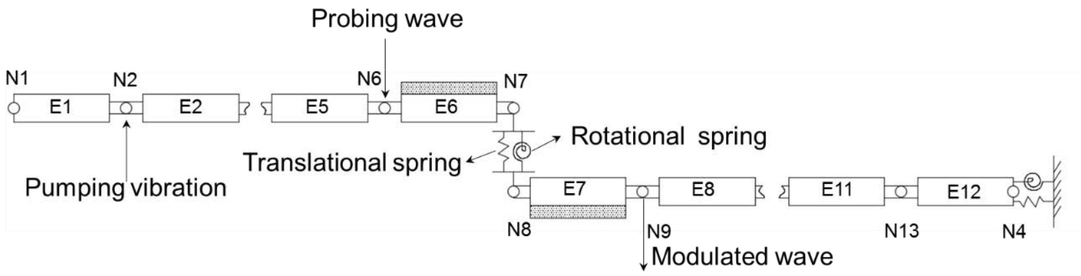

Figure 6.1 Finite element model of single-lap bolted joints

The scenario consists of two Euler-Bernoulli beam components, each containing six elements of the same length (denoted by E1~ E6) and seven nodes (N1~N7). Each node has two degrees of freedom (*DOF*s), i.e., transverse deflection, w, and rotation, θ. The right end of the joint is fixed to form a cantilever beam. A spring scenario is used to simulate the boundary condition in the clamped end and the contact condition at the lapped portion of the joint. The spring scenario comprises both translational and rotational springs that joints two beams via nodes N7 and N8, to introduce contact effect between element E6 and E7. Extra masses are added to E6 and E7 to simulate the bolt and nut (see shadowed areas in **Figure 6.1**). In the mixed excitation, the pumping vibration and probing wave are applied to the joint at nodes N2 and N6, respectively. The dynamic responses of the joint are obtained at node N9.

The equation of motion of the bolted joint under discussion is governed by

$$[M]\{\ddot{u}\}+[C]\{\dot{u}\}+[K_L]\{u\}+\mathbf{f_c}=\{F_e\}, \quad \textbf{(6.5)}$$

where $\{u\}$, $\{\dot{u}\}$ and $\{\ddot{u}\}$ are the displacement, velocity and acceleration vectors, respectively; $\{F_e\}$ represents the external excitation vector, and $\mathbf{f_c}$ signifies the nonlinear interfacial contact force vector equivalently treated as an excitation vector. Specifically, $\mathbf{f_c}$ includes non-zero elements only at the nodes within the bolted area (*i.e.*, N7 and N8), and can be defined as

$$\mathbf{f_c}=\left[0,...k_N^t(w_7-w_8)^2,k_N^r(\theta_7-\theta_8)^2,-k_N^r(\theta_7-\theta_8)^2,-k_N^t(w_7-w_8)^2,...0\right]^T, \quad \textbf{(6.6)}$$

where k_N^t and k_N^r, from **Equation (6.6)**, are the translational and rotational nonlinear stiffness of the inserted springs at N7 and N8, respectively, and are weighted with the squares of correspondingly relative displacements.

$[M]$, $[C]$ and $[K_L]$ are the global inertia, damping, and linear stiffness matrices in a dimension of 28×28, respectively, where $[M]$ and $[K_L]$ are assembled using local matrices established on elements, and $[C]$ can be ascertained according to Rayleigh damping assumption.

The inertia matrix of the bolted joints ($[M]$) is assembled by those of the beam element ([m^e]), as

$$[m^e] = \frac{\rho A l}{420}\begin{bmatrix} 156 & 22l & 54 & -13l \\ 22l & 4l^2 & 13l & 3l^2 \\ 54 & 13l & 156 & -22l \\ -13l & 3l^2 & -22l & 4l^2 \end{bmatrix}, \quad \textbf{(6.7)}$$

where ρ donates the density, A the area of the cross-section and l the uniform length of the beam element.

Similarly, the stiffness matrix of the bolted joints ($[K_L]$) can be assembled by those of the Bernoulli-Euler beam element ($[k^e]$) (see **Equation (6.8)**), and added by additional stiffness components considering the boundary condition.

$$[k^e] = \frac{EI}{l^3}\begin{bmatrix} 12 & 6l & -12 & 6l \\ 6l & 4l^2 & -6l & 2l^2 \\ -12 & -6l & 12 & -6l \\ 6l & 2l^2 & -6l & 4l^2 \end{bmatrix}, \quad \textbf{(6.8)}$$

where I signify the moment of inertia and E the Young's modulus of the beam. Specifically, Young's modulus for the unidirectional composite beam E_c is calculated from the Young's modulus of fiber E_f and matrix E_m with respect to volume fraction of the fiber V in the composite beam, as

$$E_c = VE_f + (1-\mathrm{V})E_m. \quad \textbf{(6.9)}$$

Lastly, the form of $[C]$ in **Equation (6.5)** is given according to Rayleigh damping assumption, as

$$[C]=\varsigma[M]+\chi[K_L], \quad \textbf{(6.10)}$$

where ς and χ are two constants to be estimated experimentally.

6.3.2. Results and Comparison

The unknown parameters associated with linear dynamic responses, including λ_1^t and λ_1^r in **Equation (6.2)**, and ς and χ in **Equation (6.10)**, are first estimated through fitting the linear experimental response in **Figure 6.2**, by using signal calculated based on the *FE* scenario using **Equation (6.2)**.

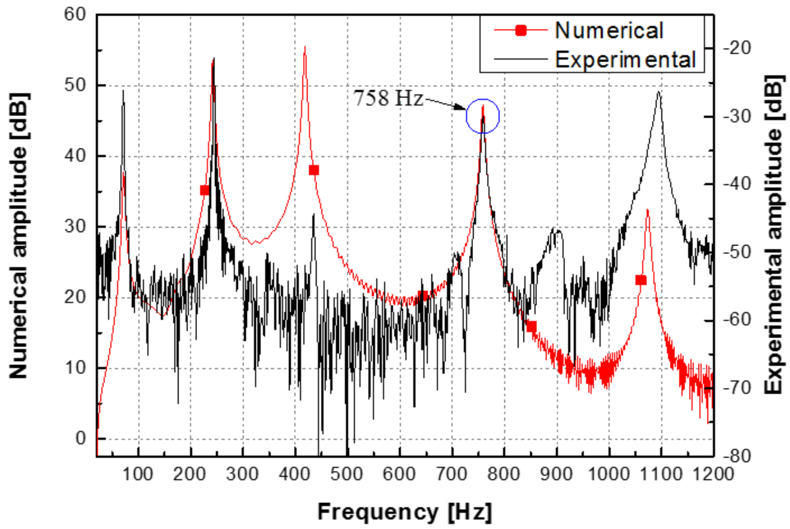

(a)

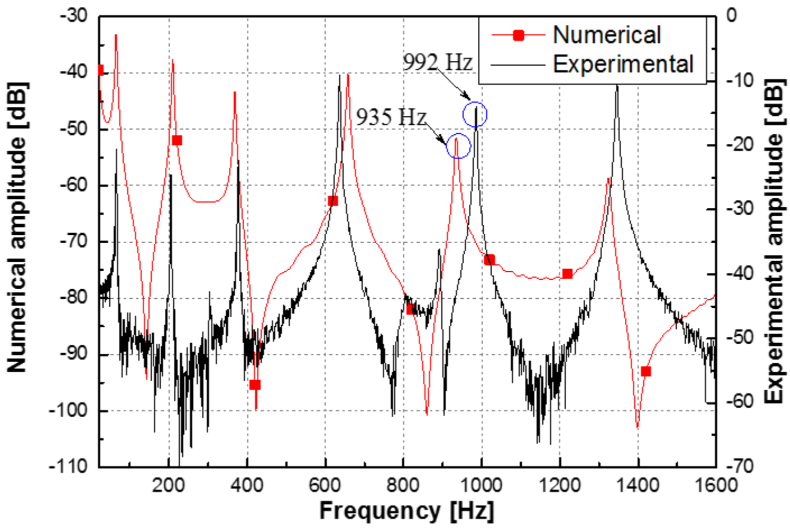

(b)

Figure 6.2 Experimental and numerical frequency responses at the low-order vibration modes of the (a) *C-C*; and (b) *Al-Al* bolted joints under a torque of 1 N·m

To be more specific, the parameters under estimation were determined when an accurate agreement between the experimental and numerical data was achieved at the natural frequencies of the first five vibration modes. Subsequently, the nonlinear parameters, i.e., λ_2^t and λ_2^r in **Equation (6.4)**, are estimated through fitting the nonlinear experimental responses by using numerical results calculated using the modified contact stiffness scenario (to be presented later), i.e., **Equation (6.4)** with $n = -0.5$.

The estimated parameters for the *FE* scenarios of *C-C* and *Al-Al* joints are shown in **Table** 6.1.

Table 6. 1 Estimated parameters for finite element simulation

Parameter	***C-C***	***Al-Al***
$\lambda_1^t \left[\mathrm{N}^{1/2}/\mathrm{m}^{3/2}\right]$	1×10^{6}	1×10^{6}
$\lambda_1^r \left[\mathrm{N}^{1/2}/(\mathrm{rad}\cdot\mathrm{m}^{1/2})\right]$	1×10^{9}	1×10^{9}
$\lambda_2^t \left[\mathrm{N}^{3/2}/\mathrm{m}^{3/2}\right]$	-1×10^{9}	-1×10^{9}
$\lambda_2^r \left[\mathrm{N}^{3/2}/(\mathrm{rad}^2\cdot\mathrm{m}^{1/2})\right]$	-1×10^{12}	-1×10^{12}
ς [s^{-1}]	20	20
χ [s]	6×10^{-7}	8×10^{-7}
ρ [kg/m^3]	1525	2691
E [Pa]	118×10^{9}	68.9×10^{9}

The excitation modes subject to the pumping vibration and probing wave are set, respectively, to be the same with those adopted in the experiment, with corresponding frequencies to be 758 Hz and 14.04 kHz for the *C-C* joint, and 935 Hz and 14.24 kHz for the *Al-Al* joint respectively. The computation procedure is shown in **Figure 6.3**.

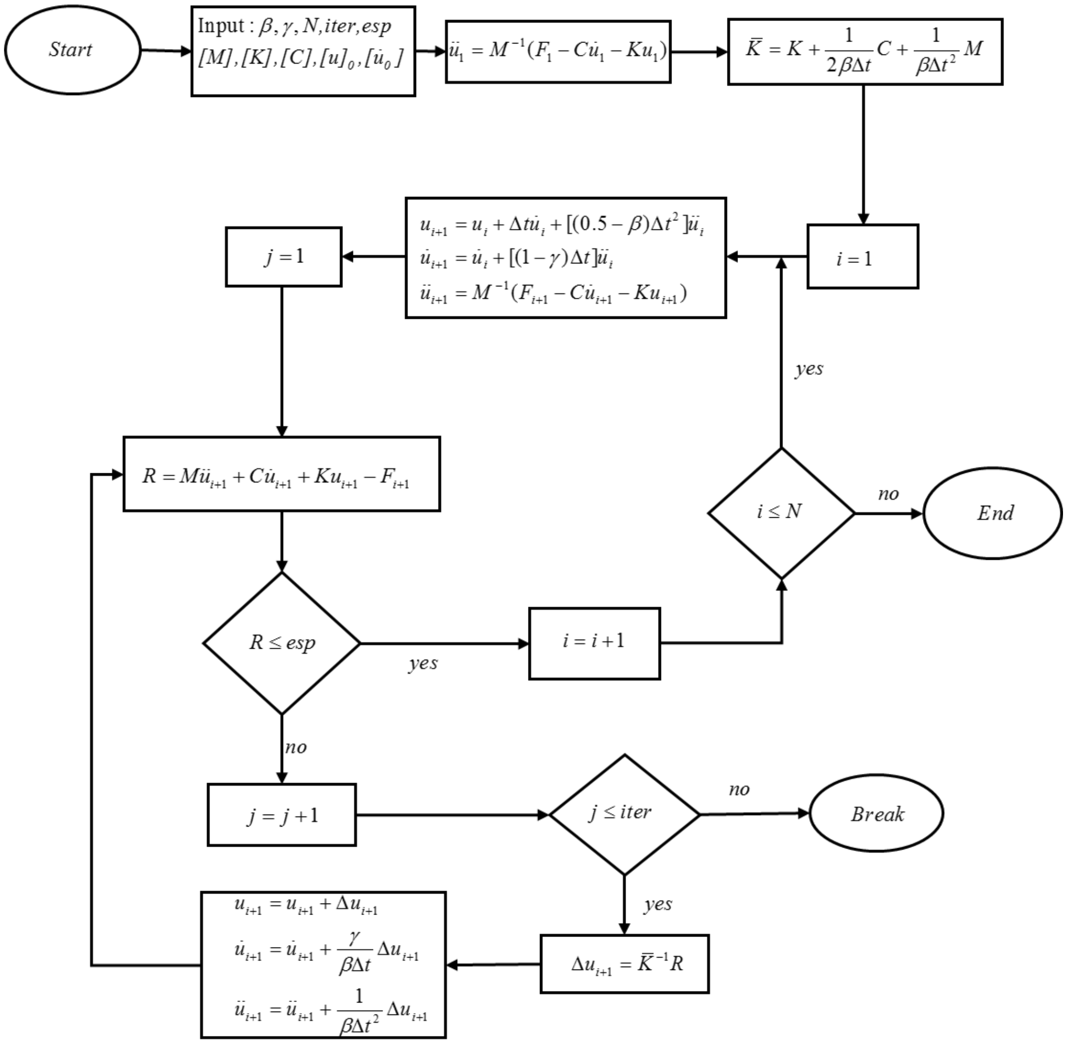

Figure 6.3 Flowchart of the proposed numerical computation, where 'num' represents the number of the total calculation steps; 'iter' is the maximum number of iteration within each step; 'esp' signifies the acceptable error; and ε , γ are adjustable parameters related to the accuracy and stability of the time scheme

Using the parameters as shown in **Table 6. 1,** representative time-domain signals of the *C-C* and *Al-Al* joints under a bolt torque of 6 N·m subject to the mixed excitation are calculated and normalized, as presented in **Figure** 6.4 (a)-(b). Two main frequency components, referred to as pumping vibration and probing wave, respectively, are observed and a considerable similarity can be seen between the numerical and experimental data.

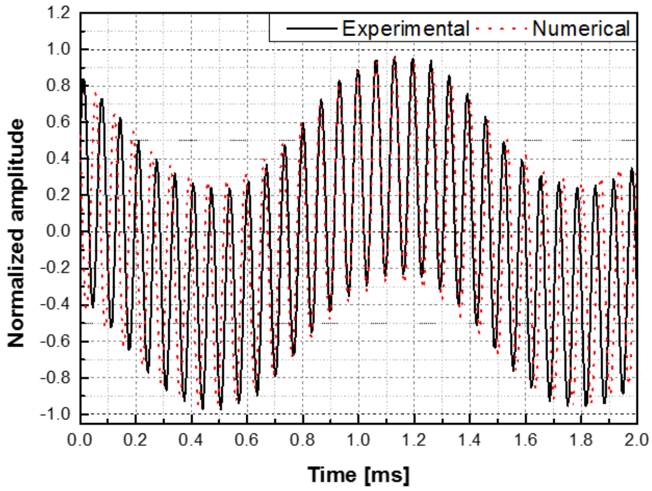

(a)

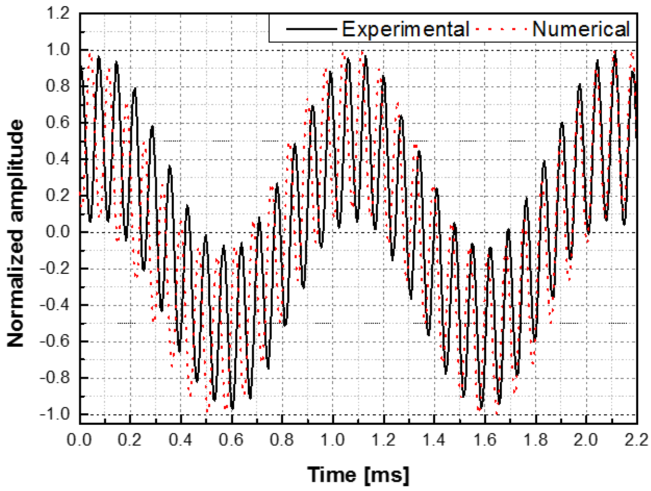

(b)

Figure 6.4 Time-domain responses of (a) *C-C*; and (b) *Al-Al* bolted joints with 6 N·m remained on the bolt, subject to numerical computation based on Scenario III and experimental measurement, respectively

For the purpose of comparison, dynamic responses of the *FE* scenario under different degrees of bolt loosening are then calculated by using three scenarios:

Scenario I: only the linear stiffness in the scenario is considered (**Equation (6.2)**);

Scenario II: the nonlinear stiffness in the scenario is considered, but the nonlinear terms are a constant (corresponding to $n = 0$ in **Equation (6.4)**); and

Scenario III: the enhanced analytical scenario is adopted, in which nonlinear stiffness is considered and the nonlinear terms vary subject to an exponential function ($n = -0.5$ in **Equation (6.4)**).

Figure 6.5 and **6.6** present the frequency responses calculated based on Scenario I when the *C-C* and *Al-Al* bolted joints under two extreme (i.e., the minimum and maximum) degrees of bolt loosening by setting the bolt torque to be 13 N·m and 1 N·m. Obviously, the absence of sidebands in the spectrum indicates the failure of Scenario I in faithfully depicting the dynamic response of the joint under a mixed excitation.

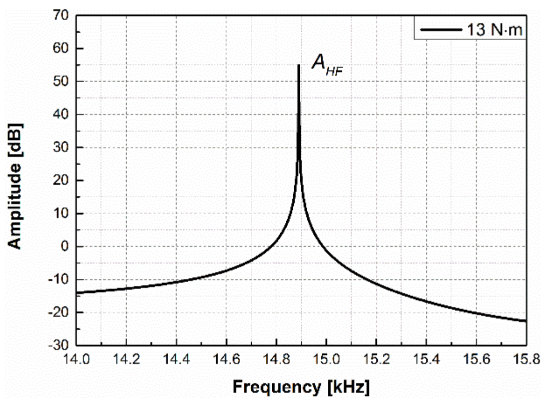

(a)

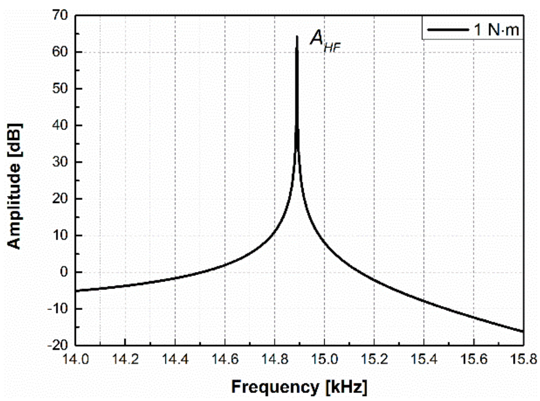

(b)

Figure 6.5 Frequency response of the *C-C* bolted joint, subject to numerical computation based on the linear contact stiffness (Scenario I) in Equation (6.2), under a bolt torque of (a)13 N·m; and (b)1 N·m

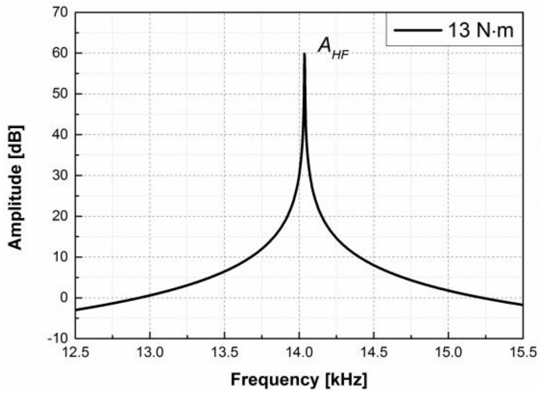

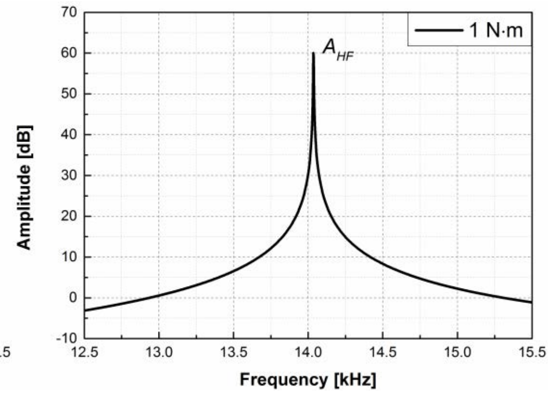

(a) (b)

Figure 6.6 Frequency response of the *Al-Al* bolted joint, subject to numerical computation based on the linear contact stiffness (Scenario I) in Equation (6.2), under a bolt torque of (a)13 N·m; and (b)1 N·m

Figure 6.7 and **6.8** compare the spectra of the composite joint, at four representative levels of bolt torques (T= 13, 9, 7 and 1 N·m), using Scenarios II and III, respectively. As mentioned in previous chapters, the joint under a torque of 13 N·m is considered as under a fully tightened condition according to the yielding strength of the composite specimen and the allowable tensile load of the bolt, whereas the joint under 1 N·m corresponds to a fully loosened condition. Under the bolt torque of 1 N·m, Scenarios II and III give rise to similar spectra, as shown in **Figure 6.7** (d) and **6.8** (d). The results using Scenario II include much higher sideband magnitudes compared with those calculated using Scenario III when the bolt torque increases. Obvious sidebands can even be captured in the frequency spectrum calculated by Scenario II for the joint under the fully tightened condition (i.e., under 13 N·m). This has revealed that Scenario II induces excessive sidebands due to the adoption of a pressure-independent nonlinear contact stiffness – a case inconsistent with the reality.

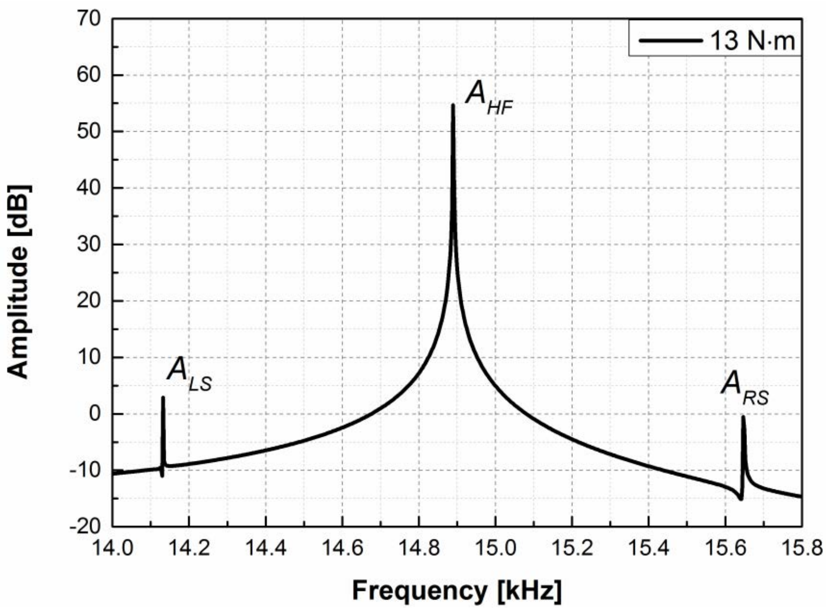

(a)

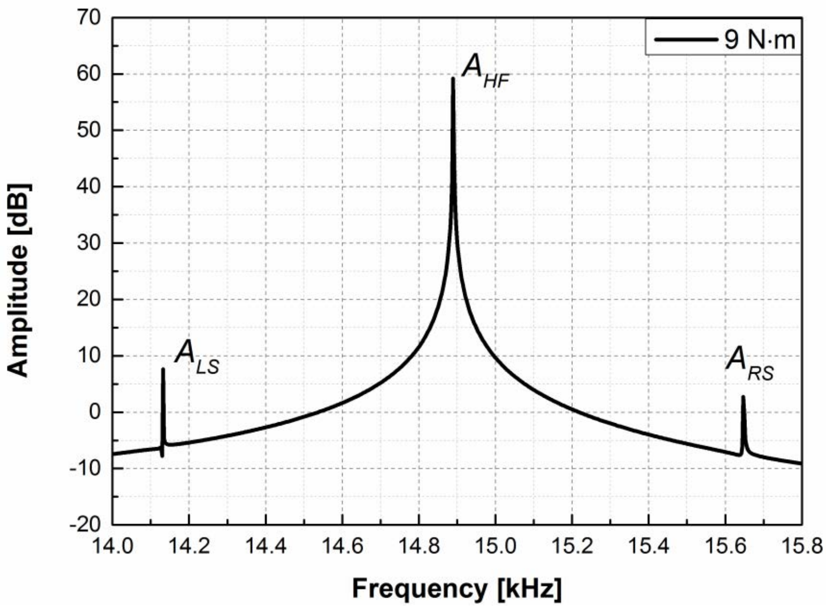

(b)

Figure 6.7 Numerical results of sideband responses of the *C*-*C* bolted joint under bolt torque levels of (a) 13 N·m; (b) 9 N·m; (c)7 N·m; and (d)1 N·m, respectively, by using contact stiffness according to Scenario II, which includes constant nonlinear terms, corresponding to n =0 in Equation (6.4)

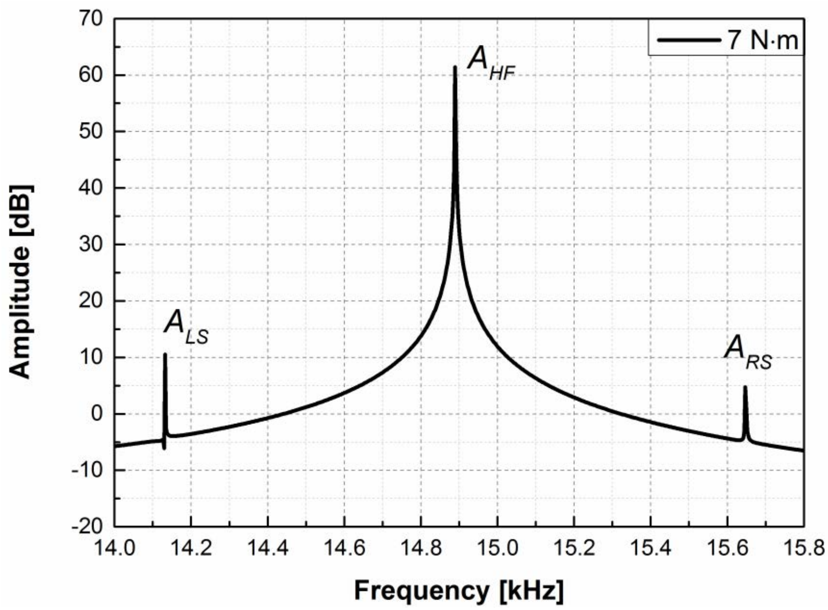

(c)

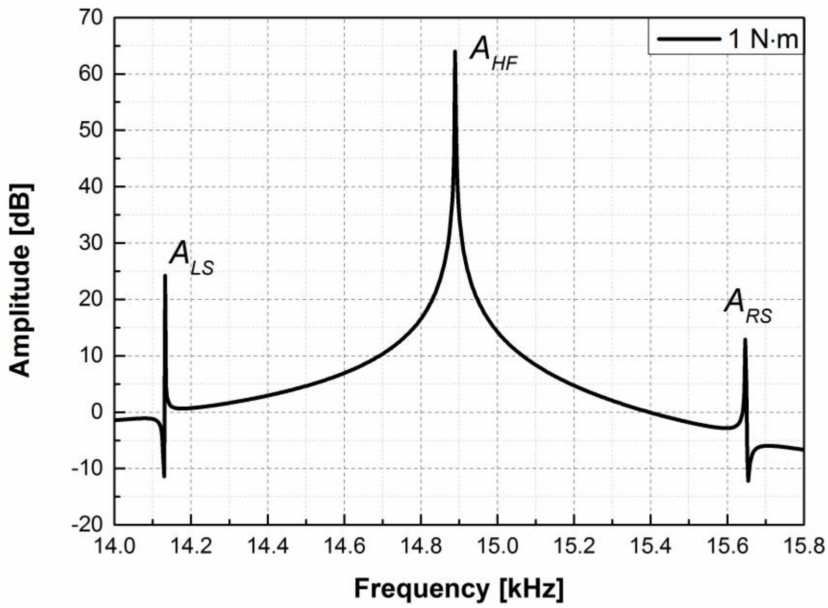

(d)

Figure 6.7 (continued)

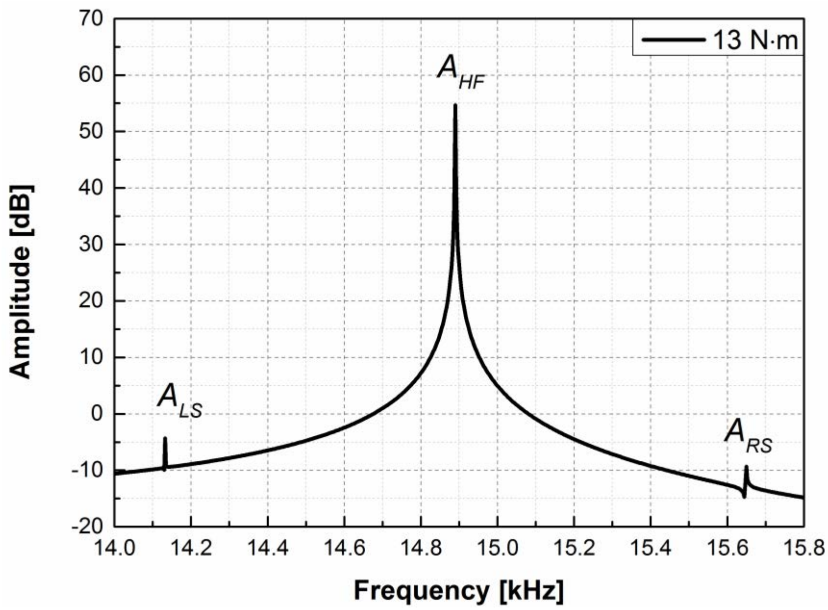

(a)

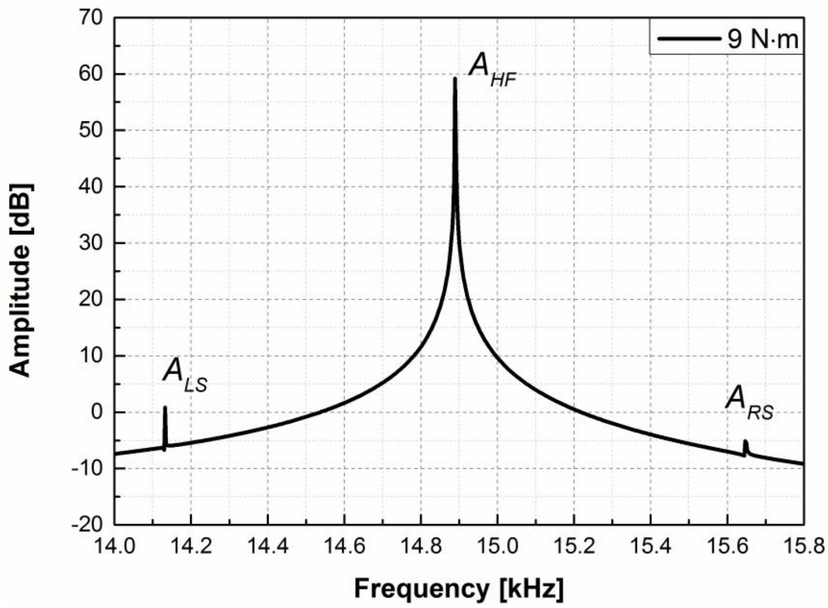

(b)

Figure 6.8 Numerical results of sideband responses of the *C*-*C* bolted joint under bolt torque levels of (a) 13 N·m; (b) 9 N·m; (c)7 N·m; and (d)1 N·m, respectively, by using contact stiffness according to Scenario III, which includes pressure-dependent nonlinear terms, corresponding to n = -0.5 Equation (6.4)

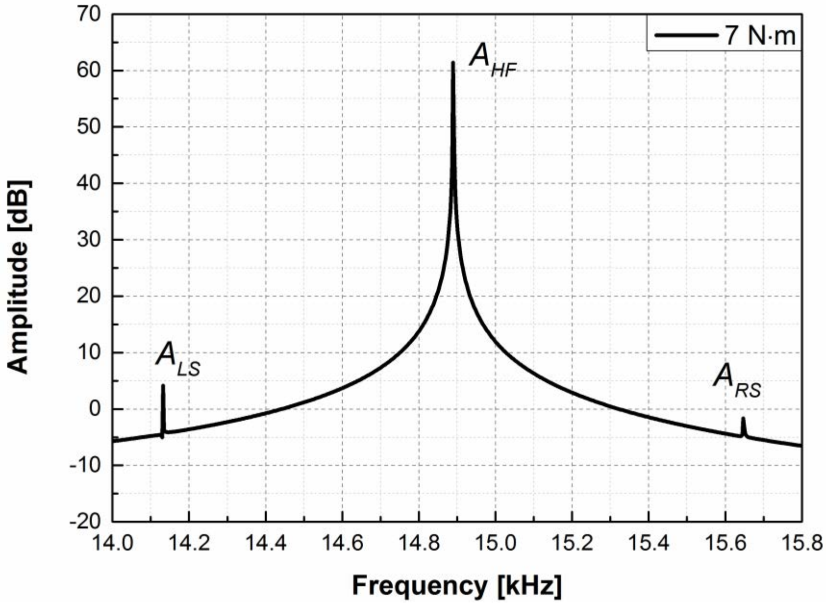

(c)

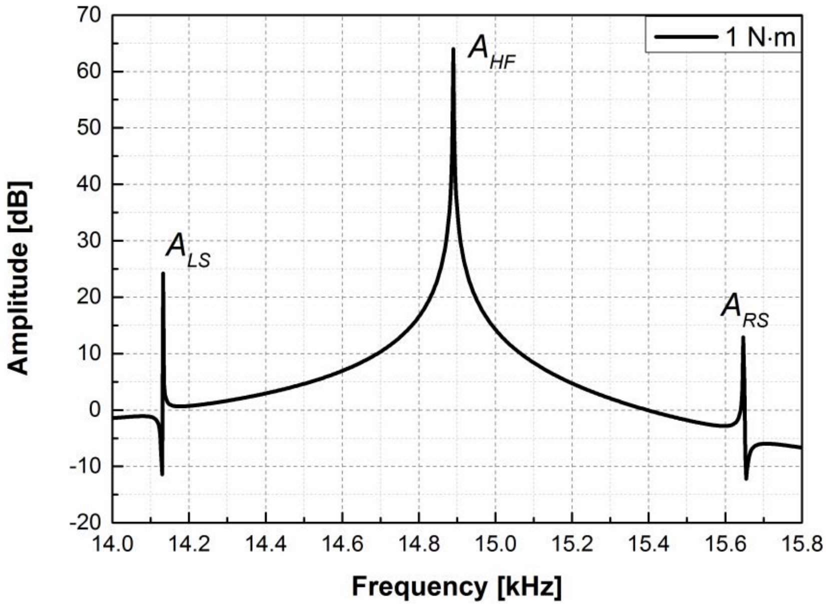

(d)

Figure 6.8 (continued)

It seems that at an early stage of bolt loosening under torque levels of 13, 9 and 7 N·m, modulated sidebands obtained by Scenario II exhibit a higher sensitivity to bolt loosening than those by Scenario III due to their magnitudes in **Figure 6.7** (a)-(c) look more significant than those in **Figure 6.8** (a)-(c). However, the validity of Scenario II is doubted when further comparison is made, by taking into account the actual data measured from experiment, as shown in **Figure 6.9** (a)-(c). Under similar levels of bolt torques, it is clear that the experimental data include much lower sideband magnitudes compared with those calculated using Scenario II. From such an aspect, it can be realized that Scenario III actually gives results much more consistent with the experimental findings. In addition, the change trend of sideband magnitudes caused by the increase in the applied torque obtained using Scenario III agrees better with the experimental results, i.e., the magnitudes increase slightly at the early stage of bolt loosening (in the torque range of 13-7 N·m) and a sharp increase in the magnitudes occurs when the torque decreases to 1 N·m from 7 N·m. It should be pointed out that the excitation frequency of probing wave in the experiment is slightly different with that presented in Chapter 5, which is caused by difference in the frequency selection of probing wave between different sets of repeated experiments due to uncertainness of bolts and diversity in the operation process of applying the torque.

The theoretical magnitude of sidebands for the *Al-Al* single-lap bolted joint under torques of 13, 9, 7 and 1 N·m calculated by Scenario II and III as exhibited in **Figure 6.10 (a)-(d)** and **Figure 6.11** (a)-(d) are compared with according experimental results as displayed in **Figure 6.12** (a)-(d).

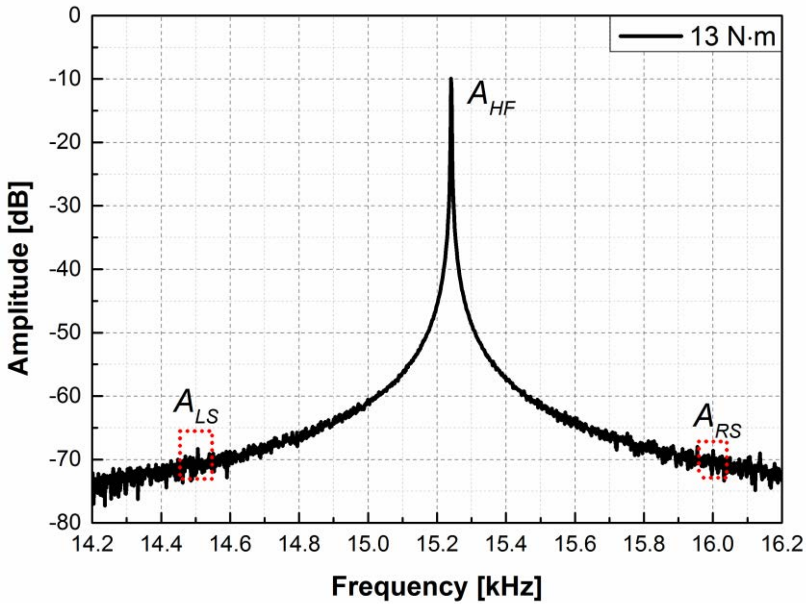

(a)

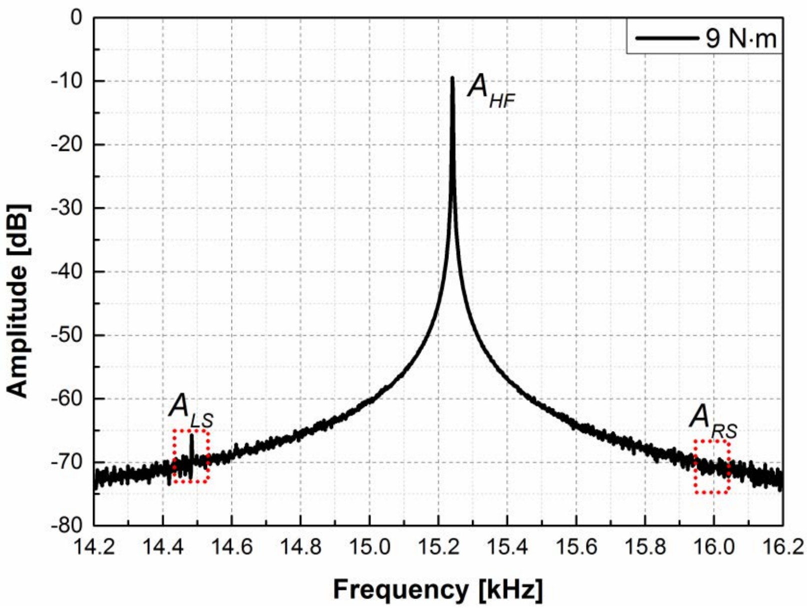

(b)

Figure 6.9 Experimental results of sideband responses of the *C-C* bolted joint under bolt torque levels of (a) 13 N·m; (b) 9 N·m; (c)7 N·m; and (d)1 N·m

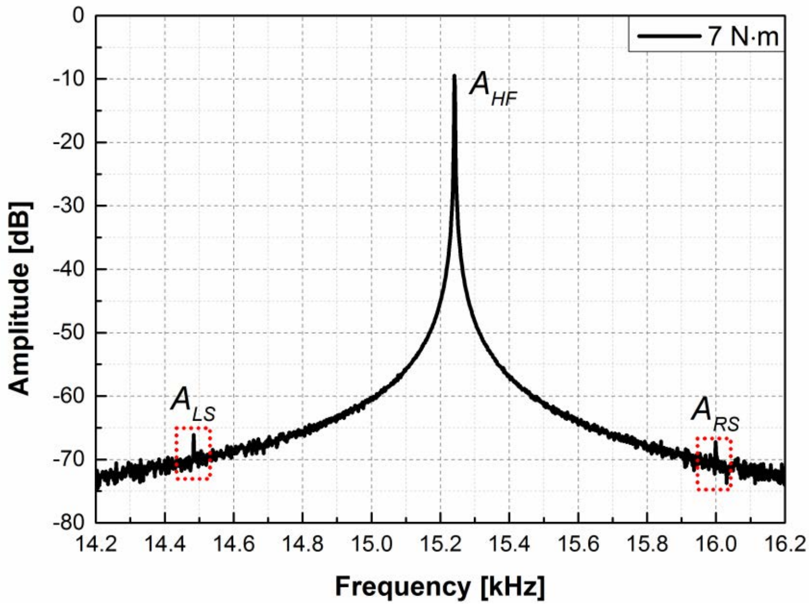

(c)

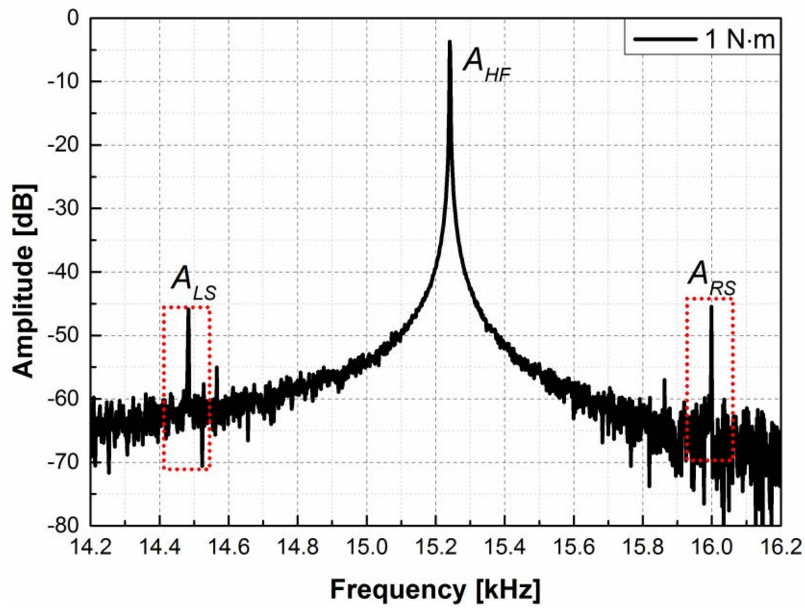

(d)

Figure 6.9 (continued)

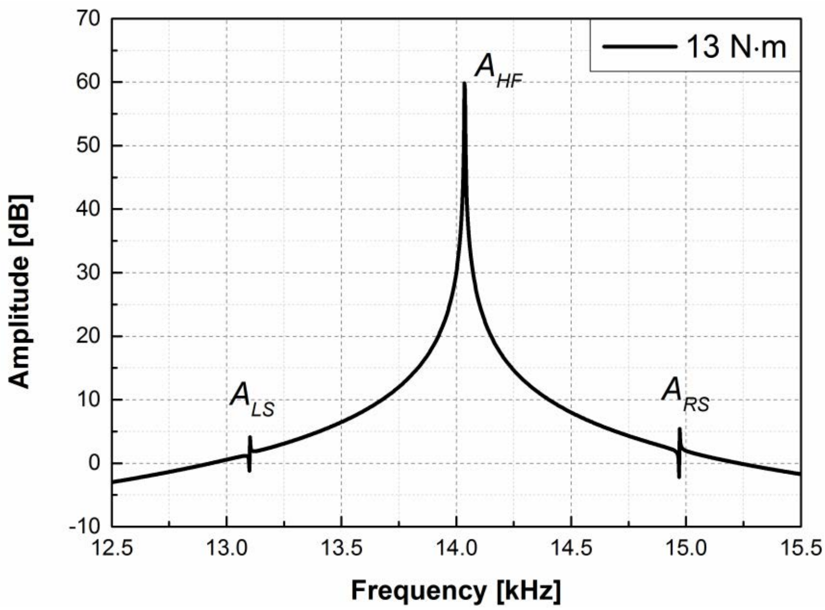

(a)

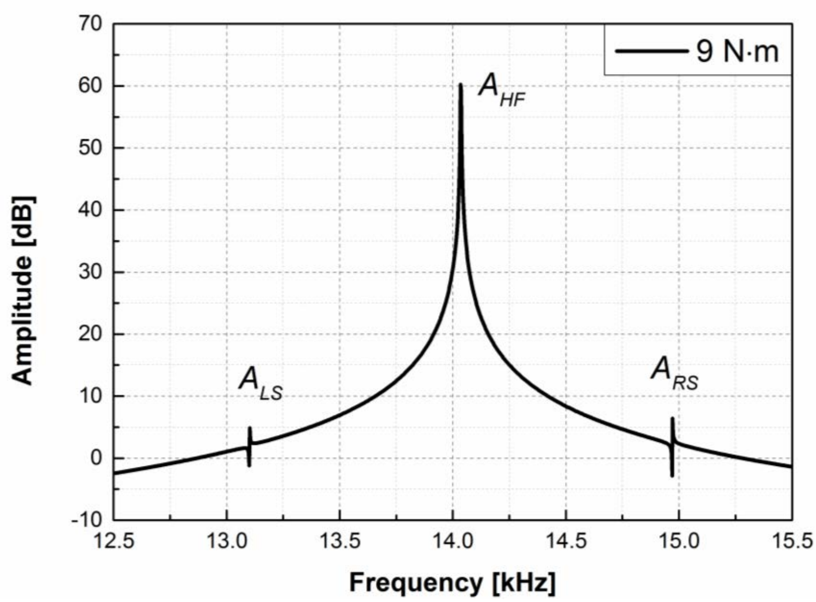

(b)

Figure 6.10 Numerical results of sideband responses of the *Al-Al* bolted joint under bolt torque levels of (a) 13 N·m; (b) 9 N·m; (c)7 N·m; and (d)1 N·m, respectively, by using contact stiffness according to Scenario II, which includes constant nonlinear terms, corresponding to n = 0 in Equation (6.4)

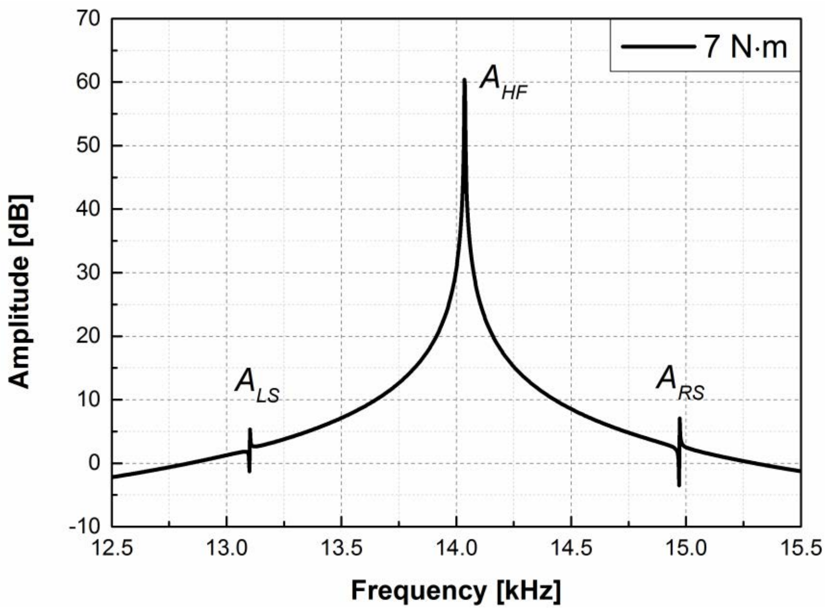

(c)

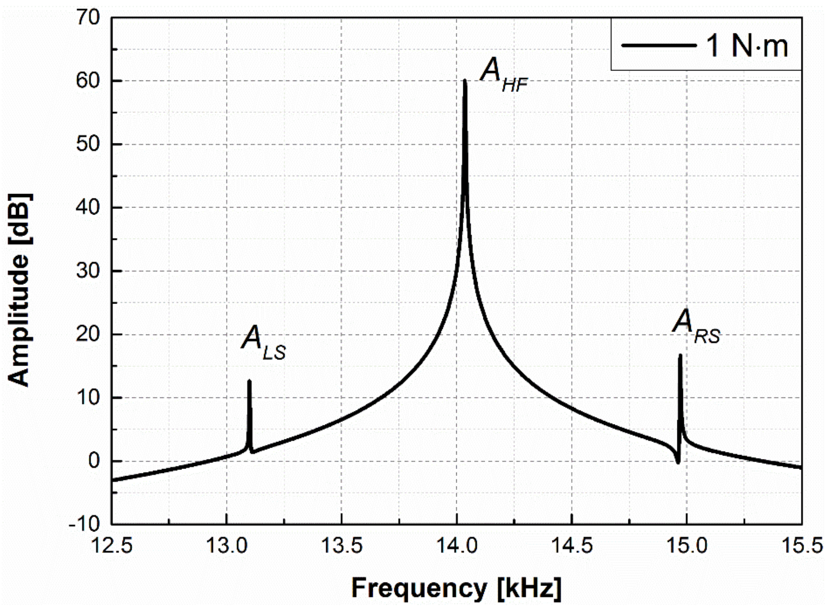

(d)

Figure 6.10 (continued)

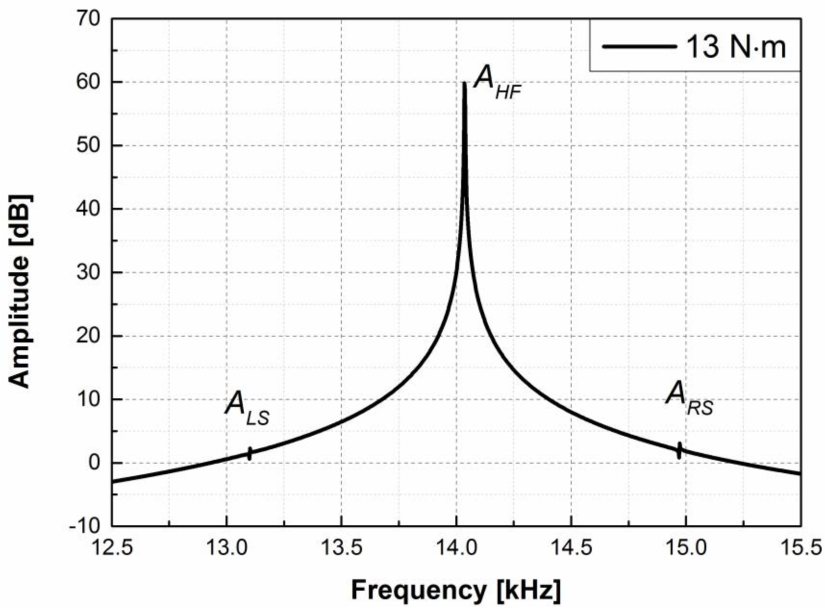

(a)

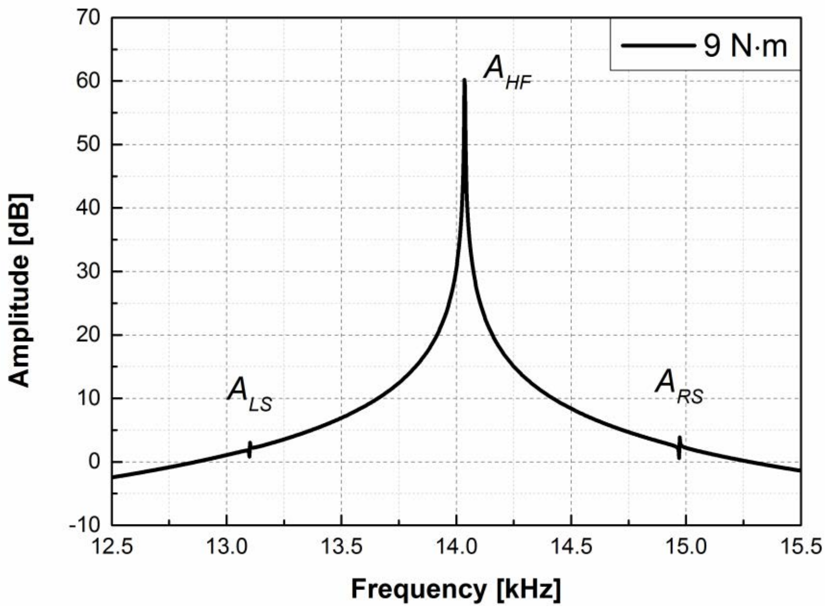

(b)

Figure 6.11 Numerical results of sideband responses of the *Al-Al* bolted joint under bolt torque levels of (a) 13 N·m; (b) 9 N·m; (c)7 N·m; and (d)1 N·m, respectively, by using contact stiffness according to Scenario III, which includes pressure-dependent nonlinear terms, corresponding to n = -0.5 in Equation (6.4)

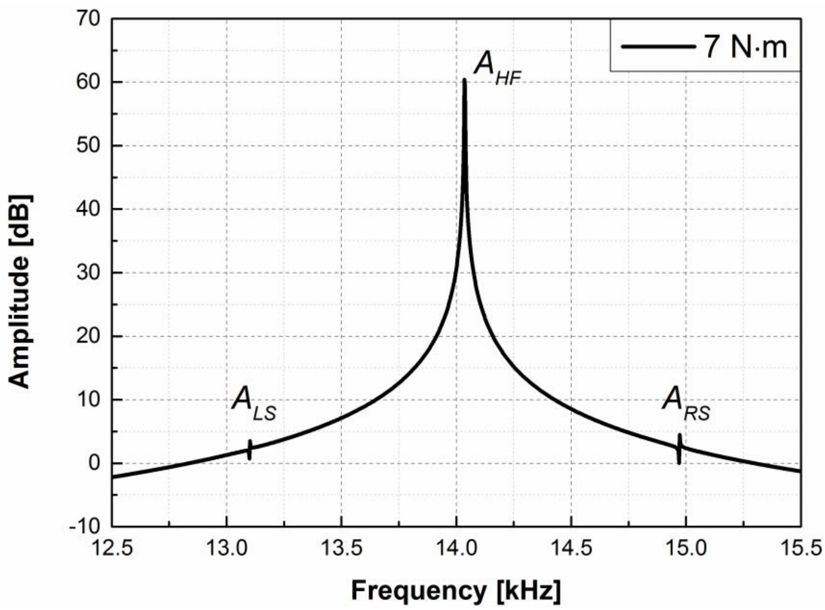

(c)

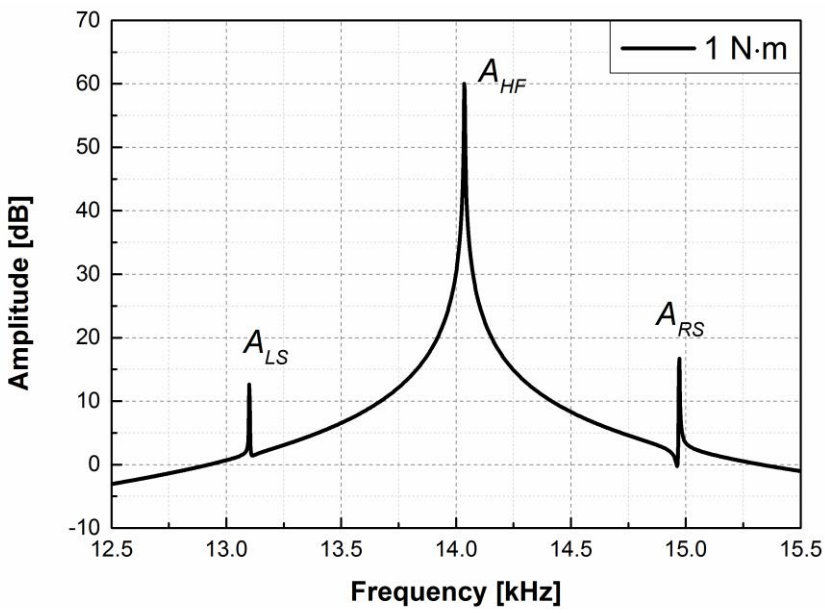

(d)

Figure 6.11 (continued)

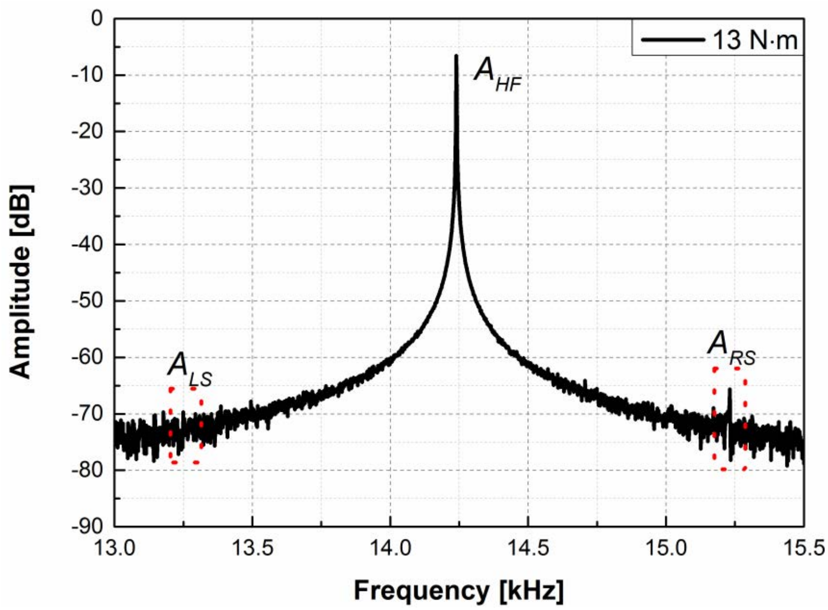

(a)

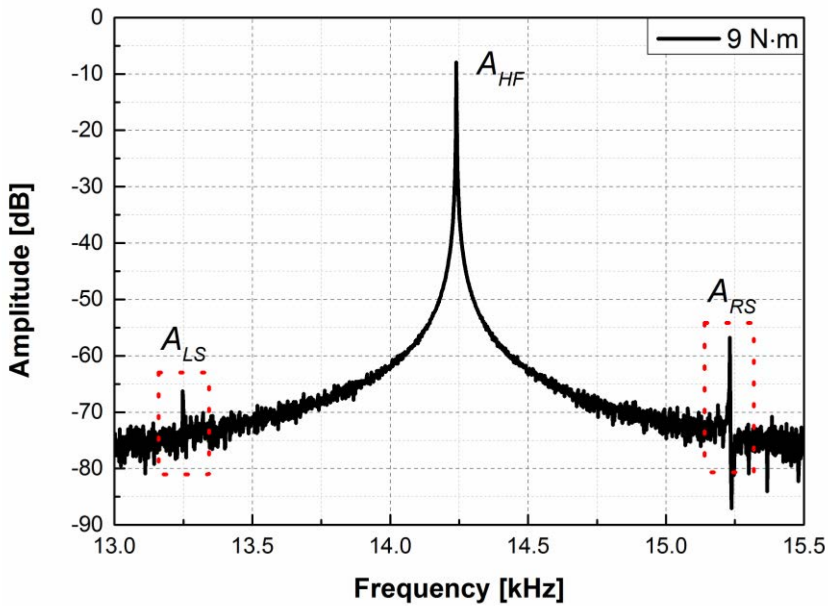

(b)

Figure 6.12 Experimental results of sideband responses of the *Al-Al* bolted joint under bolt torque levels of (a) 13 N·m; (b) 9 N·m; (c)7 N·m; and (d)1 N·m

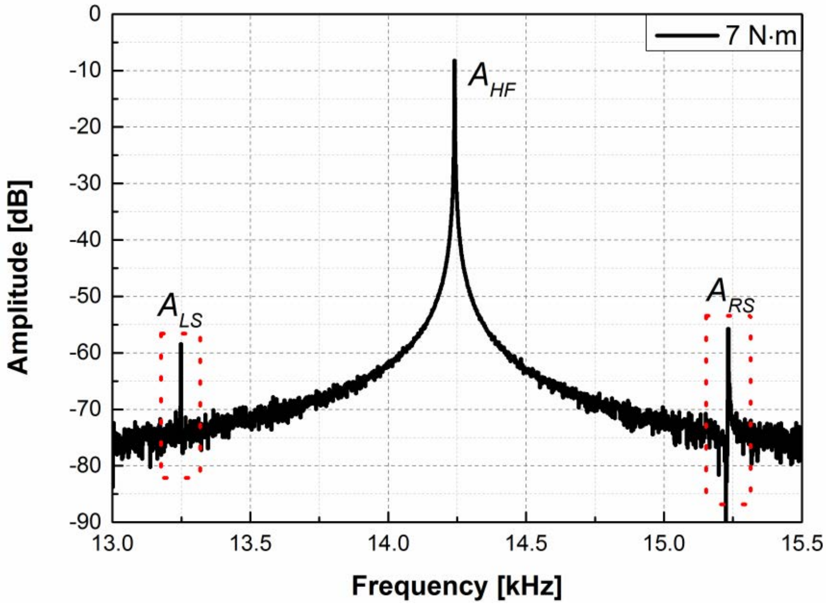

(c)

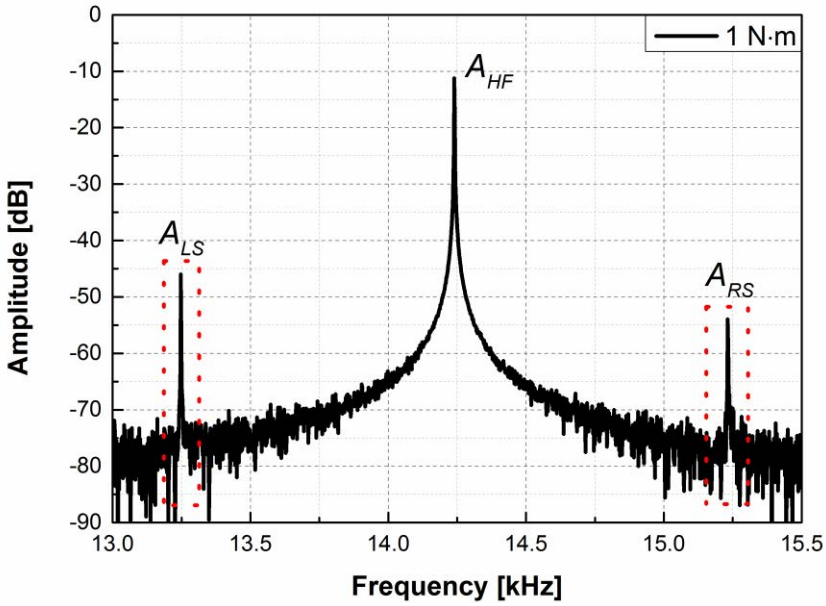

(d)

Figure 6.12 (continued)

It can be observed that left sideband (*LS*) measured from the experiment, as shown in **Figure 6.12** (a)-(c), is fairly weak at the early stage of bolt loosening and the theoretical results obtained by Scenario III show a better consistency with the experimental ones than those by Scenario II. On the other hand, a relative strong right sideband (*RS*) occurs even during the early bolt loosening in the experimental, which may arise from non-damage (non-bolt loosening)-related nonlinearity, for instance improper clamping condition at the fixed end or some other unknown mechanisms which leads to a large difference in the sensitivity to bolt loosening between *LS* and *RS*. However, when considering the variation of *RS* magnitude in the overall range due to changes in the applied torque, Scenario III still seems more reasonable compared to Scenario II.

Allowing for the fact that the magnitudes of sidebands are synergistically dependent on both the excitation intensity of the probing wave and the degree of *CAN*, the magnitudes (in the unit of dB) of actual left (LS) and right (RS) sidebands are normalized with the response magnitude of probing wave (HF) to obtain magnitudes of relative left (S_L) and right (S_R) sidebands, in order to achieve a quantitative comparison without involvement of influence of probing wave, as

$$S_L = LS - HF \text{ and } S_R = RS - HF \tag{6.11}$$

The theoretical magnitudes of relative sidebands of the *C-C* and *Al-Al* bolted joints are shown in **Figure 6.13** (a) and (b), respectively. A monotonic decrease in both S_L and S_R presents with the increase in the applied torque but with some slight difference between S_L and S_R for both joints.

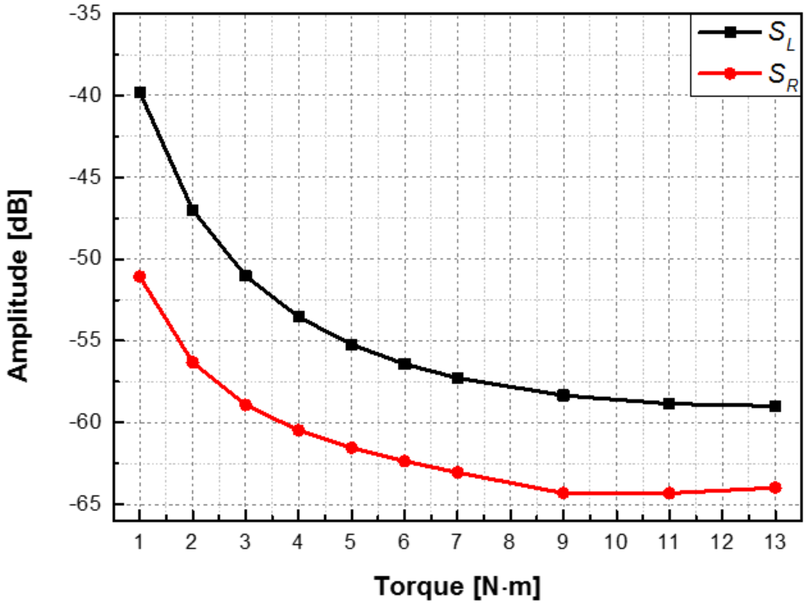

(a)

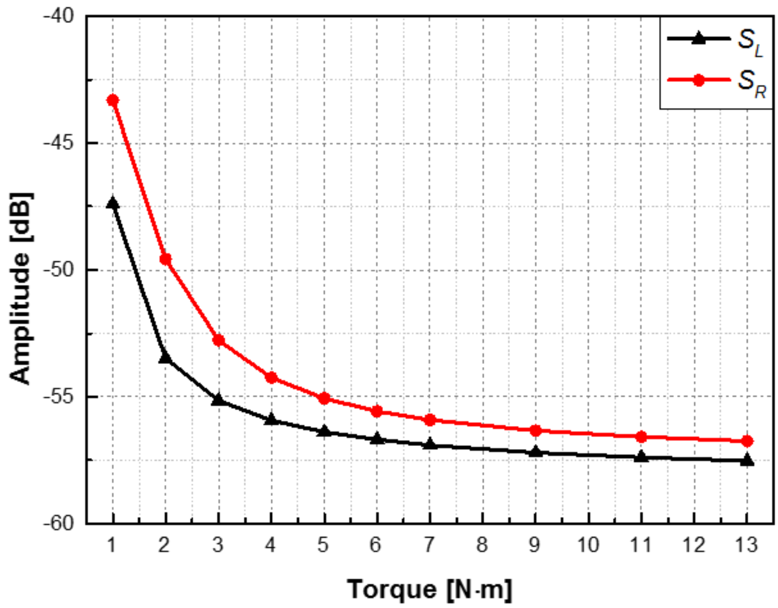

(b)

Figure 6.13 Numerical magnitude distributions of relative left and right sidebands based on Scenario III for the (a) *C-C* ; and (b) *Al-Al* bolted joints under ten different levels of bolt torques between 1 and 13 N·m

In particular, for the *C-C* joint, S_L and S_R decrease drastically when the torque increases from 1 to 9 N·m and after then moderate decreases present. For the *Al-Al* joint, when the torque varies from 1 to 7 N·m, rapid reductions in S_L and S_R occur and followed by gent decreases when the applied torque continues increasing.

Experimental S_L, S_R for the *C-C* bolted joint constructed at ten different bolt torque levels are displayed in **Figure 6.14** (a) and (b), respectively, within the entire range of bolt torques from 1 to 13 N·m. In **Figure 6.14** (a) and (b), scatter points and solid lines signify separately measured results and their averaged values, respectively, to indicate the extent of stability of data measurement. It should be noted in **Figure 6.14** (a)-(b) that the degrees of bolt loosening are actually displayed from the highest to the lowest, which is different from the presentation order in **Figure 6.9**, because of the reason that the bolt torque levels in **Figure 6.14** (a) and (b) are arranged in a naturally ascending order. From **Figure 6.14**, it can be clearly identified that an obvious change of curve tendency takes place at a certain point, probably between 6 and 7 N·m, below which nonlinear responses (i.e., S_L and S_R) to bolt loosening degree is much higher than that achieved beyond the point. In addition, there exists some difference in the sensitivity to bolt loosening between S_L and S_R. To be more specially, S_L changes observably while S_R saturates at the early stage of bolt loosening when T is no less than 7 N·m. Such an observation is consistent with the specific cases as presented in **Figure 6.12** (a) to (d), implying that bolt loosening at an early stage is of much higher difficulty to be quantified than at a serious stage.

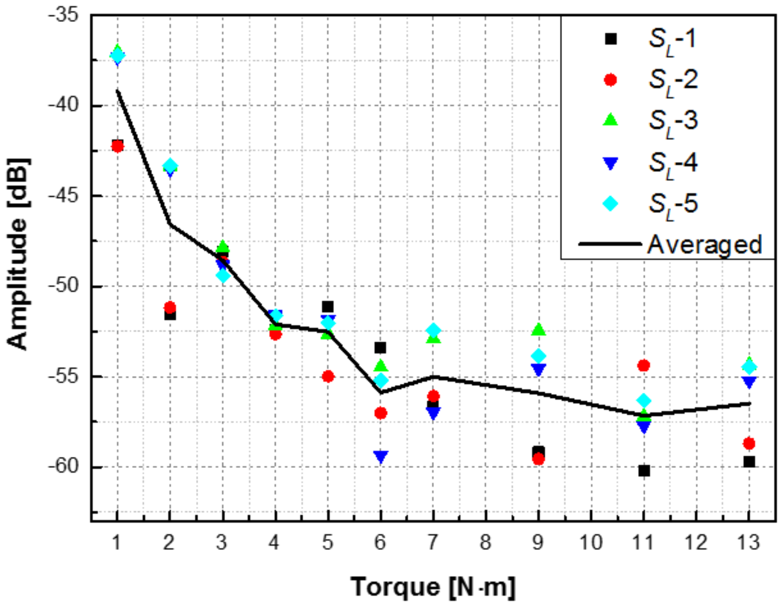

(a)

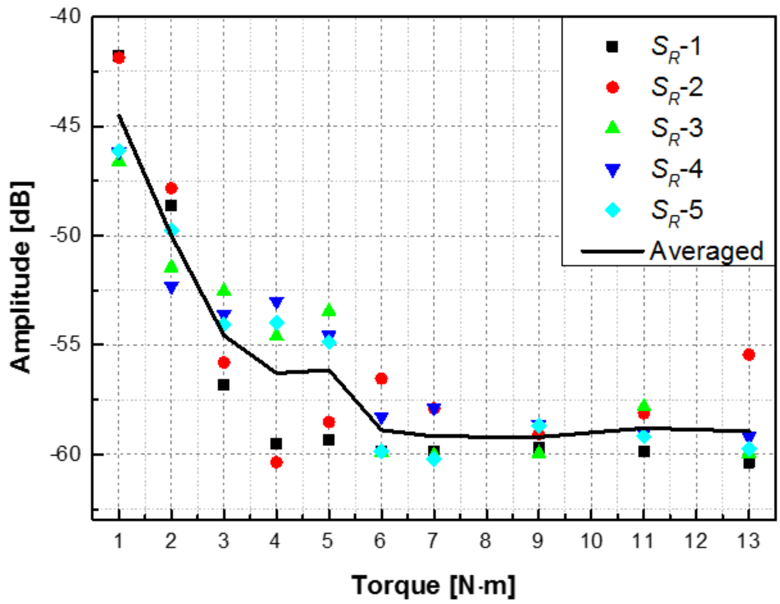

(b)

Figure 6.14 Magnitude distributions of the relative (a) left; and (b) right sidebands, constructed based on Equation (6.11), subject to experimental measurement for the *C*-*C* bolted joint under ten different levels of bolt torques between 1 and 13 N·m

By further scrutinizing the data distribution in **Figure 6.14** (a) and (b), a conclusion can be reached that the overall decline tendency of the curve sustains up to a considerably large level of bolt torque around 11 N·m, which means that the sensitivity of nonlinear responses is possible to be guaranteed in practical application at a quite early stage of bolt loosening.

Experimental S_L , S_R for the *Al-Al* bolted joint under different applied torques are displayed in **Figure 6.15** (a) and (b), respectively. From **Figure 6.15** (a) and (b), a similar change of curve tendency with that of the *C-C* joint is observed at a certain point, probably between 6 and 7 N·m. To be more specifically, S_R changes clearly while S_L almost saturates at the early stage of bolt loosening when T is no less than 9 N·m. Such an observation is consistent with the representative cases as presented in **Figure 6.12** (a) to (d), implying that the two sidebands exhibit different sensitivity to bolt loosening at an early stage, which consequently is of a much higher difficulty to be quantified than bolt loosening at a serious stage. From the observations regarding the dependence of sideband magnitudes on the residual torque of the *Al-Al* joint, it can be concluded that the *VAM*-based nonlinear method is capable of evaluating bolt loosening in the *Al-Al* joint including its early stage with an acceptable sensitivity.

To sum up, a good consistency between theoretical prediction and experiment investigation presents for both the *Al-Al* and *C-C* bolted joints. However, there exists some difference between S_L and S_R in the sensitivity to bolt loosening at the early stage. To achieve a better sensitivity for detection, the usage of *VAM*-based nonlinear index defined in Chapter 3 involving in the responses of both sidebands is meaningful in real practice. Motivated by this, both theoretical and experimental nonlinear indices constructed from the magnitudes of sidebands are comparably presented in the followings.

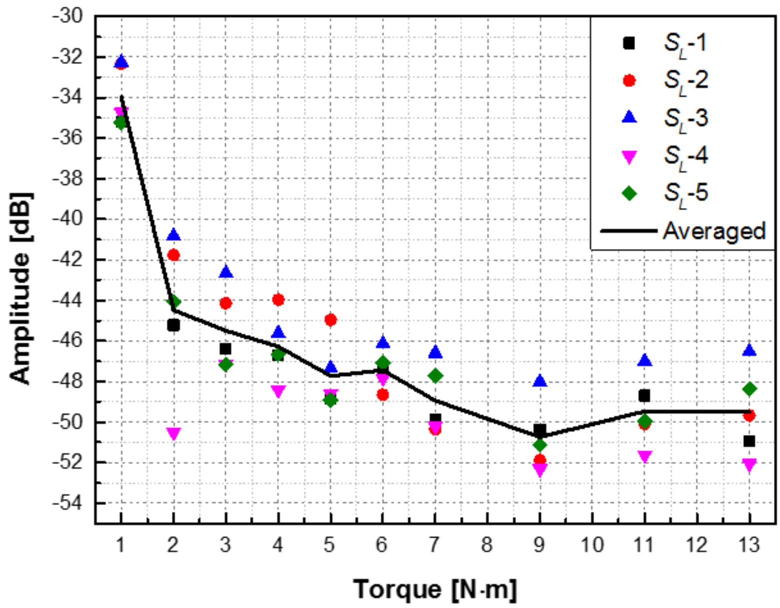

(a)

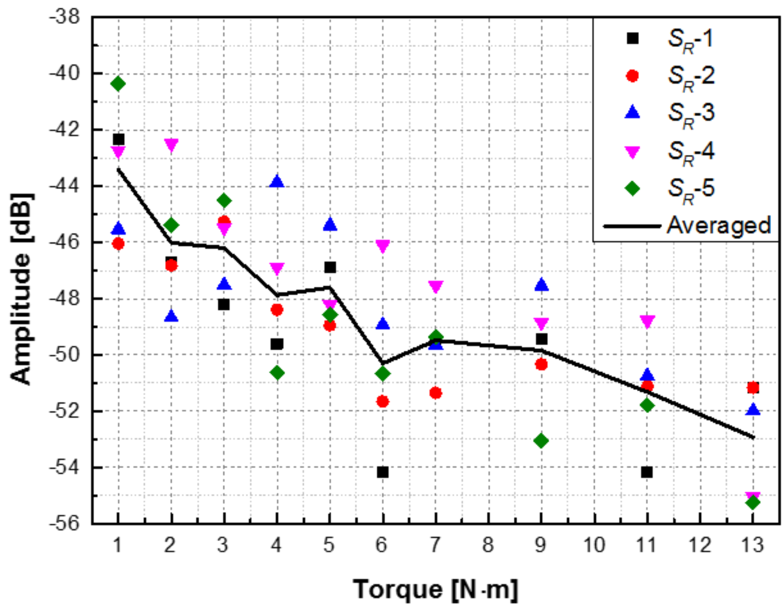

(b)

Figure 6.15 Magnitude distributions of the relative (a) left; and (b) right sidebands, constructed based on Equation (6.11), subject to experimental measurement for the *Al-Al* bolted joint under ten different levels of bolt torques between 1 and 13 N·m

To achieve a quantitative evaluation of the bolt loosening of the joints, a nonlinear bolt loosening indicator is defined using both relative left and right sidebands, as

$$\beta_{VAM} = (S_L + S_R)/2. \tag{6.12}$$

Based on respective utilizations of Scenario II and III, a more systematic analysis is made by calculating nonlinear indices using sideband responses under ten different bolt torques between 1 and 13 N·m. For the purpose of comparison, the developed bolt loosening indicator is further normalized according to

$$\beta^* = \beta_{VAM} - \beta_{ref}, \tag{6.13}$$

where β_{ref} is the reference *VAM*-based nonlinear index under the bolt torque of 1 N·m.

In **Figure 6.16** (a), the numerical results of the *C-C* joint are presented together with the experimental data, normalized using the averaged β_{VAM} values. It is clear that in **Figure 6.16** (a) the numerical results corresponding to Scenario III shows a considerably high consistency with the experimental results. The utilization of Scenario II, however, fails to coincide with the experimental data within most of the torque range. Furthermore, the sensitivity of Scenario II in characterizing bolt loosening degree vanishes when the bolt torque exceeds about 8 N·m, beyond which the curve slope becomes nearly zero, whereas Scenario III maintains its sensitivity up to a much higher torque level around 11 N·m, which is considered to be highly consistent with the experimental findings. Similar conclusions can be drawn for the *Al-Al* joint from the observations on results as exhibited in **Figure 6.16** (b).

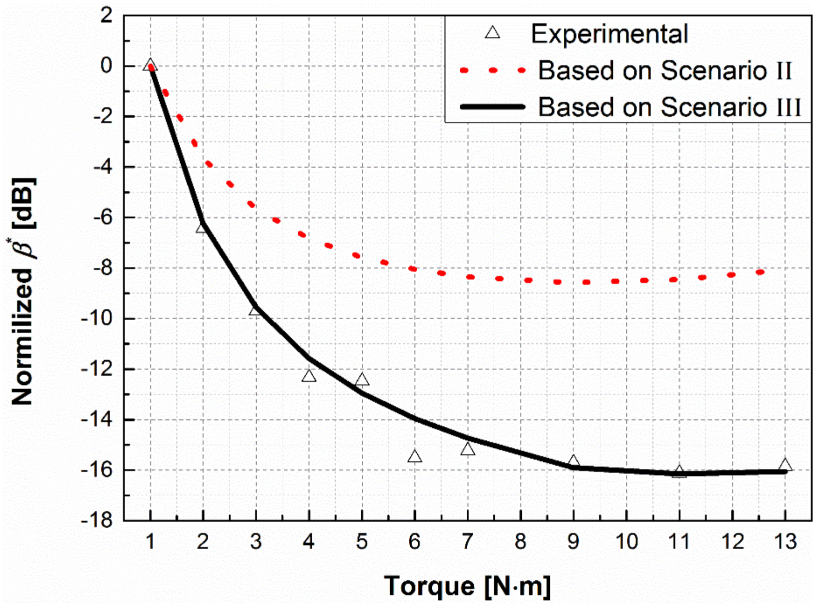

(a)

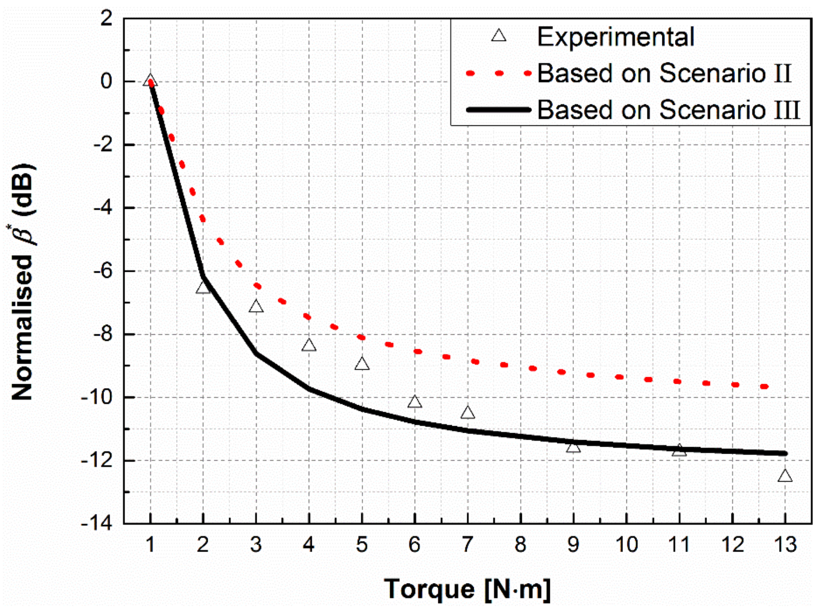

(b)

Figure 6.16 Distributions of the normalized bolt loosening indicator, β^*, as shown in Equation (6.13) subject to both experimental measurement and numerical computation, for the (a) *C-C*; and (b) *Al-Al* bolted joints under ten different levels of bolt torques between 1 and 13 N·m

The numerical results using Scenario III approach the experimental results with a better consistency compared to those obtained by using Scenario II. From the comparison in terms of agreement between the theoretical and experimental results, the proposed Scenario III is found to better describe the reliance of nonlinear index on the applied torque for the *C-C* joint.

6.4. Summary

In this chapter, contact acoustic nonlinearity (*CAN*) in *VAM*, induced by the "breathing" effect at the solid-to-solid interface of a bolted joint, is investigated analytically and experimentally, on which basis the *VAM*-inspired approach is developed to monitor bolt loosening in both composite-composite (*C-C*) and aluminum-aluminum (*Al-Al*) bolted joints. Numerical simulation based on the modified theoretical model with pressure-dependent nonlinear contact stiffness is implemented to facilitate the comprehending of generation mechanisms of *CAN* induced by a loose bolt and the dependence of nonlinear distortion, manifested as sidebands in the *VAM*-based method, on the residual torque of the loose joint. The numerical results in terms of linear and nonlinear responses of the joints under different torques subject to the mixed excitation are obtained with three types of contact scenarios and comparatively presented to reveal the relation between the degree of *CAN* and response magnitudes of modulated sidebands. From the comparisons, the sensitivity of the simulated results based on the modified scenario (Scenario III) is highly consistent with that of the experimental data. The numerical analysis has revealed that the decrease in the linear contact stiffness and the increase in the nonlinear contact stiffness, induced by the decrease of residual torque of the loose composite joint, synergistically result in the augment of sideband magnitudes. However, more studies are required to accurately measure the parameters describing the linear and nonlinear contact stiffness of the interface for different joining materials. The presented study provides a theoretical foundation, relying on which numerical analysis can be accurately conducted to facilitate the tasks of bolt loosening identification in a variety of structure types.

CHAPTER 7

Conclusions and Recommendations for Future Research

7.1. Concluding Remarks

Bolted joints are widely used to assemble primary components for engineering structures. Throughout their service lives, varied factors have the potential to initiate and accelerate the process of bolt loosening. The accumulation of bolt loosening may lead to a separation of assemblies and even a drastic failure without timely warning. To sustain structural integrity, cut down maintenance cost, and potentially extend service lives of bolted structures, over the last two decades a variety of efforts has been cast to develop effectual *SHM* using linear and nonlinear features of acousto-ultrasonics, aiming at achieving continuous and online surveillance of integrity of bolted structures.

Linear features of guided ultrasonic waves (*GUWs*), such as *WED* and *TOF*, have been widely employed to detect gross damage, but without capability of indicating the onset or severity of small-scale damage, such as fatigue cracks or early bolt loosening, which often occur in real-world structures. To achieve the task in terms of early bolt loosening detection, nonlinear features of acoustic waves, represented by *SOH*, *TOH* and modulated sidebands, have been attracting increasing research interests in recent years.

In this thesis, to facilitate a better understanding of detection philosophy of bolt loosening using linear and nonlinear features of acousto-ultrasonics, theoretical analyses are firstly conducted to derive the qualitative relation between linear/nonlinear features and the residual torque remained on a loose bolt and further define damage (bolt loosening)-related linear/nonlinear indices. The theoretical predictions are validated by detecting bolt loosening in both *Al-Al* and *C-C* bolted joints through comparably using linear and nonlinear indices. The detectability of the proposed linear and nonlinear feature-based methods is compared in terms of sensitivity to early bolt loosening and dependence on both joint configurations and joining materials.

For passive linear acoustic method, the affecting factors (i.e., the normal load, number of asperities in contact, surface properties and sliding velocity of the contact surfaces) of *AE* generation are analyzed based on micro contact theory. The energy-based and frequency-based analyses are theoretically predicted capable of characterizing *AE* signals generated from different contact interfaces (i.e., *C-C* and *M-C* contacts), and further relating them to the residual torque of a composite joint. In the experimental investigation, *IMFs* of *AE* signals, obtained by *EMD*, are used to characterize contact behaviors in a bolted composite joint under different applied torques when subject to flexural vibration. *AE* signals generated from the *M-C* and *C-C* contacts are firstly characterized using frequency analysis on the processed *IMFs*. Based on micro contact theory and baseline experiments, three main *C-C* friction related *IMFs* with different centered frequencies are physically linked to contact behaviors of asperities with different sizes at the *C-C* interface. Subsequently, *C-C* friction related *IMFs* are used to investigate the effect of applied torque on contact behaviors at the *C-C* interface of the joint. *AE* signals induced by asperity contacts at different contact interfaces (i.e., *C-C* and *M-C* contacts) in bolted composite joints are discriminated by comparing the time-presentation envelopes and the time-frequency distribution of the *IMFs* in the *HHT* spectra. The gross energy of *AE* signals shows a considerable sensitivity to changes in the residual torque of a bolted composite joint in a limited range. However, such a method fails to quantitatively detect the tightening condition of joints under vibration fatigue. *HHT* shows a higher time-frequency resolution when processing bolt loosening-induced *AE* signals, which possess non-stationary characteristics, compared to *STFT*. With usage of *HHT*-based signal characteristics, energy ratios of high-frequency *IMFs* induced by the *C-C* contact achieve an enhanced sensitivity to the decrease in bolt torque. Bolt loosening results in increases in the energy-ratios of the *C-C* contact-related *IMFs*. Based on this, vibration loosening of bolted composite joints under different torques is quantitatively correlated to the increase of energy ratios of *C-C* contact related *IMFs*. On this basis, continuous evaluation of bolted composite joints under vibration fatigue is achieved by the *HHT*-processed characteristics of *AE* signals.

For the active linear acoustic method using vibration modal parameters, resonant frequency and damping ratio are theoretically linked to the tightening state of a joint. From the experimental observation, the sensitivity of damping ratio to bolt loosening is found being much higher than that of resonant frequency. However, detectability of these two parameters is rather limited and not capable of evaluating the residual torque of a loose joint at the early stage of bolt loosening with considerable results.

For the active acoustic method based on *WED* of *GUWs*, Hertzian contact theory is used to develop a linear index, constructed from transmitted/leak energy of *GUWs* upon traversing the mating parts of a joint, to evaluate the tightening condition of loose bolts in multi-type joints. From experimental results, the *WED*-based linear index is found to increase as the applied torque increases in a single-lap bolted joint, but decreases in a cross-lap bolted joint, showing a high dependence on the joint configurations/types. Consequently, this linear index fails to predict the residual torque of the hybrid-lap bolted joint due to a contradictory change trend caused by bolt loosening of the two involved joints. Due to severe attenuation characteristics of *GUWs* propagating in composites, sensing distance plays a critical role in determining the efficiency of the *WED*-based linear index in detecting bolt loosening in the composite joints. To avoid the effect of boundary reflection, the energy envelope of first-arrival wave packet of *GUWs* are used to calculate the linear index, constructed from the transmitted energy, to characterize the residual torque remained on the cross-lap *Al-Al* bolted joint. It is found that the detectability of the *WED*-based linear method can be improved by minimizing the effect of boundary reflection, but still in a limited range. Due to the almost unchanged contact area arising from plastic deformation at the contact interface, early bolt loosening would not introduce a phenomenal change in the real contact area, as a result the detectability of such a linear feature-based method is still limited.

Given the necessity of evaluating early bolt loosening, nonlinear acoustic methods using nonlinear features (i.e., *HOH* and modulated sidebands) of acoustic waves are comparatively developed. A theoretical model is used to describe the relation between *CAN*, associated with the interaction between the contact interface of a loose joint and acoustic waves, and the residual torque of a joint. Using a single-degree-freedom system, nonlinear responses, i.e., *HOH* and modulated sidebands, of a bolted joint subject to one harmonic excitation and two mixed excitations (i.e., pumping vibration and probing wave), respectively, are theoretically correlated with the nonlinear contact stiffness, which is determined by the applied torque. Based on this, the nonlinear indices (i.e., *SOH*-based, *TOH*-based and *VAM*-based) are defined from the magnitudes of *SOH*, *TOH* and modulated sidebands for the evaluation of the residual torque of loose bolts. The accuracy of the proposed nonlinear indices is firstly experimentally verified by investigating their dependence on the intensities of pumping vibration and probing wave in both *Al-Al* and *C-C* single-lap bolted joints. β_{SOH} and β_{VAM}^{M} are found being independent of the magnitudes of *LF* and *HF*, while β_{VAM} shows a linear correlation with *LF*. The reliance of *TOH* on *LF* can be divided into two stages. Before the response magnitude of *LF* reaches a certain value, β_{TOH}

decreases with an increase in *LF* and after then it remains almost unchanged in spite of an augment in *LF*. Subsequently, to further verify their efficiencies, these four nonlinear indices are comparably adopted to identify the residual torque of loose bolts for both *Al-Al* and *C-C* bolted joints. To observe that linear responses (i.e., *LF* and *HF*) are not capable of indicating the state of a loose joint at the early stage, while nonlinear indices β_{VAM} and β_{VAM}^{M}, defined from magnitudes of modulated sidebands, persist their detectability throughout the whole range from fully fastened to fully loose, regardless of joint configurations or joining materials, showing enhanced sensitivity than the linear responses. β_{TOH} presents its efficiency in identifying the residual torque of the bolt in the whole torque range only for the *Al-Al* cross-lap bolted joint. Whereas, β_{SOH} are only capable of evaluating the leftover torque of joints when the torque is over certain value. Otherwise, due to mixed source of nonlinearity, these two *HOH*-based nonlinear indices fail to identify the state of loose joints at the late stage of bolt loosening. Lastly, to facilitate a better understanding of mechanisms of sideband generation, associated with *CAN* at the contact interface, along with its quantitative dependence on the residual torque of the bolt, numerical simulation of *VAM*-based method for detecting bolt loosening in both *Al-Al* and *C-C* single-lap bolted joints is presented. The numerical results obtained with different contact models are comparatively presented to reveal the relation between the degree of *CAN* and response magnitudes of modulated sidebands. According to the comparisons, the simulated results based on the proposed modified model show a high consistency with the experimental data. From the numerical analysis, the occurrence and increase in response magnitudes of modulated sidebands due to the presence and deterioration of bolt loosening can be attributed to a decrease in the linear contact stiffness along with an increase in the nonlinear contact stiffness. The presented study provides a reliable theoretical foundation, relying on which numerical analysis can be accurately conducted to implement the tasks of bolt loosening identification in a variety of different structure types.

The detectable loosening stage (presented by percent of fully tightening torque, i.e.,13 N·m) for the linear and nonlinear methods are shown in **Table 7.1**.

Table 7.1 Detectable loosening stage for the linear and nonlinear methods (unit: %, *NA*: not applicable)

	WED	***SOH***	***TOH***	***VAM***	***AE***	***VMP***
Al-Al single-lap	0-50	35-85	44-69	0-85		
Al-Al cross-lap	0-30	23-100	0-100	0-100		
Al-Al hybrid	*NA*	46-100	*NA*	0-100		
C-C single-lap	*NA*	54-100	31-100	0-85	31-62	0-69

To sum up, the main achievements and original contributions of this study can be briefly summarized as

- Application of *EMD* in characterizing *AE* signals generated from asperity contacts at the interfaces of bolted composite joints. Using micro contact theory, *IMFs* of *AE* signals with different centered frequencies are physically linked to contacts of asperities with different sizes. Implementation of on-line detection of bolt loosening for bolted composite joints under vibration fatigue using the *HHT*-processes *AE* signals;

- Establishment of damage (bolt loosening)-related linear index, using the linear feature of *GUWs*, i.e., *WED*, for bolt loosening identification in multi-type of joints, in conjunction with the use of advanced signal processing technique (i.e., *HT*). Theoretical and experimental demonstration regarding the dependence of the *WED*-based linear index on the joint configurations;

- Establishment of damage (bolt loosening)-related nonlinear indices, using nonlinear features of acoustic waves (i.e., *SOH*, *TOH* and sidebands) for bolt loosening characterization. Integration of *HOH*-based and *VAM*-based nonlinear indices in a single testing and implementation of these indices for quantitative identification of the residual torque of a loose joint;

- Development of a theoretical model to describe *CAN* at the contact interfaces of a loose joint and to reveal its dependence on the residual torque. Implementation of numerical simulation to uncover mechanisms of generation and evolution of sidebands due to the occurrence and deterioration of bolt loosening;

- Demonstration of advantages of nonlinear indices in detecting early bolt loosening in both *Al-Al* and *C-C* bolted joints in aspect of the dependence on joint configurations and joining materials, with comparisons to linear index.

7.2. Problematic Issues and Recommendations for Future Research

In spite of the promising results reported in this thesis, there are some problematic issues and challenges remaining for future exploration.

First, *IMFs* with different centered frequencies of *AE* signals are linked to contacts of asperities with different sizes through theoretical analysis in Chapter 4. Although a series of observations in both short-time calibration experiment and long-time fatigue experiment verify the rationality of this prediction. To extend this method for bolt loosening detection in multi-type joints with varied surface properties, it is of necessity to understand the relationship between surface properties (i.e., roughness and material types) and centered-frequencies of decomposed *IMFs* arising from asperity contacts at the surfaces. To achieve this goal, a proper theoretical contact model describing asperity contacts in the mating parts of a joint should be first developed to facilitate the subsequent numerical simulation.

Second, for *WED*-based linear method, a simplified model is used to derive the relation between transmitted/leak energy of *GUWs* upon interacting with mating parts of a joint and the residual torque of the bolt. Roughly speaking, the theoretical predictions proposed by the simplified model are consistent with experimental investigation. However, the saturation points of such a linear index with respect to increasing torques are found varied even for bolted joints consisting of the same material but with different joint configurations, i.e., single-lap and cross-lap *Al-Al* joints. This phenomenon cannot be involved in and interpreted by the simplified model. Therefore, a three-dimensional model is required for accurately describing the interaction between *GUWs* and the mating parts of a joint to consider the effect of the bolt, thread hole and joint configurations on the propagation characteristics of *GUWs*.

Third, in this study first-order classical nonlinearity is used to describe *CAN* arising from the periodical open and close of contact interfaces of a loose joint when interacting with acoustic waves. Whereas in real practice, multiple factors, including breathing behaviors, friction and hysteresis behaviors, and thermal effects, may potentially introduce *CAN* in the structural responses. Currently, it is still challenging to systematically correlate all the mentioned nonlinearity sources to the generation of nonlinear features using a single theoretical model. Thus, in this thesis *CAN* due to bolt loosening is modeled by using first-order classical nonlinearity, which is likely to provide inadequate predictions at the late stage of bolt loosening. This is because that during this loosening stage, friction, hysteresis behaviors, and thermal effects may induce an intensive degree of *CAN*, which cannot be reflected by the first-order nonlinearity. From the experimental observation, a monotonic reliance of *SOH* and *TOH* on the residual torque of a loose joint presents in a limited range, while sidebands persist the detectability throughout the whole torque range. Varied sources of nonlinearity occurring at the late stage of bolt loosening are inferred to be responsible for this disagreement in the performance of *SOH* and *TOH*. Thus, in future work a more accurate modeling of *CAN* and a detail interpretation of mechanisms regarding nonlinear feature generation of acoustic waves are two important problems to tackle. In addition, in the numerical simulation of *VAM*-based method, due to the fact that up to now contact stiffness of the interface cannot be directly measured, the parameters describing the contact stiffness are determined empirically referring to some reported studies. However, a slight disagreement between theoretical analysis and experimental results states the necessity of a systematic parameter determination in terms of contact stiffness for different interfaces. In addition, selection of excitation frequencies plays a critical role in determining detection sensitivity of *CAN*-based method, proper general and implementable criterion for frequency selection should be developed for more complex structures like two- or three-dimensional structures.

In addition, location of loose bolts using linear and nonlinear features of acoustic waves is not involved in this thesis, which is meaningful for surveillance of large structures consisting of a vast number of bolts. To achieve this goal, continuous excitation signals used in this study should be replaced with tone-burst signals to provide local information in the propagation path of guided waves. However, to produce detectable and stable *CAN* using such an excitation should be secured, which is quite challenging according to our experimental observations. Furthermore, more efforts should be directed to the validation of overall linear and nonlinear techniques in the real-world application.

BIBLIOGRAPHY

[1] J. Yang, F.-K. Chang, Detection of bolt loosening in C–C composite thermal protection panels: I. Diagnostic principle. Smart Materials and Structures 15 (2006) 581-590.

[2] J. Yang, F.-K. Chang, Detection of bolt loosening in C–C composite thermal protection panels: II. Experimental verification. Smart Materials and Structures 15 (2006) 591-599.

[3] J. Esteban, C.A. Rogers, Energy dissipation through joints: theory and experiments. Computers & Structures 75 (2000) 347-359.

[4] B. Smith, The Boeing 777. Advanced Materials and Processes 161 (2003) 41-44.

[5] Z. Su, L. Ye, Lamb wave-based quantitative identification of delamination in CF/EP composite structures using artificial neural algorithm. Composite Structures 66 (2004) 627-637.

[6] Z. Zhang, Y. Xiao, Y. Liu, Z. Su, A quantitative investigation on vibration durability of viscoelastic relaxation in bolted composite joints. Journal of Composite Materials 50(2016) 4041-4056.

[7] Y. Jiang, M. Zhang, C.-H. Lee, A Study of Early Stage Self-Loosening of Bolted Joints. Journal of Mechanical Design 125 (2003) 518.

[8] E.A. Ossa, Failure analysis of a civil aircraft landing gear. Engineering Failure Analysis 13 (2006) 1177-1183.

[9] D.J. Benac, Technical Brief: Avoiding Bolt Failures. Journal of Failure Analysis and Prevention 7 (2007) 79-80.

[10] S. Levmore, Probabilistic Recoveries, Restitution, and Recurring Wrongs. The Journal of Legal Studies 19 (1990) 691-726.

[11] M.R. Endsley, M.M. Robertson, Team situation awareness in aviation maintenance. in: Proceedings of the Human Factors and Ergonomics Society Annual Meeting, SAGE Publications, 1996, pp. 1077-1081.

[12] V. Kaminskaya, A. Lipov, Self Loosening of Bolted Joints in Machine Tools During Service. Metal Cut. Mach. Tools 12 (1990) 81-85.

[13] W. Eccles, Tribological aspects of the self-loosening of threaded fasteners. in, University of Central Lancashire, 2010.

[14] R.L. Helmreich, Culture and error in space: Implications from analog environments. Aviation Space and Environmental Medicine 71 (2000) A133-A139.

[15] P. Underwood, P. Waterson, Systems thinking, the Swiss Cheese Model and accident analysis: A comparative systemic analysis of the Grayrigg train derailment using the ATSB, AcciMap and STAMP models. Accident Analysis & Prevention 68 (2014) 75-94.

[16] U. Bjornstig, R. Forsberg, Transportation disasters. Koenig and Schultz's Disaster Medicine: Comprehensive Principles and Practices (2016) 294.

[17] J. Bickford, An introduction to the design and behavior of bolted joints, Revised and expanded, CRC press, 1995.

[18] R.A. Ibrahim, C.L. Pettit, Uncertainties and dynamic problems of bolted joints and other fasteners. Journal of Sound and Vibration 279 (2005) 857-936.

[19] T. SAKAI, Investigations of Bolt Loosening Mechanisms: 1st Report, On the Bolts of Transversely Loaded Joints. Bulletin of JSME 21 (1978) 1385-1390.

[20] T. SAKAI, Investigations of Bolt Loosening Mechanisms: 2nd Report, On the Center Bolts of Twisted Joints. Bulletin of JSME 21 (1978) 1391-1394.

[21] Y. Shoji, T. Sawa, Analytical research on mechanism of bolt loosening due to lateral loads. in: ASME 2005 Pressure Vessels and Piping Conference, American Society of Mechanical Engineers, 2005, pp. 59-65.

[22] A. Bhattacharya, A. Sen, S. Das, An investigation on the anti-loosening characteristics of threaded fasteners under vibratory conditions. Mechanism and Machine Theory 45 (2010) 1215-1225.

[23] N.G. Pai, D.P. Hess, Experimental Study of Loosening of Threaded Fasteners Due to Dynamic Shear Loads. Journal of Sound and Vibration 253 (2002) 585-602.

[24] X. Jiang, Y. Zhu, J. Hong, X. Chen, Y. Zhang, Investigation into the loosening mechanism of bolt in curvic coupling subjected to transverse loading. Engineering Failure Analysis 32 (2013) 360-373.

[25] S.D. Thoppul, J. Finegan, R.F. Gibson, Mechanics of mechanically fastened joints in polymer–matrix composite structures – A review. Composites Science and Technology 69 (2009) 301-329.

[26] S.D. Thoppul, R.F. Gibson, R.A. Ibrahim, Phenomenological Modeling and Numerical Simulation of Relaxation in Bolted Composite Joints. Journal of Composite Materials 42 (2008) 1709-1729.

[27] K.N. Shivakumar, J.H. Crews, Bolt clampup relaxation in a graphite/epoxy laminate, in: Long-term behavior of composites, ASTM International, 1983.

[28] A. Nechache, A.-H. Bouzid, Creep analysis of bolted flange joints. International Journal of Pressure Vessels and Piping 84 (2007) 185-194.

[29] Y. Xiao, Bearing deformation behavior of carbon/bismaleimide composites containing one and two bolted joints. Journal of reinforced plastics and composites 22 (2003) 169-182.

[30] Y. Xiao, T. Ishikawa, Bearing strength and failure behavior of bolted composite joints (part II: modeling and simulation). Composites science and technology 65 (2005) 1032-1043.

[31] Z. Su, L. Ye, Identification of damage using Lamb waves: from fundamentals to applications, Springer Science & Business Media, 2009.

[32] F. Chang, Introduction to health monitoring: context, problems, solutions. in: Presentation at the 1st European Pre-workshop on Structural Health Monitoring, Paris, France, 2002.

[33] H. Sohn, C.R. Farrar, F.M. Hemez, D.D. Shunk, D.W. Stinemates, B.R. Nadler, J.J. Czarnecki, A review of structural health monitoring literature: 1996–2001. Los Alamos National Laboratory, USA (2003).

[34] Z. Su, L. Ye, Y. Lu, Guided Lamb waves for identification of damage in composite structures: A review. Journal of Sound and Vibration 295 (2006) 753-780.

[35] C.R. Farrar, K. Worden, An introduction to structural health monitoring. Philos Trans A Math Phys Eng Sci 365 (2007) 303-315.

[36] A. Nair, C. Cai, Acoustic emission monitoring of bridges: Review and case studies. Engineering structures 32 (2010) 1704-1714.

[37] Z. Su, C. Zhou, M. Hong, L. Cheng, Q. Wang, X. Qing, Acousto-ultrasonics-based fatigue damage characterization: Linear versus nonlinear signal features. Mechanical Systems and Signal Processing 45 (2014) 225-239.

[38] D. Broda, W.J. Staszewski, A. Martowicz, T. Uhl, V.V. Silberschmidt, Modelling of nonlinear crack–wave interactions for damage detection based on ultrasound—A review. Journal of Sound and Vibration 333 (2014) 1097-1118.

[39] Z. Zhang, Y. Pan, Y. Xiao, Z. Zhong, Measurement and analysis of laser generated Rayleigh and Lamb waves considering its pulse duration. Acta Mechanica Solida Sinica 28 (2015) 441-452.

[40] V. Giurgiutiu, Tuned Lamb wave excitation and detection with piezoelectric wafer active sensors for structural health monitoring. Journal of intelligent material systems and structures 16 (2005) 291-305.

[41] R. Gutkin, C.J. Green, S. Vangrattanachai, S.T. Pinho, P. Robinson, P.T. Curtis, On acoustic emission for failure investigation in CFRP: Pattern recognition and peak frequency analyses. Mechanical Systems and Signal Processing 25 (2011) 1393-1407.

[42] J. Meriaux, M. Boinet, S. Fouvry, J.C. Lenain, Identification of fretting fatigue crack propagation mechanisms using acoustic emission. Tribology International 43 (2010) 2166-2174.

[43] M. Bourchak, I. Farrow, I. Bond, C. Rowland, F. Menan, Acoustic emission energy as a fatigue damage parameter for CFRP composites. International Journal of Fatigue 29 (2007) 457-470.

[44] D.G. Aggelis, N.M. Barkoula, T.E. Matikas, A.S. Paipetis, Acoustic structural health monitoring of composite materials : Damage identification and evaluation in

cross ply laminates using acoustic emission and ultrasonics. Composites Science and Technology 72 (2012) 1127-1133.

[45] S. Masmoudi, A. El Mahi, R. El Guerjouma, Mechanical behaviour and health monitoring by acoustic emission of sandwich composite integrated by piezoelectric implant. Composites Part B: Engineering 67 (2014) 76-83.

[46] I. Silversides, A. Maslouhi, G. LaPlante, Acoustic emission monitoring of interlaminar delamination onset in carbon fibre composites. Structural Health Monitoring (2013) 1475921712469994.

[47] Y. Fan, F. Gu, A. Ball, Modelling acoustic emissions generated by sliding friction. Wear 268 (2010) 811-815.

[48] K. Asamene, M. Sundaresan, Analysis of experimentally generated friction related acoustic emission signals. Wear 296 (2012) 607-618.

[49] A. Hase, H. Mishina, M. Wada, Correlation between features of acoustic emission signals and mechanical wear mechanisms. Wear 292-293 (2012) 144-150.

[50] B. Tesfa, G. Horler, F.A. Thobiani, F. Gu, A.D. Ball, A clamping force measurement system for monitoring the condition of bolted joints on railway track joints and points. Journal of Physics: Conference Series 364 (2012) 012021.

[51] T. Kundu, M.T. Alam, M. Sundaresan, Characterization of fretting related acoustic emission signals. 7650 (2010) 76500J.

[52] N.E. Huang, Z. Shen, S.R. Long, M.C. Wu, H.H. Shih, Q. Zheng, N.-C. Yen, C.C. Tung, H.H. Liu, The empirical mode decomposition and the Hilbert spectrum for nonlinear and non-stationary time series analysis. in: Proceedings of the Royal Society of London A: Mathematical, Physical and Engineering Sciences, The Royal Society, 1998, pp. 903-995.

[53] Y. Zhang, G. Zeng, D. Zhao, Y. Quan, Experimental Research on the Bolt Joints Looseness Based on HHT. Machine Tool & Hydraulics 1 (2014) 002.

[54] L. Lin, F. Chu, HHT-based AE characteristics of natural fatigue cracks in rotating shafts. Mechanical Systems and Signal Processing 26 (2012) 181-189.

[55] Y. Lei, J. Lin, Z. He, M.J. Zuo, A review on empirical mode decomposition in fault diagnosis of rotating machinery. Mechanical Systems and Signal Processing 35 (2013) 108-126.

[56] Z. Wu, N.E. Huang, A study of the characteristics of white noise using the empirical mode decomposition method. in: Proceedings of the Royal Society of London A: Mathematical, Physical and Engineering Sciences, The Royal Society, 2004, pp. 1597-1611.

[57] D. Pines, L. Salvino, Structural health monitoring using empirical mode decomposition and the Hilbert phase. Journal of Sound and Vibration 294 (2006) 97-124.

[58] R. Li, D. He, Rotational machine health monitoring and fault detection using EMD-based acoustic emission feature quantification. IEEE Transactions on Instrumentation and Measurement 61 (2012) 990-1001.

[59] G. Hearn, R.B. Testa, Modal analysis for damage detection in structures. Journal of Structural Engineering 117 (1991) 3042-3063.

[60] M. Palacz, M. Krawczuk, Vibration parameters for damage detection in structures. Journal of Sound and Vibration 249 (2002) 999-1010.

[61] H.-C. Eun, Y.-J. Ahn, S.-G. Lee, Detection of loosened bolt- joint in braced steel frame structure based on impact hammer test. (2014) 75-78.

[62] P. Razi, R.A. Esmaeel, F. Taheri, Improvement of a vibration-based damage detection approach for health monitoring of bolted flange joints in pipelines. Structural Health Monitoring 12 (2013) 207-224.

[63] K. He, W. Zhu, Detecting loosening of bolted connections in a pipeline using changes in natural frequencies. Journal of Vibration and Acoustics 136 (2014) 034503.

[64] V. Caccese, R. Mewer, S. Vel, Detection of bolt load loss using frequency domain techniques. in: Proceedings of the 15th International Conference on Adaptive Structures and Technologies, Bar Harbor, ME, 24-27 October, 2004.

[65] I. Rhee, E. Choi, Y.-S. Roh, Guided wave propagation induced by piezoelectric actuator in bolted thin steel members. KSCE Journal of Civil Engineering 16 (2012) 398-406.

[66] T. Wang, G. Song, S. Liu, Y. Li, H. Xiao, Review of bolted connection monitoring. International Journal of Distributed Sensor Networks 2013 (2013).

[67] K.Y. Jhang, H.H. Quan, J. Ha, N.Y. Kim, Estimation of clamping force in high-tension bolts through ultrasonic velocity measurement. Ultrasonics 44 Suppl 1 (2006) e1339-1342.

[68] S. Ritdumrongkul, M. Abe, Y. Fujino, T. Miyashita, Quantitative health monitoring of bolted joints using a piezoceramic actuator–sensor. Smart Materials and Structures 13 (2004) 20-29.

[69] J. Bao, Y. Shen, V. Giurgiutiu, Linear and Nonlinear Finite Element Simulation of Wave Propagation through Bolted Lap Joint. in, 54th AIAA/ASME/ASCE/AHS/ASC Structures, Structural Dynamics, and Materials Conference, 2013.

[70] Q. WANG, S.-f. YUAN, L. QIU, Study on bolt debonding monitoring of composite joint based on time-reversal method. Journal of Astronautics 6 (2007) 057.

[71] W. Tao, L. Shaopeng, S. Junhua, L. Yourong, Health monitoring of bolted joints using the time reversal method and piezoelectric transducers. Smart Materials and Structures 25 (2016) 025010.

[72] J. Ruan, Z. Zhang, T. Wang, Y. Li, G. Song, An anti-noise real-time cross-correlation method for bolted joint monitoring using piezoceramic transducers. Smart Structures and Systems 16 (2015) 281-294.

[73] J. Min, S. Park, C.-B. Yun, C.-G. Lee, C. Lee, Impedance-based structural health monitoring incorporating neural network technique for identification of damage type and severity. Engineering Structures 39 (2012) 210-220.

[74] A.N. Zagrai, V. Giurgiutiu, Electro-mechanical impedance method for crack detection in thin plates. Journal of Intelligent Material Systems and Structures 12 (2001) 709-718.

[75] S.S. Kessler, S.M. Spearing, M.J. Atalla, C.E. Cesnik, C. Soutis, Damage detection in composite materials using frequency response methods. Composites Part B: Engineering 33 (2002) 87-95.

[76] Y.-K. An, H. Sohn, Integrated impedance and guided wave based damage detection. Mechanical Systems and Signal Processing 28 (2012) 50-62.

[77] Z. Zhang, M. Liu, Z. Su, Y. Xiao, Quantitative evaluation of residual torque of a loose bolt based on wave energy dissipation and vibro-acoustic modulation: A comparative study. Journal of Sound & Vibration 383 (2016) 156-170.

[78] M. Shiwa, Y. Furuya, H. Yamawaki, K. Ito, M. Enoki, Fatigue Process Evaluation of Ultrasonic Fatigue Testing in High Strength Steel Analyzed by Acoustic Emission and Non-Linear Ultrasonic. Materials Transactions 51 (2010) 1404-1408.

[79] C. Mattei, Imaging of Fatigue Damage in CFRP Composite Laminates Using Nonlinear Harmonic Generation. 657 (2003) 989-995.

[80] F. Semperlotti, K.W. Wang, E.C. Smith, Localization of a breathing crack using nonlinear subharmonic response signals. Applied Physics Letters 95 (2009) 254101.

[81] M. Hong, Z. Su, Y. Lu, H. Sohn, X. Qing, Locating fatigue damage using temporal signal features of nonlinear Lamb waves. Mechanical Systems and Signal Processing 60-61 (2015) 182-197.

[82] D. Yan, B.W. Drinkwater, S.A. Neild, Measurement of the ultrasonic nonlinearity of kissing bonds in adhesive joints. NDT & E International 42 (2009) 459-466.

[83] M. Hong, Z. Su, Q. Wang, L. Cheng, X. Qing, Modeling nonlinearities of ultrasonic waves for fatigue damage characterization: theory, simulation, and experimental validation. Ultrasonics 54 (2014) 770-778.

[84] A.C. Rutherford, G. Park, C.R. Farrar, Non-linear feature identifications based on self-sensing impedance measurements for structural health assessment. Mechanical Systems and Signal Processing 21 (2007) 322-333.

[85] S.L. Tsyfansky, V.I. Beresnevich, Non-Linear Vibration Method for Detection of Fatigue Cracks in Aircraft Wings. Journal of Sound and Vibration 236 (2000) 49-60.

[86] A. Novak, M. Bentahar, V. Tournat, R. El Guerjouma, L. Simon, Nonlinear acoustic characterization of micro-damaged materials through higher harmonic resonance analysis. NDT & E International 45 (2012) 1-8.

[87] J. Rivi re, G. Renaud, S. Haupert, M. Talmant, P. Laugier, P.A. Johnson, Nonlinear acoustic resonances to probe a threaded interface. Journal of Applied Physics 107 (2010) 124901.

[88] G. Shui, Y.-s. Wang, P. Huang, J. Qu, Nonlinear ultrasonic evaluation of the fatigue damage of adhesive joints. NDT & E International 70 (2015) 9-15.

[89] F. Semperlotti, S.C. Conlon, Nonlinear structural surface intensity: An application of contact acoustic nonlinearity to power flow based damage detection. Applied Physics Letters 97 (2010) 141911.

[90] S. Biwa, S. Nakajima, N. Ohno, On the Acoustic Nonlinearity of Solid-Solid Contact With Pressure-Dependent Interface Stiffness. Journal of Applied Mechanics 71 (2004) 508.

[91] A. Zagrai, D. Doyle, V. Gigineishvili, J. Brown, H. Gardenier, B. Arritt, Piezoelectric Wafer Active Sensor Structural Health Monitoring of Space Structures. Journal of Intelligent Material Systems and Structures 21 (2010) 921-940.

[92] M. Zhang, Y. Shen, L. Xiao, W. Qu, Application of subharmonic resonance for the detection of bolted joint looseness, Nonlinear Dynamics, 88 (2017) 1643-1653.

[93] Z. Zhang M. Liu, Z. Su, Y. Xiao, Evaluation of Bolt Loosening Using A Hybrid Approach Based on Contact Acoustic Nonlinearity. in: 19th World Conference on Non-Destructive Testing Munich, 2016.

[94] K.E.A. Van Den Abeele, J. Carmeliet, J.A. Ten Cate, P.A. Johnson, Nonlinear Elastic Wave Spectroscopy (NEWS) Techniques to Discern Material Damage, Part II:

Single-Mode Nonlinear Resonance Acoustic Spectroscopy. Research in Nondestructive Evaluation 12 (2000) 31-42.

[95] K.E.A. Van Den Abeele, P.A. Johnson, A. Sutin, Nonlinear Elastic Wave Spectroscopy (NEWS) Techniques to Discern Material Damage, Part I: Nonlinear Wave Modulation Spectroscopy (NWMS). Research in Nondestructive Evaluation 12 (2000) 17-30.

[96] J.-J. Sinou, A review of damage detection and health monitoring of mechanical systems from changes in the measurement of linear and non-linear vibrations. Mechanical Vibrations: Measurement, Effects and Control (2009) 643-702.

[97] Y. Luan, Z.-Q. Guan, G.-D. Cheng, S. Liu, A simplified nonlinear dynamic model for the analysis of pipe structures with bolted flange joints. Journal of Sound and Vibration 331 (2012) 325-344.

[98] M. Deng, J. Pei, Assessment of accumulated fatigue damage in solid plates using nonlinear Lamb wave approach. Applied physics letters 90 (2007) 121902.

[99] M. Amura, M. Meo, F. Amerini, Baseline-free estimation of residual fatigue life using a third order acoustic nonlinear parameter. The Journal of the Acoustical Society of America 130 (2011) 1829-1837.

[100] H. Jin Lim, H. Sohn, P. Liu, Binding conditions for nonlinear ultrasonic generation unifying wave propagation and vibration. Applied Physics Letters 104 (2014) 214103.

[101] M.B. Rosales, C.P. Filipich, F.S. Buezas, Crack detection in beam-like structures. Engineering Structures 31 (2009) 2257-2264.

[102] F. Amerini, E. Barbieri, M. Meo, U. Polimeno, Detecting loosening/tightening of clamped structures using nonlinear vibration techniques. Smart Materials and Structures 19 (2010) 085013.

[103] U. Polimeno, M. Meo, D.P. Almond, S.L. Angioni, Detecting low velocity impact damage in composite plate using nonlinear acoustic/ultrasound methods. Applied Composite Materials 17 (2010) 481-488.

[104] N.P. Yelve, M. Mitra, P. Mujumdar, Detection of stiffener disbonding in a stiffened aluminium panel using nonlinear Lamb wave. Applied Acoustics 89 (2015) 267-272.

[105] A. Shah, Y. Ribakov, C. Zhang, Efficiency and sensitivity of linear and non-linear ultrasonics to identifying micro and macro-scale defects in concrete. Materials & Design 50 (2013) 905-916.

[106] R. Ruotolo, C. Surace, P. Crespo, D. Storer, Harmonic analysis of the vibrations of a cantilevered beam with a closing crack. Computers & structures 61 (1996) 1057-1074.

[107] Y. Shen, V. Giurgiutiu, Health Monitoring of Aerospace Bolted Lap Joints Using Nonlinear Ultrasonic Spectroscopy: Theory and Experiments. in: Proceedings of the 9th International Workshop on Structural Health Monitoring, Stanford University, CA, USA, 2013, pp. 23332340.

[108] D. Donskoy, A. Sutin, A. Ekimov, Nonlinear acoustic interaction on contact interfaces and its use for nondestructive testing. Ndt & E International 34 (2001) 231-238.

[109] K.-Y. Jhang, Nonlinear ultrasonic techniques for nondestructive assessment of micro damage in material: a review. International journal of precision engineering and manufacturing 10 (2009) 123-135.

[110] I.Y. Solodov, Ultrasonics of non-linear contacts: propagation, reflection and NDE-applications. Ultrasonics 36 (1998) 383-390.

[111] I. Didenkulov, A. Sutin, V. Kazakov, A. Ekimov, S. Yoon, Nonlinear acoustic technique of crack location. in: Nonlinear Acoustics at the Turn of the Millennium: ISNA 15, 15th International Symposium, AIP Publishing, 2000, pp. 329-332.

[112] K.H. Matlack, J.Y. Kim, L.J. Jacobs, J. Qu, Review of Second Harmonic Generation Measurement Techniques for Material State Determination in Metals. Journal of Nondestructive Evaluation 34 (2014).

[113] J. Kim, K.-Y. Jhang, Assessment of thermal degradation by cumulative variation of ultrasonic nonlinear parameter. International Journal of Precision Engineering and Manufacturing 18 (2017) 23-29.

[114] H. Seo, J. Jun, K.-Y. Jhang, Assessment of Thermal Aging of Aluminum Alloy by Acoustic Nonlinearity Measurement of Surface Acoustic Waves. Research in Nondestructive Evaluation 28 (2016) 3-17.

[115] G. Ren, J. Kim, K.Y. Jhang, Relationship between second- and third-order acoustic nonlinear parameters in relative measurement. Ultrasonics 56 (2015) 539-544.

[116] D. Broda, W. Staszewski, A. Martowicz, T. Uhl, V. Silberschmidt, Modelling of nonlinear crack–wave interactions for damage detection based on ultrasound—a review. Journal of Sound and Vibration 333 (2014) 1097-1118.

[117] N. Pugno, C. Surace, R. Ruotolo, Evaluation of the non-linear dynamic response to harmonic excitation of a beam with several breathing cracks. Journal of Sound and Vibration 235 (2000) 749-762.

[118] A. Bovsunovsky, C. Surace, Considerations regarding superharmonic vibrations of a cracked beam and the variation in damping caused by the presence of the crack. Journal of Sound and Vibration 288 (2005) 865-886.

[119] I. Solodov, J. Bai, S. Bekgulyan, G. Busse, A local defect resonance to enhance acoustic wave-defect interaction in ultrasonic nondestructive evaluation. Applied Physics Letters 99 (2011) 211911.

[120] W. Zhou, Y. Shen, L. Xiao, W. Qu, Application of Nonlinear-Modulation Technique for the Detection of Bolt Loosening in Frame Structure. Journal of Testing and Evaluation 44 (2016) 20150321.

[121] M. Ryles, F.H. Ngau, I. McDonald, W.J. Staszewski, Comparative study of nonlinear acoustic and Lamb wave techniques for fatigue crack detection in metallic structures. Fatigue & Fracture of Engineering Materials & Structures 31 (2008) 674-683.

[122] N.A. Chrysochoidis, A.K. Barouni, D.A. Saravanos, Delamination detection in composites using wave modulation spectroscopy with a novel active nonlinear acousto-ultrasonic piezoelectric sensor. Journal of Intelligent Material Systems and Structures 22 (2011) 2193-2206.

[123] L. Straka, Y. Yagodzinskyy, M. Landa, H. Hänninen, Detection of structural damage of aluminum alloy 6082 using elastic wave modulation spectroscopy. NDT & E International 41 (2008) 554-563.

[124] V.Y. Zaitsev, L.A. Matveev, A.L. Matveyev, Elastic-wave modulation approach to crack detection: Comparison of conventional modulation and higher-order interactions. NDT & E International 44 (2011) 21-31.

[125] U. Andreaus, P. Baragatti, Experimental damage detection of cracked beams by using nonlinear characteristics of forced response. Mechanical Systems and Signal Processing 31 (2012) 382-404.

[126] F. Aymerich, W.J. Staszewski, Experimental Study of Impact-Damage Detection in Composite Laminates using a Cross-Modulation Vibro-Acoustic Technique. Structural Health Monitoring 9 (2010) 541-553.

[127] A. Klepka, W.J. Staszewski, D. di Maio, F. Scarpa, Impact damage detection in composite chiral sandwich panels using nonlinear vibro-acoustic modulations. Smart Materials and Structures 22 (2013) 084011.

[128] A. Klepka, L. Pieczonka, W.J. Staszewski, F. Aymerich, Impact damage detection in laminated composites by non-linear vibro-acoustic wave modulations. Composites Part B: Engineering 65 (2014) 99-108.

[129] L. Pieczonka, P. Ukowski, A. Klepka, W.J. Staszewski, T. Uhl, F. Aymerich, Impact damage detection in light composite sandwich panels using piezo-based nonlinear vibro-acoustic modulations. Smart Materials and Structures 23 (2014) 105021.

[130] A. Zagrai∗, D. Donskoy, A. Chudnovsky, E. Golovin, Micro- and Macroscale Damage Detection Using the Nonlinear Acoustic Vibro-Modulation Technique. Research in Nondestructive Evaluation 19 (2008) 104-128.

[131] A. Klepka, W. Staszewski, R. Jenal, M. Szwedo, J. Iwaniec, T. Uhl, Nonlinear acoustics for fatigue crack detection - experimental investigations of vibro-acoustic wave modulations. Structural Health Monitoring 11 (2011) 197-211.

[132] I. Solodov, J. Wackerl, K. Pfleiderer, G. Busse, Nonlinear self-modulation and subharmonic acoustic spectroscopy for damage detection and location. Applied Physics Letters 84 (2004) 5386.

[133] H. Sohn, H.J. Lim, M.P. DeSimio, K. Brown, M. Derriso, Nonlinear ultrasonic wave modulation for online fatigue crack detection. Journal of Sound and Vibration 333 (2014) 1473-1484.

[134] V. Zaitsev, V. Nazarov, V. Gusev, B. Castagnede, Novel nonlinear-modulation acoustic technique for crack detection. NDT & E International 39 (2006) 184-194.

[135] G.P. Malfense Fierro, M. Meo, Residual fatigue life estimation using a nonlinear ultrasound modulation method. Smart Materials and Structures 24 (2015) 025040.

[136] J.J. Meyer, D.E. Adams, Theoretical and experimental evidence for using impact modulation to assess bolted joints. Nonlinear Dynamics 81 (2015) 103-117.

[137] J. Jaques, D. Adams, D. Doyle, W. Reynolds, Using impact modulation to identify loose bolts in a satellite structure. in: Fifth European Workshop on Structural Health Monitoring, 2010.

[138] F. Amerini, M. Meo, Structural health monitoring of bolted joints using linear and nonlinear acoustic/ultrasound methods. Structural Health Monitoring 10 (2011) 659-672.

[139] V. Baranov, E. Kudryavtsev, G. Sarychev, Modelling of the parameters of acoustic emission under sliding friction of solids. Wear 202 (1997) 125-133.

[140] J.M. Mínguez, J. Vogwell, Effect of torque tightening on the fatigue strength of bolted joints. Engineering Failure Analysis 13 (2006) 1410-1421.

[141] B.N.J. Persson, Contact mechanics for randomly rough surfaces. Surface Science Reports 61 (2006) 201-227.

[142] J. Guckenheimer, P.J. Holmes, Nonlinear oscillations, dynamical systems, and bifurcations of vector fields, Springer Science & Business Media, 2013.

[143] Y. Lu, L. Ye, Z. Su, C. Yang, Quantitative assessment of through-thickness crack size based on Lamb wave scattering in aluminium plates. NDT & E International 41 (2008) 59-68.